HABILITATIONSSCHRIFT

zur
Erlangung der Venia legendi
für das Fach Astronomie
der
Ruprecht-Karls-Universität
Heidelberg

vorgelegt von
Thomas J. Rivinius
aus Mannheim
2005

Classical Be Stars

Gaseous Discs Around the
Most Rapidly Rotating Stars

Betreffend die qualiteten / so dieſer ſternen vermuthlich in ſeiner würckhung erzeigen möchte / werden dieſelbige auß ſeinem liecht vnd farb müſſen er=lehrnet werden.

Previous page: The Be stars Pleione, Alcyone, Electra and Merope.
                          Image: NASA

Text Source: Johan Khepplern/ Röm:Kay:May:mathematicum.

                          Von einem vngewohnlichen Newen Stern, Prag, 1604

Abstract: Based on over 4000 high resolution echelle spectra this work represents one of the most extensive spectroscopic studies of Be stars and their circumstellar environment derived from a homogeneous database. The available spectra span the entire visual range and thus allow to investigate both the circumstellar environment and the star in a multi-line approach. For the circumstellar environment, the study of shell stars reinforces the understanding of a geometrically thin circumstellar disc around Be stars, seen edge-on in shell stars. Moreover, strong evidence is found that these discs are in Keplerian rotation, ruling out models of angular-momentum conserving outflowing discs as well as locked corotation. In particular spectral features like narrow shell-lines and central quasi-emission bumps require a velocity field with an almost zero radial velocity component. Next to Keplerian rotation, only locked corotation could provide this, but can be excluded since it would produce an entirely different type of line profile for the shell lines. The discs were as well shown to be governed by dynamical processes: Many discs are formed by transient outbursts and in the following show a slowly evolving pattern commensurable with a gradual outwards motion of the material, the forming of an inner empty cavity in the disc so that it rather resembles a ring, and an eventual dissipation of the disc into the interstellar space. At least for modelling spectral lines in the visual domain, it is strongly recommended to take such a structure into account. Among the central stars themselves, μ Cen and ω CMa were the most thoroughly investigated. For both is was possible to reproduce the well-known short-periodic line profile variability in great detail as non-radial pulsation in a multimode model based on four $\ell = m = +2$ modes and two $\ell = m = +3$ modes for μ Cen and a monoperiodic model with an $\ell = m = +2$ mode for ω CMa. Of 27 stars investigated for line profile variations 16 are explainable with nonradial pulsation in an $\ell = m = +2$ mode. For four more stars this is likely, but the observational data is not sufficient for a firm conclusion. Three stars exhibit a different type of periodic line profile variability. This does not necessarily exclude non-radial pulsation for these objects but probably only requires different modes than $\ell = m = 2$. Two objects show line profile variability, but the data is insufficient for any conclusion, and finally two stars were stable within the detection limits. The explanation of the line profile variations found in most early type Be stars is, therefore, nonradial pulsation. Except possibly for singular cases, other mechanisms are not required for an explanation of the short periodic line profile variations. Still, however, the process leading to outbursts and the formation of the circumstellar disc is not clear. From the usually assumed rotation rates to the Keplerian velocity several times the pulsation amplitude is missing to provide sufficient angular momentum. In order to relax this problem, recent claims that Be stars may be rotating more rapid than the canonically accepted 70 to 80 % of their critical rate are investigated. Indeed it seems possible that previous studies underestimated the effect of gravity darkening on the visibility of the stellar equatorial region, so that rotational rates higher than 80 % could have systematically remained undetected. Based on line profile modelling, an observational spectroscopic method is worked out to circumnavigate this problem by observing lines which are formed predominantly in the cooler equatorial regions. The most nearby Be star α Eri, which is known to have extreme rotational flattening, is used as test case and further promising candidate stars are identified from the database. Finally, it is shown that the accepted rotational statistics of Be stars is not in contradiction with Be stars being much closer to critical rotation than currently believed, if the gravity darkening effects are as severe as suspected.

Meinen Eltern

Contents

Preface

On 23rd of August 1866 Padre Angelo Secchi, director of the observatory of the Collegio Romano, wrote a letter to the editor of the Astronomische Nachrichten, reporting "une particularité de l'etoile γ Cassiopée". Instead of Balmer line absorption as in Sirius or Vega, it would have "une ligne lumineuse trés-belle et bien plus brilliante que tout le reste du spectre" (Secchi 1867). This was one of the first emission-line stars detected, and the first report of a Be star.

Since then, astrophysics has went on far towards the understanding of the Universe. Many aspects of Be stars are well understood nowadays, but as many questions are still open. In the past years, a concensus has been grown that these stars do have relatively thin discs in Keplerian rotation. The long standing questions whether Be stars are nonradial pulsators has found a commonly accepted answer. Results presented in the first two parts of this book have contributed their share to this development. And yet the basic question what makes a B star a Be star is still not answered. But it might be that the Be star research has finally reached a stage at which the right questions are asked; namely what process might add sufficient angular momentum to the gaseous disc to make it Keplerian, but not enough energy to make the gas escape on an angular momentum conserving trajectory. While many processes discussed in the past seem to fall short on the first problem, magnetic models require a high degree of fine tuning not to create a rapidly outflowing disc. An irony in the history of science, it seems possible that the answer to that question might be the one that has already been suggested 70 years ago by Otto Struve (1931), namely that Be stars rotate close enough to the critical limit to make equatorial mass loss into a circumstellar disc a naturally occurring mechanism.

This work is based on research undertaken in the past five years, mainly investigating high-resolution spectroscopic data. The observational data covers the entire wavelength range accessible to the human eye, and partly even more. Although the data were mainly accumulated to investigate whether Be stars do pulsate or not, the properties of these spectra allowed to address further questions once the primary science goal was reached. Therefore, following the Introduction in Chapter 1 this work is presented in three parts:

Part I discusses the properties of the circumstellar environment. The results strongly support the paradigm of a relatively thin circumstellar disc. Particular line profile types, the *central quasi emission bumps*, can only be explained in the frame of a rotationally supported disc, since they require any radial velocity components to be negligible. Similar support is obtained from the sharpness of circumstellar absorption lines. In turn, evidence presented by other authors for a thick disc or even some completely other geometry could not be confirmed to be striking (Chapter 2). Based on this picture of a thin disc, the observed long-term variations are assembled to a panorama of a disc's life. Although this is strictly valid only for early type Be stars, since the time scales in the late-type ones are too large to be observed even in a multi-year study, the observed behaviours are quite common. Discs are formed and replenished through discrete processes. When such a star-to-disc mass transfer has stopped, a slow evolution sets in, clearing the inner part of the disc and dissipating the disc through the stellar wind. As a result, the ejected mass is effectively lost from the system and not reaccreted (Chapter 3).

Whether the typical short periodic line profile variability (*lpv*) of early type Be stars is due to nonradial pulsation (*nrp*) or a rotationally bound mechanism is answered in Part II. A set of model codes that were used for this task is introduced in Chapter 4. With these codes the *lpv* of two well known objects, μ Cen and ω CMa, were reproduced in high detail (Chapter 5). The model representation of the data is excellent, even profile shapes that initially were believed to require strong non-linear processes could be reproduced. Finally, it is shown that the two objects investigated in detail are archetypical. Based on the large database accumulated, it is shown in Chapter 6 that objects with similar properties as μ Cen and ω CMa, i.e. stars with low $v \sin i$, exhibit similar variability. Other Be stars with higher $v \sin i$ are believed to differ mainly in inclination, and it is shown that the model representations of μ Cen and ω CMa can be adapted to produce *lpv* similar to those observed in higher $v \sin i$ Be stars, by just increasing the model inclination.

However, Owocki (2004) has shown that all these results provide little to no help in the basic problem of Be stars, namely the formation of the disc, as long as the paradigm of non-critical rotation at about 80% of the

critical value is kept up. In Part III it is, therefore, investigated if the the rotational velocities could be higher than measured spectroscopically by applying the usual procedures. The process believed to be responsible for such systematic errors is the gravity darkening, which renders the equator in almost critical rotators cool, hence faint, and thus almost invisible. A potential way towards an observational answer, circumnavigating those problems, is sketched in Chapter 7 and observational data proving the potential of spectroscopy to be decisive for this question is presented in Chapter 8. Finally, Part IV summarizes the findings presented here and points to new questions opened by this work.

While these main parts rather concentrate on the commonalities and the derived general behaviour of the Be stars as a class of objects, the Appendices discuss individual objects in specific details. Appendix A describes the echelle database this study is based on. Appendix B introduces the shell stars in the sample and provides the statistical basis of the findings presented in Chapter 2, while Appendix C discusses the data of the stars for which evidence for a geometrical evolution of the disc was found (see Chapter 3). Finally, Appendix D summarizes all stars in the sample exhibiting rapid line profile variability, most of which can be attributed to non-radial pulsation, as is shown in Chapter 6.

Parts of this work have already been published, like in Rivinius et al. (1999, 2001a,b, 2002, 2003) and in several conference contributions. Further manuscripts are in the editorial process of the "Astronomy and Astrophysics" Journal or in preparation. In particular figures, tables, and the purely descriptive parts of the appendices and other sections where only the immediate behaviour as seen in the data is described were taken directly from these publications, while other parts were restructured, updated, and worked over before including them into the main chapters. Individual subsections were also published in Maintz et al. (2003), and Porter & Rivinius (2003).

Acknowledgements

Chapter 1

Introduction

1.1 Astrophysical context

Be stars were defined as "A non-supergiant B star whose spectrum has, or had at some time, one or more Balmer lines in emission" by Collins (1987), who was working in earlier definitions. This definition is still in use today as working definition. However, this purely phenomenological definition includes more than one type of objects in physical terms. Although this was clear already then, this definition was formulated for the sake of applicability. Any further narrowing of the above definition which may provide a more physical description may also involve a significant amount of dedicated analysis to classify a particular star, hence rendering the definition practically inapplicable. More recently the term "Classical" Be Stars has become increasingly used to exclude Herbig AeBe stars, Algol systems and others.

In order to discriminate these physically distinct type of emission-line B-type stars, one needs to review the astrophysical context of Be stars. First, there is the star itself. Be stars, which in the context of this work will be restricted to those termed classical ones above, are the class of stars which on average rotate closest to their critical limit where the centrifugal force balances gravity. Rotation, however, is the biggest unknown in our current understanding of stellar evolution, and in particular of hot stars (Maeder & Meynet 2000). The reason for this rapid rotation is not entirely clear, and several hypotheses exist. Heger & Langer (2000) discuss the evolution of surface parameters of rotating massive stars during the Main Sequence and find that the outer layers may spin-up as a result of the evolution of the angular momentum distribution. A particularly interesting limit is the so-called "Ω limit" (or "$\Omega - \Gamma$ limit", see for instance Langer 1998) where the star rotates at its critical speed, defined where the effective gravity, taking rotation and optically thin radiation into account, becomes zero. Whether Be stars rotate *at* the critical limit or not was believed to have been answered, but as recent theoretical results highlight the answer might not be as firm as was hoped. In any case, it is clear that their high rotation places Be stars in the centre of discussions of angular momentum evolution making them one of the most significant test beds for rotationally induced instabilities.

Aside from their important role in massive star evolution studies, Be stars offer prospects for asteroseismology of the hottest objects examined so far, due to the penetrating nature of g-mode pulsations — particularly with multiperiodic Be stars. Hints exist also of magnetic fields in a few Be stars which may prompt new research into field generation mechanisms for hot stars in general. Study of Be star circumstellar environments has produced models which are starting to be applied to other hot stars which have non-spherical circumstellar gas, such as planetary nebulae and supernova progenitors (e.g. Ignace et al. 1996, 1998). Also the search for the so-called "photospheric connection", i.e. the underlying mechanism triggering large scale wind inhomogeneities in hot stars may be related to the processes leading to the formation of a Be star disc. For all these research fields, solutions to Be star problems may offer new hints to all hot stars, and of course vice versa.

In order to clarify the term "Classical Be Star", some variants of non-supergiant B type stars are summarized in Table 1.1. The above Be star definition applies to the first four rows, and even to several individual members of the other types, like β Cephei itself. Algols and Herbigs, however, are not commonly regarded as Be stars in the sense of this work. Similarly, stars like σ Ori E are not regarded as such Be stars. This is a He-strong star, which also shows emission in magnetically bound clouds, but not a disc. This star is kept separate from other He-abnormal and Bp stars as this form of circumstellar gas in magnetically locked corotation is similar to one that was proposed for the Be phenomenon.

Table 1.1: Selected spectral properties and their observed presence in different classes of non-supergiant B type stars. Circumstellar line emission formed in: 1a) equatorial decretion disc; 1b) accretion disc; 1c) co-rotating clouds. Other properties include 2) low order line profile variations; 3) radial and/or p-mode (short-period) pulsation 4) rapid rotation; 5) large scale magnetic field; 6) surface abundance anomalies; 7) binaries. A tick is not to be regarded as *sine qua non*, but rather expresses a statistically expected property; similarly a lacking entry is meant statistically only as well. Low order *lpv* is common among early-type Be stars only.

Group	1a	1b	1c	2	3	4	5	6	7
classical Be stars	✓	–	–	✓/–	–	✓	–	–	–
Herbig Ae/Be stars	–	✓	–	–	–	–	–	–	–
Algol systems	–	✓	–	–	–	–	–	–	✓
σ Ori E and similar objects	–	–	✓	–	–	✓	✓	✓	–
Slowly pulsating B (SPB) stars	–	–	–	✓	–	–	–	–	–
β Cephei stars	–	–	–	–	✓	–	–	–	–
Bn stars	–	–	–	–	–	✓	–	–	–
Helium abnormal and Bp stars	–	–	–	–	–	–	✓	✓	–

1.2 General observational characteristics

Before discussing the detailed features of Be stars, it is useful to describe some observational characteristics of an "average" Be star throughout the electromagnetic spectrum. Parts of this description are based on the HEROS database described in the Appendices, others were compiled from the literature.

Spectral lines: The photospheric absorption spectra of Be stars typically show broad absorption lines due to rotation, but are normal in terms of equivalent width, i.e. gravity, temperature, and abundance (Slettebak 1982). The emission lines of Be stars are typically double peaked, with the peak separation correlated to the observed line-width of the photospheric absorption (Struve 1931; Hanuschik 1996). Exceptions are those stars with narrow line-width, which may have only single-peaked line emission, in particular in the HI lines.

Be stars can be subcategorized into emission- and shell-line Be stars. In emission line Be stars, the central reversal between the peaks does not reach below the flux level emerging from the stellar photosphere, meaning no net absorption. The most common lines in emission are those of HI, HeI, FeII, and sometimes also SiII and MgII. In the earlier B-subtypes, weak FeIII emission might be found as well. In a given Be star the strength of the emission can be highly variable. It may disappear completely, only to return decades later.

Shell line Be stars are characterized by narrow absorption cores in addition to the broad photospheric absorption lines. Hanuschik (1996) proposed clarification of this definition and denoted a Be star as a shell star when the absorption, or the central reversal, reaches below the stellar undisturbed flux. Shell stars have the highest measured photospheric line-widths among Be stars. The emission peaks, when present, also have the largest separation. In addition to the ions mentioned above, sharp absorption lines formed by TiII and/or CrII are present, along with other ions one would rather expect in typical BA-supergiant spectra (Jaschek & Jaschek 1987).

In about two thirds of the Be stars the red and violet emission peaks of a given emission line are of equal height (Hanuschik et al. 1996). In the others, the so called violet-to-red ratio of the emission peak heights, V/R, is not unity, but cyclically variable with cycle times of years to decades. Be stars may change from the stable $V = R$ fraction to V/R-variability and back.

In the ultraviolet regime, in particular in the range of the Lyman-continuum, Be stars in an emission line phase with line widths larger than about 150 to $200\,\mathrm{km\,s^{-1}}$ show signs of enhanced wind in the resonance lines of SiIV and CIV compared to normal B stars of the same spectral type (Grady et al. 1987a, 1989). At variance, the UV spectra of Be stars in shell phases are dominated by narrow shell lines, similar to the visual domain (Doazan et al. 1991).
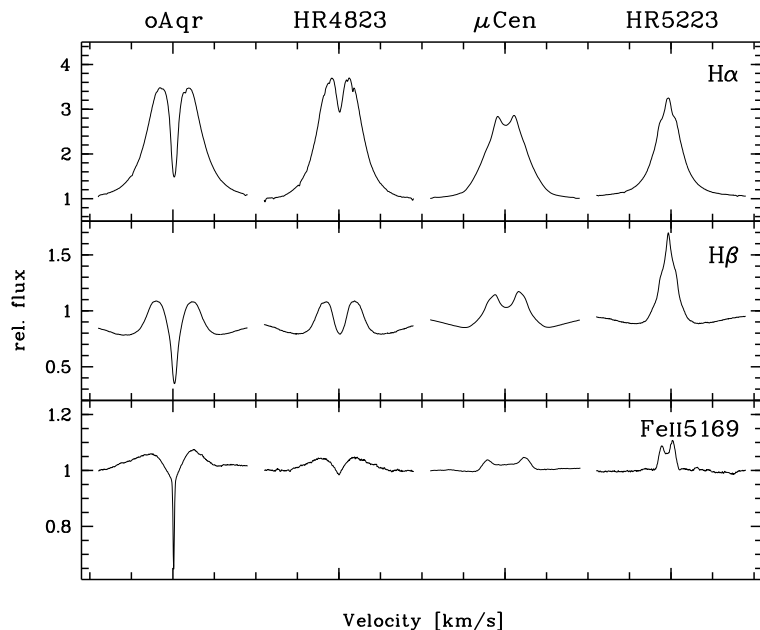
Figure 1.1: Example Be star emission line profiles, ranging from a shell Be star (left) to a single-peak emission Be star (right). Along this sequence, photospheric line-widths decrease from $\approx 260\,\mathrm{km\,s^{-1}}$ to $\approx 70\,\mathrm{km\,s^{-1}}$. The velocity tickmarks are spaced by $250\,\mathrm{km\,s^{-1}}$, larger tickmarks indicate the respective zero velocities.

The spectral energy distribution The ultraviolet spectral energy distribution of a B emission-line star does not differ significantly from the one of a non-Be star, but the Paschen continuum can be brighter than expected. Shell stars, on the other hand, show highly veiled ultraviolet spectra (Doazan et al. 1991) and their Paschen continua are typically dimmer. Depending on the amount of circumstellar matter, the spectra of both types of Be stars become dominated by free-free and free-bound emission from the disc in the near- to mid-infrared region.

In the far IR, the observed spectral energy distribution index a ($S_\nu \propto \nu^a$) changes from $a = 0.6$ to $a > 1$ in the radio regime, indicating some structural change far away from the central star (Waters et al. 1991b; Waters & Marlborough 1994).

Polarized light Almost all Be stars emit polarized continuous light (e.g. Wood et al. 1997; Bjorkman 2000b). The amount of polarization, which can be as high as 2 %, is variable and, in a given star, scales with the emission line strength, although time-lags have been observed in some cases (Poeckert et al. 1979). Polarization strength may vary also with other quantities, like the V/R ratio (McDavid et al. 2000), while the polarization angles are constant (Wood et al. 1997).

Observations of spectral line polarization have mostly yielded null results (Shorlin et al. 2002) placing an upper limit of $\sim$kG on the magnetic field. Recent reports note potential detections, but await independent confirmation, so that this claim may have to be revised in the near future.

Spatial emission distribution Nearby Be stars are prime targets for interferometric studies. Already the first studies have shown Be stars to be surrounded by flattened envelopes (Dougherty & Taylor 1992). Shell stars have higher axial ratios than emission line stars, (Quirrenbach et al. 1993, 1994) and the polarization angles are always perpendicular to the major axis of the envelope (Quirrenbach et al. 1997). The basic observational results have been confirmed by Tycner et al. (2004) for ζ Tau and a number of other stars. However, on the basis of the current envelope models, interpretations about disc opening angles and inclination are somewhat uncertain, and so further models with a discriminative power wrt. to interferometric data have to be worked out. Recent observations by Chesneau et al. (2005) and Baade (2004) also returned upper limits for the disc sizes in the mid-infrared regime at $10\,\mu$m of about 20 stellar radii for α Ara and δ Cen, respectively.

Domiciano de Souza et al. (2003) have presented the first measurement of rotational flattening of a rotating star itself for the Be star Achernar ((α Eri), and McAlister et al. (2004), by means of measuring the geometrical deformation, have found the normal B star Regulus (α Leo) to rotate with 86 % of its critical value.

1.3 Be stars discs

1.3.1 Geometrical distribution

Already early with the understanding of stellar spectra it was proposed that the emission lines are not formed in the photosphere of Be stars. The geometry and kinematics of this circumstellar material, however, remained a hotly contested subject. Only recently a consensus has been emerging about the geometric distribution of the gas.

A major step forward was made in 1992 with the first interferometric observations of a Be star by Dougherty & Taylor (1992). This radio study of ψ Per using the VLA confirmed that the geometry of the emitting circumstellar region was not spherically symmetric — ψ Per's radio emission has an axial ratio of > 2. It has long been suspected that the circumstellar gas is in the form of a disc (Struve 1931). Polarization studies (e.g. McLean & Brown 1978) have indicated that the circumstellar gas is not spherically symmetric. From the mid-1990s on, also optical interferometry has begun to produce results for Be stars. These results have confirmed the aspherical geometry of the circumstellar emission (Quirrenbach et al. 1994, 1997; Stee 1995). Indeed for those stars which have had the position angle of the disc measured it lies normally to the continuum polarization angle, as expected for scattering models (e.g. Wood et al. 1996). The available axial ratio determinations of the envelopes basically agree with the inclination estimates from the emission, but thorough determinations of this angle are model-dependant.

Several attempts have been made to determine the opening angle of the disc. Since Be shell stars are believed to be normal Be stars seen under equatorial inclination, so that the disc intersects the line of sight towards the photosphere, they can be used to constrain the disc opening angle. Statistical methods based on the number of shell stars vs. normal Be stars give values of $5°$ and $13°$, respectively (Porter 1996; Hanuschik 1996), while Yudin (2001) concludes from his statistical analysis that the half-opening angles lie in the range $10°$ to $40°$.

Independently, an upper limit of $20°$ has been derived from interferometric observations and spectropolarimetry by Quirrenbach et al. (1997), whilst Wood et al. (1997) calculate an opening angle of $2.5°$ for ζ Tauri from polarization. The latter technique is sensitive to the inner regions only which, if the disc flares, may account for the apparent inconsistency with the statistical studies which probe larger disc radii. Such a flaring at large radii, i.e. the opening angle is an increasing function of radius, was suggested by Hanuschik and is in fact well known for Keplerian accretion discs in the context of star- and planet-formation.

In summary, interferometric studies have confirmed that the geometry of the circumstellar gas is disc-like and that statistical estimates of opening angles point to a relatively thin disc. The polarization angle is perpendicular to the outer disc plane which also strongly suggests a disc structure in the inner parts, since these densest regions affect the polarization most.

1.3.2 Kinematics

Next to the geometry, also the kinematics of the circumstellar gas has received much attention in the past. Doppler shifts within the disc may reveal the velocity structure of the disc through the emission line profile. The most common profile shape is double peaked and symmetric across the line centre. But large minorities among the Be stars exhibit other profile types, such single peaked or asymmetric (e.g. see the atlas by Hanuschik et al. 1996). An asymmetry may reverse in time such that the violet and red parts of the line may be dominant at different times (termed V/R variation, discussed in detail in the following Section). This variety of profiles and behaviours makes the line profiles difficult to interpret and it is remarkable that good fits to observations have been obtained for around 25 years using relatively simple models (e.g. Poeckert & Marlborough 1978; Hummel 1994; Hummel & Vrancken 2000, to name a few).

The relative ease in modelling the line profiles has the disadvantage that an unambiguous observational determination of the kinematics is difficult, since the existing models do not well constrain it. Using a rotational velocity of $v_\phi \propto R^{-j}$, Hummel & Vrancken (2000) illustrate that it is possible to produce indistinguishable line profiles using either a Keplerian disc, or an angular momentum conserving disc by using different density structures for the disc, at least as long optically thin lines are investigated. For non-negligible optical depths the degeneracy is broken, and they find that their best fitting models have an average rotational parameter $j < 0.65$. This value is consistent with a Keplerian disc, which would have $j = 0.5$, but the result is not firm enough to be regarded as definite proof.

Next to the azimuthal velocities in the disc, also the radial velocity component is important in understanding the disc formation and dissipation processes. Line profiles from the "edge-on" Be shell-type stars are excellent diagnostics of radial outflow. These lines involve absorption of the photospheric flux throughout the whole

disc as long as the lower level of the respective transition is populated, and hence provide information on the radial velocity structure. Significant radial outward motions within the disc would produce time independent asymmetric lines with larger red components than blue, i.e. $V > R$, and blue absorption resembling classical P Cygni profiles for higher radial velocities (Waters & Marlborough 1992). As such profiles are not observed, the radial velocity is observationally constrained to upper limits. Examination of Doppler shifts in optically thin shell lines of FeII provide no evidence for radial motions within the disc (Hanuschik 2000). The kinematical evidence seems to point to a disc velocity field dominated by rotation, with little or no radial flow — at least in the regions where the kinematic signatures of emission and absorption are significant, i.e. within a few stellar radii.

1.3.3 Global disc variations

1.3.3.1 Cyclic V/R changes

For the typical double peaked emission lines, the heights of the blue- and red-shifted peaks are designated as V and R, respectively. Long-term cyclic changes in the ratio V/R are observed in many stars, taking from a few years up to decades to complete the cycle (see list in Okazaki 1997). The morphology of such cycles has been described by e.g. Hanuschik et al. (1995), using high resolution data.

Models of the circumstellar environment of a Be star based on a Keplerian disc were found to be consistent with V/R variability, if the changes are represented as a one armed density wave in the disc, precessing around the central star. Telting et al. (1994), using observations by Cowley & Gugula (1973), concluded the direction of precession to be prograde, i.e. in the sense of rotation. This has been confirmed by interferometric measurements of ζ Tau, where the photocentre of the Hα-emission is seen to move around the central star (Vakili et al. 1998). Similar observations were published by Berio et al. (1999) for γ Cas.

McDavid et al. (2000), modelling polarimetric data, required a spiral structure of the wave, rather than a plainly radial "arm", to explain phase lags in 48 Lib between Hα observations, which scan the outer parts of the disc, and polarimetric measurements affected most by the dense inner parts of the disc. Early observations of phase lags between the V/R cycles of individual lines of up to several months (see references in Baade 1985) also imply some spiral structure of the density wave in at least some stars.

Following the success in reproducing the V/R changes in great detail, theoretical explanations for these V/R variations have concentrated on one-armed density waves, i.e. $m = 1$ modes with m equal to the azimuthal wavenumber. These are the only global modes in a near Keplerian disc (suggested by Kato 1983, and applied to Be stars by Okazaki 1991). In Okazaki's model the $m = 1$ mode arises as the velocity distribution within the disc deviates slightly from Keplerian, which generates pressure perturbations and produces slightly elliptical orbits. Even for initially stochastic perturbations, viscous processes between the individual particles will tend to align the elliptical orbits more and more, so that finally the orbits will crowd around a common periastron-angle. This local overdensity is then the density wave. However, this model produced infinite oscillation periods, since the periastron angle in this model did not precess. Papaloizou et al. (1992) expanded the model and illustrated that the elliptic particle orbits precess under the action of a gravitational field containing a quadrupole component, created by the non-spherical rotating star itself, which was not included in Okazaki's model. A recent alternative to producing precession of elliptical orbits, described by Gayley et al. (2001), uses the radiative force of optically thick lines within the disc (Okazaki 1997, included the only effects of optically thin line radiation to the model). The pattern speed of the precession then is the physical background of the period of a few to some ten years for typical B star parameters. When the dense part is on the approaching side of the disc, the V peak will be higher, whilst R is enhanced when the periastron passes the receding side.

Radiative transfer modelling of one-armed density waves (e.g. Hummel & Hanuschik 1997) reproduces the V/R variation seen in the line profiles, so that the kinematic structure applied in the model of the one-armed oscillations is consistent with observation. For these one-armed density waves to build up to observational magnitudes, it is clear that the disc gas must orbit the star several times. Therefore, these models imposes a strict criterion on the velocity field within the disc: the rotational velocity must be *much* larger than any radial outflow, which again points to a (quasi-)Keplerian disc.

1.3.3.2 Transitions between emission line and shell appearance

Since emission-line and shell Be stars are explained by inclination differences and the discs are thought to be equatorial, transitions between both flavours are hardly expected. The constancy of the measured polarization angles as well propose a constant disc angle. Mild changes might be understood as due to varying radii

(Hanuschik 1996) of a flaring disc, due to changes in the innermost parts of the disc, or due to changes of the ionization balance with varying disc mass and density. However, in a few cases extraordinary variations were seen that cannot be ascribed to any of these processes. These so-called "spectacular variations" were observed in only three stars up to now, namely γ Cas (e.g. Merrill & Wilson 1941), Pleione (e.g. Gulliver 1977; Cramer et al. 1995), and 59 Cyg (e.g. Barker 1982). They not only include changes from normal emission- to shell-behaviour and back, but also significant variations in the emission line width. Given that at least the brighter Be stars were found early and have been more or less frequently observed for more than hundred years now, one can conclude that spectacular variations are extraordinary.

Hummel (1998) proposed that these variations can be explained by misaligned stellar equatorial and disc orbital planes. The intersecting nodeline then would precess around the star, so that the disc is seen edge-on in front of the star at times, but more face-on during other observations. While this is fully consistent with the observations, there are no firm theoretical explanations what could cause such a misaligned disc. Porter (1998) proposed that radiative warping of Be discs may be a possible mechanism, but it should also be noted that both 59 Cyg and γ Cas were confirmed as binaries only recently (Rivinius & Štefl 2000; Harmanec et al. 2000), which is, however, not required to induce warping, as spiral galaxies' discs show.

1.3.3.3 Be and normal B star phases

The circumstellar environment of Be stars is not only variable in the sense of the properties of the emission lines, but even a complete loss of the disc may occur, and an eventual rebuilding. This overall change of the circumstellar disc reflects in a distinct photometric signature. When a Be star is building up line emission, the Paschen continuum will brighten by up to 0.5 mag in V, while at the same time $B - V$ becomes redder, and $U - B$ bluer. In shell stars, however, the Paschen continuum dims by $\Delta V \approx 0.3$ mag compared to normal B stars, while both $B - V$ and $U - B$ redden (Harmanec 1983). This behaviour can be understood as a consequence of scattering in the disc, either looked at the disc surface from above, so that light is scattered into the line of sight, or through the edge, when light is scattered away (Poeckert & Marlborough 1978).

For instance, θ CrB showed a strong shell spectrum before 1980, but lost the shell signature in summer 1980, turning into a normal B star in the visual domain. Ultraviolet shell lines were present until late 1981, and enhanced ultraviolet wind lines finally vanished in early 1982. After that, only transiently enhanced wind lines were seen from time to time (Doazan et al. 1984, 1986a,b, 1987). Since then, the star was in a quiescent state, but remained being monitored in case the disc would appear again. In fact, θ CrB has restarted some circumstellar activity after 20 years of quiescence (see App. B), but although a weak disc signature developed it seems no persistent disc is building up. Another well known Be star, o And has meanwhile repeated several cycles of absent, weak, and strong disc (Peters 1988a; Clark et al. 2003, and references therein). An alternative to dissipating the disc through radiation driven ablation is to entrain the disc gas in the fast wind through Kelvin-Helmholtz instabilities in the shear layer between disc and wind (Bjorkman 2000a). However, both ablation and entrainment are continuous processes, so if they are acting then the disc needs to be constantly, or at least frequently enough, replenished whilst the star remains in the Be phase.

1.4 The central star

The Be phenomenon as described above can be observed in some late-O stars and early-A stars, but it is mainly confined to the B star range. Jaschek & Jaschek (1983) identified 12% of all B type stars as Be stars from the Bright Star Catalogue; subsequent work (Zorec & Briot 1997) has shown that the mean frequency of Be stars is more around 17%, although this figure is dependent on spectral subtype (e.g. the frequency may be as high as 34% for B1 stars). Most authors agree that the highest fraction of Be stars appears around spectral type B1–B2. A well known problem in all census studies is that Be stars are variable and may lose their disc, and hence emission, completely. This introduces an incompleteness selection effect towards normal B type stars. Therefore, census studies will typically provide a lower limit to the fraction of Be stars within a sample. Only in regions with diffuse nebulosity, photometric or low-resolution spectroscopic searches may give numbers contaminated by nebular emission.

1.4.1 The periodic short term variation of Be stars

The above quoted common definition term of a Be star as objects which "...have, or had at one time ... Balmer lines in emission" (Collins 1987) is tailored to one of the most enigmatic feature of Be stars — their variability.

Long term and gradual variations of the circumstellar emission and absorption lines as introduced above are in fact common to all classical Be stars. In addition however, there is also more rapid variability (e.g. Oudmaijer & Drew 1997), observable both in photometry and spectroscopy. The spectroscopic signature of this variations will be termed "line profile variability" in this work, abbreviated as *lpv*. The timescales range from minutes to a few days, sometimes present in the same object simultaneously. Such short timescales, and the spectral lines in which the variations are observed, favour either the photosphere proper or the immediate circumstellar environment as region of origin. Since rotation alone may not be sufficient to produce the disc (Slettebak 1987), the short term variations became a prime candidate to identify the additional mechanism required for a rapidly rotating B star to become a Be star.

Short term variations were readily found in most early-type Be stars (e.g. Baade 1982, 1984a; Penrod 1986; Porri & Stalio 1988), but similar searches for Be stars later than about B5 were not successful (Baade 1989a,b, and references therein). The latest type Be stars for which significant line profile variability are reported are o And (Hill et al. 1989; Sareyan et al. 1998), κ Dra (Hill et al. 1991), and θ CrB (Hubert et al. 1990), all of spectral type B6. The UV wind variability in early type Be stars is at least partially also modulated with the *lpv* periods (Peters & Gies 2000).

Cuypers et al. (1989) and Balona et al. (1992) have investigated the 32 early- and 18 late-type Be stars. They found that 90 % of those earlier than B5 are variable, while only 28 % of type B6 and later showed significant short-term variations (see also Stagg 1987). Although this is a mismatch with the fact that *no* late type Be stars are known with *lpv*-type spectroscopic variations, the trend is confirmed. Short-periodic variations were also found photometrically in the Small Magellanic Cloud (e.g. Balona 1992, for NGC 330). From these Baade et al. (2002b) selected the stars they expected to show the strongest spectroscopic signature, but obtained a null result. If this is confirmed, the paradigm that photometric and spectroscopic short-term periodic variations are two sides of the same coin needs to be reconsidered.

Baade (1982) attributed the short periodic *lpv* on timescales between 0.5 and 2 d to nonradial pulsation (*nrp*). However, Balona (1990, 1995) argued on statistical grounds the periods to be better explained by stellar rotation and attributed the *lpv* to stellar spots, and later to co-rotating clouds. In order to resolve this issue, most investigators concentrated on a few well observed objects. The most important in this list are ω CMa (Balona et al. 1999), μ Cen (Rivinius et al. 1998b; Balona et al. 2001b), ω Ori (Balona et al. 2001a; Neiner et al. 2002), and η Cen (Štefl et al. 1995; Balona 1999; Janot-Pacheco et al. 1999; Levenhagen et al. 2003). All these objects have been investigated by several groups, partly coming to different conclusions. The proponents of both pulsation and starspot hypotheses above agreed that the detection of *true* photospheric multiperiodicity would decide the issue in favour of *nrp* (Baade & Balona 1994). However, the emphasis on "true" hints at the problem: while any discretely sampled signal can be explained with multiple frequencies, the actual physical presence of such frequencies in the star is much harder to show (see Aerts 2000, for a review).

Such multiperiodicity was finally found in μ Cen (Rivinius et al. 1998b, six photospheric periods). Comparison of the line-emission outburst times of μ Cen with the beating pattern of the multiperiodicity indicates that the multimode pulsation is playing at least a triggering role in the mass transfer from star to disc, even enabling prediction of such events. This finding may prove to be the "smoking gun" for the disc formation in μ Cen, but most (early-type) Be stars seem not to have such closely spaced mode groups. Support for *nrp* also comes from other wavelength ranges: Smith (2001), investigating archival IUE data, finds the UV spectrophotometric variability of 6 stars indicative for pulsation, 8 stars do not allow clear conclusions to be drawn and only 3 stars behave as though they possess circumstellar clouds.

1.4.2 Rotational rates of Be stars

The first suggestion of the nature of the Be phenomenon was based on the on average rapid rotation of Be stars (Struve 1931), that would from an outflowing disc around a supercritically rotating star. This suggestion was based on investigations of the photospheric absorption lines, typically displaying line widths expressed in velocity units of several $100\,\mathrm{km\,s}^{-1}$. This suggestion was discussed, but rotational statistics rather pointed to an average rotation of 80 % critical rather than more than 100 %. Slettebak (1982) published a large set of linewidths along with spectral types for Be stars — an influential study as it was a relatively large and, importantly, homogeneous set of observations.

These line-width velocity measurements are taken to represent the rotational velocity of the star v multiplied by the sine of the inclination of the pole to the line of sight, or $v\sin i$. However, one must be careful in this identification though, as there is not necessarily a linear mapping between the line width and $v\sin i$. It is commonly assumed that the observed photospheric line-broadening measured in velocity units via linewidth measurements, Fourier analysis of lines, or spectral synthesis is the real $v\sin i$ of the star. However, Collins &

Truax (1995) illustrate the effects of high rotation on observational derivation of $v \sin i$: they find that stars with rotation values above $\sim 80\%$ of critical speeds are likely to produce underestimates of the true rotation speed of the star (also see Stoeckley 1968). Partly this is due to the gravitational darkening caused by rotation. With the equatorial belts less prominent due to this darkening, the largest component in the photospheric line broadening arises from an intermediate latitude, thereby producing a line width *narrower* than that from a uniformly bright stellar disc. Hence for high rotation, this yields an underestimate of a star's $v \sin i$.

An answer to the question of the fundamental distribution of the rotational speeds is of great importance to the field of Be stars as it places constraints on models of disc formation. However, the distribution of rotational velocities, is convolved with inclination to the line of sight. This is a well understood historical problem (e.g. Chandrasekhar & Münch 1950), and several numerical attempts to deconvolve the Be star $v \sin i$ distribution have been made (e.g. Lucy 1974; Balona 1975; Chen & Huang 1987). Porter (1996) adopted a slightly different approach of first dividing all $v \sin i$ values by the critical rotation rate of the star derived from spectral types. Then by assuming that the Be-shell stars are edge-on Be stars, Porter used their distribution as the intrinsic distribution of all Be stars. The results of all these studies was that Be stars do *not* rotate at their critical rotation rates. Instead, the distribution peaks at values of the above mentioned 70–80% of the critical rate with a rather small intrinsic width of the distribution. This is an interesting finding: clearly the mean rotation is high in Be star samples, pointing to rotation as an important contribution in the differentiation between normal B and Be stars. The caveat here is that observation of some stars yield rotation rates much lower than this mean value, even accounting for the inclination, making the issue less well determined. On the other hand, the studies above assume that the velocity from the photospheric line-widths is an accurate estimator of the $v \sin i$ of the star, which, as described above, may be doubtful for the fastest rotating stars. Nevertheless, as a sample, the current studies indicate that the mean rotation rate of Be stars is 70–80% of the critical value.

Examples of slower rotators are sometimes claimed and will be discussed in the following part, while other stars may actually be rotating at critical rates, what will be discussed in the third part. An example is the B3Ve star α Eri, which has been subject to the very first measurement of an axial ratio of a rapid rotator. The interferometrically determined axial ratio is 1.56 ± 0.05 as a lower limit (Domiciano de Souza et al. 2003), which is just consistent with the maximum value of 1.5 applicable to a rigid body rotating at its critical limit.

Part I

The circumstellar environment of Be stars

Chapter 2

Geometry and kinematics

2.1 Circumstellar shell lines as disc probes

Phenomenologically, shell stars are stars with strongly rotationally broadened photospheric lines and additional narrow absorption lines. Some of the latter appear roughly at the centre of the photospheric instantiation of the same atomic transition while especially those of low excitation do not have a photospheric counterpart. B-type shell stars, which typically also have Balmer emission, are commonly understood as ordinary Be stars seen edge-on, so that the line of sight towards the star probes the circumstellar, equatorial disc. On the one hand, the often strong contamination of most spectral lines by features formed in the disc poses severe problems for the analysis of the central star. On the other hand, this constellation provides special opportunities as it puts strong constraints on the disc properties by modelling the shell line formation. In the following, the generalized results are presented, while individual stars are discussed in Appendix B.

However, one of the idiosyncrasies of the research on Be stars still requires a historical detour which is the subject of the next subsection, before the properties of the disc can be investigated with the help of shell lines.

2.1.1 Exceptions from the standard model for Be stars?

As early as 1931, Struve introduced the standard model according to which Be stars rotate extremely rapidly and possess a rotating equatorial disc; and spectra of Be stars take on the appearance of shell stars, with narrow absorption lines imprinted on broad emission lines, if the line of sight passes through the disc, i.e., the star is seen equator on. Ever since this model has passed many observational tests (see previous chapter, and references therein).

However, deviations from this general scheme are sometimes claimed:

(i) There would be Be stars with narrow shell absorptions, but their stellar $v \sin i$ is low. That is, some Be stars are intrinsically slow rotators. The alternative interpretation, namely a non-disc like structure of the matter leading to the shell absorptions, among other arguments, contradicts all the recent interferometric results, see again the previous chapter for a summary.

(ii) There are Be stars that exhibit line-emission phases with and without shell absorptions, i.e. they undergo Be $\Leftrightarrow$ Be+shell transitions. This were not possible for an equatorial disc with constant orientation.

In the following, the published observational evidence for the first claim is re-discussed with the help of the collected database, while the second is confronted with recent theoretical works on disc dynamics and shell line formation.

2.1.1.1 Shell stars with low $v \sin i$?

Because Struve's model is widely accepted, this may, in fact, introduce a bias against the detection of true low $v \sin i$ shell stars. In this vain, Moujtahid et al. (1998) nominated six stars with low $v \sin i$ as candidates exhibiting 'spectrophotometric shell behaviour'. A caveat with this method is that a spectrophotometric classification as shell star is problematic, because for a shell star in the common sense the presence of absorption lines is required, whose narrowness is irreconcilable with the width of the photospheric lines. An even stronger source of concern is that the authors actually use narrow-band photometry only, not even spectrophotometric data.

For three of these six stars, observations are available from the database of this study (see App. B.1 for the description of their spectra and the justification for the following findings): 27 CMa really is a shell star, but

its $v \sin i$ was underestimated. ω CMa is an almost proto-typical pole-on and non-shell star. In spectra of this star, the circumstellar contribution to the Balmer discontinuity (BD), which was observed with HEROS, is very obviously in emission, while it should be in absorption for a shell star. HR 4074, finally, has not shown any sign of circumstellar material for more than a century (Štefl et al. 2002) so that it cannot possibly have been a shell star. Since any attempt to identify shell stars by the photometric amplitude of the BD rests on assumptions for the stellar BD, the determination of the latter was probably problematic in the cases of HR 4074 and ω CMa.

The remaining three stars mentioned by Moujtahid et al. (1998) were not observed in the HEROS project. But it is noted that two of them (HR 3135 and HR 7249) are one-sigma cases only, w.r.t. the strength of the stellar BD assumed by Moujtahid et al. (1998), and available data (e.g. in Hanuschik et al. 1996) do not point to any shell type spectra. Finally, θ Cir might be a border case between emission and shell type behaviour, but according to Hanuschik et al. (1996) the $v \sin i$ of $100 \, \mathrm{km \, s^{-1}}$, adopted by Moujtahid et al. (1998), "seems dramatically underestimated". In summary, the evidence for shell stars with low $v \sin i$ could not be confirmed.

2.1.1.2 High $v \sin i$ Be stars with only temporary shell absorption

Stars with Be $\Leftrightarrow$ Be+shell transitions are relatively rare but undoubtedly exist (see App. B.2). The mechanisms underlying these changes are not understood. But they show some characteristics that permit such objects to be clearly distinguished from conventional shell stars. Hummel (1998) summarizes those properties: In a pure emission phase, the full width of the lines is typically much narrower than in shell phases. Such a large variability in width is not seen in other Be stars. The emission heights are largest when the lines are narrow and single-peaked. Similarly, the brightness varies with the emission line width. This led Hummel to suggest a temporarily tilted or warped disc for these stars, precessing about the stellar equator. This hypothesis has not yet been tested, but it nicely explains the observations without postulating a model differing from the widely accepted disc model.

Even if the plane of the disc is invariant, shell lines may be transient. One possibility would arise the disc changing its geometrical thickness. Another one might be that the inner boundary of the disc and the stellar surface are normally rather widely separated, e.g., because the space is swept clear by a companion. It is, then, possible that the line of sight to the photosphere does not intersect the disc and no shell lines form, but the star is fully seen through the gap. Only if and when the gap between star and disc is filled with gas, which also needs to have suitable kinetic properties, shell lines can form. In conclusion, a Be star viewed nearly equator-on may possess an equatorial disc that does not intersect the line of sight, i.e. does not always manifest itself by narrow shell absorptions.

2.2 Central quasi-emission peaks

In the past two decades snap shot observations of B and Be stars have revealed that a few of them exhibit a special type of line profiles, in which the central part of the line core exhibits a weak local flux maximum. These so-called central quasi emission peaks (CQEs) were as a distinct phenomenon first noted by Baade (1990, see also Fig. 2.1). All stars in which CQEs have been found are known Be stars with one exception. This star, namely ν Pup, did not so far have a record of observed emission or shell lines. Because of this and since the features were first identified in lines of HeI in early-B sub-types and of MgII in late B stars, CQEs were considered to be primarily of photospheric nature. Consequently suggested mechanisms for CQE formation assumed a photospheric origin unrelated to the Be nature (Baade 1990; Jeffery 1991; Zorec 1994). It was however, common to all the early models that they did not seek an explanation of CQEs in terms of line emission but rather hypothesized a local deficit in absorption (see also Baade 1990).

2.2.1 Observational properties of CQEs

A first hint, that the search for an explanation of CQEs should probably be extended beyond the photosphere, was given by observations of 4 Her: In this star, CQE-like features were observed only in shell lines (Koubský et al. 1993). However, whether the two phenomena can be identified with one another, remained open.

Since the detection of CQEs requires relatively large spectral resolution, most of the available small datasets only cover few spectral lines. Accordingly, they probe a limited range of stellar atmospheric conditions and do not permit a full assessment of the possible origin(s) of CQEs.

During the collection of the HEROS database also the known stars with CQEs were observed regularly. Several stars only found in our study to exhibit CQEs were monitored for their evolution as well. Due to
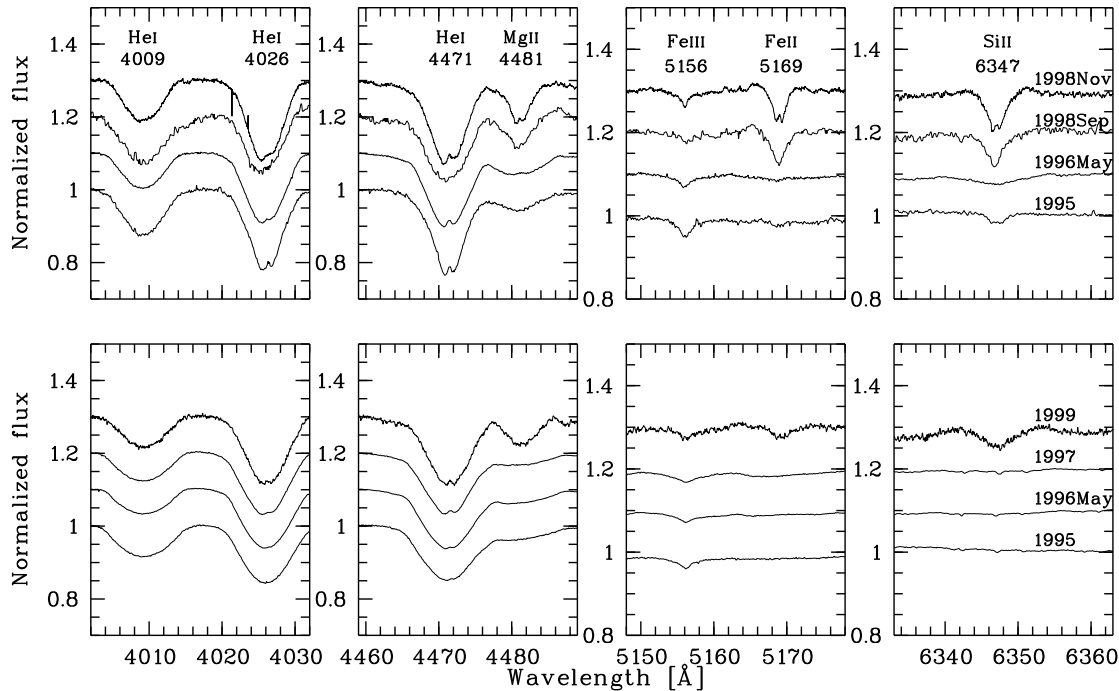
Figure 2.1: Various spectral regions of ε Cap (upper panels) and η Cen (lower panels) in several observing seasons as indicated on the right side. Note the presence of CQEs, which appear as small central reversals especially in HeI 4026, 4471 and partially also in the lines of MgII, FeII and SiII.

the nature of these cross-dispersed echelle spectra, the entire spectrum in the visual range could be obtained simultaneously with no more observational effort, in particular telescope time, than observing with a narrower spectra range would have costed. This enabled to study CQEs on a much broader basis than possible before. In the following, the prototypical cases ε Cap and η Cen are introduced in detail, together with the demonstration that also ν Pup is in fact a Be shell star. This leads to the identification of the process responsible for the formation of CQEs For more detailed notes on other objects showing CQEs see Appendix B, in particular Table B.1 for a list of such stars.

2.2.1.1 ε Capricorni

ε Cap (HD 205 637, HR 8260) is a well-known shell star with a considerable record of long-term variations, cf., e.g., Porri & Stalio (1988). These authors were also the first to report central quasi-emission features in HeI 4471, 5876, 6678, and MgII 4481 in observations obtained in Aug./Sept., 1986. Hα then exhibited emission at a peak height of 1.3 in units of the local continuum, while the absorption core reached a normalized flux of only 0.45.

HEROS spectra from 1995 show similar structures in these lines, except that the CQE was hardly visible in MgII 4481. The features are seen in most, but not all HeI lines. CQEs were not at all detected in HeI 3927, 4009, 4121, 4144, 5047, and hardly in HeI 4388. But in HeI 3820, 4026, 4471, 4713, 4921, 5015, 5876, 6678 and 7065 they were well visible. (cf. Figs. 2.1 and 2.2 for examples). While the lines without CQE exhibit purely rotationally broadened profiles, those with CQE display some unmistakable circumstellar contribution, especially in the line wings. Pure shell lines were found in FeIII 5127, 5156, SiII 6347, 6371 OIλ 8446, and weakly also in FeII. Shell absorption is as well seen in CaII and NaI lines, in addition to the sharp interstellar absorption cores. No photospheric wings were apparent in Paschen lines. The SiII 6347, 6371 absorptions showed a remarkable profile that is described best as a broad, shallow trough with flat bottom (Fig. 2.1, upper right panel). No CQE could be detected in typical *bona fide* photospheric lines such as SiIII 4553, CII 4267, or SII 5454.
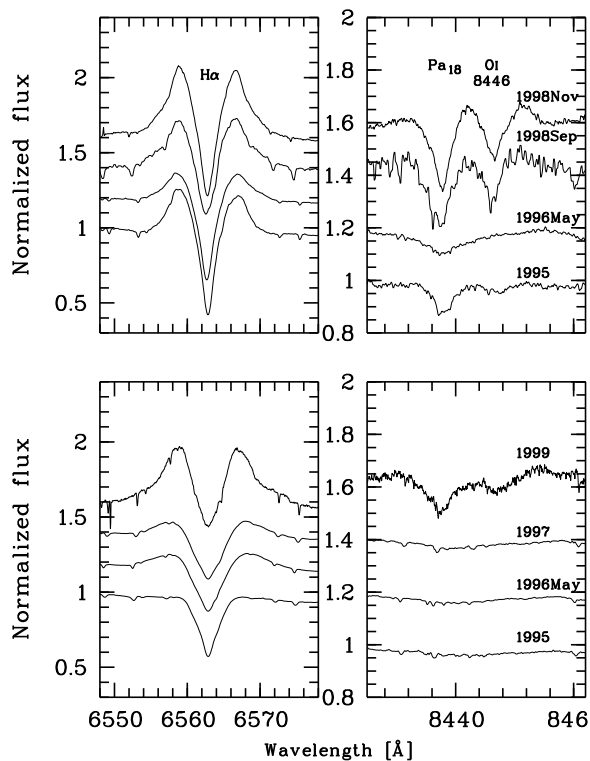
Figure 2.2: Same as Fig. 2.1 except for different spectral regions

In 1996, the strength of the Hα emission and the shell signature, but also the CQEs were weaker. The remnants of these features, seen best in HeI 4471, are now shallow and broadened. However, the MgII 4481 line seems to have developed the CQE only now, although it is very weak and extremely broad compared to HeI. In FeIII 5127, 5156, and to some small extent also in SiII 6347, broad line emission has developed. Photospheric wings now do appear in the Paschen lines.

By 1998 September, the spectrum had changed rather drastically. While FeIII absorption was nearly absent, shell lines of FeII had become strong. Other probable shell lines (cf. above) also returned, but the CQE had vanished completely, so that all HeI lines showed purely rotationally broadened profiles. The shell absorption of Hα was weaker, while the photospheric absorption wings were filled up by line emission. Only two months later, on November 20, the absorption core of Hα was again deep. As the shell absorption lines strengthened, the CQEs not only returned in the HeI and MgII 4481 lines, but for the first time in ε Cap they were also seen in purely circumstellar lines such as SiII and FeII lines. Quantitative data for the CQEs measured are given in Table 2.1.

HEROS and FEROS data, together with unpublished spectra with a resolving power of 70 000 or higher obtained with the CAT/CES on La Silla in July, 1985 and November, 1994 illustrate the long-term evolution of the CQE in HeI 6678 over many years. They are shown in Fig. 2.3. In this line the CQEs can exceed 4 % of the continuum flux and their strength is variable on a time scale of months to years. Both the visual inspection of the profiles and our quantitative measurements show a clear correlation between their strength and the depth or FWHM of the parent absorption profile. The CQE is stronger when the absorption line is deeper and narrower, i.e. when the envelope's contribution to the absorption is larger. A similar trend can be seen also in MgII and HeI in both ε Cap and η Cen. Three CAT/CES profiles from 1983 June of HeI 4471 also exhibit CQEs (in MgII 4481 even the main absorption is barely recognizable). The decrease in the FeIII/FeII ratio suggests a change in temperature (Fig. 2.1). If the concommittant increase of the Hα line emission (Fig. 2.2) is due to a replenishment of the disc, the disc would be cooler when denser. This could be plausible but can be concluded with some justification only if a more detailed modelling has ascertained that the lines due to the two ionization stages do not originate from different locations at different times.

ε Cap was suggested to be a binary with an estimated period of about 0.3 years (Abt & Cardona 1984) based on lunar occultation observations. The separation they gave was 4.7 mas. Combining all spectroscopic data available, the binarity was confirmed and a radial velocity curve could be derived. The orbital parameters abased on this curve are listed in the Appendix B. For the understanding of CQEs, however, it is only important
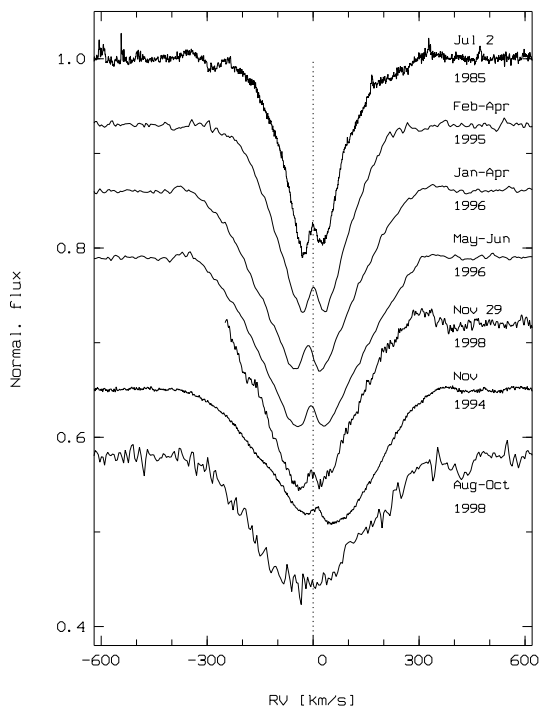
Figure 2.3: Appearance of the CQE and the parent profile of He I 6678 in ε Cap in different seasons. Profiles are arranged by decreasing depth and increasing FWHM of the absorption (from top to bottom). The radial velocity changes are due to orbital motions. The star was confirmed as binary during this study.

to keep in mind that the peak-to-peak amplitude in radial velocity is about $20\,\mathrm{km\,s^{-1}}$ (see Fig. 2.3), and this motion is reflected in the CQEs, moving the same way as the profiles they occur in. Because of this underlying variability, all measured quantities provided in Table 2.1 refer only to a single high-quality FEROS spectrum obtained on Nov. 20, 1998.

2.2.1.2 η Centauri

The first CQE in η Cen (HD 127 972, HR 5440) was reported by Baade (1983). However, they were detected in a Balmer rather than in a metallic line. Furthermore, rapid variations seemed to be present. But sorting the published data with the photometric period of 0.6424 day (e.g. Štefl et al. 1995, or Section 6.3.4) does not contradict the hypothesis of an intrinsically stable feature merely reflecting the underlying photospheric variability. In the present data, η Cen is almost a twin of ε Cap (cf. Figs. 2.1 and 2.2). Before 1999, the CQEs were best visible in He I lines, in which also some shell contribution can be recognized in the line wings. The strongest shell line is Fe III 5156, in which also weak genuine emission is detected. Measurements of the temporal development of the CQE in He I 4471 are compiled in Table 2.2. In January, 1999 the Hα emission had become stronger. Similarly to ε Cap, lowly ionized shell lines of Fe II and Si II had developed (see also Table 2.1).

2.2.1.3 ν Puppis

ν Pup (HD 47 670, HR 2451) was among the stars investigated by Baade (1989a). It exhibited a CQE quite clearly in Mg II 4481. No indication of circumstellar matter was found in previous studies. The HEROS and FEROS observations obtained from 1995 on do not show any trace of CQEs. In comparison to the earlier spectra of Baade, it is, however, not excluded that the Mg II 4481 line was deeper during his observations due to additional shell absorption, similar to, e.g., the one in ε Cap and η Cen (cf. Fig. 2.1) or to He I 6678 in ε Cap (Fig. 2.3). While this could be the result of imperfect normalization, which is notoriously difficult in echelle spectra, there is strong evidence that ν Pup is a not previously recognized bright Be shell star.

The variations of the Hα profile observed from 1995 to 1999 clearly show changes in the line profiles of Hα and Hβ of the same type as are known to occur in shell stars undergoing disc loss (Fig. 2.4), such as θ CrB. While it can hardly be speculated of the Balmer emission when the CQEs were observed it is at least clear that ν Pup is *not* an exception from the Be shell star rule for the occurrence of CQEs and thus cannot be taken as proof for a non-circumstellar origin of them.
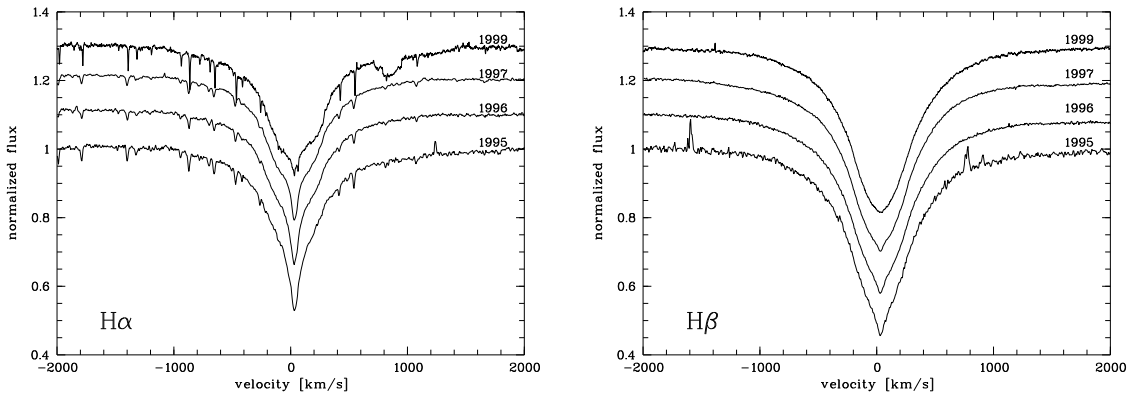
Figure 2.4: $H\alpha$ (upper panel) and $H\beta$ (lower panel) profiles of ν Pup in 1995, 1996, 1997, and 1999 (from bottom to top). In addition to numerous narrow telluric absorption lines, the FEROS $H\alpha$ profile at the top is affected by bad CCD columns. The temporal evolution clearly shows the presence of varying amounts of circumstellar matter

Table 2.1: Parameters of CQEs in different stars and lines observed with HEROS and FEROS. Strength denotes the CQE peak height above the lowest point of the parent absorption profile in units of the local continuum. The peak heights are accurate to about 0.2 percentage points, the FWHM's to about $5\,\mathrm{km\,s^{-1}}$. The error estimate of the radial velocities (RV) is about 10 % of the respective FWHM. In ω Car, the *sharp absorption core* of FeII 5169 was measured that replaces the CQEs in FeII profiles. The RV of the broad absorption was derived by measuring the wings at about half-depth of the profile

Line	Strength [%]	FWHM [$\mathrm{km\,s^{-1}}$]	$v_{\mathrm{rad,CQE}}$ [$\mathrm{km\,s^{-1}}$]	$v_{\mathrm{rad,ABS}}$ [$\mathrm{km\,s^{-1}}$]
ε Cap, 1998 Nov., FEROS				
HeI 4471	2.1	28.2	−0.2	−27.9
FeII 5169	1.6	20.3	−2.4	−1.6
SiII 6347	1.5	28.3	−0.9	−6.2
MgII 4481	0.8	30.1	5.9	−8.2
o And, 1998, HEROS				
SiII 6347	2.5	38	−25	−17.9
SiII 6371	2.3	37	−24	−18.7
FeII 5169	1.3	30	−21	−17.1
FeII 4233	1.2	28	−21	−18.9
MgII 4481	0.9	30	−21	−13.9
FeII 5317	0.8	31	−23	−12.3
ω Car, 1999, FEROS				
MgII 4481	1.0	36.8	4.7	+12.4
TiII 4395	0.7	26.7	−0.1	−11.7
FeII 5169	−8.4	9.5	1.4	−

2.2.2 Empirical conditions for the occurrence of CQEs

2.2.2.1 Properties of the circumstellar disc

From the observations described in the above text, in Table 2.1, and in Appendix B, several conditions can be derived for the occurrence of CQEs:

1. The star is an active Be shell star, i.e. it possesses a circumstellar disc seen edge-on.

2. The continuum opacity of the disc is low, while the shell lines are opaque.

Table 2.2: The temporal evolution of the CQE of HeI 4471 in η Cen

Season	Intens. CQE [%]	FWHM CQE [km s^{-1}]	v_{rad} CQE [km s^{-1}]	v_{rad} ABS [km s^{-1}]	Hα peak height
1995	0.4	34	20	-16.6	0.96
1996 Jan. – Apr.	0.5	40	15	-14.9	1.07
1996 May/June	0.4	27	10	-13.2	1.06
1997	0.8	40	10	-15.6	1.08
1999 (FEROS)	1.7	39	5	-3.1	1.35

3. The disc is not strongly developed, since then Balmer emission is typically not too strong. The outer Radius of the disc is probably small.

4. The intrinsic width and turbulent broadening of the shell lines are low.

The observational evidence is, point by point, summarized in the following:

Shell nature and orientation: The observations show clearly that CQEs occur only when shell features are also present. Often they appear in typical shell lines, but also in photospheric lines with circumstellar contributions, such as emission components in the wings of HeI lines, for instance. In lines without such contributions, CQEs were not found. This is also supported by the dynamical behaviour of CQEs, for instance in September 1998 the CQEs in HeI lines of ε Cap disappeared simultaneously with the circumstellar emission components. All stars showing CQEs are shell stars which are characterized by narrow absorption lines, mostly of singly ionized metals superimposed on the spectrum of a broad-lined B star, indicating a rapidly rotating star with a circumstellar equatorial disc viewed edge-on.

Dimensions of the disc: At the time of visibility of CQEs in the objects investigated, see e.g. the ones discussed above or o And in the Appendix, the Hα emission was relatively weak and the peak separation of the emission comparatively large. This indicates a small spatial extent of the discs from where it originates, since the total emission scales with the visible disc surface, and the peak separation scales inversely with the radius of the bulk of the disc matter (See later in this section). Independent studies confirm this: For 4 Her it is known that CQEs are present only when the disc is in the beginning of its formation process, but they disappear later (Koubský et al. 1993, 1997), and For η Cen, Coté et al. (1996) conclude from the analysis of IRAS far-IR data, which were obtained when the Hα emission probably was weak, that this star's envelope was at that time, too, small.

The strength of the Balmer emission of ω Car suggests that its disc is probably the most extended one of the observed sample of stars. However, either its intrinsic density or the column density along the line of sight (or both) do not seem to be high, judging from the depths of the shell lines. Moreover, CQEs appear with a range of prominence in different shell lines, as is demonstrated in Fig. B.11 for ω Car. In this object the FeII lines, which are supposed to be formed over the greatest range of parameters among the metal shell lines, only show narrow, pure absorption cores. Among the FeII lines, these cores are strongest in the transitions belonging to multiplet 42, which is the one most commonly observed shell line in Be stars. By contrast, the lines of MgII, TiII, and CrII, which are probably formed in a more limited region, i.e. closer to the star, *do* exhibit CQEs.

Thermal width: The above description of the observations shows unambiguously that CQEs are seen more easily in lines with higher atomic weight, i.e. lower thermal width. This is demonstrated best for ω Car and o And in Table 2.1. The FWHM of the CQEs, and with this quantity also the potential visibility, of CQEs changes from HeI to FeII. That is, the FWHM of CQEs in HeI or SiII is larger by about $10\,\text{km s}^{-1}$ than in FeII. Therefore, in HeI or SiII lines a CQE may appear in the form of a flat bottom of a profile rather than a local flux maximum separated clearly from the absorption wings. Although less clear, such a trend in FWHM can be confirmed for ε Cap in a smaller number of lines. To some extent, such a behaviour can also be seen in Fig. 5 of Koubský et al. (1997), comparing MgII to the neighbouring TiII and FeII lines. In those cases CQEs were reported in HI lines, ε Cap, and o And, it was always only at the very beginning of a shell phase in these lines, when the density and radius of the disc had not yet had much time to grow.

Line strength: Similarly, CQEs occur preferentially in the relatively strongest shell lines, i.e. when the line opacity is high.

The above set of properties probably overconstraints the formation of CQEs, as they are not independent of each other. However, this compilation provides solid empirical guidelines for an attempt to understand CQEs in the framework of shell line formation.

2.2.2.2 CQEs and disc phase transitions

Be stars are known for phase transitions from shell- or emission-type behaviour to plain B-, and then again back to the Be-appearance. Typical time scales for such cycles are of the order of decades. But there are also less spectacular changes in the appearance of the circumstellar spectrum, often on shorter time scales. It is likely that many of these variations are linked to the replenishment and subsequent dilution of the circumstellar disc.

From the rather scattered observations of CQEs it is difficult to establish a temporal profile of their life cycles. But the time scales of their variability are not incompatible with those of disc phase transitions. Moreover, the cases of ε Cap, η Cen, o And, and 4 Her suggest that CQEs are more likely to occur around the early phases of the build-up of a new disc or when the inner disc is re-filled with matter. They would weaken and eventually disappear, once the disc has reached more sizeable dimensions and greater density. Therefore, the initial speculation that CQEs are early tracers of the recurrence of a shell (Baade 1983) is still only a conjecture but now better justifies a more systematic follow-up.

2.2.3 Comparison with models for CQEs

The homogeneity of the parameters shown in Table 2.1 is rather indicative of a common origin. Because of the unquestionable circumstellar origin of at least some of the CQEs, the main focus will in Sect. 2.2.3.2 be on such an explanation. But since only stellar models have been considered in the past, the next subsection first briefly re-visits some purely photospheric models. The homogeneity of the CQEs, behaving similar in numerous lines of a wide range of ions, does not make an explanation in terms of specific non-LTE line formation very attractive, since non-LTE phenomena tend to act differently on different lines. Therefore, already these early models concentrated on more general explanations.

2.2.3.1 Photospheric origin of CQEs

These models are based either on the variation of local line strengths caused by the equator-to-pole variation of effective gravity and temperature in the presence of rapid rotation (Baade, Jeffery), which is a distinctive property of Be stars, or on differential rotation (Zorec). However, in his detailed model atmosphere calculations, Jeffery could reproduce CQEs only with the additional assumption of polar caps with lower temperature, for which no physical justification could be given. Also, the theory of gravity darkening contradicts this and instead predict hotter polar regions (see Part III). Jeffery's (1991) Table 2 provides specific criteria for observational tests of his model. CQEs should hardly be seen in HeI 4026 for any model, whereas they should be most prominent in SiIII 4553, NII 3995, and CII 4267 for early B-type stars. However Fig. 2.1, left panel, shows that HeI 4026 is particularly likely to exhibit CQEs. By contrast, in none of the other candidate lines identified by Jeffery, which are typically not formed in the disc, CQEs could be detected in any of the program stars.

Differential rotation would be less of an *ad hoc* ingredient but has not so far been required for the explanation of other observations of Be and shell stars. In the absence of rotationally induced gradients in effective gravity and temperature (von Zeipel's theorem), Zorec's (1994) model predicts the same profile for all lines with the same intrinsic line width. This is not observed. By combining differential rotation and latitudinally varying atmospheric properties, a much larger range of line profiles can be generated for an otherwise fixed set of parameters. However, as was pointed out by Baade (1990) and Jeffery (1991), this would still only work for stars with intermediate inclination angles. More specifically, Jeffery states that only $\sin i = 0.2$ to 0.8 is a possible range for the formation of CQEs, the best being 0.4 to 0.6 for most models. The fact that all known CQE stars are also shell stars effectively excludes both Zorec's and again Jeffery's model since there is ample evidence that the shells around Be stars are due to equatorially seen disc-like structures (cf. Chapter 1).

A final possibility to produce CQEs in the photosphere is a reduced polar chemical abundance of all elements showing CQEs (cf. Baade 1990). Over the broad wavelength range of the HEROS and FEROS spectra, there is no evidence of major chemical peculiarities. A still more severe problem is that, of a given ion, some lines may and others may not show a CQE. As well the restriction of the CQE-phenomenon to large values of $\sin i$ is problematic with such a global explanation. Finally, the restriction of CQEs to lines much narrower than those

from the photosphere at large cannot be construed as evidence of a circumpolar origin. Fig. 2.3 shows that the width of a given line may vary as a consequence of the *shell* contribution to this line. Moreover, such an interpretation would be at variance with all else that is known about the formation of narrow lines in Be shell stars (cf. Sect. 2.3)

In summary, the present observations of CQEs do not invalidate the principles of any of the photospheric models proposed so far. But these models simply cannot account for the observations, which evidently require a circumstellar explanation.

2.2.3.2 Circumstellar origin of CQEs

Hanuschik (1995) has computed the iso-radial velocity contours of a gaseous Keplerian disc viewed edge-on. He also derived the associated fraction of the stellar disc that is occulted by gas having a given line-of-sight velocity. The scattering and absorption of stellar photons in an opaque spectral line formed in the circumstellar gas is roughly proportional to the obscured fraction of the stellar disc. This area reaches a maximum at a radial velocity $|v|_{K,d,limb} = v_K R_d^{-1.5}$. This velocity is the projection of the orbital velocity (v_K) at the outer disc radius (R_d) on to the line of sight towards the stellar limb. Since geometry and velocity field are symmetric with respect to the orbital axis, at least as long as V/R variations are absent, two such maxima of the obscured area exist, namely one each at $+v_{K,d,limb}$ and $-v_{K,d,limb}$. Accordingly, a *local minimum in absorption* develops at zero velocity, which corresponds to a local maximum in flux, very much alike the CQEs. The principle is demonstrated in Hanuschik's Figs. 3 and 9; examples of the resulting line profiles are shown in his Fig. 8. Hanuschik's work is restricted to the case of a Keplerian disc with circular orbits, but in fact the mechanism may also work for more general discs with circular orbits, at least within certain limits. Discs with strict co-rotation, however, will not exhibit such local obscuration minima, as the obscured region for a given projected velocity will always be a straight strip parallel to the rotational axis, with the maximally obscured regions at $v = 0$.

A local minimum in *geometrical occultation* by gas with zero radial velocity always exists in a disc with Keplerian orbits seen edge-on. Whether it leads to an observable CQE depends mainly on two basic circumstances:

Outer disc radius: Because $v_{K,d,limb}$ decreases with increasing outer disc radius as $R_d^{-1.5}$, the two line profile minima are the more separated the smaller the disc is. However, if the size of the disc increases beyond some critical dimension, the separation of the two absorption maxima becomes smaller than the intrinsic line width. This means that the geometrical area of minimal occultation, widened by the turbulent and thermal motions, is larger that the size of the stellar disk seen through it. Therefore, even if it is a minimum in total area, it cannot be recognized anymore due to the lacking size of the light source behind it. In this case, the CQE disappears and a pure absorption core with a width corresponding to the intrinsic line width will appear instead. Since the ionization structure of the disc may change radially, "outer disc radius" actually denotes the outer radius at which a given line is formed. To some extent, this covers also the case of discs of finite thickness but not viewed exactly edge-on.

Turbulence and thermal broadening: Obviously, these two quantities have an interplay with the above said, and thus need to be small in order not to reduce the contrast between a CQE and its adjacent minima beyond detectability. Lines of heavier elements are, therefore, more likely to display CQEs.

Finally, the zero projected-velocity condition with respect to the stellar photosphere also implies that CQEs occur at the stellar systemic velocity. Accordingly, they would supply a very reliable means of measuring variations of the latter even in the presence of other variations. These theoretical conditions form an almost exact match of the empirical criteria for the occurrence of CQEs derived in Sect. 2.2.2. Because the inclination angle of all six stars considered will be somewhat different from 90 degrees and their vertical disc structure may not be the same as assumed by Hanuschik, the conclusion that the explanation for circumstellar CQEs is given by Hanuschik's model becomes even more robust. However, although Hanuschik's model is very successful in reproducing CQEs (and shell line profiles in general), it is not physical in that it only assumes Keplerian rotation but does not predict it. This point, therefore, requires further scrutiny, which is the subject of the following section.

2.3   Rotation of discs around Be stars

The question whether discs of Be stars are rotationally supported was considered an open issue by many not long ago, and partly still is. The major obstacle in explaining a Keplerian disc is the unknown mechanism required to supply the necessary angular momentum transfer to the disc, since even the most rapidly rotating Be stars do not seem to reach much more than $\sim$70% of the break-up velocity (e.g. Porter 1996). Two reasons may explain why this matter has for a long time perhaps not been given the emphasis that it deserves. One is the realisation that Struve's concept of a purely rotational instability was not supported by the actually observed distribution of equatorial velocities (c.f. Porter 1996). The other one is the discovery that Be stars do lose mass in a high-speed wind (cf. Prinja 1989) that is more prominent at higher stellar latitude.

However, often as a by-product of other work, clues were found for a rotational support of Be star disc during the past couple of years:

Polarisation and geometrical flatness: The very presence of a disc-like geometry, as opposed to spheroidal one, is with the least number of additional assumptions attributable to rotational flattening. This has for long been inferred from the intrinsic polarisation of Be stars (Poeckert et al. 1979). The constancy of the polarisation angle through all phases of disc transformation (e.g. Hayes & Guinan 1984) shows that the plane of the disc around single Be stars is constant in space and probably corresponds to the one of the equator. The final proof of an axisymmetric geometry has come from direct interferometric imaging (Quirrenbach et al. 1994).

Stellar $v \sin i$ and width of emission lines: The clear correlation between the stellar $v \sin i$ and the width of circumstellar emission lines and their peak-separation (Slettebak 1976; Hanuschik 1989) is also most easily reconciled with an equatorial rotating disc model.

Emission line profiles: Symmetric Hα emission lines of relatively low equivalent width often show a V-shaped central absorption. Hummel & Vrancken (2000) have modelled the absorption by the circumstellar shell, taking into account the velocity shear in the shell, obscuration of the shell by the star, and the finite size of the stellar disc. They conclude that the depth of the central absorption and consistency with interferometrically measured shell radii requires that the parameter j in the shell velocity law $v_{\rm rot}(r) = v_{{\rm rot},*} r^{-j}$ is on average less than 0.65 in their small sample of stars In this formula r is the distance from the centre of the star and $v_{{\rm rot},*}$ denotes the actual rotational velocity at the stellar surface. The value $j = 0.5$ with $v_{{\rm rot},*} = v_{\rm critical}$ corresponds to a Keplerian disc.

Outbursts: Rivinius et al. (1998c,b) have constructed a detailed temporal profile of the line emission outbursts of the Be star μ Cen, which are events of mass ejection and related to the beating of nonradial pulsation modes. It shows that matter is ejected at super-equatorial velocity which, after allowance for the relatively weakly constrained inclination angle and for plausible values of stellar mass and radius, comes at least close to the critical velocity. Kroll & Hanuschik (1997) studied somewhat less complete observations of outbursts of the same star. They find that inclusion of viscosity in the simulation of the orbital evolution of ballistically ejected matter, assuming some arbitrary mechanism, leads to the formation of a Keplerian disc from some fraction of the ejecta, while the rest falls back to the stellar surface.

V/R variability and disc oscillations: Numerous Be stars undergo cyclic variations of the ratio in strength of the violet and red components of their emission lines, V/R, with cycle lengths of the order of a few years (cf. the compilation by Okazaki 1997). Okazaki (1996, 1997) and Savonije & Heemskerk (1993) have modelled this general behaviour in terms of, respectively, retro- and pro-grade global one-armed oscillations of the disc. Actual line profile variations based on such dynamics were calculated by Hummel & Hanuschik (1997). The prograde-mode version was recently given strong observational support by interferometric observations of ζ Tau (Vakili et al. 1998) and γ Cas (Berio et al. 1999) at different V/R phases. This matter is of relevance for the disc's rotation as these models require closed elliptical, i.e. Keplerian orbits for the individual particles.

Tilted/warped discs: Hummel (1998) recently suggested that particular peculiarities in the long-term emission-line variability of γ Cas, Pleione and 59 Cyg at certain epochs may be caused by a temporary tilt or warping of a precessing disc. This explanation, too, would require the disc to be rotating.

Narrow shell lines The assumption of very small non-circular velocities in the disc is as well corroborated by the very small width of the shell lines of some stars. Hanuschik (2000) presented a Fe II 5169 profile
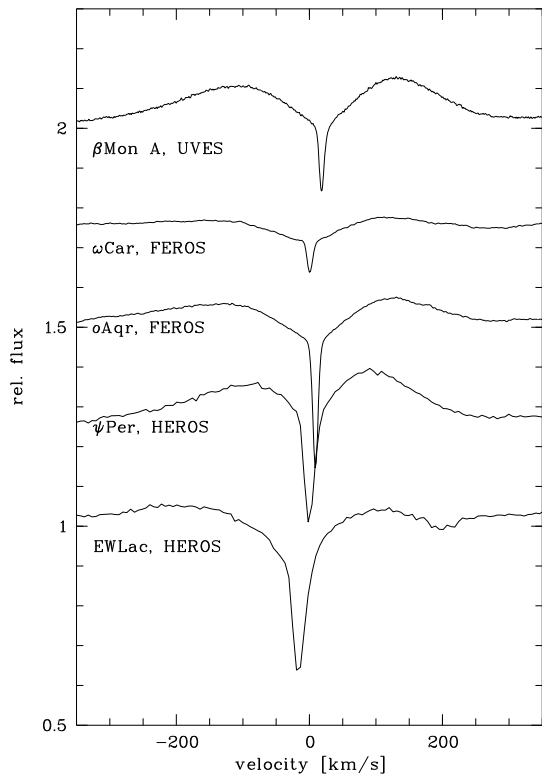
Figure 2.5: Narrow absorption cores in the FeII 5169 profile of five stars. See Table 2.3 for measured properties.

Table 2.3: Properties of the narrow cores observed in the FeII 5169 lines of four shell stars. The resolving power of UVES was $R = 80\,000$, see Appendix A for HEROS and FEROS. The stellar radial velocities $v_\star$ were taken from the General Catalogue of Radial Velocities (Wilson 1953, GCRV) and its revised edition (Evans 1967), respectively. All numbers are given in $\mathrm{km\,s^{-1}}$.

Star	instr.	resolut.	$\mathrm{FWHM_{shell}}$	v_{shell}	$v_\star$
EW Lac	HEROS	15	20	−15	−11
ψ Per	HEROS	15	17	0	−1
o Aqr	FEROS	6.3	9.1	9.0	12
ω Car	FEROS	6.3	9.6	0.7	7
β Mon A	UVES	3.8	8.4	18.6	20

of o Aqr, with a core width only a few times wider than the intrinsic thermal one, at about the stellar systemic velocity. Our spectra not only confirm this for o Aqr, but in addition show it as well for ω Car, ψ Per, β Mon A, and EW Lac (Fig. 2.5 and Table 2.3). Like CQEs, such narrow lines are present only in stars which either do not show V/R variability (o Aqr, ω Car) at all, or only weak asymmetries (ψ Per, EW Lac, β Mon A).

Given the observed spectrum of variabilities and the importance also of non-gravitational forces, it would be premature and probably even wrong to conclude from the above enumeration that the azimuthal velocity law in Be star discs is *strictly* Keplerian.

However, there can be no doubt that the discs not only are rotating, but do so in a Kepler-like way that the orbital time scale is much less than that of the non-Keplerian motion, so that Hanuschik's model is based on a reasonable approximation. Accordingly, this model does provide the correct qualitative explanation of CQEs: they are due to the line transfer in a rotating gaseous envelope and the finite size of the disc of the central star.

The inverse reasoning is also valid: Since Hanuschik's model explains CQEs, it re-reinforces independent conclusions that rotation plays an important role in supporting discs of Be stars against gravitational collapse. With respect to CQEs alone, this is, more strictly speaking, correct only for weakly developed discs. But, e.g.,

the explanation of long-term V/R variations by disc oscillations is not subject to such a limitation. Because the issue of rotation in discs of Be stars has prior to the work of Hanuschik, Hummel, and co-workers for quite some time not been very explicitly addressed, the velocity law may in some areas have been used almost as a free parameter. This may have possible repercussions. An important topic, that is worthwhile to re-visit in this connection, is the formation of discs around Be stars.

2.4   Summary

Central quasi-emission features seen in the absorption lines of some Be stars can be understood as being formed in the circumstellar disc. Purely photospheric models fail to reproduce the available observations. The coherent behaviour of the CQEs in different lines of various ions does not support a complex explanation invoking non-LTE processes. Instead, the application of Hanuschik's (1995) parametrical model for shell line formation in a Keplerian disc suggest that several circumstances strongly favour the exhibition of CQEs: The disc should be viewed edge-on, be optically relatively thin in the continuum, and have a small outer radius and little line broadening over and above the thermal width. Under these conditions, CQEs are qualitatively explained as a line transfer effect in a rotating gaseous disc when also the finite size of the stellar disc is properly taken into account. CQEs only look like emission lines but in reality are due to the circumstance that in a rotating disc there is less line absorption and scattering at zero velocity than at slightly higher or lower velocities.

CQEs, as an occultation pattern (Hanuschik 1995), form in the line of sight towards the star, at several stellar radii. CQEs, like the extremely narrow shell lines, can only occur if the radial component of the disc velocity is lower than a few $\mathrm{km\,s^{-1}}$, so that there is no strong out- or inflow, and the gas particle orbits are not too eccentric. These conditions are fulfilled by a Keplerian disc with about zero eccentricity. The only other hypothesis predicting zero radial motions, locked co-rotation, will *not* produce CQE-type absorption lines, but produce the same line-shape as rotational broadening does give the photospheric lines. In this sense, CQEs alone are already strong evidence for a Keplerian disc.

A Keplerian velocity structure is, however, also required by the current model on long-term V/R variablity. This type of variability is attributed to a density wave pattern in the circumstellar disc. In terms of celestial mechanics, this density wave consists of a common periastron of a set of eccentric Keplerian orbits, precessing about a non-spherical (rotationally flattened) star. Therefore, except when periastron or apastron are in front of the star, there will always be some non-zero radial velocity component projected against the star. Naturally, no CQEs should be formed under such dynamical conditions and in fact are not observed in V/R-variable stars. Of the 23 shell stars investigated (see Appendix B), only 4 showed neither CQEs nor long-term V/R variability. Seven were long-term V/R variable during our observations, and 12 exhibited CQEs. Not in a single star occurred long-term V/R variability and CQEs simultaneously. Taking into account also earlier observations one finds, however, that both V/R variability and CQEs may be present in the same star, but at different times. For instance ε Cap and κ^1 Aps used to be V/R variable according to the compilation by Okazaki (1997) but show CQEs now. The long-term V/R variations connected to the global density waves were found to exhibit phase lags between various lines for three out of 7 stars in our data, confirming the data summarized by Baade (1985). This supports a spiral structure of the density wave as suggested by McDavid et al. (2000), i.e. the azimuth angle of the density maximum varies with distance from the star, causing phase lags between the V/R curves of lines formed at different radii. Finally, the times when CQEs are present in a given star may be linked to phase transitions in the evolution of the circumstellar disc. CQEs seem to be more likely to occur during the early replenishment of the innermost regions of the disc.

2.4.1   Implications for disc formation

The transfer of matter to the disc with higher specific angular momentum than the one of matter co-rotating at the stellar equator remains unexplained by the current models of the Be-phenomenon. In the case of outbursts *à la* μ Cen (Rivinius et al. 1998c), it must form part of the still unknown outburst mechanism. Osaki (1998) has made a first qualitative suggestion based on the breaking of waves in the non-linear regime of nonradial pulsation. But μ Cen was found to be not representative of all Be stars, and even in μ Cen not all mass accumulated in the disc may be due to outbursts only. Therefore, other physical processes need to be considered that can build up discs around single stars.

One of the few models that have attempted this to date is the wind-compressed disc (WCD) model by Bjorkman & Cassinelli (1993). It is based on the presumably line-driven, high-velocity wind which for long has been detected in UV resonance lines of Be stars viewed at a smaller inclination angle than shell stars (e.g.

Prinja 1989). In the presence of rapid rotation, wind stream lines are deflected towards and concentrated about the equatorial plane. From there, part of the matter flows inwards back to the star but much of it leaves the star, so that a quasi-stationary disc-like concentration of circumstellar matter develops. However, as was pointed out before by Owocki (1997, private communication; see also Owocki et al. 1996 for a more complete assessment of the WCD model), this does not solve the angular momentum problem posed by Kepler-like rotating discs. The severity of the problem is only further emphasized by the explanation of CQEs by Hanuschik's model.

The sharpness, contrast, and degree of centreing within shell lines of the CQEs should also put limits on any outflow in the disc. In a numerical simulation of the WCD model, Owocki et al. (1994) obtain an outflow velocity profile in the plane of the disc, which becomes positive (i.e., outward directed) about 1 photospheric radius above the star and accelerates roughly linearly to $400\,\mathrm{km\,s^{-1}}$ at a distance of 5 stellar radii. By contrast, the IR excess observed in numerous Be stars by the IRAS satellite has been used to infer an expansion velocity at the level of $10\,\mathrm{km\,s^{-1}}$ or less (Lamers & Waters 1987). A break in the energy distribution towards the mm domain suggests a truncation of the disc or a re-acceleration of the disc matter only at very large radii (Waters et al. 1991b).

The ubiquity of V/R variations and inferred oscillations of Be star discs probably require that the observations cover at least one V/R cycle before the degree of centreing of CQEs within the shell profiles can be properly quantified. But the sharpness and contrast of the CQEs suggest already that any acceleration within the radial range of formation of the lines concerned should not be by more than $\sim 20\,\mathrm{km\,s^{-1}}$ when CQEs are present. Otherwise, the visibility of CQEs would be much reduced by the outflow velocity gradient in the line of sight similar to the effects of turbulence or other line broadening mechanisms.

With a typical pole-to-equator outflow velocity contrast of $\sim 1000\,\mathrm{km\,s^{-1}}$ vs. $\sim 100\,\mathrm{km\,s^{-1}}$ the bistability model of Lamers & Pauldrach (1991) might in this respect face a similar problem as the WCD model. This model is based on a rather sharp boundary in effective temperature near $19\,300\,\mathrm{K}$, above and below which winds are, in the Lyman continuum, optically thin and thick, respectively. In the presence of rapid rotation, the two domains could occur in one and the same star but in a region above and below, respectively, a critical stellar latitude. This model works well in explaining the enhanced density contrast of the equatorial over the polar wind in B[e] stars. However, as Lamers & Pauldrach emphasize, the model is not by itself able to produce a real disc, because the equatorial velocities of Be stars are too small. Therefore, there are no detailed numerical simulations that could be used to judge whether disc outflow velocities as low as required by CQEs and suggested by the far-IR excess are possible. If the extra mechanism necessary to (a) make the bistability model applicable to Be stars and (b) provide the angular momentum transfer were co-rotating magnetic fields or nonradial pulsation-driven outbursts, the angular momentum problem could possibly be solved at the same time. But a high disc outflow velocity would still require attention.

The current situation in explaining the formation of Be star discs is such that in all chains of observations attributed to and models developed for the formation of discs one or more links are missing to make them fully self-sufficient and -consistent. However, the one missing between the unknown mechanism that leads to outbursts as the result of some temporary increase of the nonradial pulsation amplitude and the *ad hoc* mechanism assumed by Kroll & Hanuschik (1997) presently appears to be one of the smallest ones.

Nevertheless it should be noted that, if only the rotational rate of the central star is high enough, these questions would be rather academic, since the higher the rotational rate is, the smaller these missing links become in all cases, and in a critically rotating star almost any mechanism will be able to do the job of mass ejection and angular momentum transfer to produce a *Keplerian* disc in a relatively uncontrived way.

Chapter 3

Life cycles of a Be star disc

3.1 Time dependence of the circumstellar environment

A Be star disc is usually assumed to have a relatively simple structure. Most models treat the disc parameters as varying monotonically with distance from the star in a simple analytical form. In particular, the radial density profile is typically approximated by a power law (e.g. Waters 1986; Millar & Marlborough 1999), usually justified with the equation of continuity.

Such a picture differs considerably from the ring-like models proposed in early papers explaining the origin and variability of line emission in Be stars. Struve (1931) suggests that the matter ejected at the equator due to critical rotation forms a nebulous ring, which revolves around the star and gives rise to emission lines. He mentioned Saturn's rings as a prototype of rings around Be stars. Struve demanded the envelope to be a ring as a consequence of his suggestion of supercritical rotation, rather than being based on observations. In Struve's picture, the gap would form naturally because of the angular momentum excess of the expelled material. He further pointed out that an elliptical ring might explain the Be stars with a variable violet-to-red peak intensity ratio (long term V/R variables).

Dynamical and physical properties of such rings were studied theoretically e.g. by Hazlehurst (1967), Limber & Marlborough (1968) or Huang (1972). However, the only observational motivation remained the hope to explain in this way the long term V/R variability, but this was finally shown not to require a detached disc (see Okazaki 2000, for a recent review).

Although also the variability of the line emission was recognized almost right at the beginning of Be star research, most current models nevertheless omit all time dependencies. It is usually assumed that the associated changes of the disc can be described by some suitable sequence of stationary models, in the best case by scaling the base parameters only. The only major exception is the inclusion of one-armed global oscillations responsible for the long term V/R variability (Okazaki 2000, 2001, and references therein). However, these variations have so far been treated only as perturbations of a not otherwise variable, conventional disc. The increasing number of observations of rapid, discrete star-to-disc mass transfer events may now demand some refinement of the approach to variability.

So far, these line emission outbursts seem to occur preferentially in Be stars of earlier spectral sub-types. If they are present also in the later sub-types, they must either be much weaker or much less frequent. One of the most detailed temporal profiles of such an event could be derived from observations of μ Cen. All outbursts observed in this star (Rivinius et al. 1998c) basically follow the same generalized scheme:

For an extended period of time of *relative quiescence*, the appearance of the emission lines does not change appreciably. The first signs of an upcoming outburst can be summarized as a *precursor phase*, when within a few days broad emission wings appear at the bottom of the HI line profiles, and the peak height of the emission lines drops slightly. Quasi-periodic variations in the ratio in strength of the blue and the red emission peak (V/R variability) set in. The separation of the peaks in optically thin emission lines increases. As soon as the *outburst proper* has begun, the peak height not only recovers its former strength but reaches a temporary maximum and the V/R variations terminate. After these phases of rapid changes, the spectral behaviour enters a *relaxation phase*, in which the extended wings disappear, and the peak height slowly decreases. FeII and other metal emission lines may become undetectable and/or their peak separation starts to shrink again. This phase lasts much longer than either of the previous two. The rate of change of all parameters declines with time, and gradually a new phase of relative quiescence is entered.
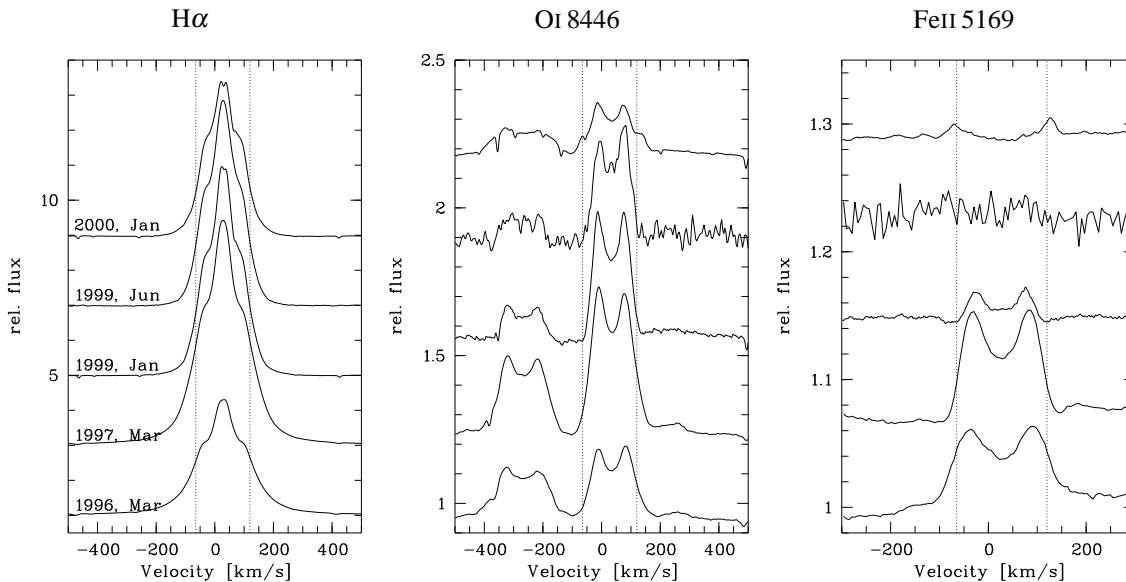
Figure 3.1: The spectroscopic evolution of ω CMa from an outburst in 1996 to the next observed outburst in 2000. Averaged data are shown for each observing run. The panel for OI 8446 also covers Paschen 14. The dotted lines indicate the narrowest observed width of the optically thin emission lines at [–65,+120] km s^{-1}. Note that the scale of the velocity axes for FeII differs from the one of the other panels.

In addition to this spectroscopic terminology, also photometric variability is observed during times of outbursts. For instance Hubert & Floquet (1998) have shown that Be stars can undergo rapid brightness increases with subsequent slower fading on the same timescales as the above described outbursts phenomena. Shell stars, being seen through the disc, in turn undergo brightness decreases with subsequent brightenings. This is explained in terms of the more massive disc after outburst contributing more scattered continuum flux if seen pole-on, but of course also scattering more out of the line of sight if seen edge-on, and the following dissipation of the respective disc.

Rivinius et al. (1998c) revived the idea of an at least temporary ring, suggesting that in some cases the disc might at times be detached from the star, instead of starting right at its photosphere, so that there would exist a relative minimum in the disc density close to the star in. The disc would, then, look more like a ring. This was derived from the varying width of disc emission lines of only a single star, μ Cen. Since then the corresponding database has been extended. In addition, emission line profiles with features indicating the simultaneous presence of two separate structures, namely an inner disc and an outer ring, are presented for two other objects. Meanwhile Roche et al. (2000) also proposed a temporary ring structure from long-term variations of the HeI emission lines of the X-ray binary X Per.

From observations of the variable peak separation of the Hα line of λ Eri, already Smith et al. (1991) drew similar conclusions as derived here. The same effect was also seen in μ Cen (Rivinius et al. 1998c). However, not only is the peak position more nearly indicative of the outer disc radius than of the inner boundary (Hanuschik et al. 1988), but dynamical results derived from Balmer emission were shown to be limited in their conclusiveness in any case due the scattering processes that affect the Hα emission (Hummel 1994) strongest. This is solved by a more thorough investigation in particular of the high velocity limits of circumstellar line emission, as opposed to the local peaks of the emission.

3.2 Observed Circumstellar line profile changes

In the following, it is attempted to assemble the available observations of disc variability and unusual disc-structures to a homogeneous picture. However, as the above section already indicates, the diversity of observed details is bewildering. This is also evident from the HEROS and FEROS observations described in Appendix C (see Fig. 3.1 for the example of ω CMa). Before any deeper investigation, it is helpful to start with a preliminary taxonomic effort to identify commonalities, although the database is probably not sufficiently complete, so that future observations may modify the summary developed in the following. Although the scope is presently

limited to the particular sample of Be stars described above and in the Appendix C, these stars are taken out of a database assembled for a different purpose, and therefore might be representative for a serendipity search.

The primary feature common to the objects in the sample is the variability of the base width of emission lines. This type of variability has been known for a long time in e.g. the Balmer lines. So, the main interest lies in the following refinements of this information:

- There is no restriction to optically thick lines. In a given Be star, all emission lines are affected, albeit with much gradation: Weak, optically thin lines may entirely vanish or (re-)appear whereas in optically thick lines the variation relative to a strong mean emission may easily not be recognized.

- Such variations can occur in perfectly symmetric profiles and independently of long-term V/R cycles.

- In particular in optically thick lines, the variability of the base width is very little connected to the one of the main peaks, which may even remain nearly constant. The waxing and waning of emission line wings is a genuine variability, in the sense that the outer limits do not change just because the profile as a whole is growing and fading. This type of change, that would be due to the wings being pushed above or below some detection threshold, is clearly distinct from what is in fact observed.

Since variability of the base width of emission lines is an integral part of outbursts, this list supplements the temporal profile of outbursts given in the introduction to this chapter.

Outbursts repeat on time scales between 1-2 months and a few years, depending on the object. The time scale for the decay of enhanced emission line wings depends on the magnitude of the outburst, but typically is of the order of a few months. Next to these changes, discs of Be stars also undergo still longer-term variations, which may take up to several decades. Such longer term changes mainly reflect in changes of the emission peak height and total emission equivalent width and are probably related to changes of the outer dimensions and the total mass content of the disc. Since they are not sufficiently sampled by the present observations, the remainder of the Chapter ignores such long-term trends, which also are less likely to be a problem for the model-approach of series of quasi-stationary models. Similarly, because all stars in this sample exhibit symmetric emission profiles, global disc oscillations, which observationally reveal themselves by cyclic long-term V/R variations, are also not considered.

In μ Cen (Rivinius et al. 1998c), and possibly also 28 Cyg (Tubbesing et al. 2000), outbursts repeat with high regularity and rather frequently. Cyclic *photometric* outbursts were detected by Hipparcos (Hubert & Floquet 1998) in a large sample of Be stars as well. For these reasons, this study adopts the concept of cyclically repeating mass loss events, in the further called outbursts, as a working hypothesis for the underlying process of the above described variability of all stars in the sample presented in Appendix C. On account of only the variability of the base width of emission lines, FV CMa would not qualify for inclusion in the present sample because it was only observed for a short time during which the respective quantities did not change. However, the similarity of these spectra to 28 CMa and especially X Per, in which variable emission line wings not only exist but temporarily took on the same shape of a second pair of discrete emission peaks with larger separation, makes it a strong candidate. DU Eri is a comparable case, but with the signature being less clear.

3.3 Disc structure

Be star discs have successfully been modelled as relatively thin, quasi-Keplerian discs. The Keplerian approximation gives a disc of rather narrow opening angle increasing with radius. The disc is typically assumed to be isothermal. The density law in the disc is commonly derived with the help of the equation of continuity: From the assumption of constant base density ρ_0 and a constant outflow speed one can immediately derive the power law index. Due to the outburst activity, however, ρ_0 is in fact variable, and hence the disc density structure becomes a free parameter. At least the remaining parameters, however, should remain unchanged in a first order approximation. Therefore, the ring as proposed in the following sections might be imagined as a Keplerian disc, in which the innermost part is missing.

3.3.1 Inner disc radius

Numerous authors have investigated which conclusions about the disc structure can be drawn from observed emission line profiles (e.g. Poeckert & Marlborough 1978; Dachs et al. 1986; Hummel & Dachs 1992; Hummel 1994; van Kerkwijk et al. 1995). The results show quite clearly that deriving robust results in terms of uniqueness of the obtained parameters is almost impossible by inspecting snap-shot emission line profiles, i.e. not taking into account the state of disc evolution.

On the other hand, the qualitative interpretation of variations of a *given disc* is much less dependent on the particulars of the correct model. For instance, $\sin i$ is the same for all observations of one star, and therefore the effect of the corresponding uncertainty in the interpretation is much reduced. If moreover lines from different ions and transitions were observed simultaneously, the need to accommodate them in a single, self-consistent description provides very strong constraints.

To first order, two circumstances are pertinent to the interpretation of the variable base width of emission lines in the present sample of Be stars:

– Virtually all currently proposed disc models include a rotational velocity profile decreasing monotonically with radius. As summarized in Chapter 2, there is even evidence that the rotational velocity law is Keplerian in good approximation. Since large-scale radial motions have observationally been constrained to be very much slower than the orbital velocities, emission from the inner regions of the disc, where the velocities are the largest, will appear in the outermost line wings. E.g. for a Keplerian disc with circular orbits, the maximum projected velocity at a given radius is

$$\Delta v_{\mathrm{edge}} = 2 v_{\mathrm{kepl}} \sin i \left(\frac{R_{\mathrm{peak}}}{R_\star}\right)^{-\frac{1}{2}}$$

– If a given disc can be assumed to be in quasi-equilibrium, i.e. radiatively, thermally, hydrodynamically, and at constant inclination angle, the only physical parameter that can change the emission formed at a given radius is the gas density.

Changes in the outer line width are observed well outside outbursts during most of the relaxation phase. As long as the interpretation limits itself to optically thin lines the combination of these two arguments implies that the variability of the emission base width is due to density variations in the inner disc. The remainder of the emission profiles often is much less affected (and/or on much longer time scales), and so this leads to the notion of the development of an inner cavity at times when the outermost parts of the wings disappear or strongly weaken. The remaining disc structure would be more reminiscent of a detached ring.

In most stars, also the separation of the emission peaks is variable. However, this quantity traces the radius of maximum emissivity of the disc for a given transition and should not be confused with the emission base width. Although changes at the inner edge of the disc, changing the base width, will typically influence the emission peak separation in the same sense (as seen e.g. in FW CMa or ω CMa), this correlation might be weak or even absent in some cases, since it also depends on the properties of the outer disc regions.

Optically thick lines need to be treated with more caution because the most extreme emission line wings must be suspected to contain a large scattering component (Poeckert & Marlborough 1978). Therefore, the observed maximal velocities in lines like Hα are not necessarily indicative of the rotation dominated ion kinematics, but rather of the temperature dominated electron kinematics. In a continuous disc, i.e. reaching down to the star, the electron density is high at small radii and the major part of the scattering wings is formed close to the star.

Still, optically thick lines can be conveniently used to illustrate a few more details, because the resulting emission line profiles depend at each line-of-sight velocity only on the surface area having this velocity. By contrast to optically thick ones, optically thin lines have to be volume-integrated, and their region of formation is typically close to the star. For Balmer lines, in turn, one can safely assume they form almost throughout the entire disc. Therefore, when an inner cavity develops in a purely Keplerian disc, optically thick emission lines

– suffer the smaller *relative* flux changes in their wings the larger the disc is, because the area having such projected velocities is smaller in comparison.

– retain the position of their peaks because the latter originate from the outermost regions of the disc, which have the largest surface area in a given velocity interval.

– have strong electron scattering wings during and shortly after the outburst, but these wings disappear during the emptying of the inner disc until they have completely vanished.

The observed variability of optically thick lines like Hα can indeed be described in such terms (see Fig. C.2, for instance), and so the above inference of a variable inner disc radius, derived from optically thin lines, is in agreement with the behaviour of optically thick lines.

The photometric observations of outburst behaviour (Hubert & Floquet 1998), i.e. brightenings and fadings, are well explainable in terms both of a variable cavity, and a solid disc of variable mass, since only the innermost part of the disc contributes significantly to the continuum flux in any case. Simultaneous spectra could discriminate between these two options, since the wings should be broad when the star is bright, but do not seem to exist but for a few cases, like ω CMa, where such a behaviour is indeed found (Štefl et al. 2003a).

3.3.2 Outer disc radius

While the last subsection concentrated on the observable effects arising from changes of the inner dimension of the disc, here it is demonstrated how the CQEs described in Chapter 2 can be used for the diagnosis of the outer boundary structure of Be star discs, and especially their variability. Hanuschik's (1995) equation [23] offers rather straightforward access to the radial disc structure, if the positions of the local minimum cusps blue- and redwards of the CQE are measured. This can be demonstrated well for the example of η Cen in 1996, when a similar outburst–relaxation sequence as in μ Cen was not only observed (Rivinius et al. 1998c) in full, but even the following outburst could be covered.

Hanuschik (1995) normalized the equation to $v \sin i$. Even assuming $\sin i = 1$, the rotation velocity of the disc at $R_d = 1\,R_\star$ is unknown. For a Keplerian disc this is the critical velocity, rather than the stellar rotational velocity as for a disc conserving angular momentum. As estimate $v_{crit} = 600\,\mathrm{km\,s^{-1}}$ is taken, being a plausible value for such an early B-type main sequence star. The cusp separation was measured for HeI 6678. These numbers were derived from data secured just after an outburst and six weeks later, just before the following outburst event. The separation of the minimum cusps Δv_{cusps} is related to the distance from the star R_{abs} up to which the lower levels of the respective transitions are populated. For HeI 6678, this is the $2^1P^0 - 3^1D$ singlet transition from 21.13 to 22.97 eV. HeI 6678 moreover shows weak emission peaks, that can be used to probe the radius R_{emi} up to which the upper level is populated sufficiently to produce net emission. Similarly, the Hα peak separation can be used to derive an estimate of the dimensions of the Hα-emitting disc. In the case of Keplerian rotation the respective equations are

$$R_{abs} = \frac{\Delta v_{cusps}}{2 v_{crit} \sin i}^{-2/3} \tag{3.1}$$

and

$$R_{emi} = \frac{\Delta v_{peaks}}{2 v_{crit} \sin i}^{-2} \tag{3.2}$$

The disc radius derived from the CQE as well as from the emission became larger during our observations 1996. It grew from 6.2 to 6.8 $R_\star$ for HeI 6678 absorption (CQEs) and from 7.3 to 8.7 $R_\star$ for the Hα emission. On the other hand, the emission radius derived from HeI 6678 emission started at 2.8 and grew to 4.8 $R_\star$. The higher outbound velocity at smaller radii is consistent with the conclusions drawn already from μ Cen (Rivinius et al. 1998c), that part of the ejected material after a burst migrates slowly outwards as a ring of enhanced density, visible as migrating emission peaks. There it merges with an already present, relatively stable disc at larger radii. It should be noted that these values are derived on the basis of simplifying assumptions, as $\sin i = 1$, and only estimated critical velocity, but the relative changes of the numbers should be reliable.

3.3.3 Discs as evolving structures

The above description leads to the notion that after an outburst the disc begins directly above the stellar surface, and a slowly outwards growing inner cavity develops. The longer the intervals between two outbursts strong enough to fill the cavity are, the more time the cavity has to grow. If the cavity is large enough, the ejecta of a later outburst will be clearly distinct from the already existing ring and in terms of emission line profiles. The combination of the changes in the emission profile morphology and width, observed best in μ Cen and ω CMa, supports this view well. The times between outbursts range from weeks in μ Cen to perhaps as much as years in ω CMa and FW CMa. Hubert & Floquet (1998) report characteristic times between outbursts of ω CMa of 200 and 330 days. The sampling of the present observations would not be sensitive to them, but the data suggest that *major* outbursts occurred only in 1996 and 2000. Something similar may be true of FW CMa, which was monitored in the same seasons as ω CMa.

In η Cen the evolution could be followed through a complete outburst sequence. The total base width of the HeI 6678 emission was observed to be 680 $\mathrm{km\,s^{-1}}$ before and 1100 $\mathrm{km\,s^{-1}}$ after the outburst, respectively. About two months later, the the total base width had decreased to 660 $\mathrm{km\,s^{-1}}$ again. Using $\sin i = 1$ and $v_{crit} = 600\,\mathrm{km\,s^{-1}}$ (see previous Section for a justification), the change of the inner disc radius during the outburst can be estimated. The inner radius of the HeI 6678 emitting region was 3.1 $R_\star$ shortly before the outburst. Directly thereafter this number was only 1.2 $R_\star$. Note that this value did not decrease smoothly, but changed rather suddenly in the wake of a discrete mass loss event. After two months, the inner edge radius had slowly grown again to 3.3 $R_\star$. Then, the star was not observed for two weeks, but afterwards it was clear that again an outburst must have occurred in the meantime, since all the velocity separations were high again.

29

Table 3.1: Evolution of inner disc radius, emission peak radii (representative of the bulk of the emitting material) and outer disc radius before, during, and after an outburst in η Cen in February 1996. For explanation of methods and symbols see Sect. 3.3.3. All dimensions are given in units of the equatorial stellar radius

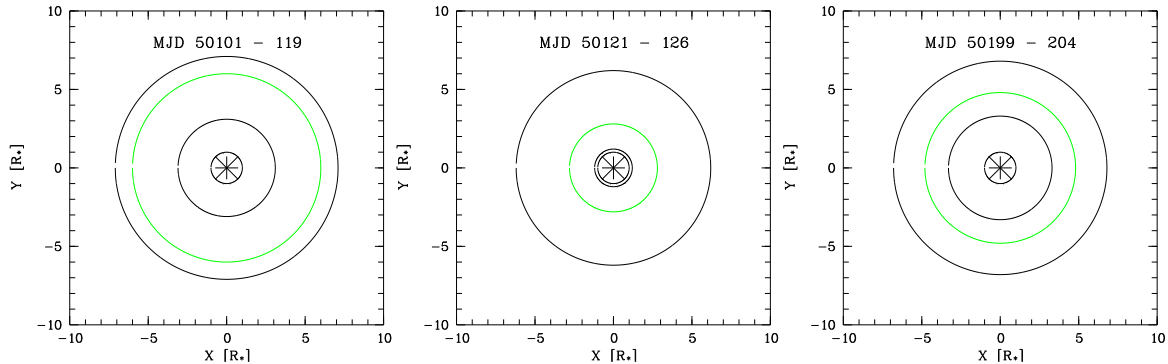| Modified Julian date	HeI6678			Hα
	inner edge v_{max}	bulk v_{peak}	outer edge CQE	bulk v_{peak}
50 101–119	3.1	6.0	7.1	9.0
50 121–126	1.2	2.8	6.2	7.3
50 199–204	3.3	4.8	6.8	8.7

Figure 3.2: Sketch of the disc structure of η Cen shortly before, after, and two months after an outburst, just before the subsequent one. The star is indicated by the crossed circle, the dark circles represent the inner and outer edges of the disc, the gray line the main bulk of emitting material. The plots base on HeI 6678 data, as described in Table 3.1 and Sect. 3.3.3

Together with the results from CQEs and emission peaks worked out in the previous section, these numbers can be assembled to a picture of the evolving disc around η Cen, summarized in Table 3.1 and sketched in Fig. 3.2. The results are based on several simplifications (e.g., $\sin i = 1$, estimated v_{crit}) so that their absolute values must be treated with care. However, the qualitative conclusion of a sudden decrease of the inner disc radius during an outburst, and the subsequent slower, smooth increase is robust. Combined with the accompanying much smaller increase of the outer disc dimensions this results in a picture, in which an inner low density region forms a while after an outburst, the next outburst fills it up again, and finally this new material possibly merges with the older ring farther out.

3.3.4 Multiple discs

It was said above that, when the inner cavity of the ring grows large, a new outburst will cause clear changes to the overall line profile. In some cases, this cavity may have grown so large, that the emission of the outer ring and the inner disk even after the outbursts would be spatially separated. This should be well observable in the line profile as some deviation from the usually smooth line profiles, e.g. some cusps unexpected in a normal profile. In fact, for ω CMa a second, morphologically distinct emission constituent was observed in 2000 while the previous one was still partly preserved (Fig. 3.1). The high velocities, if due to rotation, imply that it arises from matter close to the star. The dual structure of the OI 8446 emission profile without smooth transition between the broad base and the inner peaks as well as the evolution of the FeII emission (Fig. 3.1) support the notion that the newly ejected gas and the remainders of the old disc are not spatially connected. The outburst in 2000 possibly filled up a circumstellar low-density region in inner part of the old disc.

The Hα profile observed in 1992 by Hanuschik et al. (1996) qualifies DU Eri as a second candidate star, whose circumstellar envelope temporarily consisted of an inner disc and an outer, presumably older, ring. Unfortunately, there are no observations of other lines at the same epoch. However, in January 2000, a similar structure was observed (Fig. C.6), but not as clearly as in 1992, and no metallic emission lines could be detected for further comparison.
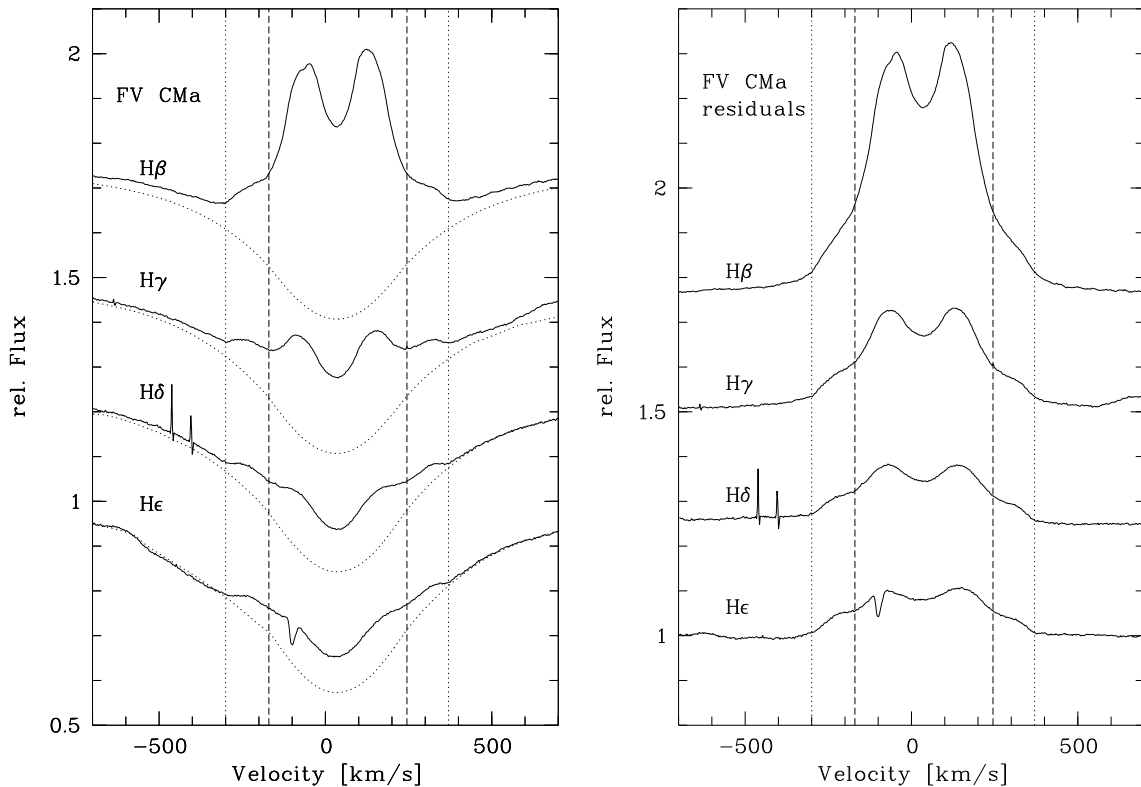
Figure 3.3: The spectroscopic evidence for two spatially separate disc constituents in the average of 13 spectra of FV CMa obtained in 2000 January. The residuals were computed by subtracting a synthetical spectrum with typical B2 IV parameters ($T_{\mathrm{eff}} = 21\,000\,\mathrm{K}$ and $\log g = 3.7$), broadened to $v_{\mathrm{rot}} \sin i = 200\,\mathrm{km\,s^{-1}}$. The observed spectra were corrected for the star's systemic velocity of $v_{\mathrm{sys}} = 35\,\mathrm{km\,s^{-1}}$. Starting from H$\gamma$ a second, wider pair of emission peaks appears to emerge towards the higher Balmer lines. The edge velocities of each constituent were estimated to $[-300,+370]\,\mathrm{km\,s^{-1}}$ for the wide and to $[-170,+245]\,\mathrm{km\,s^{-1}}$ for the narrow one and are indicated by vertical lines. The Balmer decrement is significantly shallower for the broad constituent. Residual CCD artifacts are seen on the blue side of Hδ, as well as the interstellar Ca II line in Hε.

A still stronger case in support of the dual constituents picture is represented by FV CMa. Unlike in ω CMa, a broad base in the O I 8446 emission can hardly be seen in this star because, owing to much stronger kinematical broadening, the line is blended with Pa$_{14}$. However, the similarity of O I 8446 in ω CMa to the Hβ emission of FV CMa is striking (Fig. 3.3, residuals, vs. Fig. 3.1, O I 8446, uppermost spectrum). In fact, the Balmer line profiles include two sets of edges, which bracket the velocity ranges $[-170,+245]\,\mathrm{km\,s^{-1}}$ and $[-300,+345]\,\mathrm{km\,s^{-1}}$, respectively. Starting with Hγ, the range between the two blue and the two red edges ($[-300\ldots-170$ and $+245\ldots+345]\,\mathrm{km\,s^{-1}}$) takes on the appearance of a secondary double-peaked emission constituent.

Because Balmer emission lines are easily distorted by scattering processes (Poeckert & Marlborough 1978), the translation of line widths into disc velocities and spatial dimensions is not straightforward. This affects Hα most strongly and becomes less important for the higher Balmer lines. However, in the case of FV CMa the sharpness of the edges, their equal position in all Balmer lines, and the even increasing prominence of the edges towards bluer Balmer lines (cf. Fig. 3.3) render a geometric interpretation of these values a plausible approach. This is supported by the higher Paschen lines, which are morphologically intermediate between Hγ and Hβ, as well as by the He I and metallic lines displaying emission components. The He I 5876, 6678, 7065 and Si II 6347 lines show clear emission up to $[-300,+370]\,\mathrm{km\,s^{-1}}$. This indicates that these are real gas velocities rather than scattering broadening, since scattering broadening does not produce a sharply defined edge of the emission, as seen in those lines. Lines like Fe II 5169 have the edges at $[-170,+245]\,\mathrm{km\,s^{-1}}$ in common with the Balmer lines. But their broad emission constituent does not extend over the full range of $[-300,+370]\,\mathrm{km\,s^{-1}}$.

Application of the relation between projected rotational velocity and inner disc radius (Sect. 3.3.1) and the assumption that the broad emission component belongs to a disc starting right above the stellar surface, which leads to $2v_{\mathrm{kepl}}\sin i \geq 670\,\mathrm{km\,s^{-1}}$, imply that the narrow component originates from a ring with an inner radius of at least $2.6R_\star$. This number will be higher still if also the inner disc is detached from the star. However, this is not too likely as it would require an even higher Keplerian velocity at the stellar surface. Furthermore, the difference in the Balmer decrement of both constituents in FV CMa is indicative of a higher density in the supposed inner disc than in the outer ring.

In order to explain their observations of X Per, Roche et al. (2000) have independently proposed a multiple-disc structure. Because of the other stars under consideration here and in App. C only o And is a known binary, it appears plausible that the variability at the inner edge of the disc of this system is unrelated to the presence of a companion. Neutron stars orbiting Be stars have for long been realized to be promising probes of the disc structure. The present observations suggest this even more strongly. Note also that a disc with two different constituents of different radii has been postulated before by Hanuschik et al. (1988) on account of the inflection points seen in Hα emission lines such as those of ω CMa and μ Cen, because of their appearance also dubbed "winebottle profiles". However, Hummel (1994) later showed that a smooth radial run of the ratio of the local line broadening by gas motions to non-coherent scattering reproduces such profiles of optically thick lines quite satisfactorily, so that these these winebottle profile shapes are not related to the process proposed here.

3.4 Discussion

3.4.1 Alternative hypotheses

For discs of the kind considered here, there is only one other plausible *general* mechanism to explain a variable base width of the optically thin emission, namely a varying tilt angle of the disc (Hummel 1998). However, for random orientations w.r.t. the Earth, one would expect either that increases and decreases in line emission and base width in a given star take the same time or that sudden increases followed by slow decreases are roughly equally frequently observed as the inverse (slow increase followed by sudden decrease). The present database is at variance with both. Neither can the change of the base width at roughly constant emission peak separation (Fig. C.5) be explained by varying tilt angles.

For several stars discussed above, circumstances specific to them or a particular event may as well lead to similar observational effects. So for instance in FV CMa the temporarily enhanced emission wings in the Balmer lines could be caused by a transient local overdensity. However, this would not explain that in stars like ω CMa the emission lines of FeII and SiII vanish completely and return only after a new burst when also the broad wing component in Balmer lines appears again. Neither can it account for the variable base width of the optically thin emission lines. In those cases where the development of the emission lines after an outburst could be observed in sufficient detail, the temporary emission at high velocities always decreased monotonically and roughly homologously with time. Therefore, the simultaneous presence of two distinct emission constituents as in FV CMa is also for this reason much more plausibly attributed to two outbursts at different times than to a radially outward moving density enhancement, superimposed on an otherwise unchanged disc. This, in turn, re-reinforces the inference of a transient inner low-density region.

Moderate increases in the base width of optically thin lines, i.e. by less than about $20\,\mathrm{km\,s^{-1}}$, like in FW CMa, might be explainable by variable turbulence. But the difference in base width of more than $200\,\mathrm{km\,s^{-1}}$ observed in 28 Cyg (Tubbesing et al. 2000, and Fig. C.5) certainly cannot be attributed to this effect.

However, again the plain fact that a single explanation is possible for all those cases favours it over a set of individual ones. Moreover, it would be surprising if such very different mechanisms would lead to the rather homogeneous variability patterns observed in the present sample of stars.

3.4.2 Synopsis of the formation of inner disc cavities with physical processes

The present observations do not offer direct evidence as to whether the matter leaving the inner disc rains back to the star or moves to larger distances. Both from the observational and theoretical point of view, however, it is quite probable that a disc in an early-type Be star cannot persist for a long time without on-going star-to-disc mass transfer. The coming and going of Balmer line emission in μ Cen, when it did not have a persistent disc (Baade et al. 1988; Hanuschik et al. 1993), probably provides the observational confirmation for the quick dissipation of a weakly developed disc. Other cases of disc decay have also been observed frequently and were discussed before, so that here only the theoretical arguments are listed.

A viscous decretion model succeeds in explaining more observational details of Be star discs than most other models (for a discussion see Porter 1999; Okazaki 2001). This type of model, however, by necessity leads to an outflow, starting to gain significant radial speed only at higher radii than probed by visual spectroscopy. Radiation pressure by itself is insufficient to overcome gravity at the photospheric level, except for the earliest B spectral subtypes. Even in these, however, the winds observed are weaker than those observed in most Be stars. The rotational support of matter in the disc may give the radiation much more leverage there, since the radiation force can take its time to act on the gas, which is not falling back anymore. As well already the stellar wind alone occurring in the earlier B subtypes may entrain disc material and so erode the disc.

Outward motions superimposed to a (pseudo-)Keplerian disc pose the well-known angular momentum problem, which makes it difficult to explain the very existence of such discs. In numerical simulations, Kroll & Hanuschik (1997) studied the trajectories of particles ejected from a rapidly rotating star in explosive events. They found that a collisional exchange of angular momentum takes place, which permits some particles to settle in an orbit and forces others to fall back to the star. Conceivably, radiative and/or viscous perturbations of the inner edge of the disc lead to processes with a similar effect. Moreover, in the viscous decretion model, the disc is not Keplerian everywhere but probably becomes angular momentum conserving in its outer parts (Okazaki 2001), thereby alleviating the problem.

In order for viscous decretion discs to survive for many decades, the mass-supply to the disc needs to be either continuous or composed of discrete events with a repetition time significantly shorter than the viscous timescale (cf. Okazaki 2001). The outburst periods of 29 and 54 days in μ Cen (Rivinius et al. 1998a) satisfy this criterion easily. In the Hipparcos database, Hubert & Floquet (1998) identified 14 candidate stars with photometric cycle lengths between 20 and 500 days. This is still considerably shorter than the viscous timescale of typically 5 years.

Model calculations by Gayley et al. (2001) and mainly aimed at explaining long-term, precession-like variations of the overall structure of Be star discs provide a first numerical description of the dynamical influence of the stellar radiation on a Keplerian disc. Because of the shadowing effects of spectral lines, the radiative driving of a gas outflow requires the presence of velocity differences in order to be able to further accelerate the gas. Therefore, the radiation from a central point source would have no effect on a Keplerian disc because the velocity profile is flat in the radially outward direction. Only the finite angle subtended by the stellar photosphere at each location in the disc provides the required velocity differences required.

This model would be most effective in the case of low-density discs while the self-shadowing of lines in high-density discs could even let it fail. In fact, a sufficiently high density at the beginning of the formation of a disc might be required for the survival of the disc (leading to the interesting question whether early-type Be stars can develop a disc only because of their outbursts). If the same process is also involved in the later dispersal of a disc, some further ingredients are probably necessary for the full explanation.

Finally, a very effective circumstellar broom as well as angular momentum booster could obviously be made of magnetic field loops. They could be small and weak enough to not be detectable with current instruments so that observational constraints would be difficult to supply.

3.4.3 Implications for the modelling of discs

The observations presented here call for time-dependent refinements of the models of Be star discs at the interface to the star (as also noted by Okazaki 2001). Even in the absence of multi-constituent structures as in FV CMa, the inner disc radius should be treated as a free parameter. It may be possible that only after an outburst there is no significant density minimum between photosphere and disc. However, during these early stages the validity of the assumption of equilibrium becomes questionable.

If the described variability of the inner disc regions is indeed due to outbursts of the central star, it is probably essential to keep in mind that outbursts do not seem to be common, or may even be absent, in late-type Be stars. With the exception of o And, all stars of the present sample have spectral types between B1 and B3 (as have the 14 Hipparcos stars mentioned in the previous subsection). Therefore, the results of this work may well not be pertinent to the discs of Be stars of all spectral types. On the other hand, there is mounting evidence that among the early sub-types outbursts are very common.

The inner variability appears to have little to no effect on the outer disc regions. Typically observed outflow velocities in Be star discs are only a few $\mathrm{km\,s^{-1}}$, as was shown in the previous Chapter and the references therein. This at least applies to the populated ring. Closer to the star, the sweeping of the inner cavity is more effective. In this way the ring forms a reservoir, from which the flux of matter in the outer disc regions is fed. Unless such a reservoir empties significantly, it has a damping effect on the amplitudes of perturbations propagating through it.

Therefore, the density power laws derived from infrared and radio data using the equation of continuity (Waters 1986) should describe these regions well, as the assumption of a constant mass flow might be a good approximation for the outwards dissipation of the ring, even if the feeding from inside is due to an eruptive process.

3.4.4 Discs and winds

For more than a decade, observations with the *International Ultraviolet Explorer* (IUE) satellite have been one of the governing factors in the research of Be stars. However, much of this work was dominated by an intensive dispute about the geometry of the exophotospheric regions. The main points were the interpretation of the optical low-velocity circumstellar emission and absorption lines due to lowly ionized gas and the high-velocity lines from highly ionized species found by IUE. While some authors counted this as evidence of a radial stratification similar to the solar photosphere and chromosphere, others ascribed the former line types to an equatorial disc and the latter to a polar wind. A first access to the vast amount of observations and interpretations can be obtained through the monograph by Underhill & Doazan (1982) and the literature cited therein.

Now, that the observations no longer need to explain the geometry but the known geometry can help to better understand the observations, it is worthwhile to briefly re-visit some of the loose ends in light of the progress made since. The following points come to mind:

Polar winds: Advocates of the flat-disc model resorted to the hypothesis that the fast wind filled the space above and below the disc. The notion of a polar wind also seemed to be helped by the decrease in effective temperature and, thereby, radiative driving, from pole to equator as a result of rotationally induced gravity darkening. However, the key study based on the largest sample of Be star spectra obtained with IUE does not support this at all: Grady et al. (1987a, 1989) found that in Be stars with $v \sin i$ less than about $150 \, \mathrm{km \, s^{-1}}$ the winds were not any stronger than in ordinary B stars. The authors surmised that there might be Be stars which rotate too slowly to develop a polar wind. But this distinction is not supported by any other circumstance. If, conversely, it is assumed that (early-type) Be stars do form a reasonably homogeneous group, the conclusion must be that the wind excess of Be stars over B stars forms neither at the pole nor very close to the star: It is the result of ablation of the disc by the stellar radiation.

Wind/disc correlations: Both wind and disc are highly variable in many Be stars. The lack of a clear correlation was used as a supporting argument by the disc camp, whereas the other one claimed superiority because the variations were not completely uncorrelated. The notion of a disc being created, or replenished, by outbursts and then being gradually dispersed through the wind can explain such a loose relation without any effort. More importantly, neither of the two historically competing models would be able to explain observations like those of θ CrB: After a Be-shell phase, the star entered a B star phase between March and October 1980, i.e. no trace of circumstellar material was observed since October 1980 in the visual domain. Yet, the IUE observations showed shell lines in e.g. SiIV 1394, AlIII 1863, and FeIII 1896 until about December 1981 (Doazan et al. 1986b) and a continuous wind excess in CIV 1548 with relatively low expansion velocities until March 1982 (Doazan et al. 1984, 1986a). Now, if the excess wind is merely the result of the demolishment of the disc rather than its formation, this is unavoidable because the much larger optical thickness of the UV resonance lines makes them still visible when the column density is far too low for Balmer and optical metal lines. After March 1982, decreasingly frequent signs of a temporarily enhanced wind were observed at several occasions in θ CrB, having higher expansion velocities than before (Doazan et al. 1987). These might have been indications of failed disc formation, as sketched at the end of Sect. 3.4.2. Such a scenario can be easily adapted to explain observations of λ Eri and 66 Oph (Barker & Marlborough 1985; Barker 1986; Grady et al. 1987b; Peters 1988b), if it is assumed that the excess wind is strongest during the sweeping of the inner ring cavity, i.e. after an outburst.

Discrete Absorption Components (DACs): At one time or the other, DACs are observed superimposed to the wind lines of virtually all luminous OB stars (Howarth & Prinja 1989). Massive observing campaigns with IUE found them to repeat cyclically in many objects, and the commonly accepted explanation is by shocks arising at so-called co-rotating interaction regions (CIRs). In some stars, there is also evidence of CIRs developing due to stellar nonradial pulsation (Howarth et al. 1998).

The same models are undoubtedly also applicable to Be stars. However, in Be stars with enhanced winds DACs account for a very much larger fraction of the equivalent width of UV wind lines than

in more luminous OB stars, and on average also appear to occur more often. Moreover, at least some fractions of the DACs in Be stars do not seem to repeat cyclically, but are quasi-stationary on timescales much longer than the typical flow times. This has led some authors to infer special physical conditions in the atmospheres of Be stars. But it is rather probable that the gradual destruction of the disc, and the dynamical response of the disc matter to this process, do not proceed in a smooth and continuous fashion. It is, therefore, conceivable that the different roles of DACs in Be and more luminous OB stars is only the result of the presence of a decaying disc.

The work of Telting & Kaper (1994) might support such a hypothesis, as they found the occurrence of DACs in γ Cas strongly correlated with the V/R ratio of the disc's Balmer emission. They concluded that the material forming the DACs comes from the density wave rather than from the star, leaving the disc outwards on a trajectory resembling the case of conservation of angular momentum. Such a scenario would also be compatible with the model by Okazaki (2001).

Very rapid variability: Variations within hours mainly concern DACs. Therefore, the same conjectures as before suggest the same change in paradigm: The combination of wind and disc instabilities may well make the assumption of special physical processes in Be stars unnecessary.

3.5 Conclusion

It seems necessary to adjust somewhat the picture of the discs around early-type Be stars. Instead of a stationary disc structure with constant, moderate outflow, several observed cases show indications for a varying radius of the inner disc edge, i.e. at times forming a ring. The appearance of a disc in contact with the stellar surface seems limited to the immediate times of outbursts. Due to a process yet to be identified, part of the ejected matter attains sufficiently high angular momentum to form a roughly Keplerian disc. For instance, this may be due to the collisional exchange of angular momentum between particles, in which case the angular momentum donators would return to the star.

After a dynamically stable disc has formed, intrinsic instabilities of the disc, starting at the inner edge, e.g., due to sheer, and the stellar radiation pressure itself or the stellar wind driven by it gradually excavate the disc, which may be re-filled by subsequent outbursts. Simultaneously to the growth of the inner disc radius, also measurements of the mean and outer disc radius indicate expansion. All these properties typically follow a saw-tooth pattern, steeply changing during outburst and gradually returning afterwards. The excavation of the inner disc, eventually turning into a gradual erosion of the entire disc, accounts for the differences between the winds of Be and B stars. If no further, sufficiently strong outbursts take place the disc will be completely dissolved.

The *direct* observations of a varying inner disc radius are limited to the cases described in this chapter and in Appendix C. However, not only are several other, but less conclusive indicators seen more frequently (e.g. varying peak separation), but the evolution from a disc into a ring is closely correlated with circumstellar outbursts, which are common for early-type Be stars. Therefore, it seems plausible to assume that the mechanisms at work to form a ring are also effective in other, if not all, early-type Be stars.

Part II

Be stars as pulsating stars

Chapter 4

Nonradial pulsation modelling

4.1   Stellar pulsation

Stars are typically regarded as stable. They take millions or even billions of years to evolve. However, next to this irreversible aging stars need not to be "stable" in a static sense during their evolution. Many stars in fact undergo pulsations on timescales between minutes and years. The most fundamental pulsation is the radial mode with no nodelines both on the surface or in the radial direction. As the star becomes bigger and smaller, not only the radial velocity of the surface changes, but like any expanding/compressing gas the star also becomes cooler and hotter again. These objects typically vary distinctly in brightness and colour. Stars may not only pulsate radially, however. Next to the radial modes, there are the non-radial ones. Imagine some free-falling fluid in a spacecraft: it will have spherical shape, unless it is externally excited by some force. Before reaching the stable spherical shape again, there will be damped wobbles. This, in a sense, is externally excited nonradial pulsation (*nrp*) in a multitude of modes.

Nonradially pulsating stars behave similarly. But since these pulsations are excited from inside the star and are going on for millions of cycles, they appear more ordered as most modes are damped, and typically only one or few high-amplitude modes are excited in an *nrp* star. The selection process which mode precisely will be excited with detectable amplitude and which will not be visible is not understood. However, it is an observational fact that in many stars one or a few modes stand out with high amplitude, even if theory predicts dozens to hundreds of unstable modes. The excitation process resembles a Carnot-process where the role of the valve is played by a layer inside the star that turns opaque with increasing temperature due to ionization processes and becomes transparent again during the following expansion phase. In B stars this so called κ mechanism is, other than in Cepheids, not acting on Helium-opacity, but on Iron-group metals. When such a layer is close to the stellar surface, stellar pulsation may be excited. On the surface *nrp* manifests itself as a global wave pattern, which travels around the star parallel to the equator. The repetition of the wave pattern wrt. the line of sight causes the periodic behaviour. This global wave pattern can be described by means of quantum numbers ℓ and m, characterizing the total number of oscillation nodelines on the star and and how many of them cross the equator, respectively, (see Fig. 4.1). While such *nrp* might be very subtle, like in the Sun, for other stars like the Be stars, however, the induced variability may look so violent that it was first claimed that, if this were pulsation, the star would be disrupted (see also Sect. 1.4.1). It has been claimed that there is no such excitation mechanism to induce pulsation in low-order modes in the vicinity of the Be star parameter range (Balona & Dziembowski 1999). Recent studies by Townsend (2005), however, have shown that the SPB instability strip, responsible for the low-order *g*-mode pulsation in the Slowly Pulsating B stars, moves up the main sequence if rotation is included more completely into the stability computations.

4.2   Computing the stellar surface parameters with BRUCE

Townsend (1997a,b) has published two model codes to compute the pulsational profiles of rotating stars. The first, BRUCE, computes the physical variations of the stellar surface, while the second, KYLIE integrates a spectral profile from these data. It should be noted that BRUCE does *not* compute eigenmodes, but the mode parameters like period etc. have to be fixed as input. Thus, the computations are not self-consistent, but the more complete methods in this sense are also more restricted in terms of rotational speed.

The first step performed by BRUCE is to compute the non-variable mean stellar surface, and then to apply
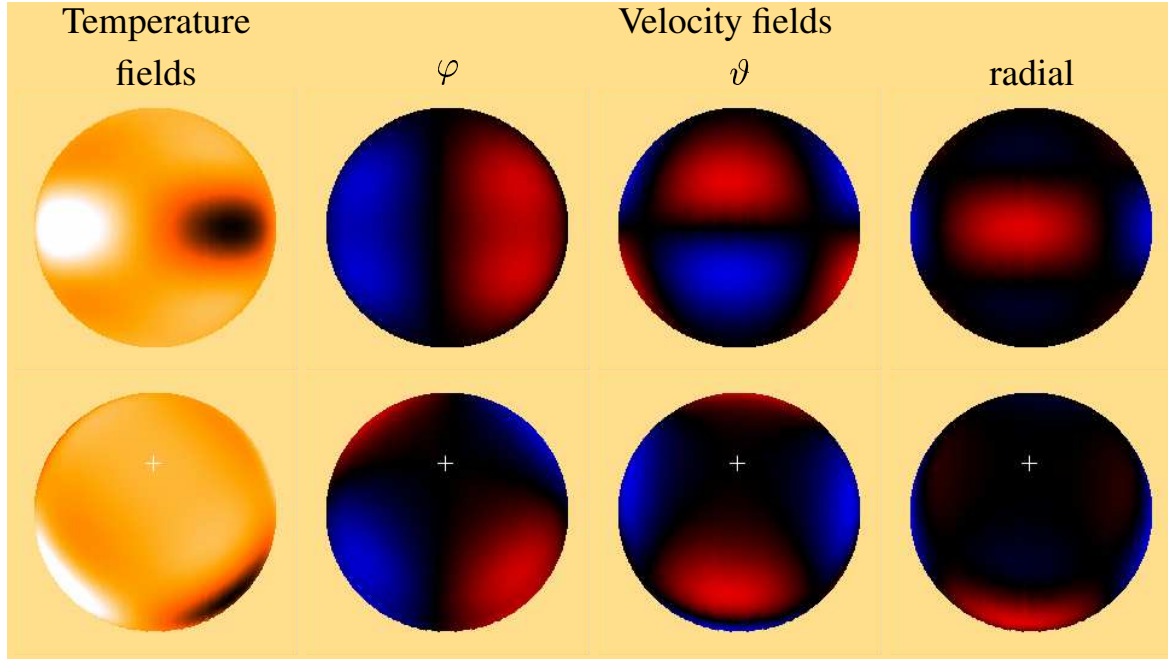
Figure 4.1: The pulsational variations of the stellar surface as computed by the model BRUCE for an $\ell = 2, m = 2$ mode. This is a so-called sectorial mode with two node-lines ($\ell = 2$), both of which are in longitudinal direction ($\ell - |m| = 0$). This causes the nrp-pattern to repeat twice along the stellar circumference. Although the number of node-lines in latitude should be zero for the radial velocity field, this is only a first order approximation due to the effects of rotation and some additional weak features might be noticeable towards the poles. The same model is shown for equator-on (upper row) and almost pole-on orientation, as ω CMa is seen from Earth (lower row, the "+" marks the rotational pole). Since the pulsation is almost adiabatic, the changes in pressure also cause the temperature to vary locally. The radial motions are a factor of almost 10 slower than the horizontal ones, while the φ- and ϑ-amplitudes are about equal. These three velocity fields are co-added and projected onto the line of sight to compute the observed spectrum.

the disturbances due to the variability to it. To compute the undisturbed stellar surface of a rapidly rotating star the critical fraction will be defined as

$$w = \frac{v_{\text{rot}}}{v_{\text{crit}}} \tag{4.1}$$

where v_{crit} is the speed the star could rotate at most before the photospheric material would leave the star into orbit. It is important to note that the definition of w through the rotational speed is different from that through the angular velocity, since the increasing radius is included in the former, while in the latter it is not. For an observational work, however, the velocity definition is more easily applicable. The simplicity of dealing with observed velocities on the other hand means that, computing the critical velocity for a given star, one has to take into account the rotational flattening at critical rotation, i.e. an axial ratio of polar to equatorial radius of 1:2 under the assumption of uniform rotation, so that

$$v_{\text{crit}} = \sqrt{\frac{GM_\star}{R_{\text{eq}}}} = \sqrt{\frac{GM_\star}{1.5R_{\text{p}}}} \tag{4.2}$$

Again assuming uniform rotation, the actual flattening at sub-critical rotation can be expressed as

$$\frac{R_{\text{p}}}{R_{\text{eq}}} = 1 - \frac{1}{3}w^2 \tag{4.3}$$

The resulting oblate form of the stellar surface alters the total surface area seen, but it also changes the angle of view towards any given surface element. This will not only influence the limb darkening to be applied, but also the projected surface area and hence the weight this surface element will be given for the integration over the visible surface.

Next to the oblateness the most obvious effect of rapid rotation is the so called gravity darkening. As von Zeipel (1924) stated, a rapidly rotating star cannot have a uniform surface temperature and be in equilibrium. Instead, if a non-convective envelope is assumed the local surface temperature depends on the local effective gravity, which varies as a function of colatitude ϑ:

$$T(\vartheta) = T_{\mathrm{p}} \frac{g(\vartheta)^{\beta}}{g_{\mathrm{p}}} \tag{4.4}$$

The canonically assumed value of β for early-type stars with geometrically thin, non-convective atmospheres is 0.25 (Hadrava 1992, discussing the limitations of this parametrization). The atmosphere will become convective at $w = 1$, but this process is little investigated and is neglected here, since it is unknown how this influences gravity darkening. The local radius $R(\vartheta)$, needed for the effective gravity $g(\vartheta)$, is computed numerically.

The pulsational surface wave pattern (see Fig. 4.1) in the non-rotating case is expressed as a single spherical harmonic with the fundamental numbers ℓ and m. However, when rotation becomes significant, the actual pattern is no more a single spherical harmonic, but has to be approximated by a series of these functions. Still it is possible, though, to assign a given mode such numbers from the general appearance, i.e. which spherical harmonic dominates the pattern. Generally spoken, the wave pattern corresponding to these dominating mode numbers becomes more and more concentrated towards the equator with increasing rotation and the the contributions at higher latitudes weaken to neglectable amplitude. The technique used to calculate the rotational modifications to the pulsational modes, following Lee & Saio (1990), is particularly well-suited for long-period pulsators, with respect to the fundamental radial oscillation period, and thus for g-modes, in which the restoring force is the gravity. Most other codes specialize in short period pulsation modes, where radial motions dominate, called p-modes for "pressure". These two wave types can be imagined as ocean- vs. sound-waves. BRUCE accounts for the Coriolis forces completely, but neglects the centrifugal forces. Therefore, for extremely rapid rotation even this model will not be completely correct. The input for BRUCE are the stellar parameters, the angular pulsational mode indices (ℓ and m) and their respective amplitudes. BRUCE is able to perform multi-mode modelling, but does not take into account interactions between the pulsational modes, it just co-adds the perturbations due to each mode linearly. Townsend (1997a,b) and the commented BRUCE sourcecode describe these procedures in detail.

4.3 Stellar atmosphere models

For the computation of the observable stellar variability from the perturbations of the stellar surface by BRUCE, the intrinsic observables for each surface element are needed. The NLTE model grid of intensity spectra used by Townsend (1997a), and a similar NLTE flux spectra grid by Gummersbach et al. (1998) unfortunately were too limited to be used for this work both in the $\log g$–T_{eff} plane, as it does not cover the cool equator regions in a gravity-darkened star, and in the number of ions computed. Therefore, for integrating the line profile variability the intrinsic profiles were interpolated from the models introduced below.

4.3.1 Atmosphere structure (ATLAS 9)

Next to their NLTE work, Gummersbach et al. (1998) have as well computed a grid of ATLAS 9 atmospheric models for different metalicities. Since then these authors recomputed and extended the grid, now reaching from $T_{\mathrm{eff}} = 3\,000\,\mathrm{K}$ to $50\,000\,\mathrm{K}$ in steps of $1000\,\mathrm{K}$, and from the lowest numerically converging $\log g$ to an upper limit of $\log g = 5.0$ in steps of 0.1 dex. From these data a subset of solar metalicity models with a microturbulence of $\xi_{\mathrm{micro}} = 8\,\mathrm{km\,s}^{-1}$ was selected. This subset covers the range of $4\,000\,\mathrm{K} \leq T_{\mathrm{eff}} \leq 30\,000\,\mathrm{K}$, and $\log g \leq 5.0$. The lower boundaries were chosen to be able to model also very rapid rotation, which causes an equatorial temperature significantly lower than T_{eff}.

4.3.2 Intrinsic line profiles (BHT)

ATLAS 9 provides the atmospheric structure needed as an input to model the intrinsic line profiles of a stellar surface element. For the spectral synthesis the BHT LTE code by Baschek et al. (1966) was used. Next to computing metal line profiles in LTE, this code is able to use different approaches for HeI lines than for metal lines, as it computes the HeI profiles following specialized theories (Barnard et al. 1974; Gieske & Griem 1969). Because of the spectral peculiarities, especially of the HeI triplet lines, their intrinsic profile can differ

41

Table 4.1: Ions and abundances used by BHT to compute the synthetical spectra.

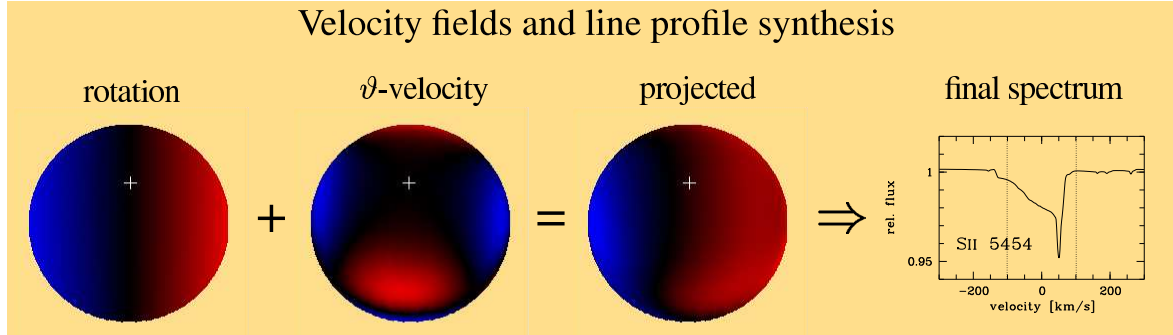| Ion:	HI	HeI	CII	NII	OI	OII	NeI	MgI	MgII
Abundance:	12.00	10.95	8.25	7.91	8.45	8.45	9.08	7.50	7.50
Ion:	AlIII	SiII	SiIII	SII	CaI	CaII	FeII	FeIII	
Abundance:	6.21	7.33	7.33	6.96	6.16	6.16	7.37	7.37	

Figure 4.2: For the cases of μ Cen and ω CMa the velocity field as seen from Earth is dominated by the undisturbed rotation and the ϑ-velocity for a pole-on star. At the approaching limb of the star (blue), the co-added ϑ-amplitude increases the total approaching velocity, being responsible for the extended ramp on the blue wing of the final spectrum. At the receding limb, rotation and ϑ-velocity have different signs, thereby *reducing* the maximal projected velocity. A large part of the receding hemisphere is, therefore, projected into a narrow velocity range, causing the spike. The modelled SII 5454 line is shown for illustration.

significantly from a Gaussian or Lorentzian profile shape. Only for the HeI 4471 line the code faced some problems, as for temperatures around 20 000 K and high $\log g$ the code execution stopped. For these parameter sets, the line was removed from the list of lines to be computed and later approximate interpolations from the neighbouring parameter sets were included for this particular spectral line.

To account for the typically non-solar metalicity of B-type stars in the local vicinity, the abundances were adopted from Kilian (1992, 1994). For each of the selected atmosphere models above, a synthetic spectrum was calculated from 3900 Å to 6750 Å that included in total 6756 spectral lines. The microturbulence for the BHT calculations was set to $\xi_{\mathrm{micro}} = 2\,\mathrm{km\,s}^{-1}$. These synthetical spectra form the grid of input profiles, on which the spectroscopic modelling was based.

4.4 Integrating the surface parameters with KYLIE

BRUCE computes the surface parameters of the pulsating star for a mesh of about 25 000 points on the visible part of the stellar surface. For instance, Figs. 4.1 and 4.2 have been constructed from the BRUCE output. The computed pulsational perturbations, superimposed on the equilibrium configuration of the rotating stellar surface, include pulsational velocity fields in all three directions (r, ϕ, θ), temperature changes, variations in the visible surface area and finally the variations in the viewing angle of a given surface element.

KYLIE, then, computes observable quantities from these perturbation fields. To obtain the observable spectrum of the computed pulsational phase, the local spectra for the surface elements are taken from the above introduced input grid of precomputed data. The limb darkening coefficient to be applied at the given viewing angles can be strongly variable across a spectral line, reaching even negative values. However, Townsend (1997a) showed that this is of little importance for *lpv* modelling. The limb darkening was, therefore, adopted to be constant for line profile synthesis. According to Townsend this is an acceptable simplification.

Finally, the computed local spectra are shifted according to the projected local velocity field component. This is done on a logarithmic wavelength scale, so that the full wavelength range of 3900 Å to 6750 Å is computed in a single step. Then, these local spectra are co-added using the projected surface area and the Planck-function of the local temperature as weighting factors. A schematic overview of this procedure is given in Fig. 4.2 for the most important perturbation in a Be star, the velocity field.

Chapter 5

Modelling individual Be stars

5.1 μ Centauri

The first step to explore the capabilites of the *nrp* model code provided by Townsend (1997a) was to apply it to the most extensive dataset in the HEROS collection. At this time, these were the spectra collected of μ Cen. During the work, ω CMa reached a similar prominence and is, therefore, presented later in this Chapter.

The Be star μ Cen ($=$ HR 5193 $=$ HD 120 324; B2 IV-Ve) was an intensively studied object well before this work already. One of the more recent studies of its observational properties was given by Rivinius et al. (1998c,b), who also references to previous work. They found six coherent periods present, which fall into two groups. Within each group, the periods differ only by a few percent and the spectroscopic appearance is very similar. The labour-intensive modelling is, therefore, limited to the strongest period in each group, and will only in later sections be extended to a multimode model.

5.1.1 Finding the best model parameters

For each of the two strong periods ($\mathscr{P}_1 \approx 0.5$ d and $\mathscr{P}_5 \approx 0.28$d) several pulsation modes were tested. For each mode considered hundreds of different parameter sets were computed. Therefore, the first evaluation of how the models compare to the data had to be performed automatically. To do so, the observed profiles were phased in eight bins ($\Delta\phi = 0.125$) and the residuals from the averaged line profile were calculated. For the model, which calculates sixteen equally spaced phase steps ($\Delta\phi = 0.0625$), profiles from odd and even phase steps were merged, and then treated similarly for comparison with the data.

Then, the model residuals were cross-correlated against a fixed reference, namely the extreme blueshifted phase (chosen for the sake of unambiguity) of the observed phase-binned profiles, to derive the phase shift of the model compared to the data. Because this coarse grid, as a first step, was only computed with a fixed amplitude (see also Sect. 5.1.1.2), the residuals were normalized to reduce the impact of such an approach, since the χ^2 technique is very sensitive to amplitude differences. In the following step, the χ^2 of the model residuals from the observations was calculated for each bin according to the derived phase. The individual χ^2 values were averaged over all eight bins and the full profile width.

The best model is then the one that fulfils the following constraints best:

1. plausible stellar parameters

2. good matching variability for both $\mathscr{P}_1$ (minimum χ^2) and $\mathscr{P}_5$ for one and the same stellar parameter set, but differing in ℓ and/or m, amplitude, and co-rotating period

Previous analyses have revealed a couple of variation properties that can be used as further constraints:

3. The capability of the model to explain features like spikes and ramps occurring cyclically at times of high amplitude due to constructive interference of two or more modes of the $\mathscr{P}_1$ to $\mathscr{P}_4$ group (Sect. 4 of Rivinius et al. 1998b)

4. The occurrence of backward travelling bumps apparent only in very high quality data (Baade 1991). That these are barely visible in the actual HEROS data is probably a consequence of the data quality, as it can be seen very well in Baade's (1991) CES data. If the models were degraded to HEROS quality by the

Table 5.1: Adopted stellar parameter ranges for the coarse grid. Note that i is calculated for each v_{rot} assuming either of the two considered values of $v_{rot} \sin i = 130, 160 \, \text{km s}^{-1}$.

Parameter		Range
Radius, $R_{\star,\text{polar}}$	$[R_\odot]$	4.0 … 6.0, step 0.4
Temperature, $T_{\text{eff,polar}}$	[kK]	20, 22, 24
Mass, $M_\star$	$[M_\odot]$	7, 8.5, 10
Equ. rotation, v_{rot}	$[\text{km s}^{-1}]$	200 … 400, step 40
$v_{rot} \sin i$ to compute i	$[\text{km s}^{-1}]$	130, 160

addition of photon noise and degrading to $R = 20\,000$, the retrograde features would hardly be visible anymore.

5. The variability outside the limits given by the projected rotational velocity, especially having a node of low variability at, or close to, $v_{rot} \sin i$ (Rivinius et al. 1998b).

5.1.1.1 Initial guess parameters

Physical parameters for μ Cen have been computed using Walraven photometry by de Geus et al. (1989). They obtained $T_{\text{eff}} = 20\,500 \, \text{K}$, $\log g = 3.94$, $\log L_\star/L_\odot = 3.6$, and a distance of 145 pc. The HIPPARCOS distance is a little greater, $162 \pm^{21}_{17}$ pc. Brown & Verschueren (1997) derived $v_{rot} \sin i = 130 \, \text{km s}^{-1}$ from high resolution echelle spectroscopy, while Slettebak (1982) gave $v_{rot} \sin i = 155 \, \text{km s}^{-1}$. This relatively low value and the shape of emission line profiles point towards a low-to-intermediate inclination (Hanuschik et al. 1996). For a rapidly rotating star, however, the values for T_{eff}, $\log g$, and $\log L_\star$ cannot be translated directly into parameters like radius and mass using standard calibrations. Due to the rotational deformation, the observationally derived radii, luminosities, and temperatures depend on the inclination angle (see below and Part III) due to gravity darkening and rotational deformation. Therefore, from these observations only the boundaries of the parameter grid, for which pulsational model calculations were performed, can be derived.

The input stellar parameters required by the model are polar radius $R_{\star,\text{polar}}$, polar temperature $T_{\text{eff,polar}}$, mass $M_\star$, the rotational velocity v_{rot}, and the inclination i. Since the latter two, for modelling a given star, are not independent but connected via the measured $v_{rot} \sin i$, only certain combinations $< v_{rot}, i >$ are acceptable. Thus a complete set of parameters is given by $R_{\star,\text{polar}}, T_{\text{eff,polar}}, M_\star$ and $< v_{rot}, i >$.

Due to gravity darkening in a rapid rotator, the polar temperature will be higher than the one inferred from observations. On the other hand, the gravity darkening gives extremely low temperatures only in a small equatorial band. Since the models do not depend too much on the polar temperature, only three values with a 2000 K step size were tested. Similarly, the main influence of the mass is that it will alter the critical velocity of the star and, therefore, the rotational deformation. The dependency was not found to be sensitive, however. Significantly Stark-broadened lines were not modelled at this stage, so that it was enough to consider only three values that were selected such that any main sequence B 1 to B 2 star has a mass within the used limits (e.g. calibration by Balona 1995). The limits for the radius were chosen with similar considerations in mind as for the mass, but since the model is more sensitive to radius, six steps were computed to ensure smooth variations between two neighbouring parameter sets.

For $v_{rot} \sin i$ good observational estimates exist. Since, however, the value of v_{rot} has the second most important effect on the resulting modelled *lpv*, six steps were calculated for v_{rot} from the lowest believable value, estimated from the fact that μ Cen is certainly not viewed edge-on or close to edge-on, i.e. $i < 50°$, up to the critical velocity. For each v_{rot} two inclinations were computed, so that the observationally derived values of $v_{rot} \sin i$ are bracketed. Table 5.1 lists the grid of parameters chosen. This leads to a total of 648 stellar parameter sets to be calculated for each mode. Parameter sets yielding physical impossibilities, such as super-critical equatorial velocities, or for which the computed local surface parameters would exceed the limits of the synthetical atmosphere grid (Sect. 4.3), were not computed.

5.1.1.2 Coarse modelling grid

The amplitude for this initial modelling was fixed to $A_1 = 15 \, \text{km s}^{-1}$ for $\mathscr{P}_1$ and $A_5 = 7 \, \text{km s}^{-1}$ for $\mathscr{P}_5$ as the maximal physical particle velocity on the stellar surface. The variation power of the models computed this

way differed from the observed one by up to about $\pm 50\%$. However, the characteristics of the variability are relatively stable against amplitude variations. Except for a few special cases discussed below, changing the model amplitude only scales the variation power. The normalization of the residuals (Sect. 5.1.1) is therefore justified and leads to reliable results.

For the parameter range given in Table 5.1, all twelve modes with $\ell \leq 3$ and $m \neq 0$ were tested on $\mathscr{P}_1$. Only zonal modes ($m = 0$) were excluded *a priori*, since their variability pattern would not show phase propagation, due to their axisymmetry. Modes with $\ell \geq 4$ are not expected to have corotating periods within the possible range, i.e. yielding an observed period of twelve hours. Of the modes tested, most retrograde modes could be excluded safely after brief inspection. This is so because the stellar rotation is not fast enough in these cases to make the variability look prograde to the observer. The retrograde ($\ell = 1, m = +1$) mode, however, is an exception, as it was the formally best candidate mode (Table 5.2), and the retrograde ($\ell = 2, m = +2$) mode was found to actually appear prograde to an observer due to rotation. The prograde ($\ell = 3, m = -3$) mode resulted in either a single or a triple-peaked power distribution, while the observed variability of $\mathscr{P}_1$ appears as double-peaked, so this mode was excluded. Similarly, the prograde ($\ell = 2, m = -2$) mode showed significant mis-matches in the power distribution.

All parameter sets with slow rotation ($v_{\mathrm{rot}} < 320\,\mathrm{km\,s^{-1}}$) were significantly poorer at reproducing the observations than the fast ones. In all cases the lower inclination for a given v_{rot} had a lower χ^2, indicating that the $v_{\mathrm{rot}} \sin i$ is closer to $130\,\mathrm{km\,s^{-1}}$ than to $160\,\mathrm{km\,s^{-1}}$. This is supported by visual inspection of the data, since the profiles modelled with $v_{\mathrm{rot}} \sin i = 130\,\mathrm{km\,s^{-1}}$ are only slightly narrower than the observed ones, while for the ones with $v_{\mathrm{rot}} \sin i = 160\,\mathrm{km\,s^{-1}}$ the difference is larger.

The corotating period is calculated from the observed one using

$$\sigma_{\mathrm{corot}} = \sigma_{\mathrm{obs}} + m\Omega_{\mathrm{rot}}. \tag{5.1}$$

Obviously, if Ω becomes large for (observed) negative m and a given σ_{obs}, σ_{corot} may become numerically negative. At first sight this seems unphysical, but a close look reveals a special situation: This is equivalent to a change in sign of m, i.e. a physically retrograde mode, and a negative *observer's* period. Recasting the above equation as

$$\sigma_{\mathrm{obs}} = \sigma_{\mathrm{corot}} - m\Omega_{\mathrm{rot}} \tag{5.2}$$

makes clear that a negative observer's period is not at all unphysical. It is just the mathematical designation for a co-rotating retrograde mode, which is observed prograde due to rapid rotation. This kind of mode can also be shown for ω CMa to be able to model the observed variability excellently (see Sect. 5.2 below). Of the calculated modes, only these, plus one with ($\ell = 1, m = +1$) and the modes with $m = -1$ were found to match the observations well enough to warrant further evaluation (Table 5.2, the best χ^2 achieved was 3.06, the worst values being higher than 10).

Modelling of the variability attributed to $\mathscr{P}_5$ leads to very similar constraints, i.e. that the lower $v\sin i$ gives better agreement between models and observations, and that a very high rotational velocity in connection with mostly small radii will result in a better model reproduction of the variability. Therefore, at this stage, modelling $\mathscr{P}_5$ is not useful in constraining further the best parameter set. On the other hand, the best models found for $\mathscr{P}_1$ are in the same region of the parameter space as the best models for $\mathscr{P}_5$. This can be understood as an indication that the stellar model parameters are sound.

5.1.1.3 Determining the pulsation mode

To finish the computations for one parameter set takes on average nine minutes on a P III 500 MHz processor running LINUX. For the coarse grid, a total of about 16 000 models were computed for $\mathscr{P}_1$ and $\mathscr{P}_5$ on a double processor system, taking about $1\frac{1}{2}$ months of pure computing time. The "impossible" parameter sets leading to supercritical rotation and other unphysical behaviour were sorted out beforehand. Given the time-expensive computations, the number of possible modes from Table 5.2 has to be narrowed down further fro a more detailed investigation.

As Fig. 5.1 shows, the χ^2 method is a good measure for judging the general quality of a model. However, it misses significant details, that are as important in the modelling as the overall quality of fits, e.g. points 3 to 5 of the above list on page 43.

Modes with m $= -1$: The ($\ell = 1, m = -1$) mode does not show as pronounced a blue-to-red propagation across the whole line profile as the observational data. Instead there is almost no variability in the centre of the line. It turned out that modes with the same m, but different ℓ, spectroscopically do not appear different from

Table 5.2: The formally best matching modes (χ^2 test on the residuals from the observed C II 4267 profiles) and the corresponding parameter sets found in the coarse grid for $\mathscr{P}_1$. The first two columns give the mode indices, the next five the stellar input parameters radius, temperature, mass, rotation and inclination. In the second table again the first two columns give the mode indices, the next four four show the equilibrium (i.e. non-pulsating) configuration of the rotating model star, while the last three list the corotating period and the χ^2. The *lpv* of these C II 4267 and the six modes listed here are shown in Fig. 5.1.

ℓ	m	$R_{\star,\mathrm{polar}}$ [$R_\odot$]	$T_{\mathrm{eff,polar}}$ [K]	$M_\star$ [$M_\odot$]	v_{rot} [km s^{-1}]	i $^\circ$
1	1	4.4	20 000	8.5	320	24.0
1	−1	5.6	20 000	8.5	400	19.0
2	2	4.0	20 000	8.5	400	19.0
2	−1	4.8	20 000	7.0	400	19.0
3	2	4.0	24 000	8.5	400	19.0
3	−1	6.0	20 000	10.0	400	19.0

ℓ	m	$\dfrac{\mathscr{P}_{\mathrm{rot}}}{\mathscr{P}_{\mathrm{crit}}}$	$\dfrac{R_{\mathrm{equ}}}{R_{\mathrm{pol}}}$	$\dfrac{T_{\mathrm{eff,equ}}}{T_{\mathrm{eff,pol}}}$	$\mathscr{P}_{\mathrm{rot}}$ [hours]	$\mathscr{P}_{nrp,\mathrm{corot}}$ [hours]	χ^2
1	1	0.65	1.16	0.84	19.40	7.43	3.06
1	−1	0.91	1.38	0.59	23.51	24.64	3.12
2	2	0.77	1.25	0.76	15.14	20.41	3.13
2	−1	0.93	1.40	0.56	20.47	29.18	3.20
3	2	0.77	1.25	0.76	15.14	20.41	3.36
3	−1	0.87	1.34	0.65	24.35	23.77	3.91

each other in principle, but in detail. This is the consequence of a rather polar orientation, since m is the number of nodelines crossing the pole. The ($\ell = 2, m = -1$) and ($\ell = 3, m = -1$) modes show increasing differences in the behaviour of the line wings. The ($\ell = 2, m = -1$) mode, which spectroscopically looks like the most acceptable candidate among the $m = -1$ modes, has an associated photometric peak-to-peak amplitude of 0.05 mag (Table 5.2), which is unacceptably high. In general, the $m = -1$ modes reproduce the data at a rough level, but not in detail (Fig. 5.1).

The ($\ell = 1, m = +1$) mode: The ($\ell = 1, m = +1$) mode was formally the best ($\chi^2 = 3.06$). However, it has several drawbacks that makes it an inferior candidate to the ($\ell = 2, m = +2$) mode discussed below. First, it has a co-rotating period of only about seven hours, which is not plausible for a g-mode. Could it, then, be a p-mode? In principle yes: the model value of $k = 0.71$ would be small enough. However, there are three other arguments. Firstly, it cannot explain the power outside the limits of $v_{\mathrm{rot}} \sin i$ as described in Sect. 5.1.1. Furthermore, it does not exhibit the retrograde feature apparent in the ($\ell = 2, m = +2$) mode. Lastly, this mode is unable to explain the observed spikes.

Modes with $m = +2$: The two modes computed with $m = +2$ look quite similar, except that the variability is generally concentrated more towards the outer line wings for $\ell = 3$. The variability outside the limits of the projected rotational velocity is clearly reproduced by these modes, and both modes show as well retrograde features. Finally, if the amplitude of the $m = +2$ modes are increased, they start forming spikes and ramps, just as in the observed profiles, during times of beating of $\mathscr{P}_1$ to $\mathscr{P}_4$, i.e. high constructive amplitude. The formation of these features is due to the same effect as in ω CMa, where also an ($\ell = 2, m = +2$) mode is thought to be present (Sect. 5.2). The pulsational properties of both modes differ in so far as an $\ell = 3$ mode with the same co-rotating period requires higher temperature perturbations than an $\ell = 2$ mode. Although the photometric variability is small in both cases, this is mostly due to the low inclination. Already the ($\ell = 2, m = +2$) mode requires several thousand Kelvin variability at the equator with the parameters derived from the coarse grid. Even though these extreme variations are concentrated to a very small region around the equator only, the mode requiring the less extreme values, ($\ell = 2, m = +2$) is preferred, mainly because the resulting non-linearity for ($\ell = 3, m = +2$) would be too strong to be readily believed. The final solution given below needs less extreme variations, but the argumentation in favour of ($\ell = 2, m = +2$) remains untouched.
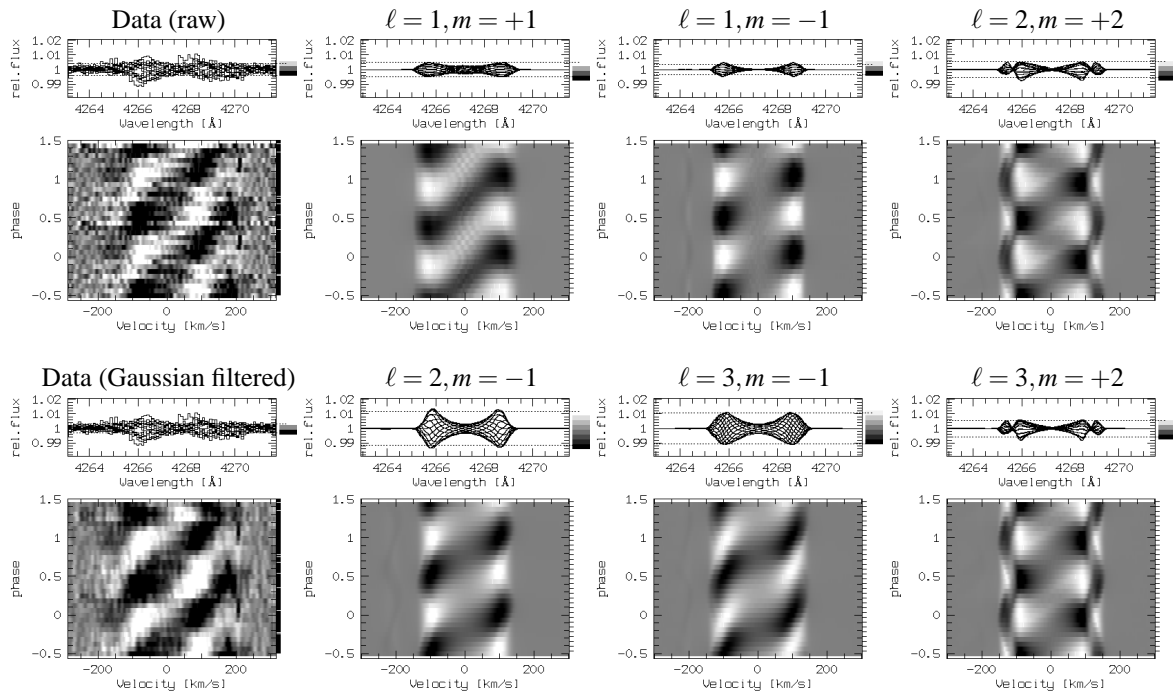
Figure 5.1: Comparison of CII 4267 data to the best matching modes taken from the coarse grid (Table 5.2). We show the residuals only, as the variations are at a level of $\approx 1\,\%$, while the line itself has a depth of the order of $\approx 10\,\%$, which does not give enough contrast of the variations compared to the profiles to be displayed as a grayscale image. Given that sufficient data are available for constructing the mean spectrum, however (in our case more than 400 spectra taken over a couple of years), the residuals are defined unambiguously. Although the CII 4267 line was chosen with special regard to symmetry, the stellar variability seen in the data is still not completely symmetric. At the moment, no solid explanation can be given for this.

Table 5.3: Adopted stellar parameter ranges for the fine grid to model the ($\ell = 2, m = +2$) mode.

Parameter		Range
Radius, $R_{\star,\text{polar}}$	[$R_\odot$]	$3.0 \dots 4.6$, step 0.2
Temperature, $T_{\text{eff,polar}}$	[kK]	23
Mass, $M_\star$	[$M_\odot$]	8.5, 9.0, 9.5
Equ. rotation, v_{rot}	[km s^{-1}]	$340 \dots 500$, step 20
$v_{\text{rot}} \sin i$ to compute i	[km s^{-1}]	134, 138, 142
Amplitude A	[km s^{-1}]	10, 13, 16

5.1.1.4 Fine modelling grid

For this latter mode, models for about a thousand additional stellar parameter sets were computed with a finer mesh in parameter space to obtain the most accurate match and an estimate of the uncertainties. Since the best matching model for the ($\ell = 2, m = +2$) mode was located at the edge of the coarse grid, the explored parameter space was extended to smaller radii and higher rotational velocities. On the other hand the temperature, which was found to play a minor role only, was fixed at 23 000 K. For the pulsational amplitude, three values were allowed for. All parameter values are compiled in Table 5.3.

It turned out that the parameters are not independent. The model properties are somewhat degenerated in the critical rotation fraction $w = v_{\text{rot}}/v_{\text{crit}}$. All models with $w \approx 0.77$ are similarly good. Therefore increasing v_{rot} while lowering the inclination i, will give a comparable match if also a lower radius and/or a higher mass is adopted. Because the degeneracy is not complete, this works only to within some limits, however.

In Fig. 5.2 the χ^2 for all models computed for the fine grid is plotted against the different stellar parameters varied. The final parameter set is given in Table 5.4. The minimum obtained χ^2 was 2.73, while the overall
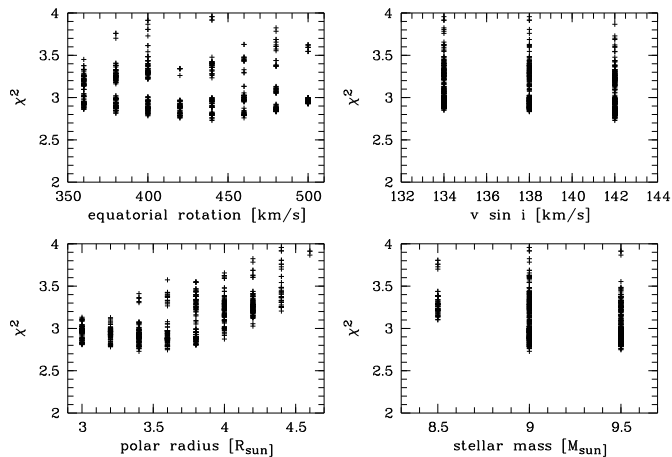
Figure 5.2: The distribution of χ^2 values computed from the fine model grid against the model parameters varied.
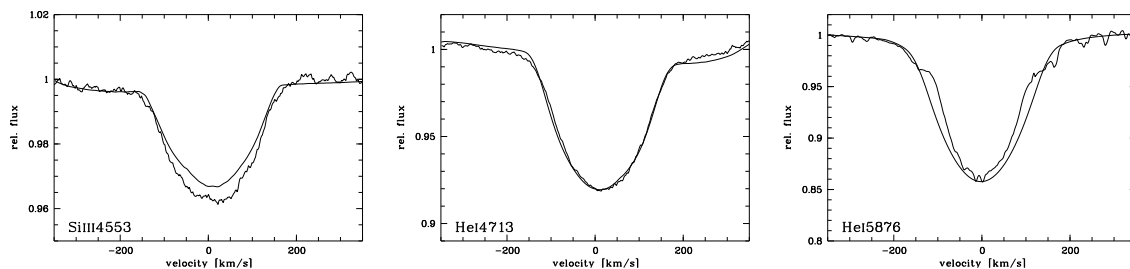

Figure 5.3: Comparison of the observed average line profiles in the low emission state of 1999 to the average profiles derived from the final model for $\mathscr{P}_1$ shown in Fig. 5.4.

minimum for the coarse grid was only 3.13 for this mode ($\ell = 2, m = 2$), and 3.06 for ($\ell = 1, m = 1$). Since the models for $\mathscr{P}_5$ are not decisive in terms of stellar parameters, one model was calculated for each mode with the stellar parameters found by modelling $\mathscr{P}_1$. The ($\ell = 3, m = +3$) mode was found to match the observations better than any other mode for $\mathscr{P}_5$. Figures 5.4 and 5.5 show the model calculations for $\mathscr{P}_1$ and $\mathscr{P}_5$ and five different spectral lines, respectively.

5.1.2   Derived stellar and pulsational parameters

In Sect. 5.1.1 six conditions were listed to be fulfilled by a good model. The details of the line profile variability that should be modelled have already been discussed above. In addition, the mean modelled line profiles match the observed ones well (Fig. 5.3). Considering that the underlying parameters were chosen to model the line profile *variations* rather than the profiles themselves, the agreement is remarkable. But are the derived stellar parameters plausible? In particular the radius of $3.4\,R_\odot$ for a $9\,M_\odot$ star, and the the rotational velocity of $440\,\mathrm{km\,s^{-1}}$, do not seem to be. It is true that $440\,\mathrm{km\,s^{-1}}$ is rapid, and even among the equatorially-viewed shell stars it is unusual. For comparison, 48 Lib is believed to rotate at $400\,\mathrm{km\,s^{-1}}$ (Slettebak 1982). However, in terms of critical fraction $w = v_{\mathrm{rot}}/v_{\mathrm{crit}}$ μ Cen is still an average Be star with $w = 0.76$ (Table 5.4).

Another interesting effect to take into account is what is understood as luminosity and effective temperature. In Sect. 5.1.1.1 the observed luminosity $\log L_{\mathrm{obs}} = 3.6$ and effective temperature $T_{\mathrm{eff,obs}} = 20\,500\,\mathrm{K}$ are given. Despite the polar temperature of $23\,000\,\mathrm{K}$, the model of μ Cen with the parameters listed in Table 5.4 would appear as a star with $\log L_{\mathrm{app}} = 3.46$ and $T_{\mathrm{eff,app}} = 20\,760\,\mathrm{K}$, because the observer sees large parts of the hot polar caps face-on and the equatorial regions limb-darkened. The actual area of the stellar disc on the celestial plane would correspond to a stellar radius of $R_{\star,\mathrm{app}} = 4.17\,R_\odot$, since the rotational flattened ellipsoid basically is seen from above, the direction from which the largest extension is seen.

The high polar model temperature of $23\,000\,\mathrm{K}$ is, therefore, in full agreement with an observed effective temperature of $20\,500\,\mathrm{K}$. The true luminosity in the sense of energy emitted over 4π steradian is, however, $\log L_{\mathrm{true}} = 3.32$ only. This radiation is emitted through a total stellar surface corresponding to a sphere with
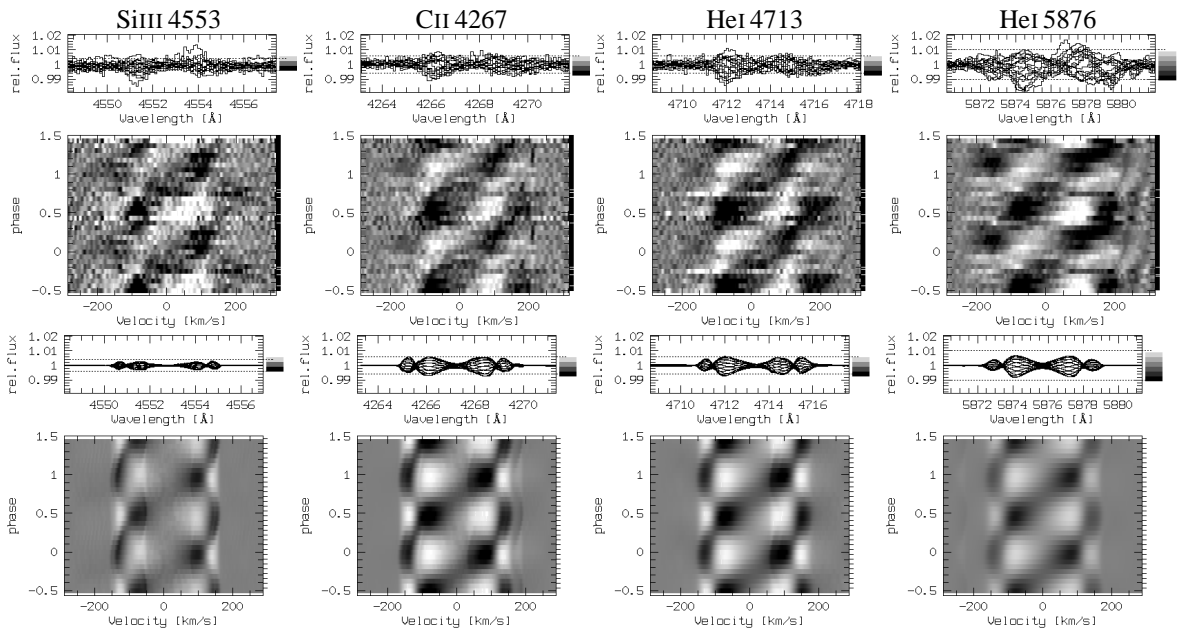
Figure 5.4: Comparison of the observational data for five spectral lines to the final model for $\mathscr{P}_1$ ($\ell = 2, m = +2$). The grayscales are the same for the data and model of each line (but may differ from line to line) to allow an estimate of the accuracy of the model amplitude. It suits the data well, with the exception of HeI 5876. This line can be strongly affected by photospheric NLTE effects, but also by circumstellar emission. The asymmetric variability, like in HeI 4144 could not be reproduced by the model.
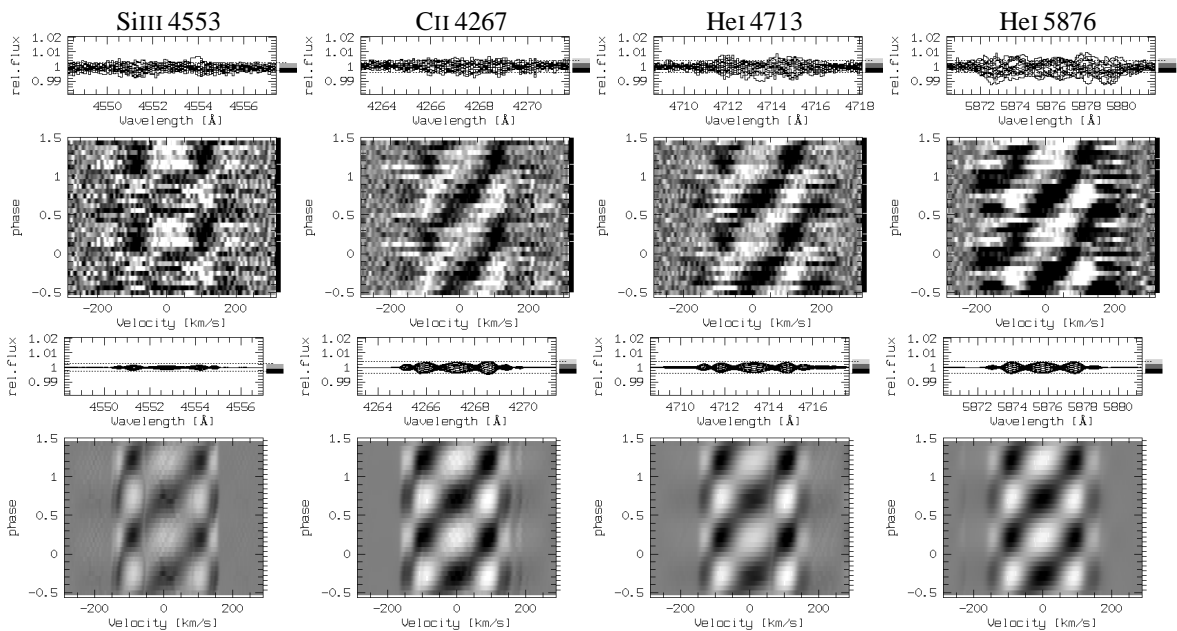
Figure 5.5: Like Fig. 5.4, but for $\mathscr{P}_5$ ($\ell = 3, m = +3$). For HeI 5876 the amplitude difference between observation and model is less pronounced.

$3.89\,R_\odot$, which would then have $T_{\rm eff,spherical} = 19\,770\,{\rm K}$.

The rather small radius is more of a concern. Calibrations, such as that of Balona (1995), give 4.75 to $6.55\,R_\odot$ for a B2 IV-V star. The calibration by Harmanec (1988) lists $4.28\,R_\odot$, $8.62\,M_\odot$, and $23\,120\,{\rm K}$ for a B2V star. The rotational flattening not only increases the equatorial radius, but also shrinks the polar radius by up to $7\,\%$. This number has been taken from Moujtahid et al. (1999), who derives $R_{\rm equ}/R_{\rm pol} = 1.5$ for critical rotation , but $R_{\rm equ}/R_{\rm norot} = 1.44$ and, therefore, $R_{\rm pol}/R_{\rm norot} = 0.93$. One should be aware, however, that other authors give different numbers for $R_{\rm pol}/R_{\rm norot}$ (e.g. Sackmann 1970). In any event this is the number that has to be compared to the polar radius of the model $3.4 \pm .3\,R_\odot$. The difference between the calibration values for B2 stars and the model polar radius of μ Cen is then 15 to 20%. This makes the radius undoubtedly low, but certainly not unbelievable. Theoretical calculations of stellar evolution typically yield smaller radii than calibrations, in a range similar to the one derived here. For instance the models of Claret (1995) give a ZAMS radius of $3.68\,R_\odot$ for a $9\,M_\odot$ star.

On the other hand, observational determinations of the radius of μ Cen as an individual star have to be compared to the *apparent* model radius of $4.17\,R_\odot$ (see above paragraphs), which is larger because in the model one sees the rotationally flattened star almost pole-on. This is still smaller than what e.g. Harmanec (2000) derived, namely $5.28 \pm .07\,R_\odot$. However, such determinations face a number of problems. μ Cen is a member of the Sco OB2 association (Upper Cen Lup, UCL). Nevertheless, since the UCL is very extended, the mean cluster parallax is not a good approximation of the distance to μ Cen. Additionally, recent results by de Bruijne (1999) indicate that μ Cen is closer to the Earth than indicated by Hipparcos ($\pi = 7.10 \pm 0.38$ mas instead of 6.19 ± 0.71 mas). Finally, the assumption that the bolometric correction (B.C.) is a function of $T_{\rm eff}$ only, is not valid for rapidly rotating stars (e.g. Pérez Hernández et al. 1999). Instead, not only the temperature see above, but also the B.C. is a function of $T_{\rm pole}$, w, and inclination. While it is not attempted to derive a final conclusion here, the above discussion shows that the model of μ Cen cannot be rejected on the basis of existing stellar parameter studies.

Telting & Schrijvers (1997) found that modes with the same ℓ look similar, while in our study this is the case for the same m (Fig. 5.1). However, the study by Telting et al. gave this result with greater confidence for modes with higher ℓ than studied here, and while the present models are for g-modes, they investigated p-modes. Following their Figures 3 to 8, the relation between ℓ and $\Delta\phi$ becomes less tight with low inclination and high k, both of which is the case for the present models. Moreover, with decreasing inclination they find that the phase propagation of a feature across the full profile $\Delta\phi \propto m$ rather than $\Delta\phi \propto \ell$ as for higher inclination. This becomes plausible if one recalls that m is the number of nodelines through the pole, so that the *nrp*-pattern seen pole-on is very similar for all modes with the same m. Therefore, these results are not contradictory to the findings of Telting & Schrijvers.

5.1.3   Testing the results

The final criterion is whether the actually observed line profiles and line profile variability can be reproduced by the model also for other spectral lines, in a complete multi-mode approach, and for datasets not used in the analysis. A variety of tests were performed to compare the model to own data, but also to results published by other investigators.

5.1.3.1   Parameters derived from observations and model

In order to construct a multi-mode model, the amplitudes of the individual modes need to be constrained. As a first-guess the model was started with the observed radial velocity amplitudes for the maximum physical velocities of each mode. However, these quantities cannot be taken as amplitude directly, since the position of a bump is due to convolution of rotation and pulsational velocities. Thus a cross-check against the corresponding quantities predicted by the model is required. To do this, the expected line profiles for all more than 400 Heros observations were computed and re-analyzed in the same way as the originally observed data. The periods and phases derived from all Heros data (Table 5.4; Rivinius et al. 1998b) were used, the circular phases are given for $MJD = 50\,000.0$, which is $JD - 2\,450\,000.5$).

Within the limits of the time series analysis discussed in Rivinius et al. (1998b), the analysis of the model-reconstructed dataset gave the same results as the original data for periods and phases. However, not unexpectedly because of what was said above, it turned out that the variability is better reproduced with somewhat different amplitudes than derived from the radial velocity variations. Model parameters of all modes and of the star are given in Table 5.4. The amplitude given is the maximum physical velocity due to that mode, $|v|_{\rm max}$, regardless of direction. The analysis results for any mode in this multimode model are somewhat different

Table 5.4: Characteristics of the final multiperiodic model. For the input parameters the estimated uncertainties are given. The circular phases refer to MJD=50 000. For a discussion of the Table see Sect. 5.1.2.

Stellar model			
R_{pole}	$(3.4 \pm .3)\,\mathrm{R_\odot}$	R_{equ}	$4.21\,\mathrm{R_\odot}$
$\log g_{\mathrm{pole}}$	4.33	$\log g_{\mathrm{equ}}$	3.86
T_{pole}	$(23 \pm 2)\,\mathrm{kK}$	T_{equ}	$17.6\,\mathrm{kK}$
M	$(9.0 \pm 1.0)\,\mathrm{M_\odot}$	v_{rot}	$(440 \pm 40)\,\mathrm{km/s}$
i	$(19 \pm 3)°$	$v_{\mathrm{rot}}\sin i$	$143\,\mathrm{km/s}$
$\mathscr{P}_{\mathrm{rot}}$	$11\overset{\mathrm{h}}{.}615$	$v_{\mathrm{rot}}/v_{\mathrm{crit}}$	0.759
$R_{\mathrm{eq}}/R_{\mathrm{crit}}$	0.825		
$T_{\mathrm{eff,spherical}}$	$19.77\,\mathrm{kK}$	$\log L_{\mathrm{true}}$	$3.32\,\mathrm{L_\odot}$
$T_{\mathrm{eff,app}}$	$20.76\,\mathrm{kK}$	$\log L_{\mathrm{app}}$	$3.46\,\mathrm{L_\odot}$

$\mathscr{P}_1$ parameters		$\mathscr{P}_2$ parameters		$\mathscr{P}_3$ parameters	
$\ell = 2$	$m = +2$	$\ell = 2$	$m = +2$	$\ell = 2$	$m = +2$
$\mathscr{P}_{\mathrm{obs}}$	$-12\overset{\mathrm{h}}{.}0702 \pm 1$	$\mathscr{P}_{\mathrm{obs}}$	$-12\overset{\mathrm{h}}{.}1804 \pm 2$	$\mathscr{P}_{\mathrm{obs}}$	$-11\overset{\mathrm{h}}{.}8686 \pm 3$
$\mathscr{P}_{\mathrm{corot}}$	$11\overset{\mathrm{h}}{.}193$	$\mathscr{P}_{\mathrm{corot}}$	$11\overset{\mathrm{h}}{.}099$	$\mathscr{P}_{\mathrm{corot}}$	$11\overset{\mathrm{h}}{.}372$
ϕ_0	$323°$	ϕ_0	$54°$	ϕ_0	$233°$
A	$15 \pm 2\,\mathrm{km\,s^{-1}}$	A	$6 \pm 2\,\mathrm{km\,s^{-1}}$	A	$3 \pm 2\,\mathrm{km\,s^{-1}}$
k	3.706	k	3.664	k	3.825

$\mathscr{P}_4$ parameters		$\mathscr{P}_5$ parameters		$\mathscr{P}_6$ parameters	
$\ell = 2$	$m = +2$	$\ell = 3$	$m = +3$	$\ell = 3$	$m = +3$
$\mathscr{P}_{\mathrm{obs}}$	$-12\overset{\mathrm{h}}{.}3926 \pm 4$	$\mathscr{P}_{\mathrm{obs}}$	$-6\overset{\mathrm{h}}{.}7537 \pm 1$	$\mathscr{P}_{\mathrm{obs}}$	$-6\overset{\mathrm{h}}{.}9920 \pm 2$
$\mathscr{P}_{\mathrm{corot}}$	$10\overset{\mathrm{h}}{.}929$	$\mathscr{P}_{\mathrm{corot}}$	$9\overset{\mathrm{h}}{.}072$	$\mathscr{P}_{\mathrm{corot}}$	$9\overset{\mathrm{h}}{.}173$
ϕ_0	$332°$	ϕ_0	$306°$	ϕ_0	$153°$
A	$3 \pm 2\,\mathrm{km\,s^{-1}}$	A	$6 \pm 2\,\mathrm{km\,s^{-1}}$	A	$3 \pm 2\,\mathrm{km\,s^{-1}}$
k	3.533	k	2.435	k	2.489

from the corresponding single-mode model, but only at the level of a few percent. The main reason is probably that the sampling for the multimode model was the same as for the data, while for the single mode check-models only one cycle each was calculated with 16 model profiles. Now with these complete sets of stellar and pulsational model parameters, more demanding test than reproducing the data used for the analysis can be performed.

5.1.3.2 Detailed modelling

Baade's 1987 spectra: The next test was to model the He$\textsc{i}$ 6678 variability observed by Baade with the CAT/CES (Rivinius et al. 1998c). This data was taken in 1987, almost ten years before the main campaign on μ Cen started. In Fig. 5.6 the observed data are compared to the model. Obviously, the time elapsed had an influence on the accuracy of the phasing, which was one of the reasons why it was not used for the analysis. But still the pattern can be recognized with some shift of about 0.15 day. The uncertainties of $\mathscr{P}_1$ over this time can add up to about 0.05 day only, but since this is the best constrained of all six periods, the others may introduce larger shifts. The individual contribution of a single period uncertainty to the overall effect of all six periods can hardly be estimated and, therefore, not be used to improve the periods. A difference that cannot be explained this way is that the retrograde feature apparent in the third panel from above and the prograde feature in the second panel from above are much stronger than modelled. However, in the other panels the features are of comparable strength. Since μ Cen also shows aperiodic processes in this line, the visibility of these two individual features could have been enhanced by stochastic variations.

The 1999 observation of Balona et al.: Balona et al. (2000) recently cast doubt on the period analysis presented by Rivinius et al. (1998b). This was already answered by Baade et al. (2000) from the point of view of period analysis. But whether the observations published by Balona et al. (2000, their Fig. 2) can be
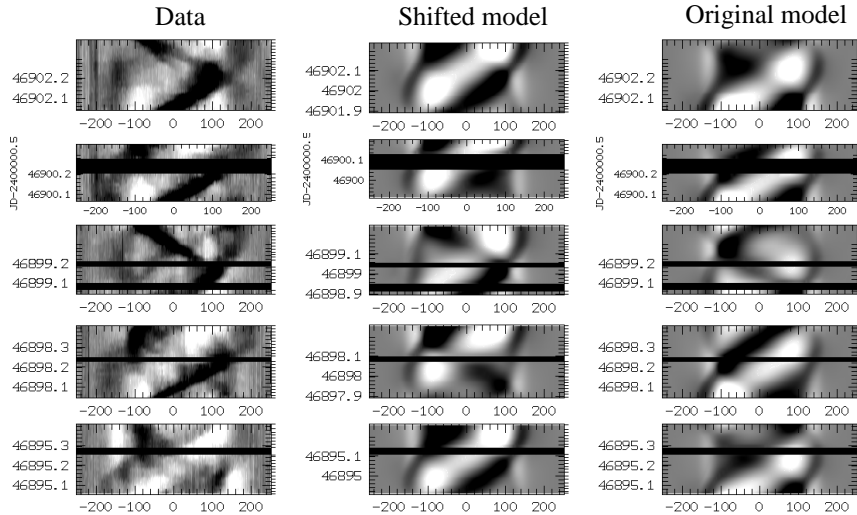
Figure 5.6: CAT data of HeI 6678 taken during five nights in April 1987 (left) and the modelled *lpv* (right). Additionally, the modelled pattern is computed with a time shift of -0.15 day (middle left), which was found to give a better match than the unshifted model. Given that the major part of the data for the period analysis dates from 1995 to 1997, however, this is within the uncertainties of the six contributing periods and phases. The relative strengths of the ridges and valleys in the flux residuals differ somewhat between observation and model, but in principle observed features are reproduced by the multiperiodic nrp-model. The variations at velocities higher than $\pm v \sin i \approx 140 \mathrm{km\,s}^{-1}$ and the presence of backward (right-to-left) traveling bumps in both observations and model are the most striking features reproduced.

reproduced by a multimode *nrp* model still seems a conclusive check. To do so, the dates of observations were extracted from their Fig. 2. Then, the five lines they show were modelled with the parameter values of Table 5.4, and the variability was co-added. With exactly the same periods and phases as derived from the HEROS data obtained between 1992 and 1997, Balona et al.'s (2000) figures, showing spectra taken in 1999, could be very satisfactorily reproduced. Especially the nightly alternating appearance, used as a major argument against the $\mathscr{P}_1$ period, is well explained by interference effects. Therefore, the *nrp* model for μ Cen is complete in the sense that the model is able to reproduce the periodic part of the spectroscopic variability for any epoch within the limits imposed by uncertainties of the periods and phases.

5.1.3.3 Extreme conditions

In the present multimode computations, the most extreme conditions were searched to have an estimate of the minimum and maximum net variability that occurs at times of low and high constructive interference of all modes, respectively. For instance, in modelling the observations by Balona et al. (2000), carried out at the minimum combined amplitude (Baade et al. 2000, their Fig. 1), a maximal true velocity amplitude on the star of $|v|_{\mathrm{max}} \approx 12 \mathrm{km\,s}^{-1}$, maximal fractional radial displacement $|\Delta R|/R \approx 0.002$, and maximal fractional temperature variation $|\Delta T|/T \approx 0.08$ is found.

At the other extreme, the modelling of the CAT/CES data taken in 1987 during times of high constructive interference gave $|v|_{\mathrm{max}} \approx 33 \mathrm{km\,s}^{-1}$, maximal fractional radial displacement $|\Delta R|/R \approx 0.015$, and maximal fractional temperature variation $|\Delta T|/T \approx 0.24$. However, the latter pulsational configuration exceeds the linearity limits, especially in v_{rot} and T, moreover the author of the BRUCE-code recommends care in taking large temperature amplitudes at face-value (Townsend, priv. comm.). One may, nevertheless, say this is unphysical. But since this is not a stationary configuration that had developed by itself, but rather has been forced by the beating of otherwise linear pulsations, this might in turn even be the instability leading to the bursting ejection of material. Additionally, although $v = 33 \mathrm{km\,s}^{-1}$ is greater than the speed of sound (typically $\approx 20 \mathrm{km\,s}^{-1}$), this does not necessarily mean that shocks will develop. This is strictly valid only for fully stochastic motions. For ordered motions, it is rather the local velocity shear over some kind of coherency length, that is limited by v_{sonic}. For pulsation, this velocity shear depends strongly on the mode characteristics. The importance of this coherency length becomes clear if one recalls that ordered motions like rotation increase from $0 \mathrm{km\,s}^{-1}$ at the
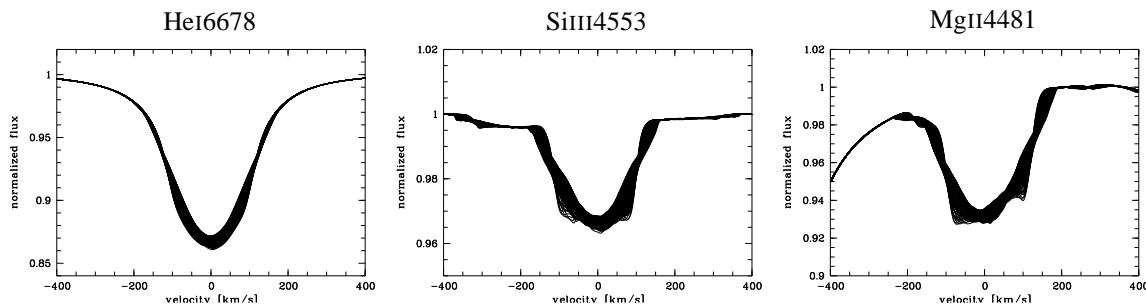
Figure 5.7: Modelling of spikes at times of high pulsation amplitude in μ Cen. The spikes are reproduced at the observed positions, about $\pm 90 \ldots 100\,\mathrm{km\,s^{-1}}$, and with the observed relative strengths between individual lines, strengthening from He I 4471 to Si III 4553 and Mg II 4481, but too weak in general.

pole to about $20 \times v_{\mathrm{sonic}}$ at the equator without shocks.

5.1.3.4 Periodic high velocity spikes

Rivinius et al. (1998b) discussed the presence of phase locked high velocity spikes, resembling those in ω CMa. They seem to be present at times of high combined velocity amplitude only. Results on ω CMa (Sect. 5.2) show that spikes are indeed a high amplitude phenomenon, occurring because the star is viewed pole on and the pulsation is dominated by horizontal velocities. Since both is also the case for μ Cen a series of model calculations, taking into account all six modes, was computed for an epoch of high combined amplitude, indeed showing spikes (Fig. 5.7).

5.2 ω Canis Majoris

While μ Cen was from the beginning of the project intended as a test case for *nrp* modelling, the pole-on Be star ω (28) CMa (HD 56 139, HR 2749, B3IVe, $m_{\mathrm{V}} = 4.03\,\mathrm{mag}$) has increasingly gained attention in recent years. The two main reasons for this interest are the very strong, but rare outbursts, one of which started recently in 2001 (Štefl et al. 2001, 2003a), and the well known short periodicity. This was analyzed most recently by Štefl et al. (2003b) and modelled by Balona et al. (1999), who declared *nrp* would not be able to explain the behaviour of the *lpv*.

Although the periodic line profile variability (*lpv*) was the first to be seen in a Be star, detected by Baade (1982) with $\mathcal{P} = 1.37\,\mathrm{day}$, the *lpv* properties indeed did not seem favourable for a test. The variations are so strong, that they were not believed to be modellable with a normal, linear model. In fact, investigations since turned up many more line profile variable Be stars, of which ω CMa exhibits the most prominent short periodic *lpv* known of all Be stars. Nevertheless many investigators regarded the object as proto-typical, and this stance could finally be confirmed, as will be shown in Chapter 6. The periodicity was confirmed by many authors using different data sets (e.g. Harmanec 1998; Štefl et al. 1999; Balona et al. 1999). The *lpv* was present at least for the past 20 years, and fully coherent between 1996 and 2000. In times of outburst, however, either phase or period may shift somewhat (Štefl et al. 2003b). No other coherent stellar period is known for ω CMa.

As said above, Balona et al. (1999) did not succeed in reproducing the *lpv* of He I 6678 assuming *nrp*, while an (ad-hoc) model based on variable local linewidth (e.g. by non-uniform micro-turbulence across the stellar surface) could reproduce the He I 6678 at least in principle. But Maintz et al. (2000), exploring a larger parameter space than considered by Balona et al. (1999), were able to model the *lpv* of ω CMa not only for He I 6678, but for all lines in the visible spectrum in high detail. This study was reperformed and expanded for this work, using the same methodology as for μ Cen.

5.2.1 Initial guess parameters

5.2.1.1 Pulsational mode

During the intensive modelling of μ Cen it became clear that profile features like spikes and ramps could not be reproduced for modes other than $m = +2$ and a negative sign of the observed period (see Sect. 5.1.1.2 and Eqn. 5.2 for explanation). Therefore, also following Baade (1982), it was decided to concentrate on $\ell = 2$,
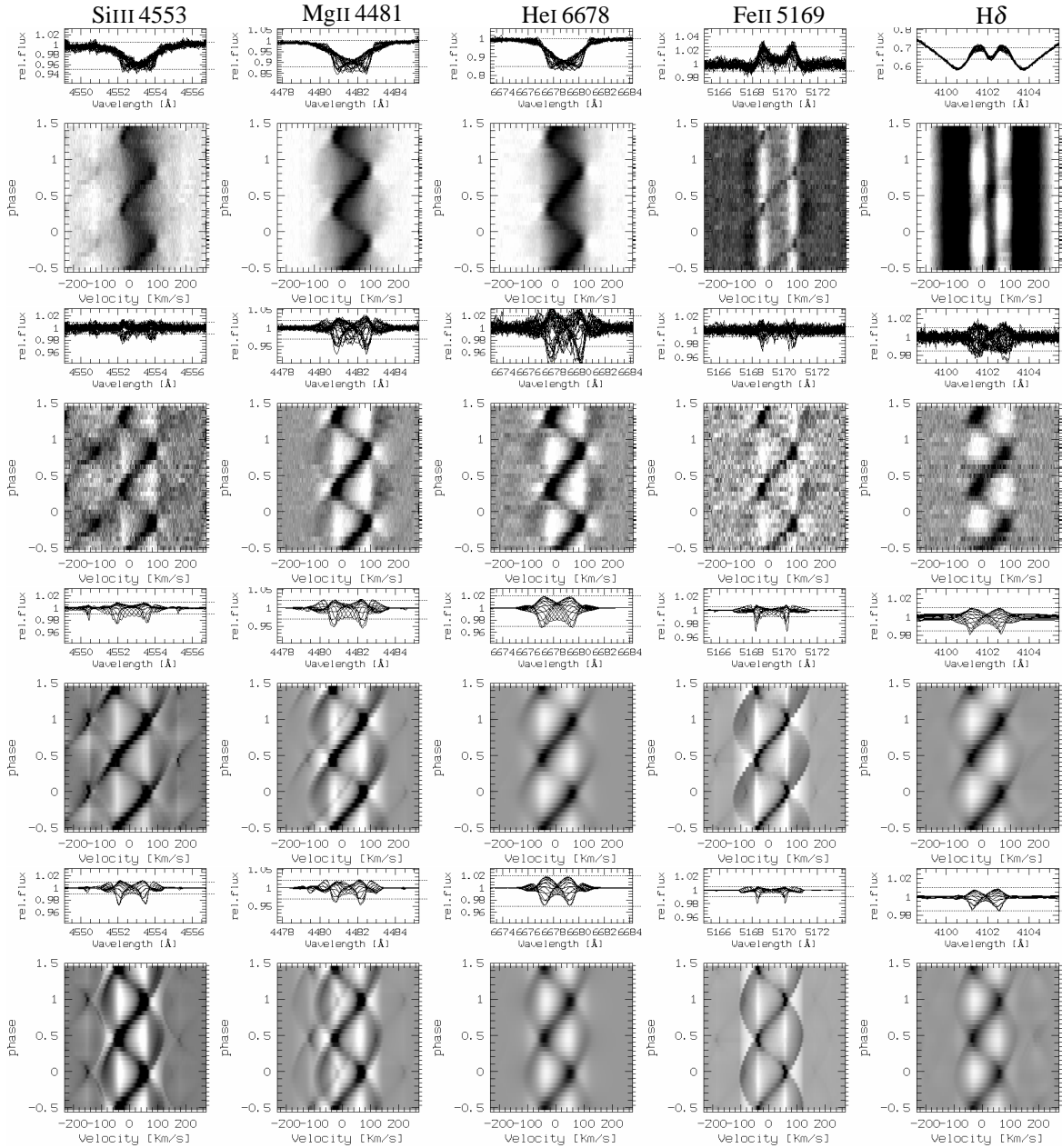
Figure 5.8: In order to minimize the influence of the emission contribution, not the absolute line profiles (top row: overplot of spectra, second row: phased "dynamical" spectrum) are considered for modelling, but the residuals from the mean profile (third row: phased "dynamical" residuals). The models computed with the two best matching parameter sets (see Sect. 5.2.1.2) are shown in the fourth row from top (lower $v_{\rm rot}$) and the bottom row (higher $v_{\rm rot}$).

$m = +2$, sign$(\sigma_{\rm obs.}) = -1$ for modelling. Numerous spot checks with other modes, including those with sign$(\sigma_{\rm obs.}) = +1$, and reasonable stellar parameter sets confirmed that the *lpv* cannot be accounted for by modes other than $\ell = 2, m = +2$ or $\ell = 3, m = +2$. In a pole-on oriented star like ω CMa, these modes do not bear strong observational differences, but the $\ell = 3, m = +2$ mode requires higher amplitudes in temperature and geometric distortion to yield a similar reproduction of the observations as does $\ell = 2, m = +2$. Since the amplitudes are already quite strong, compared also to the local sound speed, for $\ell = 2, m = +2$ this mode, with sign$(\sigma_{\rm obs.}) = -1$, is adopted as the pulsational mode also of ω CMa.
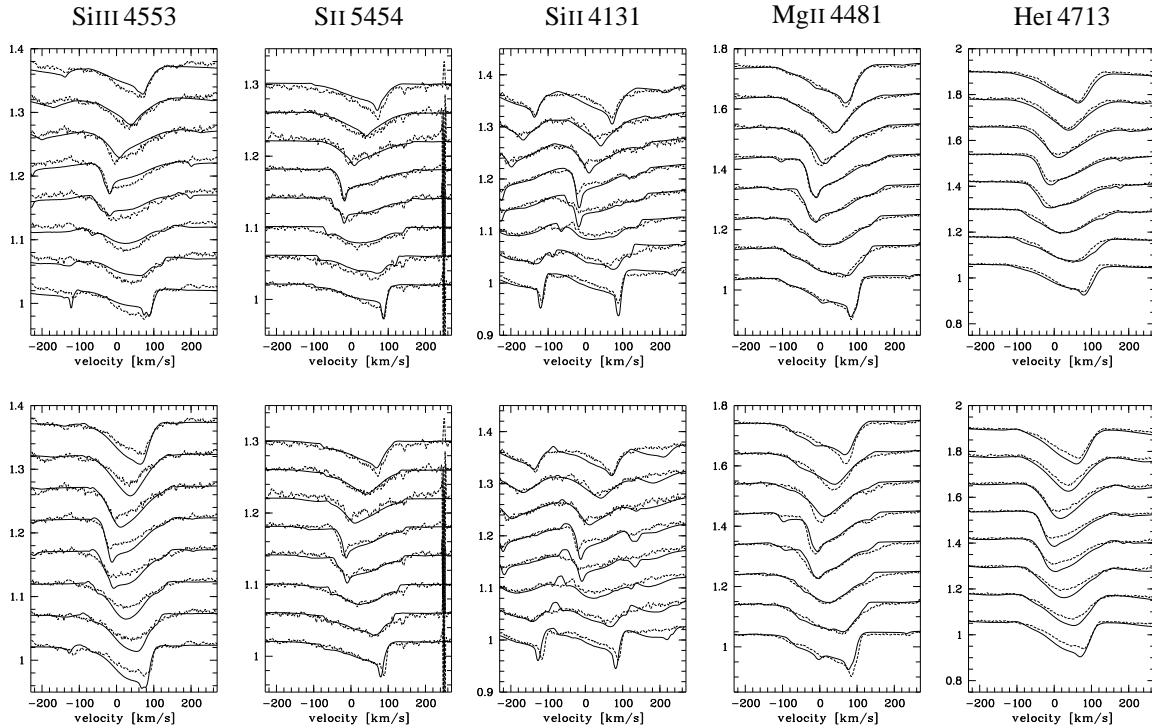
Figure 5.9: Comparison of modelled (solid) and observed (dashed) *lpv* for the lower and higher v_{rot} (upper row: 250 km s^{-1}, and lower row: 350 km s^{-1}, repectively). Besides the spectral lines indicated on top, some panels also contain neighboring blended lines. Phase increases from bottom to top. The observational data of SII 5454 shows CCD artifacts at about 140 km s^{-1} and 250 km s^{-1}. Only every other of the 16 computed phase steps is shown in order not to overload the plot.

5.2.1.2   Model parameters

For further modelling to obtain the closest agreement between model and observations, a wide grid across plausible combinations of stellar parameters and pulsation amplitudes was computed, like for μ Cen. For ω CMa this grid covered three polar effective temperatures (18, 20, and 22 kK), three masses (8, 9, and 10 M$_\odot$), five polar radii (4.5, 5, 5.5, 6, and 6.5 R$_\odot$), and five rotational velocities (200, 250, 300, 350, and 400 km s^{-1}) at five projected values ($v \sin i = 85, 90, 95, 100,$ and 105 km s^{-1}). The limits were selected to cover all plausible parameter combinations for a star normally classified around B2-3 IV. However, note that the example of α Eri has shown recently that rapid rotation close to critical values may severely affect these numbers (Domiciano de Souza et al. 2003).

Close to local minima, a finer grid mesh was used. In total, synthetic spectra for several tens of thousands of parameter sets were computed. For each parameter set, sixteen profiles for the HeI 4713 line were computed in equidistant phase steps across one pulsation cycle. For comparison, the 32 spectra observed in January 1999 with FEROS were also phase-binned into 16 steps. The HeI 4713 line was chosen for its low sensitivity to circumstellar influences. The best matching parameters were, then, determined using a χ^2-test, just as for μ Cen. Two local minima were found in the χ^2 distribution. One is close to the parameters published by Maintz et al. (2000), while the other, being deeper but also narrower, is at lower rotational velocities of $v_{\mathrm{rot}} = 250$ km s^{-1}.

The χ^2 values typically range from 8 to 11 for the $\ell = 2$, $m = +2$–mode, but will be significantly higher for other modes. In order to compare the quality of the parameter sets, more spectral lines in addition to HeI 4713 were computed and visually compared with the observations. In the following both these parameters sets (Table 5.5) are discussed.

5.2.2   Modelled line profile variation

The two lower rows of Figure 5.8 show the residual variability for both selected parameter sets in grayscale representation. The residual variability of the displayed spectral lines is reproduced well, also for those of

55

Table 5.5: Stellar and pulsational input parameters for modelling the *nrp* with the lower v_{rot} of $250\,\mathrm{km\,s^{-1}}$ (left) and $350\,\mathrm{km\,s^{-1}}$ (right). Also shown are several derived parameters. k is the ratio of horizontal-to-vertical velocity amplitude components. For an explanation of the meaning of the "apparent" parameters in a rapidly rotating star see Sect. 5.1.2.

Input parameters		
	$250\,\mathrm{km\,s^{-1}}$	$350\,\mathrm{km\,s^{-1}}$
Polar radius, R_{polar}	$5.0\,R_\odot$	$6.0\,R_\odot$
Polar temperature, $T_{\mathrm{eff,polar}}$	$18\,000\,\mathrm{K}$	$22\,000\,\mathrm{K}$
Mass, M	$11\,M_\odot$	$9\,M_\odot$
Rotation, v	$250\,\mathrm{km/s}$	$350\,\mathrm{km/s}$
Inclination, i	$24°$	$15°$
ℓ	2	2
m	$+2$	$+2$
$\mathscr{P}_{\mathrm{obs.}} = \mathscr{P}_{\mathrm{inert.\ frame}}$	- 1.37 days	- 1.37 days
Full Amplitude $A = \lvert v_{\mathrm{max}}\rvert$	$45\,\mathrm{km/s}$	$35\,\mathrm{km/s}$

Derived parameters		
Rotational period, $\mathscr{P}_{\mathrm{rot}}$	1.09 days	1.10 days
Critical period, $\mathscr{P}_{\mathrm{crit}}$	0.52 days	0.89 days
Critical velocity, v_{crit}	$529\,\mathrm{km/s}$	$436\,\mathrm{km/s}$
$\mathscr{P}_{\mathrm{corot}}$	0.91 days	0.92 days
k	5.41	2.65
polar gravity, $\log g$	4.08	3.84
equatorial gravity, $\log g$	3.94	3.28
true luminosity, $\log(L/L_\odot)$	3.321	3.718
apparent luminosity, $\log(L/L_\odot)$	3.363	3.891
apparent T_{eff}	$17\,281\,\mathrm{K}$	$19\,658\,\mathrm{K}$
apparent radius	$5.370\,R_\odot$	$7.606\,R_\odot$

partly circumstellar origin like Hδ. This includes the strong absorption peaks ("spikes") and accompanying broad absorption wings ("ramps") on respective opposite sides of the line profile, present in the phases of extreme asymmetry. Such structures are found in the majority of all spectral lines, although with with variable prominence, and were previously described by Baade (1982, for MgII 4481 and HeI 4471) and Štefl et al. (1999, for HeI 6678). Since both parameter sets would be acceptable judged by the residual variability, further comparison is based on the variability of the absolute line profiles.

In Fig. 5.9, the variations of modelled and observed absolute line profiles are shown for both parameter sets. Several lines of different ions with presumably minimal emission contribution were selected. Keeping in mind that the parameter sets were selected exclusively on the base of the HeI 4713 residual *lpv*, both parameter sets reproduce well the absolute line profile variability in general, but also show some problems.

The local χ^2 minimum for the slowly rotating parameter set is about 6.9 (Fig. 5.10), compared to a mean value of about 9. The local minimum is narrow with respect to the stepsize of the coarse model grid. The modelled HeI 4388 line shows that the $\log g$ is too high for the slow v_{rot} parameters, since the wings are too broad. The same effect is even more visible in modelled Balmer lines. Clearly the mass-to-radius ratio is too high for a star classified as luminosity class IV. Comparing the SiII to the SiIII line also makes clear that the model temperature is slightly too low. The rotation rate of $w = 0.5$ critical is very low compared to Be stars in general (see e.g. Chauville et al. 2001; Yudin 2001). On the other hand, the spikes are perfectly positioned and the line strengths are well reproduced for SII and MgII.

For the minimum marking the rapidly rotating model the χ^2 reaches only 7.9 (Fig. 5.10), with a FWHM of about 3 times the stepsize of the coarse grid. While the lower mass and, hence, lower $\log g$ of this parameter set reproduce the wing broadening better, the temperature is somewhat too hot and the overall reproduction of
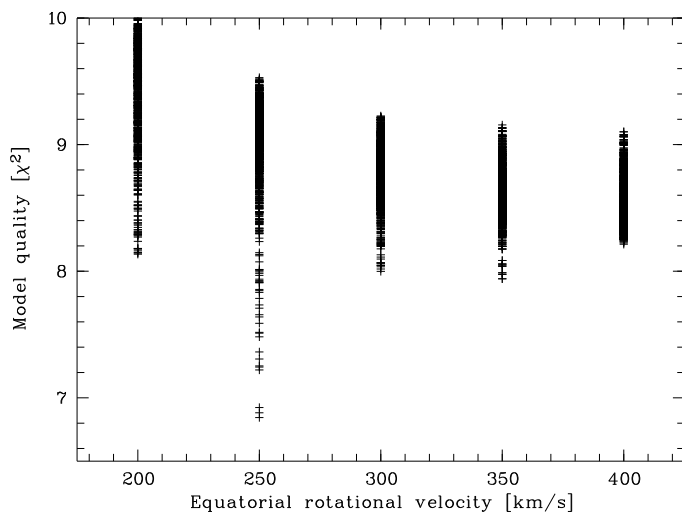
Figure 5.10: The χ^2-values of the coarse model grid (compared to the observations) plotted against the rotational velocity of the respective model. See Sect. 5.2.2 for discussion.
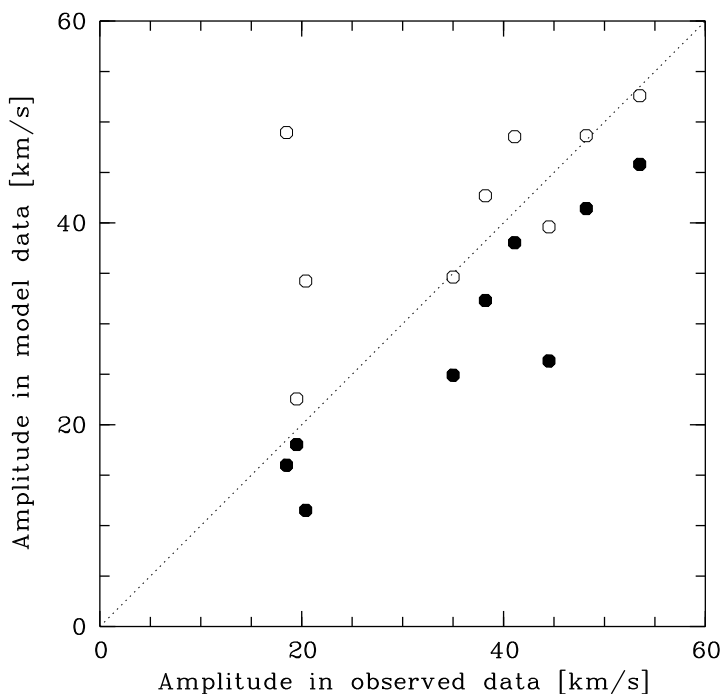

Figure 5.11: Comparison of the line core velocity amplitudes, measured in the observational data (Štefl et al. 2003b) vs. the lower v_{rot} (open circles) and higher v_{rot} (filled circles) models for a number of lines.

the *lpv* is inferior compared to the slow rotating model. Common to all modelled lines, the position of spikes, which in the model depends mostly on $v \sin i$ and amplitude, are too close to the line centre. However, the rapid rotation of $w = 0.8$ is well in agreement with the expectation for a Be star.

The RV-amplitudes of spectral lines were found to differ both from line to line, but also from season to season (Baade 1982, Štefl et al. 2003b). While the latter can be explained due to influences of the variable circumstellar contribution, the first is a property of the *lpv* itself, and should therefore be reproduced by the model computations. Fig. 5.11 shows the amplitudes of nine spectral lines (HeI 4387, 4471, 4713, 6678, 4026, 4144, MgII 4481, NeI 6402, and SiIII 4553) measured in the observations (Table 2 of Štefl et al. 2003b) and for both model parameter sets. Both agree in general well. But while the rapidly rotating model is slightly worse for lines with high RV-amplitude, the slowly rotating one fails completely for two of the lines with low RV-amplitude, namely HeI 4026 and 4144.

5.2.3 Absolute stellar parameters

Several determinations of fundamental stellar parameters of ω CMa have been published.

From optical and infrared photometric measurements, taken shortly before an outburst in the late 70s and early 80s, Dachs et al. (1988) derived $T_{\text{eff}} = 20\,000$ K, $\log g = 4.0$, and $R_\star = 5.2\,R_\odot$ using $E(B-V) = 0.06$ mag. The measured V magnitude was 3.81 and 3.92, respectively. For the same epoch, but using spectrophotometric data, Kaiser (1989) derived $T_{\text{eff}} = 18\,600$ K and $\log g = 3.4$ with $E(B-V) = 0.04$ mag. Including also the envelope in the flux model, Dachs et al. (1989) derived $T_{\text{eff}} = 18\,000$ K, $\log g = 4.0$, and $R_\star = 5.2\,R_\odot$ with a total (i.e. inter- and circumstellar) $E(B-V) = 0.05$ mag.

Harmanec (2000) got $T_{\text{eff}} = 17\,100$ K and $R_\star = 9.91\,R_\odot$, based on the Hipparcos parallax of $\pi = 3.53 \pm .58$ mas, $V_0 = 4.0$ mag, and spectral type vs. parameter calibrations, but did not publish which $E(B-V)$ he used. If the spectrophotometric values mentioned above are recomputed using the Hipparcos distance and theoretical ATLAS 9 fluxes, radii close to the one obtained by Harmanec (2000) are derived. Chauville et al. (2001), finally, derived $T_{\text{eff}} = 21\,500$ K and $\log g = 3.81$. This represents a surprisingly large range of parameters for such a bright and nearby star, but is not an unprecedented case: in α Eri the very same is seen, which is most likely a consequence of almost critical rotation (see Part III). Comparison with spectral line modelling in Fig. 5.9 shows that $T_{\text{eff}} = 18\,500$ K and a $\log g$ of about 3.5 (which is between the values in Tables 5.5 and 5.5) seem acceptably close to the true average surface parameters. The spectral type of B3 IV agrees with these parameters as well. Such a spectral type, however, is incompatible with a radius of almost $10\,R_\odot$ but, depending on which calibration is used, rather should be in the order of 5 to $7\,R_\odot$, which is also the range of (polar) radii derived by *nrp* modelling.

The radius determinations depend on the measured and theoretical fluxes, and the distance. Although there are claims of systematic errors in the Hipparcos database (Pinsonneault et al. 1998), such errors are probably not required to explain the discrepancy. Looking at the LTPV photometry shown in Štefl et al. (2003a), confirmed by Hipparcos photometry (see Fig. 8 in Harmanec 1998), the "quiescent ground state" is at least $V = 4.05$ mag, if not fainter. This means the spectrophotometric fluxes obtained by Dachs et al. (1989) have to be corrected not only for the extinction A_V of about 0.015 mag, but also for the envelope excess flux of about 0.13 mag.

The recomputation of the derived radius then becomes $8.6^{+2.5}_{-1.5}\,R_\odot$, taking into account both parallax errors and T_{eff}-$\log g$ uncertainties. The parameters for the more rapidly rotating model (Table 5.5) lie well within this range. The lower radius-to-mass ratio of this parameter set is as well compatible with a subgiant star rather than the closer to ZAMS values of in Table 5.5. All this, including the lower total pulsation amplitude of $35\,\text{km s}^{-1}$, make the higher v_{rot} parameters of Table 5.5 the favoured ones in the end. The intrinsic errors of the parameters derived by modelling the pulsational variability are related to the width of the minimum in the χ^2 distribution. Given the FWHM of the local minimum of the favoured parameter set (Table 5.5), they are estimated to be roughly 1.5 times the stepwidth of the input grid, giving $\sigma_{R_\star} = 0.75\,R_\odot$, $\sigma_{T_{\text{eff,polar}}} = 3000$ K, $\sigma_{M_\star} = 1.5\,M_\odot$, $\sigma_{v_{\text{rot}}} = 75\,\text{km s}^{-1}$, $\sigma_i = 5°$, and $\sigma_A = 8\,\text{km s}^{-1}$. It should be noted that these error estimates disregard potential systematic errors, which to investigate would be beyond the scope of a paper dedicated to an individual star.

5.2.4 Formation of ramps and spikes

Spikes and ramps result from a pole-on geometry in combination with high horizontal pulsation velocities in an $|m| = 2$ mode in conjunction with a high amplitude of several tens of percent of the projected linewidth $v \sin i$. Since the movements on the stellar surface in ϑ direction are not projected with $\sin i$ (at variance to movements in φ, like rotation), the contrast of the *lpv* due to the pulsation will be enhanced for intermediate to low inclination angles, as long as the rotational broadening is still sufficient for Doppler mapping of the stellar surface. The velocity excess of the *lpv* beyond $v \sin i$ is the total horizontal amplitude, that co-adds to the projected rotational velocity.

To illustrate the formation of these features, a set of models of SII 5454 was computed for the same pulsational phase (namely 0.0), but for different velocity amplitudes (Fig. 5.7). A spike becomes apparent with increasing amplitude at the red part of the line profile getting sharper and sharper. Corresponding to this spike, a ramp develops on the blue side of the profile. This combination can be explained by looking at the projected surface velocities. The projected surface velocity of a non-pulsating model ($A = 0$) increases monotonically across the visible stellar disc from $-v \sin i$ to $+v \sin i$. At the phase when the spike is formed, the pulsation velocity field of an $|m| = 2$ mode, however, is rather of a hyperbolic shape. For instance, for the formation of a spike on the red side, like in Fig. 5.7 the projected pulsational velocity field will be zero in the centre and $-A$ at both stellar limbs. Co-adding both fields gives a total velocity of $-v \sin i + (-A)$ at the approaching limb of the star, causing the ramp at velocities exceeding $v \sin i$ (namely by $|A|$), while on the receding side the co-addition
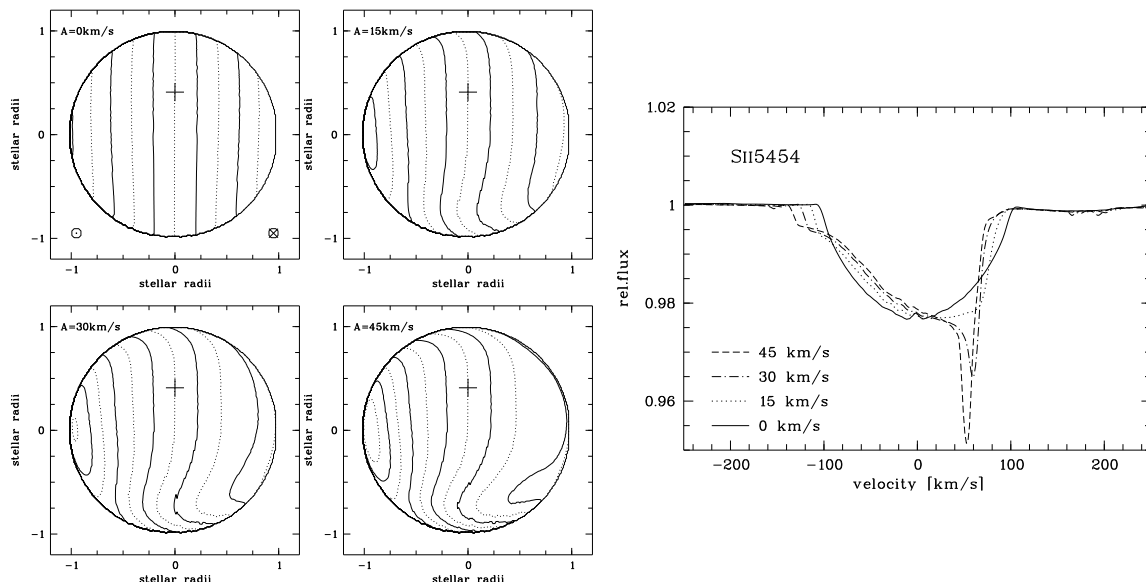
Figure 5.12: Left Panel: Contours of the projected velocity field for a pole-on non-radial pulsator Contours are plotted every $20\,\mathrm{km\,s^{-1}}$, from -100 to $+100\,\mathrm{km\,s^{-1}}$. The stellar pole is marked by a cross and also marks the zero projected velocity contour. Note that for plotting purpose the geometrical deformations were neglected. The leftmost panel shows the pure rotational velocity field, indicating also the sense of rotation by symbols in the lower corners. Right panel: Resulting profiles from the velocity distribution sketched in the left panel. The solid line represents the non-pulsating, but rotating profile. The small central bump is an effect of the latitudinal temperature variation due to gravity darkening. The blueshifted ramp exceeds the stellar $v\sin i$ by about the velocity amplitude of the respective model, while the spike's position is roughly at $v\sin i$ minus this amplitude.

gives $+v\sin i + (-A)$. If A is sufficiently large, at least in the same order of magnitude as $v\sin i$, this causes the steep shoulder of the profile at the red edge and the spike, because no part of the visible hemisphere will be seen at full $v\sin i$ and in turn a larger fraction of the stellar disc will be projected into the spike's velocity range than without pulsation (Fig. 5.7, left panels).

The presence of spikes and ramps can thus be explained naturally as due to high amplitude g-mode pulsation of $|m| = 2$ in a pole-on seen star within the scope of non-radial pulsation. In modes with higher $|m|$ it depends whether $|m|$ is even or odd. In the first case, basically similar features will appear, though weaker. For the latter, spikes at both sides will simultaneous present, so will be ramps half a cycle later. In both cases, additional subfeatures within the line profile will be present. The requirement of high horizontal amplitude limits the possible modes to retrograde ones in Be stars: For prograde modes the co-rotating period is quite short, so that the ratio of horizontal-to-vertical amplitude becomes small (i.e. the mode is getting p-mode characteristics) and the pulsational motions are dominated by the vertical ones. The necessary high horizontal amplitudes would require full amplitudes likely to disrupt the star for prograde modes.

5.2.5 Periodic line profile variability during outbursts

Štefl et al. (2003b) have shown that the *lpv* of some lines changes during outbursts. For these lines the prograde travelling bump weakens or even disappears, and the retrograde travelling feature strengthens (Fig. 5.13, observed data, see also Štefl et al. 2003b). The lines with typically strong circumstellar emission contribution, like the Balmer lines, O I 8446, and Fe II 5169 are affected most, while lines like Mg II 4481 show a weaker effect and purely photospheric lines like Si III 4553 remain unaffected. Since this behaviour has been observed in both the 1996 and 2001 outbursts, it is likely to be a general property of outbursts of ω CMa and, presumably, of the outbursts in other (low $v\sin i$?) Be stars as well. One possibility to explain this is certainly interaction of the variable photosphere with the disc, which at times of outbursts reaches down to the star itself. This could either be some "lighthouse effect" as proposed by Penrod (1986) or the extension of the pulsational velocity field into the disc due to mass-loss (wave leakage).

But there might be another mechanism that could explain this behaviour with fewest possible additional
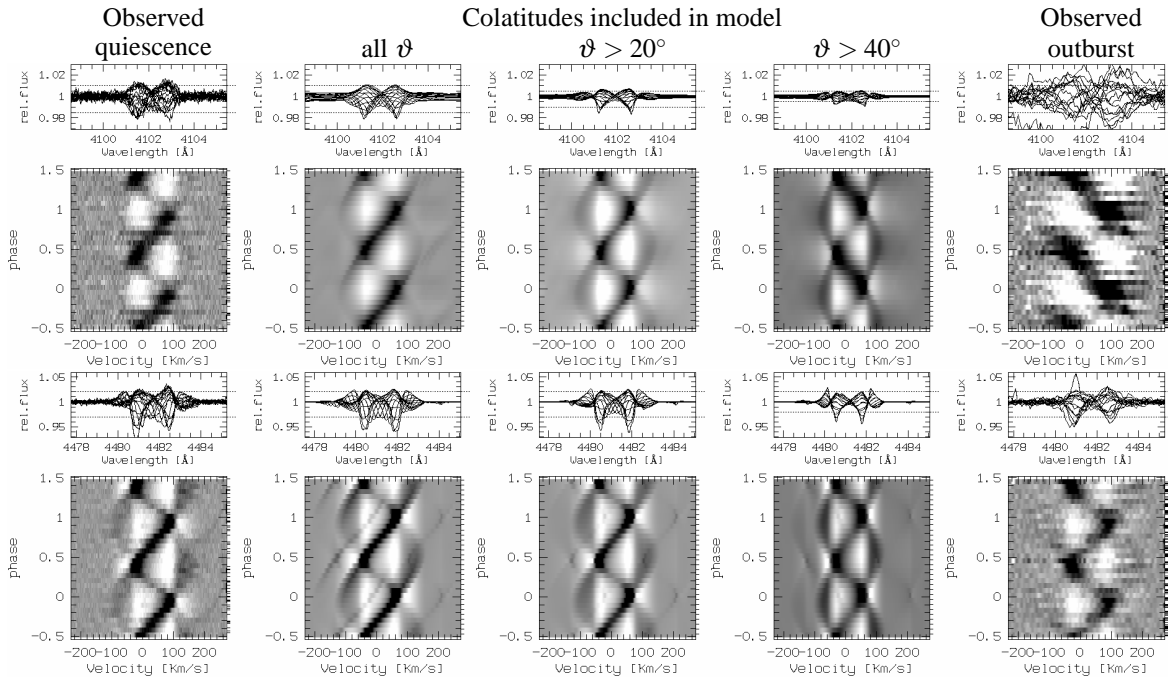
Figure 5.13: Line profile-variability during quiescence and outburst for Hδ (top row) and MgII 4481 (bottom row). To the very left and right observations during quiescence and outburst are shown, respectively. In the middle columns the model (lower v_{rot}, Table 5.5) is shown if the entire visible hemisphere is integrated (all ϑ), and if only stellar latitudes above 20° and 40°, respectively, are taken into account. See Sect. 5.2.5 for a physical interpretation.

assumptions. The disc, being in contact with the photosphere during an outburst, is optically thick at least in the Balmer lines and, though less, probably also in the other mentioned lines (Millar et al. 2000). Assuming this has no effect on the pulsation itself, supported by the largely unchanged behaviour of lines like SiIII 4553 (except a slow phase drift, see Štefl et al. 2003b), the disc will veil the equatorial region as seen by the observer, but only for optically thick lines. This, however, can easily be tested with an *nrp* model: Only points on the stellar disc above some stellar colatitude ϑ are taken into account by KYLIE for computing the observable spectrum (Fig. 5.13).

In fact, the basic behaviour of Hδ and similar lines is reproduced by such a "ϑ-limited" model. To create this effect, the star needs to be veiled up to quite high colatitudes of about 30° to 40° above the equator. Though this seemingly contradicts results that Be star discs only have less than $\approx$ 20° degree opening angle at the inner edge (Hanuschik 1996; Quirrenbach et al. 1997), the disc is certainly not in an equilibrium configuration during an outburst.

This would mean that the disc is optically completely thick in the Balmer and similar lines, and relatively optically thin in the continuum. There might still be some scattering of light even for photons originating from lines like SiIII 4553, but this does not destroy the line profile completely. On the other hand, at least some scattering in the continuum is also required to explain the light changes during outbursts. Polarization measurements indeed typically derive electron optical depths τ_e of the order of unity (e.g. McDavid 2001).

However, such a modified model does not completely explain the observed variability. The ϑ-limited variability should become weaker compared to the full-disc one, (see Fig. 5.13, overplots of the residual variability) while it is in fact observed to be even stronger in Hδ. Similarly, the velocity range of the *lpv* should become narrower, but this is not observed, again in Hδ it becomes even wider. The mean profile of the Hδ during and outside outburst differs by higher wings, possibly due to enhanced Thomson scattering (see Štefl et al. 2003a, their Fig. 3). While the model does not look too bad for MgII 4481 and similar lines, at least in Hδ (and the other Balmer lines) additional variability must be present, that still may require to invoke star–disc interaction mechanisms as discussed above.

5.3 Summary

The photospheric *lpv* of μ Cen and ω CMa were modelled as non-radial pulsation for spectral lines of different ions, using the simulation codes BRUCE and KYLIE by Townsend (1997b). The adopted pulsation mode is $\ell = 2, m = +2$ with a negative observer's period for both cases. This means that the pulsation, being retrograde in the corotating frame, is seen prograde in the observer's frame due to the rapid rotation. The residual variability is reproduced in high detail in all modelled lines, regardless if those lines have emission contribution or not. The absolute line profiles are not reproduced equally well as the residual *lpv* in ω CMa, but this can be attributed to mismatches of the global stellar parameters, for which no unique solution could be found. In any case, this is not a problem of the *nrp* hypothesis itself. For general astrophysical considerations the stellar parameters with higher rotational velocity are preferred as final ones for ω CMa, although the *lpv* is reproduced with not quite as high accuracy as with the lower rotational velocity (see Table 5.5).

That the *lpv* is due to pulsation rather than due to circumstellar material, concurs with the finding by Štefl et al. (2002). They did show that HR 4074, a star of similar spectral type and $v \sin i$ as ω CMa, shows almost identical *lpv*, although the only reported emission episode of this Be stars dates back more than a century. Since it is hardly believable that HR 4074 could have maintained any circumstellar material without showing line emission for such a time, its *lpv* must be of photospheric origin.

Chapter 6

Be stars as a class of pulsating stars

Studies of individual Be stars, like the ones in the previous chapter, are immensely labour intensive. While such works are required to answer questions about the nature of the *lpv* in detail, a generalized picture of Be star line profile variability (*lpv*) might be obtained best from a study of many objects, using a database as homogeneous as possible. With the large HEROS database (Appendix A, or e.g. Kaufer 1998, for an overview), such an approach is attempted here. One of the parameters influencing the appearance of Be stars most most is $v \sin i$. While in the previous Chapters of Part I this has been worked out in particular for the emission line properties, it is in fact true as well for the *lpv*. Since, in Be stars as rapid rotators, $v_{\rm rot}$ covers a much smaller range than does $\sin i$ (the photospheric line broadening points to about 70 to 80 % of the critical velocity, see Yudin 2001, and references therein as well as Part III), this would suggest that the viewing angle, i, has a large effect.

If so, there might be a standard model that can describe the periodic, the transient, or both variabilities in a fair fraction of all early-type Be stars. Such a model could, then, be studied further for possible implications for the explanation of the Be phenomenon. In the following, the HEROS/FEROS database is mined in full for both periodic and transient photospheric variability.

6.1   Period search-techniques

Be stars are known to undergo long-term changes due to the varying amount of circumstellar matter, potentially affecting the results of period determinations. Echelle spectra, however, offer the advantage to investigate a large number of lines. At least some lines can always be found which are known to be hardly formed in the disc, and thus should be only little affected by these long-term changes. In early type Be stars these are typically lines of ions like Si III, or higher-term He I lines, e.g. those at 4026 or at 4388 Å. Though it cannot be entirely excluded that part of the spectra are affected by transiently present pseudo-periods (in particular for those objects observed only in a single season), for most targets the results are ascertained by multi-seasonal observations and the limitation to lines uncontaminated by emission. Even if the photosphere is highly veiled, a comparison of the variation strength with the emission in the respective line provides a hint towards the region the variation is seated in.

In such lines as above mentioned, first the mode, i.e. the position of the line centre, was measured automatically and a period search using a Fourier technique based on Scargle's (1982) algorithm performed. The results were checked against a period search on the full line profile, i.e. applying the above Fourier technique to the change of local intensities with time across the line width. In objects where multiple periods were found, these were iteratively removed using the procedure described by Kaufer et al. (1996). This procedure is fitting a sine-wave to the data, and repeating the Fourier-transformation on the residuals to find the next period.

Besides returning a consistent period by both techniques and in the entire profile, a coherent phase propagation across was required across the profile for acceptance as significant period (for instance, see Figs. 1 and 7 of Rivinius et al. 1998b, also describing the period search method in detail). In other words, pure scatter plots as phase diagrams were rejected. The results of the period search are listed in Table 6.1, while the residual *lpv*, sorted with the respective period, is shown in Figs. 6.1 and 6.2, indicating the coherency of the phase propagation. Appendix D provides further information and comments on each object individually.

Table 6.1: Be stars in the sample for which spectroscopic periods could be established. The error of these periods in frequency space can be estimated from the overall observing length in Table A.1. The photometric periods are taken from various sources discussed in detail in Appendix D. For photometric periods that agree with the main spectroscopic period (or one of its aliases) the amplitudes are typeset in italic. The spectroscopic *lpv* is of ω CMa type (see Sect. 6.3.1) in all listed stars, except for λ Eri, κ CMa, and *o* And.

Name	HR	periods		photom.
		spectr.	photom.	amplit.
		[d]	[d]	[mag]
α Eri	472	1.291	1.26[1]	*0.020*
DU Eri	1423	0.577:	0.654[2]	0.020
DX Eri	1508	1.267	1.267[3]	*0.015:*
λ Eri	1679	0.702	0.702[4]	*0.010*
10 CMa	2492	1.338	1.338[2]	*0.007:*
κ CMa	2538	0.548	1.337[2],1.408[5]	0.015:
ω CMa	2749	1.372	1.47,1.37[6]	*<0.005*
FW CMa	2825	0.839	—	—
	3642	1.130	—	—
	4009	0.650:	—	—
	4074	2.318	—	—
PP Car	4140	0.504:	—	—
δ Cen	4621	1.139:	1.923[4],0.55,1.1[7]	*0.010*
	4625	1.686	—	—
μ Cen	5193	0.503	1.06[8]	<0.005
η Cen	5440	0.577	0.64[9]	0.030
χ Oph	6118	0.649:	> 0.45[2]	0.025
66 Oph	6712	0.452	—	—
28 Cyg	7708	0.648	0.64[10]	*0.025*
31 Peg	8520	0.724:	—	—
o And	8762	0.694	1.58,0.79,0.69[11]	*0.019*

References: [1]Balona et al. (1987); [2]Hubert & Floquet (1998); [3]Štefl & Balona (1996); [4]Balona et al. (1992); [5]Balona (1990); [6]Štefl et al. (1999); [7]Percy et al. (2002); [8]Cuypers et al. (1989); [9]Štefl et al. (1995); [10]Balona (1995); [11]Sareyan et al. (1998).

6.2 Generalized pulsation model

The line profile variations associated to the detected periods will in the following be compared to the pulsational model representations of μ Cen and ω CMa as presented in Chapter 5. These models were shown to explain the *lpv* of these objects very well, namely with a monoperiodic retrograde sectorial pulsation modes with indices $\ell = m = +2$ for ω CMa and a group of such modes together with a group of weaker $\ell = m = +3$ modes for μ Cen. In order to avoid problems arising from multiperiodicity of μ Cen, the following is mainly based on the model for ω CMa, but results have been cross-checked against the model of μ Cen. Since ω CMa, however, is the Be star with the most pronounced *lpv* it is not *a priori* clear that it is a typical member of its class. It has been mentioned already that differences in $v \sin i$ of individual Be stars are largely due to different inclination i, as all Be stars are rapid rotators. Thus, if ω CMa were typical and could be observed at higher inclination, its *lpv* should not differ from the observations of typical high $v \sin i$ Be stars. The differences in the *lpv*s of low and high $v \sin i$ Be stars, however, are quite pronounced, and the transition between both forms is not explained easily without modelling:

– The variability, concentrated in the wings in low $v \sin i$ stars becomes more evenly spread over the profile width at high $v \sin i$.

– Ramps exceeding $v \sin i$ and spikes become less pronounced and finally undetectable at $v \sin i$ between 150 and 200 km s^{-1} and beyond.

– The variability contrast, generally high and about equal for HeI and metal lines in low $v \sin i$ stars decreases as the inclination becomes more equatorial. The variability becomes undetectable with our data in metal lines, but remains visible, though weakly, in HeI lines.
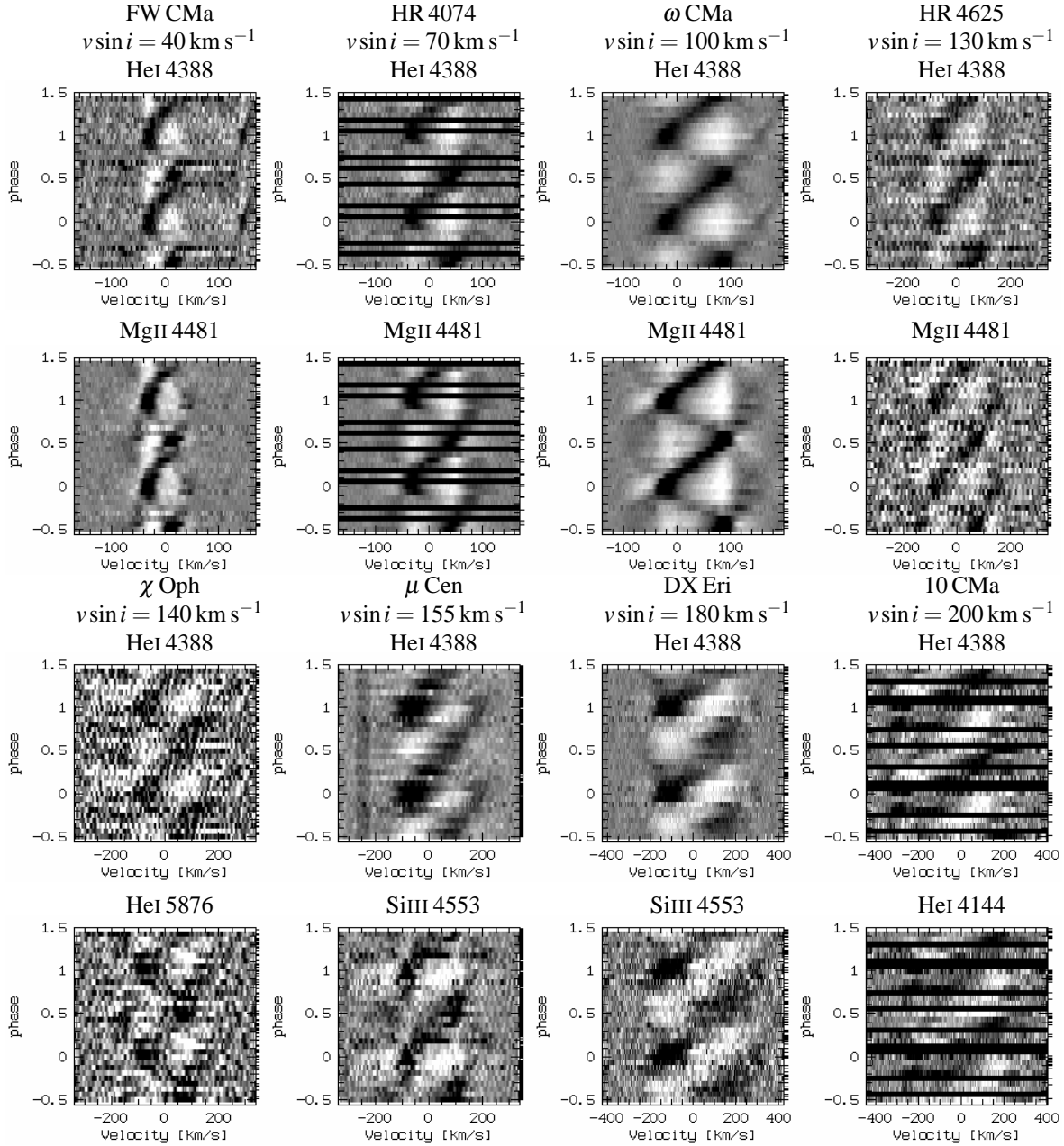
Figure 6.1: Phased main *lpv* in HeI 4388 and MgII 4481 of ω CMa like Be stars with low and intermediate $v\sin i$. Note the typical variability of the far wings (beyond $v\sin i$) in antiphase to the core, seen better in metal lines like MgI 4481 than in HeI lines. In stars with variability too weak to be detected in metal lines, a second HeI line is shown. The periods are given in Table 6.1.

The behaviour of the pulsational model for ω CMa at low $v\sin i$, i.e. the formation of spikes and ramps was already discussed in Chapter 5. Using the model parameters for ω CMa, but changing the inclination at which the model star is observed, four pulsating Be star models were computed for $v\sin i = 40, 80, 160$, and $320\,\mathrm{km\,s^{-1}}$ (Fig. 6.3). It is easily seen that the above listed points, which a model should explain, are in fact solved by *nrp*:

Due to projection effects on the pulsational velocity fields, such *g*-mode pulsation is *always* seen with about its true physical amplitude, while the maximal rotational velocity is projected with $\sin i$. This immediately explains the decrease of variability contrast with increasing inclination. In high $v\sin i$ stars the modelled variability as well exceeds the limits of $v\sin i$, just as in low $v\sin i$ stars, where it causes the ramps and spikes, but since the excess is equal to the true physical pulsation amplitude, this is much less obvious in more equatorial objects, so that ramps should only faintly be seen in observed data with noise contribution, if detectable at all.
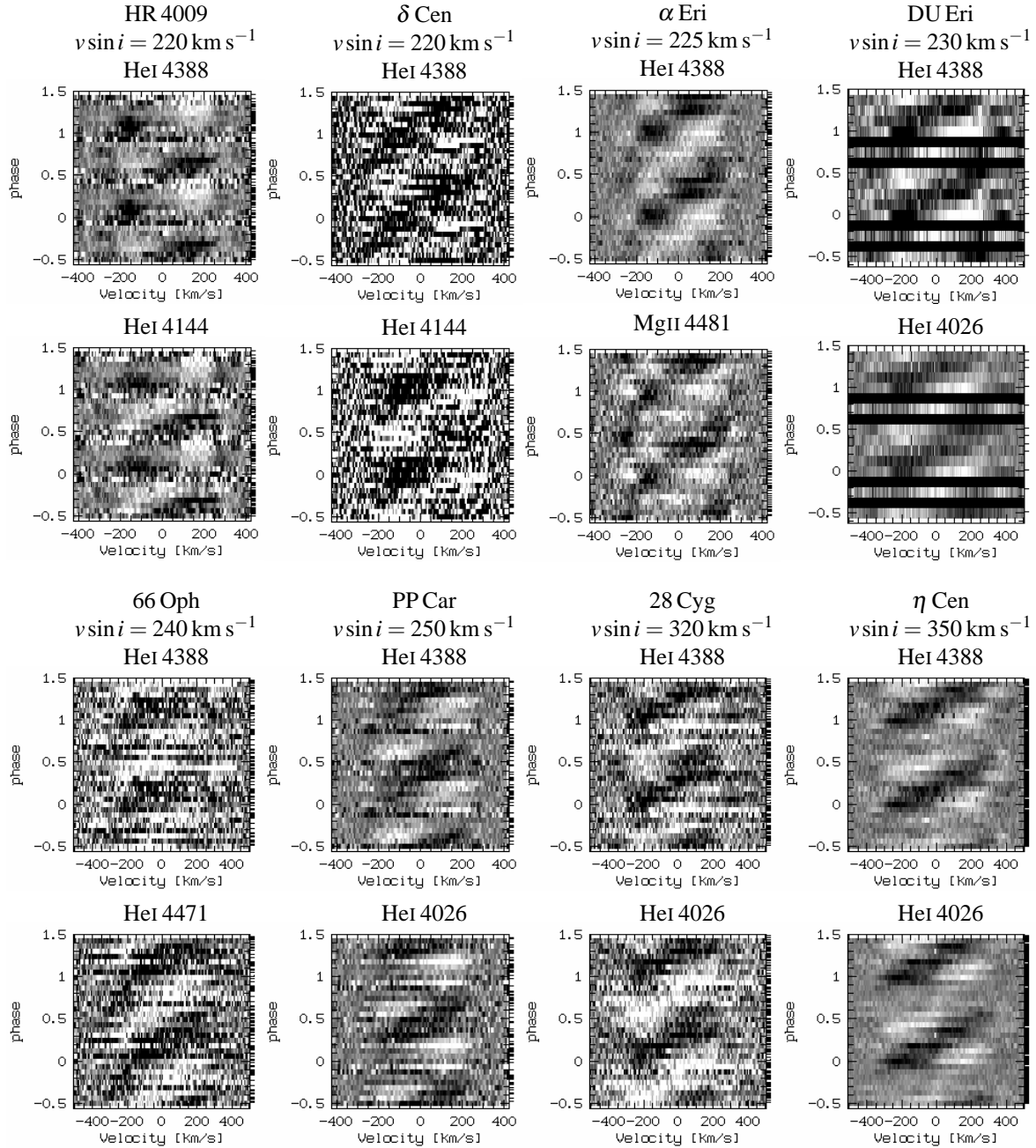
Figure 6.2: Phased main *lpv* of ω CMa like Be stars with intermediate to high $v\sin i$. The periods are given in Table 6.1.

The differences between HeI and metal lines arise from the different intrinsic line width of the species. For metals, the width is dominated by relatively low thermal broadening, while HeI and HI also undergo Stark-broadening effects. The smaller this intrinsic line width is, the more prominent spikes are. On the other hand, since the lines with prominent spikes are typically weak ones, these lines are too shallow to be observable in high $v\sin i$ stars.

The *lpv* of μ Cen and ω CMa have been computed quantitatively with physically state-of-the-art line profile and pulsational velocity-field modelling. Due to the individually different stellar parameters, like mass, radius, temperature etc., the comparison with other objects is comparably qualitative and based on the phenomenological appearance of the *lpv*. Nevertheless, the similarity of Fig. 6.3 with the observed *lpv* in Figs. 6.1 and 6.2 is striking.
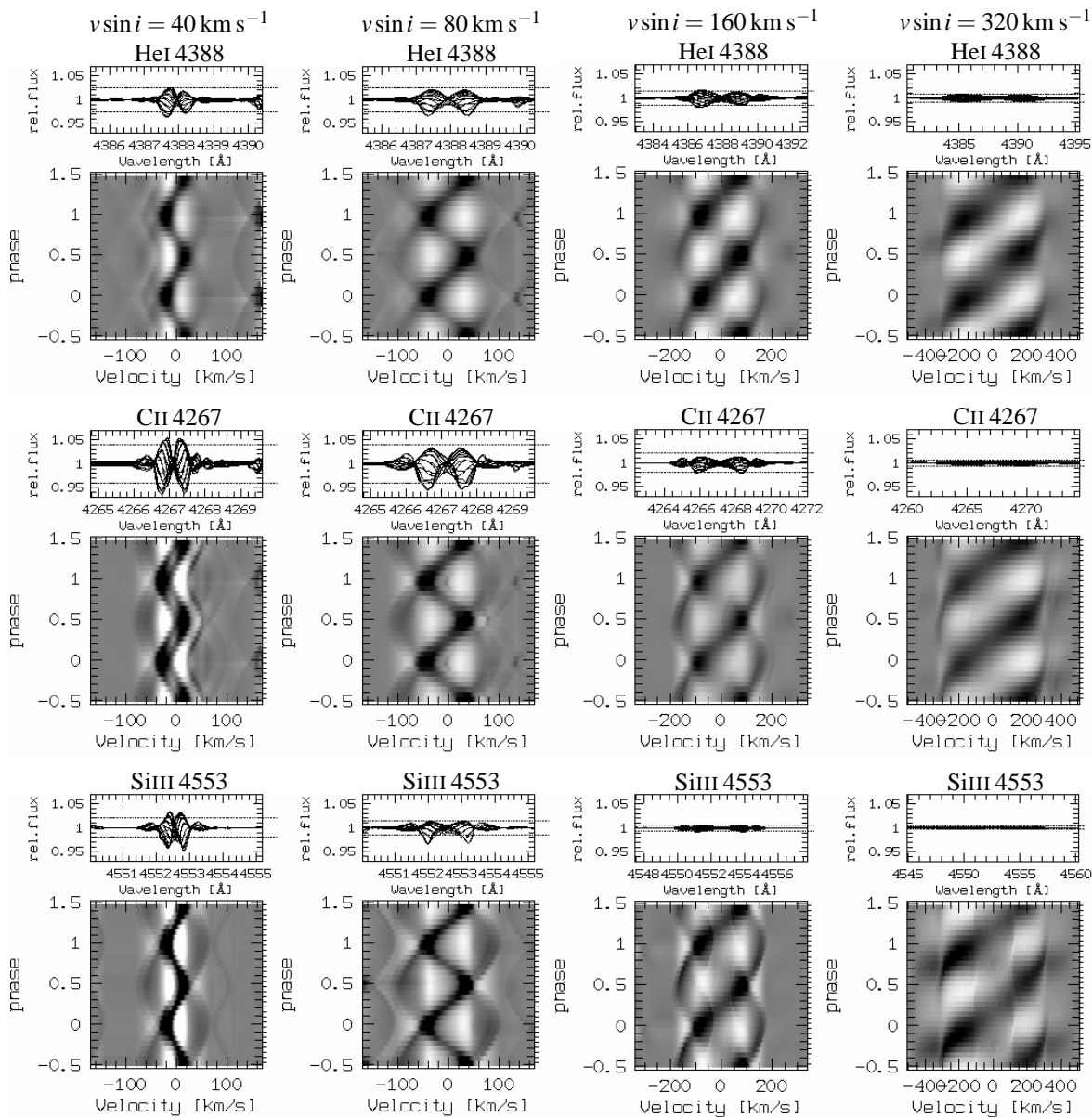
Figure 6.3: Phased *lpv* for ω CMa-like pulsation, computed for $v \sin i$ values of 40, 80, 160, and 320 km s^{-1}. Shown are He I 4388, C II 4267, and S III 4553 The residual variability overplotted on top of each grey-scale picture gives an impression of the decrease of visible contrast with increasing $v \sin i$.

6.3 Types of line profile variations

6.3.1 ω CMa like Be stars

ω CMa is compared to other Be stars in two steps: First, the observed *lpv* is contrasted to observations of other low $v \sin i$ stars, then the high $v \sin i$ model (see above) is compared to high $v \sin i$ Be stars. Despite the extraordinary strong *lpv* of ω CMa commonalities with other low $v \sin i$ stars, exhibiting weaker *lpv*, can readily be identified. Besides FW CMa, HR 4074, and HR 4625 also χ Oph shows enhanced ramps, though quite weakly, and for μ Cen a detailed modelling resulted in the same pulsational mode as was derived for ω CMa in Chapter 5. In all cases, the phase propagation of the variability $\Delta\phi$ across the profile is about 0.6 to 0.7 of the full cycle. All the above mentioned early-type Be stars have $v \sin i < 160$ km s^{-1} (Fig. 6.1).

For the two remaining low $v \sin i$ stars in Table 6.1, 31 Peg and HR 3642, our database is insufficient to investigate the *lpv*. However, the spikes present in 31 Peg (Fig. D.5) and the published spectra of HR 3642 (Carrier et al. 2002) support the similarity with ω CMa also of these stars (cf. Appendix D and Figs. D.1 and

D.5) for further information.

Since these 8 stars represent a significant fraction of *all* early-type low $v \sin i$ Be stars brighter than 6th magnitude (Slettebak 1982, lists 31 Be stars with $v \sin i < 150 \, \text{km s}^{-1}$, of which 23 are of type earlier than B4), it can be concluded that early-type low $v \sin i$ Be stars in general share a common type of *lpv*. The remaining ones not mentioned here have not been observed in our programme, or only single spectra were taken. But there is no reason to assume principally different behaviour for those, since most stars were selected on account of their brightness and coordinates.

If ω CMa is representative of low $v \sin i$ stars, and the difference between low and high $v \sin i$ is mainly the inclination, ω CMa should also look like any high $v \sin i$ Be star if it could be observed equator-on. While it is not really feasible to tilt the star, this can easily be tested with the model (Sect. 6.2). Comparing Fig. 6.3 to Figs. 6.1 to 6.2 it becomes apparent that also most high $v \sin i$ stars are explained by the model of ω CMa, tilted to appropriate inclinations (DX Eri, 10 CMa, HR 4009, δ Cen, α Eri, DU Eri, 66 Oph, PP Car, 28 Cyg, and η Cen).

Of the variability of 20 periodic Be stars listed in addition to ω CMa in Table 6.1, six low to intermediate $v \sin i$ stars are directly comparable to ω CMa, ten intermediate to high $v \sin i$ ones are explainable assuming the same pulsational parameters as for ω CMa, but different inclination. Two more stars with scarce data, but sufficient to derive a period, are compatible with *nrp* as well. For two stars, HR 5223 and ω Ori a period could not be given, but note that the observed *lpv* does not contradict an interpretation as ω CMa-like *nrp*. The three remaining objects with periodic *lpv* unlike ω CMa are discussed in Sect. 6.3.3.

In addition, the phased *lpv* presented in the literature also suits the presented model well in many cases. This is not only true for visual comparison of the spectra, like e.g. in HR 3642 (Carrier et al. 2002), or PP Car (Porri & Stalio 1988). But for stars where mode identifications have been attempted, typically sectorial modes with similar values of ℓ and m are derived, as by Neiner et al. (2002) for ω Ori (see also Table D.1). The long-term coherency of the observed periods also provides an upper limit to potential binary effects. Since no periodic $O - C$-type variations are found, the Be star must reside close to the centre of mass of any presumable binary system (unless all such systems would be pole-on w.r.t. the orbital plane).

6.3.2 Photospheric multiperiodicity

For several stars, multiperiodicity was claimed from spectroscopic data. For at least part of these stars, the additional periods are present in the same photospheric lines as the main periods, meaning they arise from the photosphere as well. This multiperiodicity is in fact another strong and independent argument to ascribe the *lpv* to non-radial pulsation.

In one of the best investigated cases, μ Cen, six photospheric periods are present, grouped around 0.503 d and 0.28 d (Rivinius et al. 1998b). Tubbesing et al. (2000) found a similar grouping for the main period of 28 Cyg, using the lsw97 and ca98 subsets of the data presented here (see Appendix A for the definition of the observing runs). A preliminary analysis of the additional Ondřejov data confirms the two reported periods at 0.64 and 0.62 d. The main period of η Cen could also be shown to be double, namely 0.577 and 0.565 d (see Appendix D). In 66 Oph (Floquet et al. 2002) and λ Eri (Kambe et al. 2000) shorter periods with larger phase propagation than the main one were reported, but due to unfavourable sampling, S/N, and resolving power they could not be confirmed in the available data. From the published properties, however, these periods seem comparable to the *lpv* of the short period group in μ Cen.

6.3.3 Objects with discrepant or no photospheric *lpv*

The observed *lpv* of three investigated objects is not explained by an *nrp* model *á la* ω CMa. These are κ CMa, λ Eri, and o And, shown in Fig. 6.4. However, the *lpv* of these stars, too, generally looks like the one one would expect from *nrp*. So, it might just require higher values of ℓ and m than for ω CMa to explain the observed behaviour in terms of *nrp*. Kambe et al. (2000) in fact propose tesseral *nrp* modes, i.e. $\ell \neq |m|$, to model the *lpv* of λ Eri, which might also apply to the similar *lpv* of κ CMa. However, at least λ Eri and κ CMa are extraordinary active even on shortest timescales of less than an hour. Such activity can be found in other stars as well, but it certainly is on a high level in these two. Whether or not this discriminates these stars from other Be stars or rather is an additional feature is not clear at present, however.

For o And the multiperiodicity, observed photometrically in many different seasons, points to *nrp* as explanation. The *lpv* of o And differs mainly in phase propagation across the profile from the one of other Be stars, which here is about 1 (meaning the feature is visible over a full cycle, just disappearing redwards when a new one appears on the blue side) as opposed to typically 0.6...0.7 cycles in the other objects. Some testing with
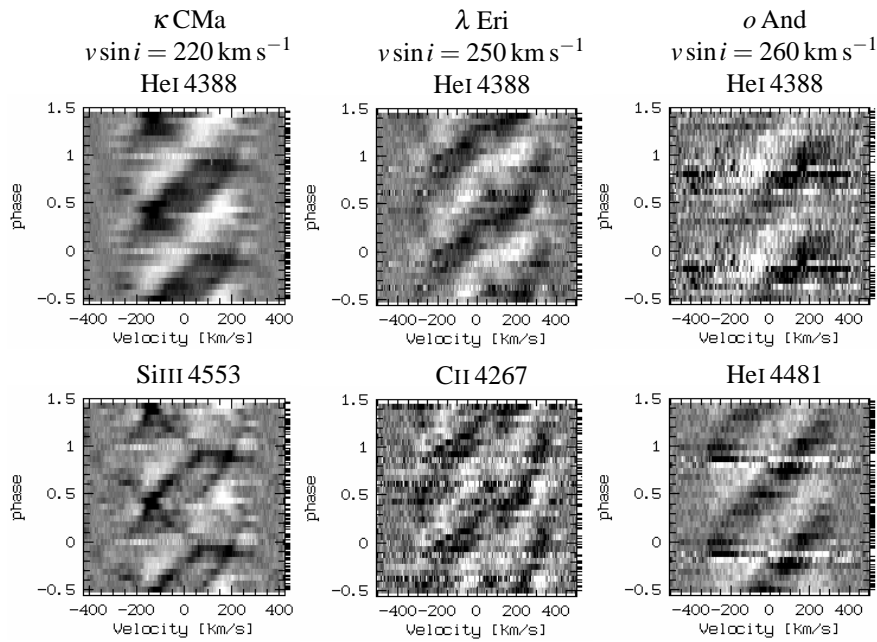
Figure 6.4: Phased *lpv* of the Be stars which do not show ω CMa-like behavior, discussed in Sect. 6.3.3.

the *nrp* model code confirms that such a phase propagation would easily be explainable by a sectorial mode, i.e. $\ell = |m|$, with ℓ higher than 2. In a mode with lower ℓ, i.e. $\ell = 1$, the phase difference should be even less. On the other hand, the strongly variable amplitude was attempted to be explained as an effect of variable magnetic activity, and Sareyan et al. (1998) favour a rotational activity hypothesis together with differential rotation to explain the multiperiodicity. In any case the $\ell = m = 2$ mode explaining the *lpv* of most other Be stars cannot readily be applied to these three objects.

Two of the investigated stars, α Ara and ι Ara, did not show any *lpv*, although photometric periods are reported and sufficient spectroscopic data was obtained. If periodic *lpv* is present in these stars, it must be weaker than in the other objects. For λ Pav the data is too scarce for classification, but *lpv* is present. The *lpv* of π Aqr, finally, does not fit any of the above descriptions (see Appendix D and Figs. D.6 and D.7), but recent high-resolution spectra in a dense monitoring by Peters et al. (2004, priv. comm., and Tennessee Conference Poster) were attributed by them to *nrp*-typical variability in a higher (*p*-)mode than easily identifiable in our data.

6.3.4 Secondary circumstellar (transient) periods

Four stars in the sample exhibit secondary periods within 10 % of their main photospheric ones (Table 6.2). Taking into account the lines these periods are seen in, namely ones usually formed in the upper photosphere and the close circumstellar environment (e.g. Mg II 4481, He I 6678, blue Balmer lines etc., see Štefl et al. 2003b), and their typically transient appearance during outbursts only, already Štefl et al. (1998) attributed them to the circumstellar environment. Although not due to *nrp*, these periods shall at least be described more phenomenologically here, and only preliminary hypotheses are presented for their physical nature.

The phase diagrams of the secondary periods are shown in Fig. 6.5. For μ Cen only the best sampled event is shown. The patterns look rather similar to each other for non-shell stars, but differs drastically for the shell star η Cen. Other than for the photospheric *nrp* pattern, there seem to be little further aspect effects. This also points to a circumstellar origin of the *lpv*. The various short-lived periods in μ Cen support an interpretation as orbital timescale of circumstellar matter ejected shortly before. This is not so easy for the other three objects, where the secondary variability is phase-coherent at least over weeks to months (ω CMa, κ CMa), and even years (η Cen). Similar behaviour was also observed in λ Eri by Kambe et al. (1998), who called them intermittent periods.

In any case, contrary to the *nrp* connected to the primary periods, the secondary periods have to be attributed to processes that strongly interact with or reside in the disc. This could be an additional *nrp* mode on the stellar
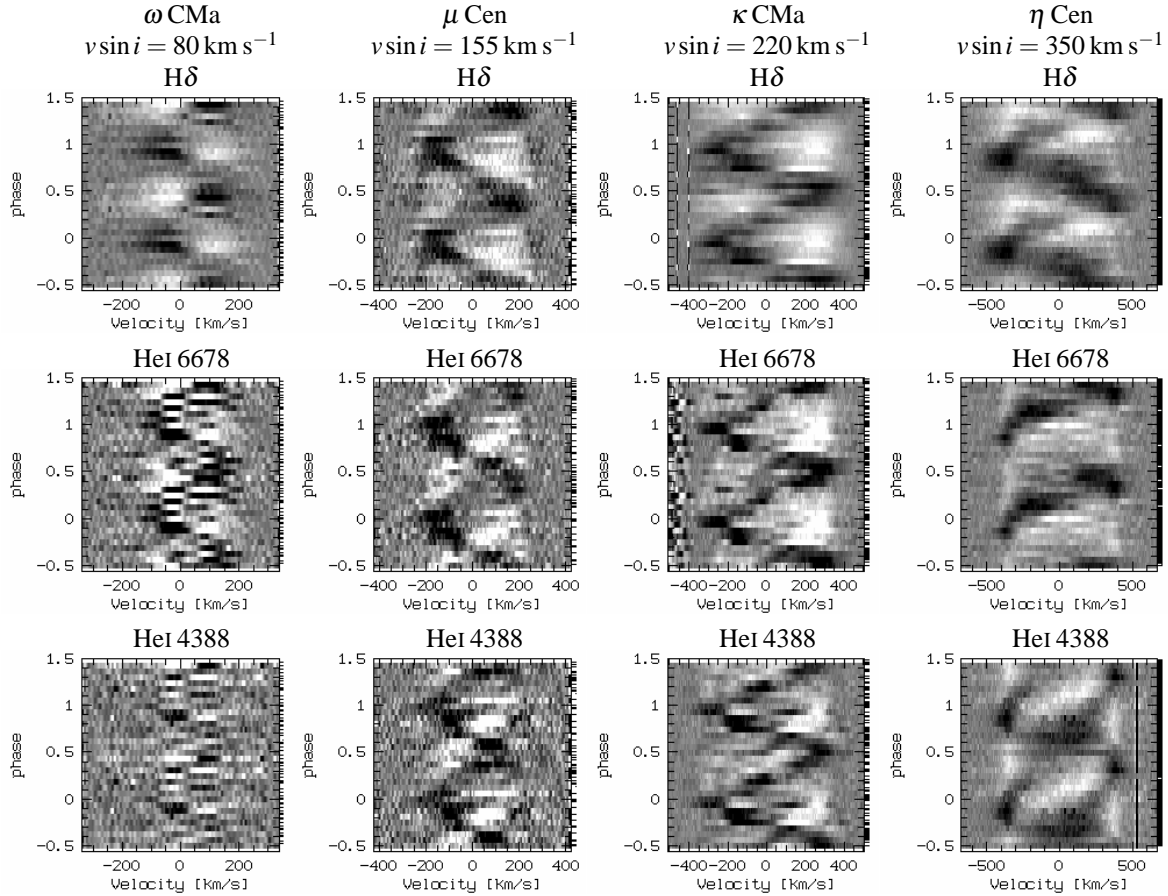
Figure 6.5: *Lpv* phased with transient periods of four Be stars discussed in Sect. 6.3.4, shown for Hδ and two HeI lines. The high scatter in the HeI lines of ω CMa is due to the main period, that is too strong to be completely averaged out in a data string of 45 spectra obtained during the few weeks of the outburst. The periods are given in Table 6.2.

Table 6.2: Secondary (transient) periods of Be stars.

Name	HR	main period [d]	secondary period [d]
κ CMa	2538	0.548	0.617
ω CMa	2749	1.372	1.470
μ Cen	5193	0.503	$\approx$0.622
η Cen	5440	0.577	0.643

surface having an inhomogeneous temperature distribution, but since purely photospheric lines do not show any trace of the secondary periods, such mechanisms are not very likely.

- – Alternatively, the secondary periods could be the rotational ones of the stars, which interact with the disc through magnetic processes. But the *nrp* modelling results for ω CMa point to a significantly shorter rotation period of about 1.1 d, compared to the transient period of 1.47 d. On the other hand, Neiner et al. (2003) recently has found a period of 1.2 d in ω Ori in addition to the main photospheric one of about 1.0 d, which seems connected to magnetic field modulation, and thus to be rotational. The period is prominent only in the UV wind, however, and only hardly present in optical lines.

- – Finally, despite their stability, the secondary periods could entirely be intrinsic to the inner disc, e.g. as the period of a density disturbance. The secondary period of η Cen, remaining phase-coherent over
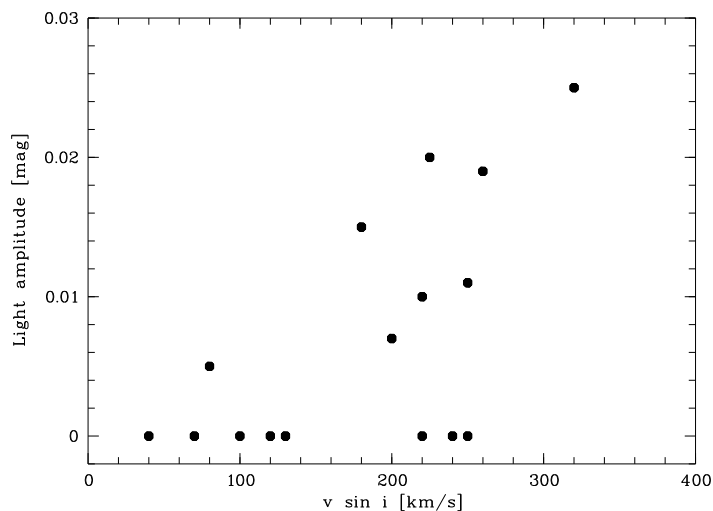
Figure 6.6: The photometric amplitude attributed to the main photospheric period, as derived from spectroscopic data, plotted vs. the $v \sin i$ of the star.

several years, is hardly explained by such an interpretation, however.

Although no firm answer can currently be given, the striking differences in the appearance of the secondary *lpv* from line to line, e.g. in η Cen (Fig. 6.5), can hardly be explained with photospheric line formation properties, but most likely require NLTE effects to be taken into account.

6.3.5 Photometric vs. spectroscopic periods

Most of the objects investigated spectroscopically here were also subject of photometric campaigns. Other than the photospheric periodic *lpv*, which is relatively easy to disentangle from circumstellar effects by using different lines, the photometric variations not only include the periodic photospheric variability, but also the circumstellar changes on all different timescales between hours and decades, convolved into a single number. Photometrically determined periods, therefore, have to be taken with care, especially since transient secondary periods might additionally be present (Štefl et al. 1999). Searching the literature for photometric periods of the 21 stars with identified periodic *lpv* in our sample (Table 6.1), we found the following:

- In 8 stars, no photometric period was detected. These stars typically have low to intermediate $v \sin i$.

- In 5 stars, the periods agree, and no further period is present. These stars typically have intermediate to high $v \sin i$.

- In 5 stars, the periods do not agree. There is no range in $v \sin i$ clearly preferred in these objects.

- In 3 stars, several periods were detected, including the main spectroscopic one. Since this is not always the one with the largest light amplitude, identification of the main period, meaning here the photospheric and long-term coherent one, is only possible if spectroscopic data is taken into account.

On the other hand, there are many later-type Be stars with well-defined photometric periods, which hardly show any variability in spectroscopic data. Some of them were also observed within the framework of this project, but even with FEROS data *lpv* was not found, confirming again the negative result of Baade (1989b). *o* And, B6 III, the latest-type object *lpv* is detected in, is already an exceptional case both in terms of spectral type and the *lpv* pattern.

A spectroscopic study of early-type low $v \sin i$ Be stars in NGC 330 in the SMC gave negative results, i.e. *lpv* was not found at all, although photometric periods are well established (Baade et al. 2002b) and the observational data should have enabled a detection, if the *lpv* properties were the same as for Galactic Be stars. This may point to different variability mechanisms of Be stars in the Magellanic Clouds than in our Galaxy, although further data is needed to ascertain these results. Clearly, photometric studies need to be assisted by spectroscopic observations in order to allow the unambiguous identification of the photometric variability belonging to the periodic *lpv* (see also Sect. 6.3.6 below). Simultaneous observations with both techniques are even required to understand the nature of the additional photometric variability on short timescales.

Only for the objects where the photometric variations connected to the pulsation could be isolated, further predictions by the *nrp* hypothesis can be tested. Other than for the *lpv*, which is Doppler-enhanced at low $v \sin i$, the photometric variability is measured with a broadband filter in the continuum. Therefore, the observable

amplitudes should decrease with $v \sin i$ if the physical amplitudes on the stellar surface are comparable for individual objects. To test this prediction, amplitudes were taken from HIPPARCOS data (Percy et al. 2002) for four stars with consistent main photospheric *lpv* and photometric periods, and from Balona et al. (1987) for α Eri. For three more stars with ambiguous periods, the photometric amplitude for the main one is given by Štefl et al. (1999, ω CMa), Percy et al. (2002, δ Cen), and Sareyan et al. (1998, *o* And). For the 8 stars without any period being detected in photometry, zero amplitude was assumed. With the exception of three outliers, these stars form a well defined band from zero amplitude at low $v \sin i$ to 0.025 mag at high $v \sin i$ (Fig. 6.6). The three outliers are PP Car, 66 Oph, and HR 4009, having intermediate $v \sin i$ of about 200 to 250 km s^{-1} but no detected photometric periodicity. These stars are not the most intensively observed ones, however. The spectroscopic *lpv* is quite weak, partly only recently detected (see Appendix D). Therefore, the assumption of similar physical amplitudes on the stellar surfaces might not hold for these three stars.

6.3.6 The rotational modulation hypothesis

This hypothesis ascribed the periodic *lpv* to circumstellar clouds slightly above the photosphere, which supposedly are forced into co-rotation by magnetic effects. The main arguments in favour of this were:

1. *The photometric* lpv *periods and rotational periods deduced from v* sin *i and spectral type are statistically identical to within* $\sigma = 7\%$ *(Balona 1995)*. Statistical problems with this analysis were already addressed by Baade (1996). In addition, especially for lower $v \sin i$ the determination of the main periods by photometry alone is often ambiguous (see Sect. 6.3.5 and Table 6.1). The true rotational velocities and radii of individual Be stars, used to derive the rotational periods, are not well constrained, either.

2. *The Balmer lines vary on top of the emission, therefore the variation must be circumstellar.* This argument is easily disproved, since the line profiles of non-shell stars are linear superpositions of photospheric and disc contribution. Without cross-checking *pure* emission and *pure* absorption profiles such a claim cannot be made. As was shown in Chapter 5, the *lpv* on top of the Balmer lines of ω CMa is well explained by photospheric *nrp*. Similarly, the residual variability patterns are easily misinterpreted as due to physical emission or absorption. Such claims require the undisturbed profiles to be known. However, the travelling bumps due to *nrp* are neither emission nor absorption, but only a redistribution of the local photospheric equivalent width contributions from the stellar surface in velocity space. Accordingly, the undisturbed profiles can only be derived from detailed modelling.

   Independent support against a circumstellar interpretation of the *lpv* is also given by Štefl et al. (2002). They found HR 4074 to be almost a twin of ω CMa *lpv*-wise, but without any trace of line-emission for at least a century, thus eliminating any potential circumstellar contribution.

3. *The complicated appearance of the* lpv *is not explainable by* nrp. Note that of the seven stars investigated in detail to support this stance, three are shell objects (ζ Tau, Balona & Kaye 1999; η Cen Balona 1999; and ε Cap Balona & Lawson 2001) for which a circumstellar contribution of the disc to the absorption lines is not surprising. The example of η Cen above illustrates the difficulties of the analysis of such objects. For the other Be stars, (ω CMa, Balona et al. 1999; ω Ori, Balona et al. 2001a; μ Cen, Balona et al. 2001b; and λ Eri, Balona & James 2002) refer to Appendix. D, Table D.1 and the references therein.

Among the objects for which enough data is available for an independent investigation, only the case of λ Eri (Balona & James 2002) clearly withstands an explanation as an ω CMa-like Be star, i.e. as non-radial pulsator in an $\ell = m = 2$ mode. This is not a principal problem of the *nrp* hypothesis, however (Sect. 6.3.3). For ζ Tau and ε Cap, the data is not sufficient to countercheck the results for these stars in the light of *nrp*, but none of the published results seem to pose principal problems, certainly less than seemingly did η Cen. The dependence of photometric amplitude on inclination (see above, Fig. 6.6) and the presence of *lpv* spanning the full range of $\pm v \sin i$ (and more) would require the circumstellar clouds to concentrate above the equator. The prominence of the *lpv* in nearly pole-on stars, much stronger than in the equator-on ones, is not explainable by equatorial corotating clouds, but requires a velocity field dominating the *lpv*.

6.4 The short periodic variations of Be stars

A total of 27 early-type Be stars were investigated for this purpose, using more than 3000 spectra. Two of them, μ Cen and ω CMa, were investigated and modelled in great detail. λ Eri is sometimes referred to as

prototypical for the *lpv* of early-type Be stars. However, as the data shows it is in fact a rather unusual case. Line profile variable Be stars should, therefore, not globally be called λ Eri-type stars anymore.

Most of these objects undergo line emission outbursts. In the case of μ Cen the outburst timing could be attributed to the multiperiodic *lpv* already by Rivinius et al. (1998a,b). Two more stars with similar multiperiodic properties were identified, 28 Cyg (Tubbesing et al. 2000) and η Cen, without being able to establish such a close connection to the outburst timing as in μ Cen, however. Other objects showing outbursts are equally well observed, but only a single pulsational *lpv* period is present (ω CMa above, or ω Ori: Neiner et al. 2003, for instance). Some stars show additional periods during outbursts, located in the near circumstellar environment. These secondary, transient periods might even dominate the photometric behaviour. It is not clear whether all observed occurrences of transient periods can be explained by a single mechanism, like orbital motion of ejected gas, or some phenomenon phase-locked to the underlying photosphere. Additional, aperiodic short-lived phenomena are present in several stars, but the data presented in this do not allow to determine their nature.

The analysis and modelling of the periodic line profile variability of μ Cen and ω CMa revealed them to be non-radial pulsators with $\ell = m = +2$. Then, it was tested whether such *nrp* can explain other early-type Be stars as well, assuming that the differences in morphology of the *lpv* arise almost entirely from differences in the individual inclination of the objects. This test was performed by

1. comparing the observed variability of ω CMa to that of other low inclination Be stars

2. comparing the *nrp* model of ω CMa, tilted to more equatorial viewing angles, to Be stars with higher $v \sin i$

It turned out that, in addition to μ Cen and ω CMa, 14 more objects show periodic *lpv* well explainable by *nrp* with $\ell = m = 2$. For four more stars this is likely, but the observational data is not sufficient for a firm conclusion. Three stars exhibit a different type of periodic *lpv*. This does not necessarily exclude *nrp* for these objects but probably only requires different modes than $\ell = m = 2$. Two objects show *lpv*, but the data is insufficient for any conclusion, and finally two stars were stable within the detection limits (see Table D.1 in Appendix D). Summarizing this part of the work, the low-order *lpv* seen in the large majority of early-type Be stars is due to non-radial pulsation, typically with $\ell = m = 2$. The relevance of this result for the understanding of the Be phenomenon still remains to be evaluated; late-type Be stars, being much less photospherically active, indicate either that there is no causal link or that early- and late-type Be stars require different explanations.

Part III

Be stars as rapidly rotating stars

Chapter 7

Modelling rapidly rotating stars

7.1 Stellar rotation

Our knowledge about stars and stellar evolution has advanced steadily over the last decades. It is thus natural that effects that were dismissed as second order in the beginning are regaining focus now. Among these, stellar rotation is one of the more important. Be stars were identified as being the most rapidly rotating group of stars. Even conservative studies, which might be well underestimated as the following sections may show, claim an average of 70 to 80 % of the respective's star critical rotation for Be stars.

For instance, this affects the evolution of the chemical structure as a function of radius, since it is changed by meridional circulation. Hence the stellar evolution paths and the position in the Hertzsprung-Russell-Diagram a star occupies at given zero-age mass and evolutionary stage are altered. In addition, as was discussed already in Sect. 5.1.2 several observational concepts used for non-rotating stars are not valid for rotating ones. This obviously applies to the relation between spectral energy distribution and the concept of effective temperature as a single number characterizing the stellar surface, since the surface of a rotating star has a temperature varying with latitude. This is a bit different for the luminosity, since such a number still exists, characterizing the total energy output of the star, but the observational understanding and measurement techniques break down due to lack of spherical symmetry. For an observer, it is thus not only crucial to measure the rotational velocity in terms of the critical one, but also the inclination angle of the star must be determined. In this sense, rotation not only adds the often quoted "third dimension" to the Hertzsprung-Russell-diagram, but for an observer attempting to place a star in it even a fourth one, the inclination. This part outlines a potential way to solve this problem.

The parameter discrepancies found for μ Cen (Sect. 5.1.2) and ω CMa (Sect. 5.2.3) might be caused by rotational effects, and in the following Chapter 8 a further example is introduced, for which test observation have been performed and are compared to result derived with other techniques.

Comparing Figures 7.2 and 7.4 might indicate the problem different methods to derive the parameters are facing. While photometric and spectrophotometric methods will see the star as in the continuous light, i.e. as in Fig. 7.2, spectroscopic methods will derive parameters from a surface distribution as presented in Fig. 7.4. This has not been investigated in detail, but next to the obvious fact that all methods will yield a temperature below the polar one, but higher than the equatorial one, it can not be taken for granted that all methods will be affected in the same way and by the same degree.

7.2 Fundamental stellar parameters

For a discussion of the effects of rapid rotation it is helpful to define the critical fraction at which a star rotates as

$$w = \frac{v_{\text{rot}}}{v_{\text{crit}}} \tag{7.1}$$

with the critical rotation being defined as the Keplerian velocity *at the equator*. Note that an alternative definition using the angular velocities is used sometimes, and both numbers are not comparable one to one, except for zero and unity values. Calculating the critical velocity for a given star, one has to take into account deformation
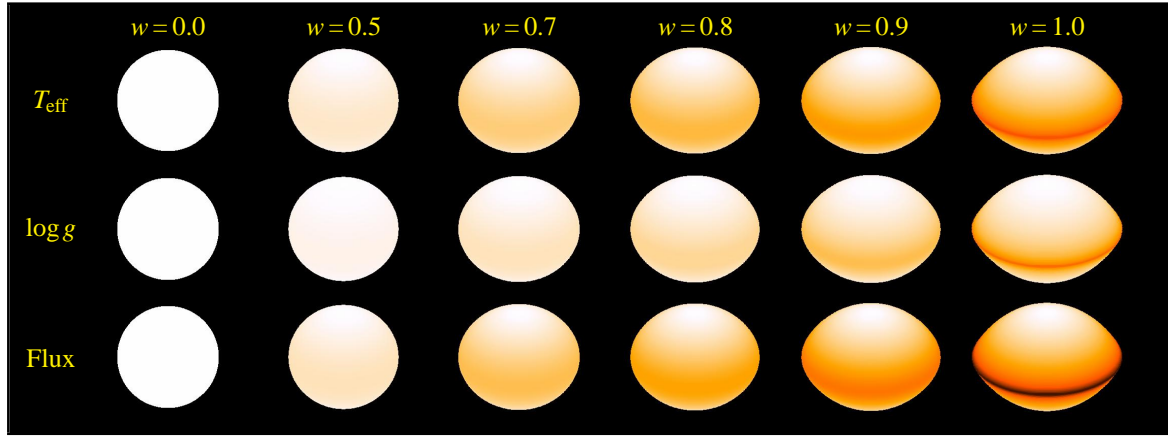
Figure 7.1: Latitudinal variation of surface parameters of rapidly rotating stars as function of critical fraction. The "Flux" shown is $\propto T^4$, without yet taking limb darkening effects into account.

in terms of rotational flattening at critical rotation (i.e. an axial ratio of 1:2), so that

$$v_{\text{crit}} = \sqrt{\frac{GM_\star}{R_{\text{eq}}}} = \sqrt{\frac{GM_\star}{1.5R_{\text{pole}}}} \qquad (7.2)$$

The only fundamental parameter remaining unchanged by rotation is the mass. The changes of the other parameters in *global* terms were quantified by Sackmann (1970). Under the assumption of uniform rotation Sackmann estimated the changes of the other fundamental parameters as a function of the critical fraction w and derives relatively minor influences for B-type stars.

Massive stars do actually not rotate uniformly, as assumed by Sackmann, but during the main sequence stages the deviations from this assumption are not too big (Maeder & Meynet 2000; Heger et al. 2000). Since Bodenheimer (1971) also found that Sackmann's results do not strongly depend on the assumption of uniform rotation, the numbers given there are adopted as typical for B-type stars. In this case the luminosity drops with w^2 by about 7% at critical rotation, while the polar radius drops by maximally 2% in the same manner. This change in luminosity is less than if one takes into account the change of surface area and gravity darkening alone, so that the polar temperature has to rise to yield these values. The following parametrization is adopted for comparisons with non-rotating stars with respect to luminosity, polar radius, and polar temperature.

$$\log L_\star(w) = \log L_\star(0)(1 - 0.07w^2) \qquad (7.3)$$
$$R_{\star\text{p}}(w) = R_{\star\text{p}}(0)(1 - 0.02w^2) \qquad (7.4)$$
$$T_{\text{p}}(w) = T_{\text{p}}(0)(1 + 0.123w^2) \qquad (7.5)$$

Townsend et al. (2004) recently also have investigated the variation of the actually measured parameters with rotation in terms of the effective shift of position in the HRD a B star will experience as the rotational rate increases. While the amount of the shift is a function of the critical fraction, by up to 2 spectral subtypes and/or one luminosity class, the direction is determined by the inclination angle. A pole on star will appear more luminous at the same temperature compared to its non-rotating counterpart, while an equator-on star will seem cooler at the same luminosity.

Townsend et al.'s results of relatively a strong dependence of the parameters on w and i are only an apparent contradiction to the results by Sackmann. The reason is that Townsend et al. gave the actually observable parameters, but an observer is not able to determine global parameters straightforwardly. As stated above, this is because the information is obtained from a tiny fraction of the 4π steradian sphere the star emits radiation into, and then recomputed to the full sphere by usually assuming spherical symmetry of the radiation field. To investigate the latter effect in detail, the changes of the true parameters due to spinning up a given star have to be taken into account for the model input parameters.

Next to the oblateness the most obvious effect of rapid rotation is the so called gravity darkening. As von Zeipel (1924) stated, a rapidly rotating star cannot have a uniform surface temperature and be in equilibrium.
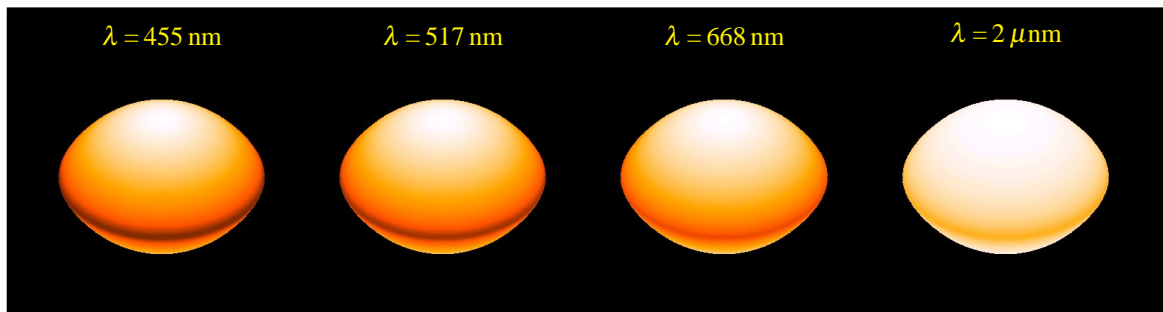
Figure 7.2: Surface flux distribution as function of wavelength. In the blue range, the differences are stronger than in the red and infrared due to the shift of the flux maximum towards the red with decreasing temperature.

In addition to the above mentioned meridional flows, it is usually assumed that the local surface temperature depends on the local effective gravity, which varies as a function of colatitude ϑ:

$$T(\vartheta) = T_{\mathrm{p}} \frac{g(\vartheta)^{\beta}}{g_{\mathrm{p}}} \tag{7.6}$$

The canonically assumed value of β for early-type stars with geometrically thin atmospheres is 0.25, with the limitation that it applies only to geometrically thin and non-convective atmospheres.

Figure 7.1 shows the effects of increasing rotation on stellar shape, local surface gravity and temperature. As an estimate, the local total flux is shown as $\propto T^4$. With respect to the following Section, it should be noted that the equator emits less flux in a rapid rotator, but it is not so little as to render the equator bolometrically invisible, except maybe for 100 % critical rotation. This changes somewhat if the Planck-function is looked at the individual wavelengths. As Figure 7.2 shows, the blue domain, where the lines are which are typically used to determine $v \sin i$, is more affected than red.

7.3 Line profiles in rapidly rotating stars

In order to derive the rotational properties, all techniques usually applied rely on the comparison of a template profile with the measured one. The more basic ones just parametrize the full width of the line, more sophisticated ones for instance compare the Fourier-transformed of the profiles, and in particular the position of the first minimum, which is closely related to the width. Obviously, the determination of rotational speed is critically depending on the choice of the template profiles. They are often constructed by convolving either the spectrum of a non or slowly rotating reference star, or a non-rotating model spectrum, with a rotational broadening function.

Such a method assumes that the parameters important for line formation do not vary across the stellar surface. In light of the principles presented in the previous section, this is simplified. It was thought for long that this effect was of little importance, but theoretical computations in the past years pointed to the possibility that this was oversimplified.

Collins & Truax (1995), and more recently Owocki (2004) and Frémat et al. (2004), noted that above a threshold of about 80 % of the critical value the normally assumed roughly linear relation between true stellar v_{eq} and the observed linewidth parameter may break down. Initially, it was suspected that this would be due to continuum limb-darkening. In this case, the limb regions with the largest line-of-sight velocity component would be basically invisible and the question of critical rotation unanswerable by spectroscopy alone.

Owocki (2004) pointed out that the major effect should rather be gravity darkening, making the equatorial regions of a rapid rotator very cool. They would be rather dim compared to the rest of the visible surface, so that these regions would hardly contribute to the line profile and thus not be seen by spectroscopic methods. However, a closer look at the spectral lines being formed in a B star shows that while this is true for the ions usually utilized to determine $v \sin i$, for transitions being strong at cooler temperatures the situation is just reversed. These would be enhanced at the equator, so that selected spectral lines might in turn help to solve the problem posed by the commonly used lines. It might even be possible to detect lines of ions that would not be expected in a non-rotating star of that type, depending how cool the equator gets. For early type B stars the typical equatorial temperature may drop as low as 10 000 K. At such temperatures, however, only few

Table 7.1: Sketch of formation of line profiles by lines being formed all over the stellar surface, preferably at the poles and at the equator, respectively. See Fig. 7.3 for the respective shapes.

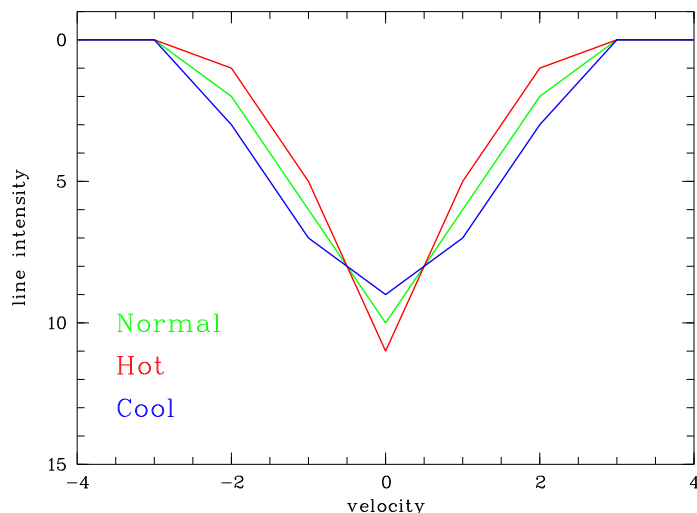| "normal"						"hot"						"cool"				
		2						3						1		
	2	2	2				2	2	2				2	2	2	
2	2	2	2	2		1	1	1	1	1		3	3	3	3	3
	2	2	2				2	2	2				2	2	2	
		2						3						1		
2	6	10	6	2		1	5	11	5	1		3	7	9	7	3

Figure 7.3: The profiles shape types for the three formation scenarios sketched in Table 7.1.

non-Balmer lines have significant strength, so that detection and modelling of such lines requires excellent signal-to-noise ratios.

Besides the plain presence of unexpected lines, the rotationally broadened profiles of temperature sensitive lines will react on gravity darkening. A line formed mainly at the pole will be only moderately broad and have a narrow core. This was already shown by Hutchings (1976) and Hutchings & Stoeckley (1977) for the ultraviolet regime, where the flux effects are most severe (cf. Fig. 7.2), but according to the results presented by Townsend et al. (2004) and in this work this is also important for the visual domain. By contrast, in an equatorially formed line the core would be missing from a normal uniform-disk profile, so that it would appear broad with a nearly flat bottom. The principle formation of these three profile types is demonstrated by Table 7.1 and Fig. 7.3.

According to these considerations, the BRUCE/KYLIE package (Townsend 1997b, see also Chapter 4) provides an excellent toolbox to check the critical-rotation hypothesis by means of realistic line profile modelling.

Figure 7.4 shows detailed surface models following the principle sketched in Table 7.1 and Fig. 7.3. It is easily seen that the strong lines usually utilized in early type B stars to measure $v \sin i$, such as those of HeI or the SiIII triplet around 4560Å, are not ideally suited because they hardly scan the equator. The same applies to the lines typically used in mid-B stars, such as those of SiII or MgII. In turn, one can identify lines well suited to measure the full width in Fig. 7.4. For early early-type B stars, these would be FeII lines formed predominantly at the equator, while SiII lines are formed all over the stellar surface. In mid-type B stars, only FeII lines are formed at sufficiently equatorial regions to track the full rotational speed.

The resulting line profiles for an early-type B star are shown in Figure 7.5. The inclination for profile modelling presented in this Figure was chosen such that $v_{eq} \sin i = 260\,\mathrm{km\,s^{-1}}$ in all cases, but with increasing actual rotational speed, and thus critical fraction. It is easily seen that at constant true $v_{eq} \sin i$ the actual line width decreases for the HeI 4713 line when the v_{eq} increases. This line is one of those exhibiting little non-rotational broadening, showing the effect clearly. The closer the parameters get to the critical rotation, the
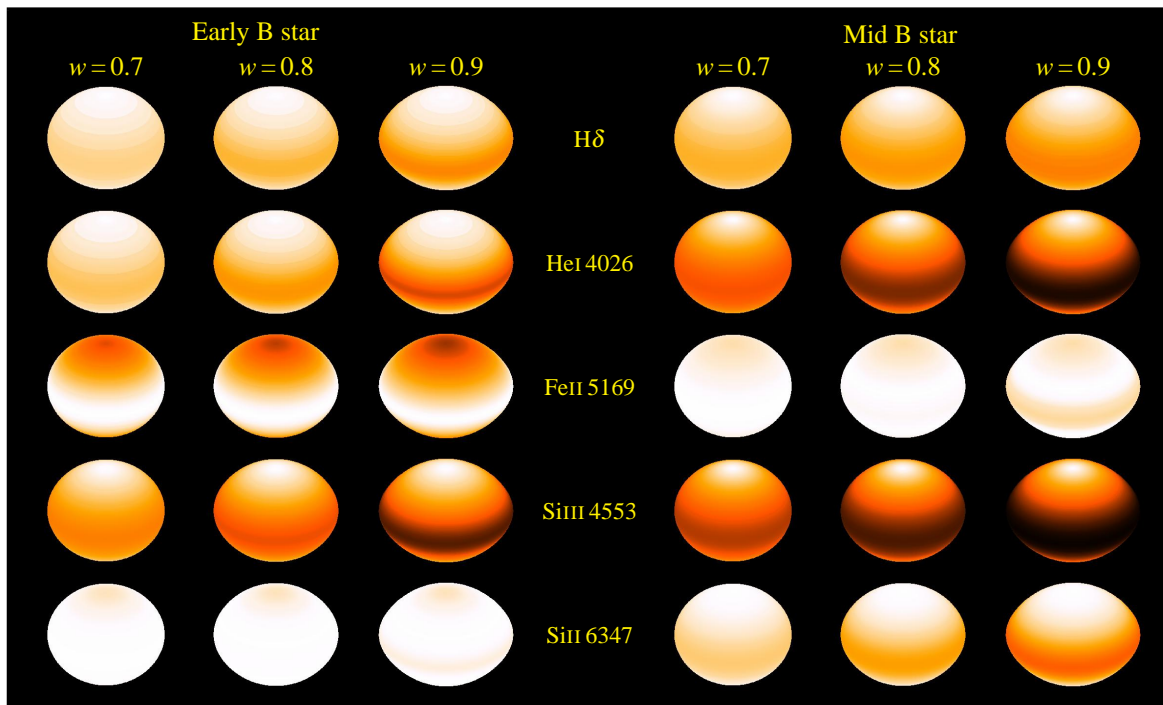
Figure 7.4: Latitudinal variation of line formation from 70 % to 90 % critical. Typical parameters were chosen for an early type main sequence B star and a mid-type one. Light areas contribute larger equivalent width to the integral absorption profile than darker ones. These contributions have been weighted with the Planck function for the local temperature, but no further effects like limb darkening were applied for this figure.

smaller will be the rotational velocity actually measured. This is just a different view of the above noted upper threshold of 80 % for the determination of the critical fraction. Other HeI lines like those of 4026 and 4471 are affected the same way, but due to the strong Stark-broadening this less is obvious to the plain eye.

In contrast, such a width change at given $v \sin i$ does not occur in the FeII 5169 profile. Therefore, this line is theoretically well suited for the determination of true rotational velocities. In practice, problems occur because the line is typically weak, requiring a signal-to-noise-ratio higher than achievable in a single shot observations with common detectors. In addition, such observations are feasible only with well understood instruments, since instrumental effects also limit the signal-to-noise.

Next to these instrumental problems, in the class of the most rapid rotators, the Be stars, this line is the second after the Balmer lines to show emission, which makes the detection of the line width unreliable, if emission presence cannot be firmly ruled out, e.g. by simultaneous $H\alpha$ observations proving a diskless state.

The next Chapter deals with observational question in greater detail and presents some data of test observations, showing that nevertheless the above sketched method is promising, if care is taken.

7.3.1 Unsolved problems of rotating stellar atmospheres

The theory of atmospheres of rapidly rotating stars as sketched above is still only a first order approximation. The validity of many of the assumptions is not really sure or even provenly wrong, but at presence the best approach available.

Among these problems is that the von Zeipel theorem with the adopted parametrization of $\beta = 0.25$ is valid only for non-convective atmospheres. However, this is what happens with a stellar atmosphere at critical rotation: It becomes convective. It is assumed here that these effects become severe only very close to the critical limit, so that the models presented below, rotating of the order of 90 to 95 % critical, still represent the actual properties of the atmosphere well enough for our purpose.

Similarly, the conventionally adopted axial ratio of 1 : 1.5 is derived for a hydrostatically stable ball of gas, i.e. with the help of the Roche-approximation. Yet, one of the physical implications of the von-Zeipel theorem is that such an atmosphere cannot be in hydrostatic equilibrium. Instead, a flow pattern through the stellar interior from the core along the rotational axis to the poles, on the surface to the equator and back inwards to
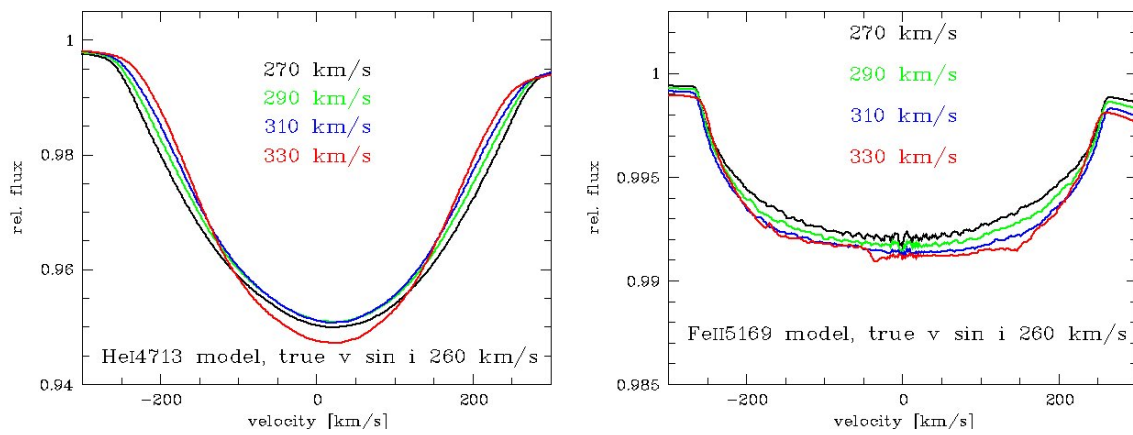
Figure 7.5: Line profiles modelled with BRUCE/KYLIE showing the narrowing vs. flat-bottom effect sketched in Fig. 7.3. The wiggles seen in the profiles are numerical artifacts, except in the $330\,\mathrm{km\,s^{-1}}$ profile for FeII, where a neighbouring line formed at the cool equatorial belt becomes strong and blends with FeII

the core will form, which is called the meridional circulation.

Observations of α Eri (Domiciano de Souza et al. 2003) may indicate that actual stars might have an axial ratio larger than 1.5, since the observed ratio for this star is $1 : 1.56 \pm 0.05$. This value even is a lower limit, since it assumes equatorial inclination, which can be excluded on ground of the non-shell nature of α Eri. Based on these measurements, Jackson et al. (2004) have proposed alternative flattening scenarios, but also an observational effect can not be ruled out on ground of present data.

Chapter 8

Observational evidence

In the previous Chapter, the possibility of almost critical rotation being undetected by classical observational methods was introduced on theoretical grounds. Here, observations supporting such a rapid rotation are presented for individual stars. It is explored whether Be stars as a group in general might be such objects, and whether the available observations would commensurate with this hypothesis. The southern Be star Achernar was chosen as a test object, since recent interferometric observations strongly suggest very rapid rotation of this object. It has a measured axial ratio of about 1:2, which is indicative for critical rotation.

8.1 α Eridani

8.1.1 Constraining the input parameters

Being the ninth brightest star in the sky, spectra of high quality were easily available from our database described in the Appendices. Strong emission lines have never been observed in Achernar, but even these are completely absent since early 1999. Spectra taken with FEROS in January, 1999 still show some emission, but in Hα only, which had fully disappeared in May–July, 1999 and January, 2000. This is important since equatorial, i.e. low-excitation lines may be contaminated by a contribution from the disk, having a similar temperature. Like most early-type Be stars, α Eri pulsates nonradially (see App. D), but does so too weakly to significantly affect this test. Moreover, a phase-averaged profile of all FEROS data was used for comparison with the calculations. The non-pulsational input parameters to BRUCE, mass, polar radius, polar temperature, equatorial velocity, and inclination angle, were constrained as follows:

Achernar is mostly classified as B3 Ve, sometimes also as B4 IVe. The equivalent widths, notably of He I, crudely agree with a *temperature* of about 16 000 to 17 000 K (see e.g. Leone & Lanzafame 1998). However, spectrophotometric determinations, mostly based on Balmer discontinuity and UV data, give lower values of about 14 000 to 15 000 K (Kaiser 1989 summarizes several works). Quick reconnaissance calculations with BRUCE/KYLIE confirmed that it is possible to reproduce the intensities of the spectral lines with a disk-averaged temperature of about 16 000 to 17 000 K, but not with lower temperatures. Therefore, the subsequent detailed modelling was required to yield parameters values resulting in this range for the disk-averaged temperature. Because the results could qualitatively explain also the method-dependent discrepancies between temperature determinations (cf. the previous Chapter), calculations at different temperatures were not performed.

The spectral type implies a *mass* around six solar masses. Its quantitative impact on the model is, together with the radius, to set the critical equatorial velocity and the polar gravity. For the given purpose, the exact value of the mass is only moderately relevant as significantly Stark-broadened lines were not modelled and the effect of higher critical velocity can partly be compensated for by adjusting other input parameters.

Interferometric measurements gave a uniform disk *radius* of about 9 R$_\odot$ (Code et al. 1976). This seems very large for a B3 V star, but is consistent with parallax, effective temperature, and apparent magnitude. Moreover, it was confirmed by the first scientific measurements with the VLTI (ESO press release 23-01). Therefore, the input parameters were required to be consistent with such a radius. More precisely, the area visible to the observer was constrained this way. In fact, other more recent VLTI measurements deduced an axial ratio of 1.56 and radii of 7.7 and 12 R$_\odot$ in polar and equatorial direction, respectively (Domiciano de Souza et al. 2003).

The value for the projected *rotational velocity*, $v \sin i$, of Achernar is adopted by most authors as 225 km s^{-1}, given by Slettebak (1982). Other recent determinations fall in the same range to within the errors; they were

Table 8.1: Stellar input parameters for modelling the line profiles of α Eri. Also shown are several derived parameters. For an explanation of the meaning of the 'apparent' parameters in a rapidly rotating star see Rivinius et al. (2001b, Sect. 6.1).

	Model 1	Model 2
Input parameters		
Polar radius, R_{polar} [R$_\odot$]	7.7	8.2
Polar temperature, $T_{eff,polar}$ [K]	22 000	19 500
Mass, M [M$_\odot$]	6	6
Rotation, v_{eq} [km s^{-1}]	300	240
Inclination, i	65°	75°
Derived parameters		
rotational period, $\mathscr{P}_{rot}$ [day]	1.86	2.18
critical velocity, v_{crit} [km s^{-1}]	315	305
equatorial radius R_{eq} [R$_\odot$]	11.05	10.33
projected axial ratio (on sky-plane)	1.37	1.24
polar gravity, $\log g$	3.44	3.39
equatorial gravity, $\log g$	2.25	2.87
equatorial temperature, [K]	11 040	14 460
true luminosity, $\log(L/L_\odot)$	3.88	3.79
apparent T_{eff} [K]	16 866	15 928
apparent radius [R$_\odot$]	9.11	9.12
apparent luminosity, $\log(L/L_\odot)$	3.77	3.75

mainly derived from the stronger HeI lines. According to the discussion in the previous chapter, the projected velocity could be higher if the v_{eq} was closer to its critical value. Thus, the conditions are $v_{eq.} \sin i \geq 225$ km s^{-1} and $v_{eq.}/v_{crit.} \geq 0.7$, also setting a lower limit to the *inclination angle* of about 50°. An upper limit results from Achernar not being a Be shell star. This means that the equatorial disc, when present, does not intersect the cone of sight from the observer to the photosphere. Since it is commonly assumed that the opening angle of equatorial disks does not exceed $2 \times 15°$, the permissable range of the inclination is confined to values between 50 and 75°.

Following the above criteria and guided by a number of spot checks, two models were selected to illustrate the observable differences between a 95 % critically rotating model for Achernar (Model 1 in Table 8.1) and the more conventionally assumed parameters (Model 2 in that Table).

8.1.2 Results

The parameters derived for each of the two models are compiled in the lower part of Table 8.1. The *apparent* effective temperature and radius were computed by averaging them over the stellar disc in the same way as the profile was synthesized. They were, then, used to determine the *apparent luminosity*. Note, however, that this apparent luminosity is an *a-posteriori* estimate using disc-averaged parameters, not a quantity integrated over the stellar disc by the model itself. The true luminosity emitted over 4π steradian is also given.

Figure 8.1 shows the resulting surface distribution of the Planck function at visual wavelengths. Also visualised are the local contributions to the equivalent widths of several spectral lines, computed from the local T_{eff} and $\log g$-values and weighted with the flux at the respective wavelengths. HeI lines are clearly inappropriate to determine the rotation of almost critically rotating B-stars, since their line profiles do not carry any information from that region. The problem is less severe, but still visible for a rotational rate of about 80 % critical (Fig. 8.1, upper and lower row, respectively). Lines like the ones of FeII should be better suited.

Next, the model package was used to compute also the actual spectral line profiles for various transitions. The results are shown in Fig. 8.2. Just as expected, the HeI lines, e.g. at 4713 and 6678 Å, are reproduced about equally well by either model. For FeII 5169 or SII 5454, however, the more slowly rotating model clearly falls short of the observations not only in reproducing the line widths but also the flat-bottomed shape of FeII 5169.
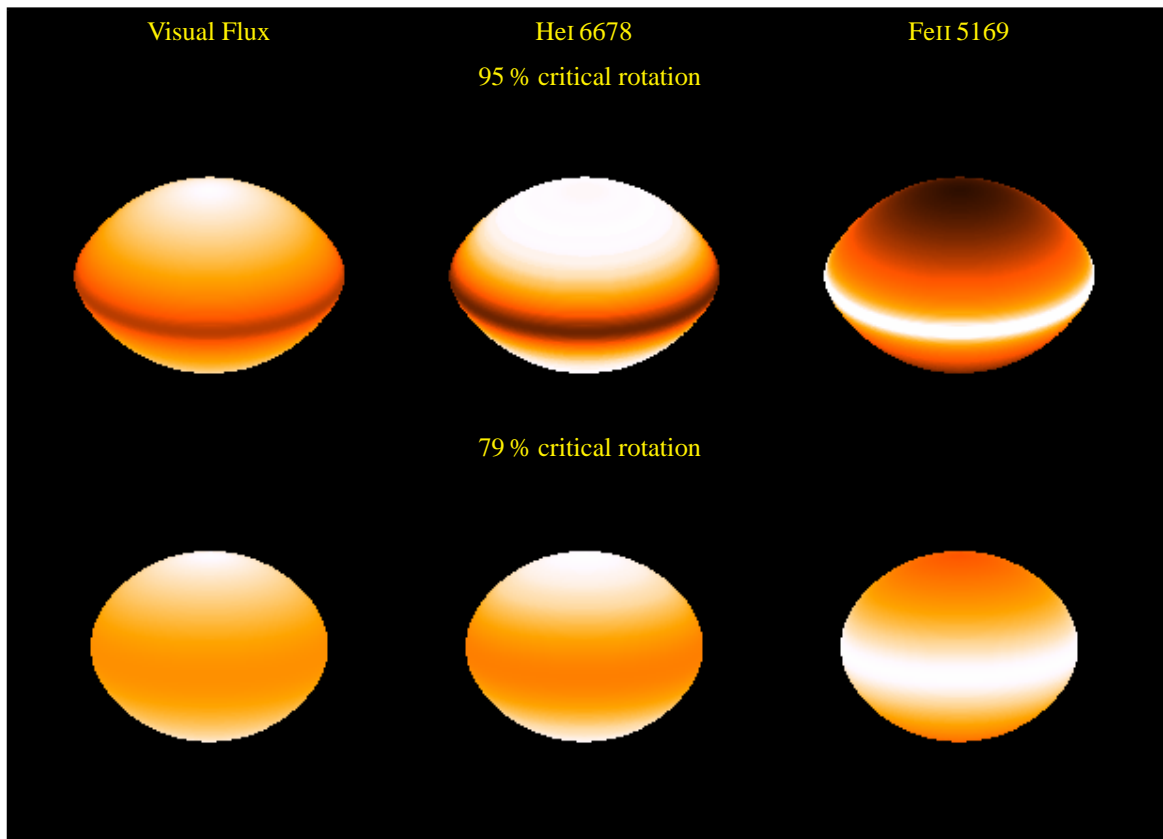
Figure 8.1: Surface distribution of flux and equivalent width contribution for important lines at two different rotational rates for Achernar. For parameters see Table 8.1 The geometry is shown as projected onto the sky plane.

This is not an observational problem (e.g., caused by imperfect continuum normalisation), because other FeII lines observed with FEROS exhibit a similar shape.

Unfortunately, although the FEROS data are well exposed, they turned out to be S/N-limited by instrumental effects. It was not possible to take them into account for the reduction, since they varied on a night to night base. Observations of Achernar with UVES at the VLT unit telescope Kueyen have been obtained to overcome this limitation, but are not yet finally reduced. Preliminary results as presented in Fig. 8.3, however, confirm the general appearance of the line profiles as observed with FEROS, and thus the above considerations hold.

8.1.3 Achernars rotation

The $v \sin i$ of Achernar is larger by almost 20 % than given in the literature. This means, that also the equatorial rotational velocity of Achernar must be much higher than conventionally thought. In particular the fractional critical velocity, $w = v_{eq}/v_{crit}$, of the star probably lies above 90%, not at about 70 to 80 %.

Recently, the axial ratio of the stellar disc of Achernar, as projected on the sky plane, was determined by the VLTI to be 1.56 ± 0.05 (Domiciano de Souza et al. 2003). This is even *larger* than the maximally permitted value of 1.5, if solid body rotation at the critical limit is assumed. Since the inclination is less than 90°, this result becomes even more non-conventional. While the present Model 2 results in an observable axial ratio of only 1.24, Model 1 gives 1.37, which is still lower than observed but at least alleviates the problem somewhat. The star may not rotate as a solid body, but the VLTI observations are not yet sufficiently complete for aperture synthesis, so that there still might be some leeway.

Does such high a rotation rate solve, at least qualitatively, the problem of the discrepant temperature determinations, ranging from around 14 000 K (Kaiser 1989, and references therein) to more than 20 000 K (Chauville et al. 2001)? The temperatures at the low end are typically derived from measurements of the Balmer discontinuity and so correspond to a relative lack of UV flux. At very fast rotation, this is expected because the circum-equatorial flux is emitted at much lower temperatures (see Fig. 8.1) so that the UV flux is substantially
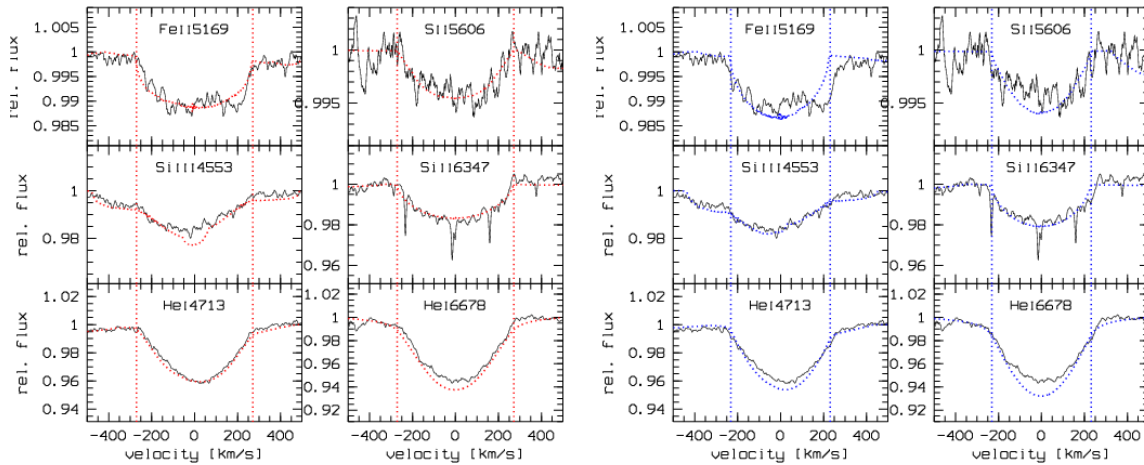
Figure 8.2: Line profiles of selected ions in α Eri. The profiles were calculated for a 95 % critically rotating star and $v_{eq} \sin i = 272\,\mathrm{km\,s^{-1}}$ (left panel) and one rotating at 79 % only with the conventional $v_{eq} \sin i = 232\,\mathrm{km\,s^{-1}}$ (right panel, see Table 5.5 for full parameters). Flat-bottomed line profiles as in FeII cannot be reproduced with slower rotation. The central bump in FeII 5169 is not due to any circumstellar material, but might be due to the nearby MgI 5173,5184 lines already being formed at the cool equator and blending with FeII 5169. The SiIII 4553 line is blended on both sides with FeII lines. The sharp absorptions in the SiII 6347 line are of telluric origin.
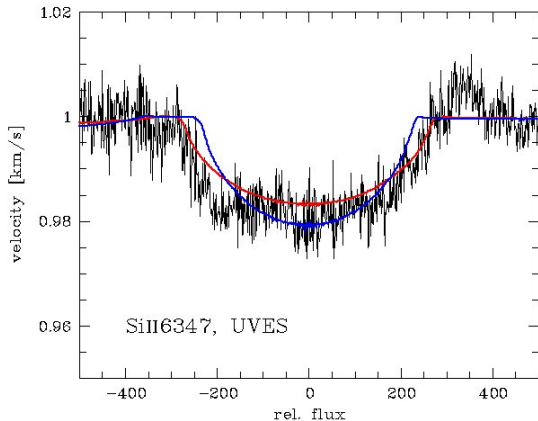

Figure 8.3: A UVES spectrum of the SiII 6347 line of Achernar, confirming the results derived from the FEROS data about the higher $v \sin i$ of about $270 \mathrm{km\,s^{-1}}$ and the flat-bottomed profile-shape.

reduced. This is also the outcome of a study by Frémat et al. (2004). Temperatures at the high end would become understandable if they were derived from spectral lines, that are formed mainly in polar regions, e.g. from HeI 4471 as done by Chauville et al. (2001). Since the latter line due to numerical problems is not modelled very well by the BRUCE/KYLIE implementation used for the present calculations, a direct comparison cannot be presented. However, the good agreement between observations and computations of numerous other lines and ions makes this straightforward qualitative conclusion fairly robust.

When the apparent temperature and radius in Table 5.5 are combined with the Hipparcos parallax to compute the apparent V-magnitude, Model 1 comes out too bright by almost 0.4 mag (in comparison, the very low interstellar extinction towards α Eri is a negligible source of error). However, to finally settle this issue the code will have to be expanded as to compute the emerging flux in physical units directly, instead of making a detour via the disk-averaged parameters.

8.2 Candidates from archival data

α Eri is the most nearby Be star, but otherwise not expected to be too different from other ones. As it is the first one checked for critical rotation by methods overcoming the gravity darkening problem, the results may potentially be generalized to all Be stars. To check on this, the FEROS/HEROS database was searched for further candidates. However, the required combination of very high data quality and temporary absence of a
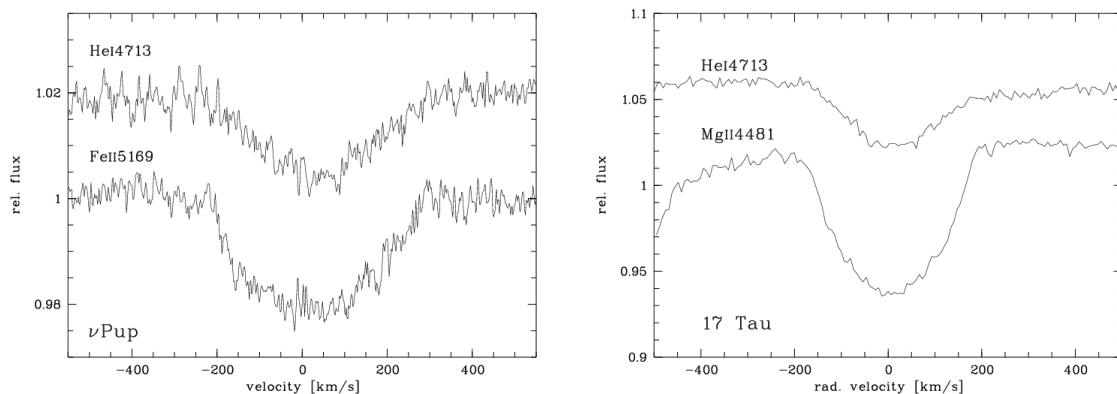
Figure 8.4: The profiles of HeI 4713 and FeII 5169 in ν Pup and HeI 4713 and MgII 4481 in 17 Tau (Electra), respectively. These late-type Be stars are much cooler than α Eri. In ν Pup most of the stellar disc contributes to the FeII and MgII lines, giving the latter a normal rotational profile. By contrast, the formation of HeI lines is concentrated towards the pole, leading to narrower wings as well as a more pronounced core. At the time of the observations (2000 January), the spectral lines were virtually free of circumstellar contributions; also Be stars later than B6 are not known to be nonradial pulsators.

circumstellar disk was up to now fulfilled in only a few cases. ν Pup (HR 2451, B8 III) was found to be a shell star (see Chapter 2 and App. B), but had lost all circumstellar contribution by 1999, so that the profiles obtained in 2000 are fully photospheric. Though modelling has not yet been attempted, the profile distortions thought to be characteristic of critical rotation are undoubtedly present (Fig. 8.4). Electra, a Be star in the Pleiades of type B6 III is a similar case. Although the emission is not completely absent, it is very weak and undetectable even in the Balmer lines except for Hα and Hβ, similar to what was seen in ν Pup in the late 1990's.

In conclusion, high signal-to-noise spectroscopy offers prospects to constrain the profile shape of extremely rapidly rotating stars sufficiently well. In this way, it could complement interferometric work by extending its scope to fainter magnitudes and, therefore, more representative statistics. This is desirable because an inter-ferometric determination of the axial ratio will, for a while, remain feasible for the most nearby Be stars only; moreover, interferometry will — even when combined with low-resolution spectroscopy and using aperture synthesis techniques — have to be concerned about contamination by the circumstellar disk so that the number of available target stars is further reduced. But as the unexpectedly high VLTI axial ratio of Achernar illustrates, the spectroscopic method needs to be calibrated against direct measurements.

For cross-calibration also Bn stars might be used. A recent publication by McAlister et al. (2004) shows the geometric flattening ratio on the plane of the sky of the B7 Vn star Regulus to be 1.32. Assuming an inclination of 90° they derive a rotation of 86 % critical. This could also be a worthwhile candidate for spectroscopy, even though its rather late B-type spectrum will make it very difficult to detect suitable spectral lines.

8.3   Be star rotational statistics

Porter (1996) investigated the rotational velocities of shell stars. The basis of his work was that all shell stars are ordinary Be stars viewed about equator-on so that $\sin i$ would be close to unity. Accordingly, the observed distribution in $v \sin i$ of shell stars provides the most straightforward way of determining the distribution of the equatorial velocities of Be stars. The determination of the equatorial velocity distribution of Be stars from shell stars only offers another decisive advantage in addition to its simplicity. If a sample of Be stars with supposedly random inclination angles is analyzed, this sample stands a certain risk to be biased against stars with large inclination angle. The increased width of the emission lines makes them more difficult to detect than the narrower line emission resulting from smaller inclination angles (see Fig. 8.5). Moreover, for optically thick emission lines, their flux is roughly proportional to the projected area rather than the volume. This again favours the detection of Be stars with low $v \sin i$. By contrast, shell stars are easy to detect.

The database of shell stars compiled in Appendix B is somewhat more complete than the one available to Porter (1996). Furthermore, Porter assumed all objects to be of luminosity class V. The re-analysis presented below differentiates between different luminosity classes. While Porter did not have access to a homogeneous set of observations, the present database permitted all $v \sin i$ values to be put on one common scale. Omitted
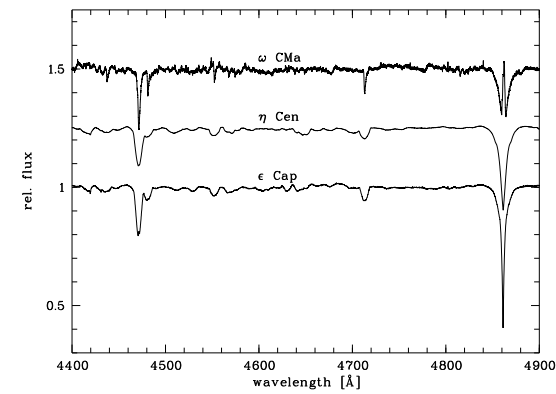
Figure 8.5: The part of the wavelength range used in the MK classification process. The pole-on star ω CMa is clearly recognized as a Be star. ε Cap would probably also have been classified as Be-shell star even in lower quality spectra. However, η Cen, having a weak shell signature could easily be missed. This illustrates that Be stars with narrow emission lines are easier to find, which may introduce biases in samples of Be stars.
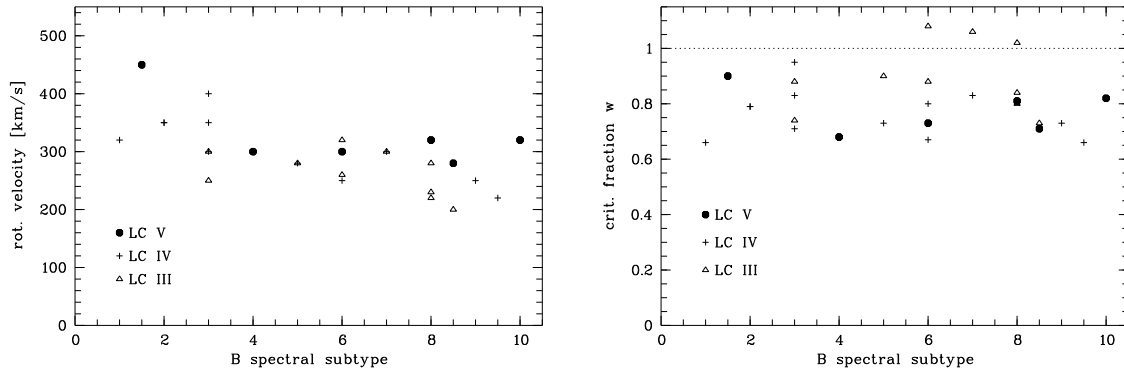

Figure 8.6: The values of $v \sin i$ (left panel) and w (right panel) of the shell stars in Table B.1 (i.e. the ones listed in the upper part) plotted against spectral subtype. While the rotational velocity depends on spectral type, but little on luminosity class, the critical fraction is largely independent of spectral type.

from the analysis were the three stars, which have shown only intermittent shell features although their line-emitting discs where well developed. It is, therefore, doubtful whether their $\sin i$ is similarly close to unity as for the main sample. Since they only account for 10% of the stars in Table B.1, their non-consideration is not critical anyway especially since neither their $v \sin i$ nor their $w \sin i$ values appear to exhibit systematic deviations.

A full re-determination of rotational velocities is beyond the scope of this work. More importantly, this will only make sense after the question has been answered whether critical rotation has not so far been found in Be stars because the traditional methods used exclude this, as as proposed in the previous sections. However, because such an error would be systematic, and the present sample is homogeneous, this does not invalidate the results obtained here. If a re-scaling is necessary, this can easily be applied later.

The expected uncertainty of an individual value of w arises from $v \sin i$, which has a typical error of about 10%, and the uncertainties in spectral type and luminosity class. From a comparison of the values given by Slettebak (1982) with determinations by Moujtahid et al. (1998) and Chauville et al. (2001), an uncertainty of up to one spectral subclass and one luminosity class can be deduced. The value of v_{crit}, taken from Table 2 of Yudin (2001), should therefore be accurate to within 20%. The errors are dominated by the uncertainty of the spectral classification.

Repeating Porter's analysis, it is found that the mean critical fractional rotation of Be stars at large is $\overline{w} = 0.81$ with $\sigma = 0.12$ (see also Fig. 8.6). Broken down by luminosity class, the results are $\overline{w}_{\mathrm{LCV}} = 0.77 \pm 0.08$, $\overline{w}_{\mathrm{LCIV}} = 0.76 \pm 0.09$, and $\overline{w}_{\mathrm{LCIII}} = 0.89 \pm 0.13$. The corresponding mean equatorial velocities are $\overline{v}_{\mathrm{LCV}} = 328 \pm 61$ km s^{-1}, $\overline{v}_{\mathrm{LCIV}} = 306 \pm 51$ km s^{-1}, and $\overline{v}_{\mathrm{LCIII}} = 264 \pm 39$ km s^{-1}. Although there seems to be a trend towards lower v but higher w with decreasing luminosity class, the errors are too large to ascertain its significance.

The above value of $\overline{w}$ is slightly larger than Porter's (1996) result. However, since the spectra available for the present study permitted low $v \sin i$ outliers to be corrected, this is not surprising.

More interesting is that the width of the peak at $\overline{w} = 0.81$, namely $\sigma = 0.12$, is narrower still than the estimated intrinsic uncertainties of individual determinations of w of about 20%. The error estimates made

above are, therefore, conservative. But even if the true error in individual values of w was as small as 10%, the width of the peak in their distribution would be not or only marginally resolved. Since there must also be a genuine spread in w, this might signal that the true $\overline{w}$ is higher but that the observational scale of w is truncated. This could lend some additional support to the growing suspicion (cf. the discussion above) that, above some threshold in the true rotational velocity, the width of strong spectral lines no longer increases with the equatorial velocity. In any event, the derived $\overline{w} = 0.81$ should be regarded as a lower limit.

Part IV

Summary and Conclusions

Be star disks

The first part of this work dealt with the properties of the circumstellar disks of B emission line stars. It is helpful to restrict the initial discussion to shell stars. It is meanwhile commonly accepted that these stars do not form an intrinsically distinct group among Be stars, but appear special only due to their inclination angle close to 90°. The circumstellar disk is seen edge on and the light from the star passes through it, opening various possibilities for the analysis of the disk properties and avoiding potentially ambiguous results due to unknown inclination angles.

The first topic of interest is the rotational law of such a disk. For stars with symmetric emission profiles it was shown by various means, namely the formation of CQEs and the narrowness and position of shell lines, that the radial motions in the disk must be very small, i.e. less than a few $\mathrm{km\,s^{-1}}$, so that the individual particle orbits must be circular. This is in principle also the case for forced co-rotation, but as was shown in this case CQEs cannot form as well and forced corotation would also lead to some very significantly different spectral signatures in other respects. In particular, the Keplerian velocity at the stellar surface would not be a natural upper limit for the maximum observed kinematic velocity. In fact no velocity larger than this limit was observed up to now, in turn they are typically smaller. Other velocity law, such as angular-momentum conserving ones, require out- or inflow with velocities higher than measured. Thus, although circular Keplerian orbits are not explicitly proven for stars with CQEs or narrow shell absorption, all alternatives are either disproven or highly unlikely.

There are stars, however, which do not show CQEs or narrow shell lines, but still are shell stars. These are the stars undergoing what is called long term V/R variability, where cyclically either the violet or the red peak becomes dominant over the other. There are models explaining such changes as in- and outflowing motions. However, to invoke such a process is not required. There is a theoretical model explaining the V/R variability by a density wave. This model relies on elliptical Keplerian orbits (Okazaki 1991), i.e. that the individual orbits have non-zero eccentricity and a co-aligned periastron angle. Elliptical orbits, other than circular ones, do have non-zero radial motions, even if they are Keplerian. In full agreement with the model hypothesis, no star with such a V/R-pattern shows CQEs or narrow shell lines. The principle of Occam's razor demands to explain these properties with the least number of assumptions. Since the observations mentioned in the above paragraph already strongly support Keplerian rotation, and the ones noted in present one also do not require a different mechanism, although one is possible, the following conclusion can be drawn:

1.: Most findings strongly support a well-known description for disk particle orbits around the central star: Kepler's laws. No result is at variance with this hypothesis.

The disks of Be stars are typically changing with time. Only for a few late type Be stars the emission lines are stable over more than decades. In particular for earlier type stars the emission lines, as signatures of the disk structure, are variable on timescales ranging from minutes and days in spectral line presumably forming in the immediate vicinity of the star, over weeks and months for the outbursts believed to replenish the disks up to years and even decades for the V/R cycles and sometimes even complete losses of the disk.

While for the most rapid variations and the physical mechanism itself no hypothesis was presented in this work, it became clear that outbursts are so common that one should regard them as the standard way to replenish a Be star disk. The subsequent evolution of the emission lines indicate a thinning of the material close to the star, so that an inner cavity in the disk forms. Available observations of the last stages before the complete destruction of a disk also indicate that the gas is dissipated outwards together with the stellar wind. The immediate physical mechanism is unknown in detail, but related to the either the stellar wind eroding the disk through viscous processes, or the UV-radiation itself that accelerates the disk material outwards as wind directly.

2.: The star-to-disk mass-transfer is of an episodic nature rather than of a steady one. After an outburst, the disks evolve structurally outwards.

Stellar pulsation

The fuelling of the disks though an episodic process may provide hints towards the nature of this process. Is was claimed that the existence of rapid line-profile variability (*lpv*) in an early-type B star is an almost as good criterion for the Be nature as the presence of emission itself (Baade & Balona 1994). Although this is somewhat

over-exaggerated, the overlap between both groups is so large that some causal connection of both properties is likely. A purely rotational nature of the *lpv* can not strictly be excluded for any given star. However, contrary to the the modelling in terms of non-radial pulsational variability a rotational explanation would require a highly individual model for many stars. For instance the *lpv* properties of high- and low-inclination stars differ systematically, which is naturally explained by the pulsation hypothesis as a property of the inclination itself. In terms of the rotational hypothesis, however, both types of objects would need to have a different variation process, which is unphysical since the inclination is not an intrinsic stellar property.

3.: The short-periodic spectroscopic line profile variations found in Be stars are of nonradial pulsational nature in most cases.

Unfortunately, initial hopes that the above mentioned causal connection between *lpv* and Be-nature would be straightforward, i.e. the first causing the latter, turned out to be deceptive for a generalized explanation. In a few stars, like μ Cen, η Cen, or 28 Cygni pulsational multiperiodicity with closely spaced periods may provide this link through beating processes leading to an outburst when the combined amplitude is high. In most investigated objects however, no pulsational multiperiodicity was found. Since these stars were partly investigated at least as thoroughly as the above three objects, the negative result cannot be ascribed to selection effects and biases.

The problem then is that under the current assumptions for the rotational velocities of Be stars the monoperiodic pulsation alone can not provide sufficient kinetic energy and angular momentum to the stellar surface material to form a rotationally supported circumstellar disk (Owocki 2004). The required Δv between the rotation and the Keplerian speed is in order of $100 \, \mathrm{km \, s^{-1}}$. Since the typical pulsational amplitudes are of the order of 10 to $20 \, \mathrm{km \, s^{-1}}$, a pulsational ejection falls short several times of the required speed. Also stochastic resonance amplification, where the turbulent velocities reaching up to the local speed of sound of about $20 \, \mathrm{km \, s^{-1}}$ stochastically add to some fraction of the particles in the right direction is not able to reach the required velocity.

4.: The pulsational energy is typically not sufficient to eject material into a Keplerian disk

This is further strengthened by the detailed modelling of the pulsational variations, since the modes found to reproduce the behaviour best are those with a retrograde phase-velocity wrt. stellar rotation. In these modes, the density maximum of the wave falls together with the maximal retrograde group-velocity of the particles, which would make an ejection into a Keplerian orbit least efficient compared to prograde modes.

Rapid rotation

The inability of nonradial pulsation to provide the required angular momentum opens two possible solutions: Firstly, the mechanism could be an entirely different one. However, most promising candidates have been excluded or are less likely than pulsation. Secondly, the underlying assumption about the required additional angular momentum might not be correct and instead much less additional velocity is required to reach the orbit for a surface particle. Since this would also require to dispute long-standing answers to the questions of Be star rotation, a re-investigation of this quantity must be carefully justified.

In the past decades such a possibility was mentioned every about 10 to 15 years (Hutchings & Stoeckley 1977; Collins & Truax 1995), but hardly taken further, as there seemed to be more promising possibilities. Meanwhile, the angular momentum problems mentioned above have brought this question back to focus. Indeed earlier results that the line-width becomes independent of rotational speed for the usually used lines were theoretically confirmed by Townsend et al. (2004). Test observations presented here confirm this for the most nearby Be star Achernar and indicate that such a mechanism might be more general in a number of other Be stars. Also the statistics of Be star rotation suspiciously clusters where the decoupling of the line-width from the actual rotation is expected, at about $0.8 \, v_{\mathrm{crit}}$.

5.: The rotation of Be stars might be much more rapid than commonly believed. Observational methods to accurately redetermine the true rotational speed were introduced and need to be applied to a full sample of objects

These methods rely on high-precision spectroscopy and/or interferometry with large baselines. For the latter, available facilities include the CHARA Array of the Center for High Angular Resolution Astronomy on Mount

Wilson on the northern hemisphere, and the ESOs VLT-Interferometer on the Southern one, in particular when observing with the Auxiliary Telescopes will be offered to the community.

As was mentioned on the very early pages of this book, Be star research has not yet found the final answer to the question what constitutes the Be phenomenon. But it might have reached a stage at which the right questions are asked.

Bibliography

Abt, H. A. & Cardona, O. 1984, ApJ, 285, 190

Abt, H. A., Levato, H., & Grosso, M. 2002, ApJ, 573, 359

Adelman, S. J. 2002, Informational Bulletin on Variable Stars, 5307, 1

Aerts, C. 2000, in ASP Conf. Ser. 214: IAU Colloq. 175: The Be Phenomenon in Early-Type Stars, 192

Baade, D. 1982, A&A, 105, 65

—. 1983, A&A, 124, 283

—. 1984a, A&A, 134, 105

—. 1984b, A&A, 135, 101

—. 1985, A&A, 148, 59

—. 1989a, A&AS, 79, 423

—. 1989b, A&A, 222, 200

Baade, D. 1990, in NATO ASIC Proc. 316: Angular Momentum and Mass Loss for Hot Stars, 177

Baade, D. 1991, in Rapid Variability of OB-stars: Nature and Diagnostic Value, 217

—. 1996, Be Star Newsletter, 31, 7

Baade, D. 2004, unpublished data

Baade, D. & Balona, L. A. 1994, in IAU Symp. 162: Pulsation; Rotation; and Mass Loss in Early-Type Stars, 311

Baade, D., Dachs, J., van de Weygaert, R., & Steeman, F. 1988, A&A, 198, 211

Baade, D., Rivinius, Th., & Štefl, S. 2000, in ASP Conf. Ser. 214: IAU Colloq. 175: The Be Phenomenon in Early-Type Stars, 224

Baade, D., Rivinius, Th., & Štefl, S. 2002a, The Messenger, 107, 24

Baade, D., Rivinius, Th., Štefl, S., & Kaufer, A. 2002b, A&A, 383, L31

Baize, P. 1992, A&AS, 92, 31

Ballereau, D., Chauville, J., Zorec, J., & Morrell, N. 2000, in ASP Conf. Ser. 214: IAU Colloq. 175: The Be Phenomenon in Early-Type Stars, 562

Balona, L. A. 1975, MNRAS, 173, 449

—. 1990, MNRAS, 245, 92

—. 1992, MNRAS, 256, 425

—. 1995, MNRAS, 277, 1547

—. 1999, MNRAS, 306, 407

—. 2002, Journal of Astronomical Data, 8, 1

Balona, L. A., Aerts, C., Božić, H., et al. 2001a, MNRAS, 327, 1288

Balona, L. A., Aerts, C., & Štefl, S. 1999, MNRAS, 305, 519

Balona, L. A., Cuypers, J., & Marang, F. 1992, A&AS, 92, 533

Balona, L. A. & Dziembowski, W. A. 1999, MNRAS, 309, 221

Balona, L. A., Engelbrecht, C. A., & Marang, F. 1987, MNRAS, 227, 123

Balona, L. A., James, D., Lawson, W. A., & Shobbrook, R. R. 2000, in ASP Conf. Ser. 214: IAU Colloq. 175: The Be Phenomenon in Early-Type Stars, 220

Balona, L. A. & James, D. J. 2002, MNRAS, 332, 714

Balona, L. A., James, D. J., Lawson, W. A., & Shobbrook, R. R. 2001b, MNRAS, 324, 1041

Balona, L. A. & Kaye, A. B. 1999, ApJ, 521, 407

Balona, L. A. & Lawson, W. A. 2001, MNRAS, 321, 131

Barker, P. K. 1982, ApJS, 49, 89

—. 1986, PASP, 98, 44

Barker, P. K. & Marlborough, J. M. 1985, ApJ, 288, 329

Barnard, A. J., Cooper, J., & Smith, E. W. 1974, J. Quant. Spectros. Rad. Transf., 14, 1025

Baschek, B., Holweger, H., & Traving, G. 1966, Abhandlungen der Hamburger Sternwarte 8, 1, 26

Berio, P., Stee, P., Vakili, F., et al. 1999, A&A, 345, 203

Bjorkman, J. E. 2000a, in ASP Conf. Ser. 214: IAU Colloq. 175: The Be Phenomenon in Early-Type Stars, 435

Bjorkman, J. E. & Cassinelli, J. P. 1993, ApJ, 409, 429

Bjorkman, K. S. 2000b, in ASP Conf. Ser. 214: IAU Colloq. 175: The Be Phenomenon in Early-Type Stars, 384

Bjorkman, K. S., Miroshnichenko, A. S., McDavid, D., & Pogrosheva, T. M. 2002, ApJ, 573, 812

Blow, G. L., Chen, P. C., Edwards, D. A., Evans, D. S., & Frueh, M. 1982, AJ, 87, 1571

Bodenheimer, P. 1971, ApJ, 167, 153

Brown, A. G. A. & Verschueren, W. 1997, A&A, 319, 811

Budovičová, A. et al. 2005, A&A, in prep.

Carrier, F., Burki, G., & Burnet, M. 2002, A&A, 385, 488

Chandrasekhar, S. & Münch, G. 1950, ApJ, 111, 142

Chauville, J., Zorec, J., Ballereau, D., et al. 2001, A&A, 378, 861

Chen, H. & Huang, L. 1987, Chinese Astronomy and Astrophysics, 11, 10

Chesneau, O., Meilland, A., Rivinius, Th., et al. 2005, A&A, in press

Claret, A. 1995, A&AS, 109, 441

Clark, J. S., Tarasov, A. E., & Panko, E. A. 2003, A&A, 403, 239

Code, A. D., Bless, R. C., Davis, J., & Brown, R. H. 1976, ApJ, 203, 417

Collins, G. W. 1987, in IAU Colloq. 92: Physics of Be Stars, 3

Collins, G. W. & Truax, R. J. 1995, ApJ, 439, 860

Coté, J., Waters, L. B. F. M., & Marlborough, J. M. 1996, A&A, 307, 184

Cowley, A. & Gugula, E. 1973, A&A, 22, 203

Cramer, N., Doazan, V., Nicolet, B., de La Fuente, A., & Barylak, M. 1995, A&A, 301, 811

Cuypers, J., Balona, L. A., & Marang, F. 1989, A&AS, 81, 151

Dachs, J., Hanuschik, R., Kaiser, D., & Rohe, D. 1986, A&A, 159, 276

Dachs, J., Kiehling, R., & Engels, D. 1988, A&A, 194, 167

Dachs, J. & Lemmer, U. 1991, in Rapid Variability of OB-stars: Nature and Diagnostic Value, 103

Dachs, J., Poetzel, R., & Kaiser, D. 1989, A&AS, 78, 487

de Bruijne, J. H. J. 1999, MNRAS, 310, 585

de Geus, E. J., de Zeeuw, P. T., & Lub, J. 1989, A&A, 216, 44

Delgado-Martí, H., Levine, A. M., Pfahl, E., & Rappaport, S. A. 2001, ApJ, 546, 455

Denizman, L., Koktay, T., Hack, M., & Eker, T. 1993, Ap&SS, 208, 135

Divan, L. & Zorec, J. 1982, in IAU Symp. 98: Be Stars, 61

Doazan, V. 1976, in IAU Symp. 70: Be and Shell Stars, 37

Doazan, V., Marlborough, J. M., Morossi, C., et al. 1986a, A&A, 158, 1

Doazan, V., Morossi, C., Stalio, R., & Thomas, R. N. 1986b, A&A, 170, 77

Doazan, V., Morossi, C., Stalio, R., Thomas, R. N., & Willis, A. 1984, A&A, 131, 210

Doazan, V., Rusconi, L., Sedmak, G., & Thomas, R. N. 1987, A&A, 173, L8

Doazan, V., Sedmak, G., Barylak, M., & Rusconi, L. 1991, ESA SCIENTIFIC PUBLICATION ESA-SP, 1147

Domiciano de Souza, A., Kervella, P., Jankov, S., et al. 2003, A&A, 407, L47

Dougherty, S. M. & Taylor, A. R. 1992, Nature, 359, 808

Evans, D. S. 1967, in IAU Symp. 30: Determination of Radial Velocities and their Applications, 57

Fabregat, J. & Adelman, S. J. 1998, A&A, 329, 579

Floquet, M., Neiner, C., Janot-Pacheco, E., et al. 2002, A&A, 394, 137

Frémat, Y., Zorec, J., Hubert, A. M., et al. 2004, in IAU Symposium 215, 23

Fracassini, M., Pasinetti, L. E., & Pastori, L. 1977, Ap&SS, 49, 145

Galkina, T. S. 1990, Izvestiya Ordena Trudovogo Krasnogo Znameni Krymskoj Astrofizicheskoj Observatorii, 82, 14

Gayley, K. G., Ignace, R., & Owocki, S. P. 2001, ApJ, 558, 802

Gieske, H. A. & Griem, H. R. 1969, ApJ, 157, 963

Grady, C. A., Bjorkman, K. S., & Snow, T. P. 1987a, ApJ, 320, 376

Grady, C. A., Bjorkman, K. S., Snow, T. P., et al. 1989, ApJ, 339, 403

Grady, C. A., Sonneborn, G., Wu, C., & Henrichs, H. F. 1987b, ApJS, 65, 673

Gulliver, A. F. 1977, ApJS, 35, 441

Gummersbach, C. A., Kaufer, A., Schaefer, D. R., Szeifert, T., & Wolf, B. 1998, A&A, 338, 881

Hadrava, P. 1992, A&A, 256, 519

Hadrava, P. 2002, `http://www.asu.cas.cz/~had/fotel.html`

Hahula, M. E. & Gies, D. 1994, in IAU Symp. 162: Pulsation; Rotation; and Mass Loss in Early-Type Stars, 100

Hanuschik, R. W. 1989, Ap&SS, 161, 61

—. 1995, A&A, 295, 423

—. 1996, A&A, 308, 170

Hanuschik, R. W. 2000, in ASP Conf. Ser. 214: IAU Colloq. 175: The Be Phenomenon in Early-Type Stars, 518

Hanuschik, R. W., Dachs, J., Baudzus, M., & Thimm, G. 1993, A&A, 274, 356

Hanuschik, R. W., Hummel, W., Dietle, O., & Sutorius, E. 1995, A&A, 300, 163

Hanuschik, R. W., Hummel, W., Sutorius, E., Dietle, O., & Thimm, G. 1996, A&AS, 116, 309

Hanuschik, R. W., Kozok, J. R., & Kaiser, D. 1988, A&A, 189, 147

Hanuschik, R. W. & Vrancken, M. 1996, A&A, 312, L17

Harmanec, P. 1983, Hvar Observatory Bulletin, 7, 55

—. 1984, Bulletin of the Astronomical Institutes of Czechoslovakia, 35, 164

—. 1988, Bulletin of the Astronomical Institutes of Czechoslovakia, 39, 329

—. 1994, Be Star Newsletter, 29, 15

—. 1998, A&A, 334, 558

Harmanec, P. 2000, in ASP Conf. Ser. 214: IAU Colloq. 175: The Be Phenomenon in Early-Type Stars, 13

Harmanec, P. 2002, in ASP Conf. Ser. 279: Exotic Stars as Challenges to Evolution, 221

Harmanec, P., Božić, H., Percy, J. R., et al. 2002, A&A, 387, 580

Harmanec, P., Habuda, P., Štefl, S., et al. 2000, A&A, 364, L85

Harper, W. E. 1934, Publ. Dom. Astrophys. Obs., 6, 207

Hayes, D. P. & Guinan, E. F. 1984, ApJ, 279, 721

Hazlehurst, J. 1967, Zeitschrift f. Astrophysik, 65, 311

Heger, A. & Langer, N. 2000, ApJ, 544, 1016

Heger, A., Langer, N., & Woosley, S. E. 2000, ApJ, 528, 368

Hill, G. M., Walker, G. A. H., Dinshaw, N., Yang, S., & Harmanec, P. 1988, PASP, 100, 243

Hill, G. M., Walker, G. A. H., & Yang, S. 1991, A&A, 246, 146

Hill, G. M., Walker, G. A. H., Yang, S., & Harmanec, P. 1989, PASP, 101, 258

Hiltner, W. A., Garrison, R. F., & Schild, R. E. 1969, ApJ, 157, 313

Howarth, I. D. & Prinja, R. K. 1989, ApJS, 69, 527

Howarth, I. D., Townsend, R. H. D., Clayton, M. J., et al. 1998, MNRAS, 296, 949

Huang, S. 1972, ApJ, 171, 549

Hubert, A. M. & Floquet, M. 1998, A&A, 335, 565

Hubert, H., Hubert, A. M., Chatzichristou, H., & Floquet, M. 1990, A&A, 230, 131

Hummel, W. 1994, A&A, 289, 458

—. 1998, A&A, 330, 243

Hummel, W. & Dachs, J. 1992, A&A, 262, L17

Hummel, W. & Hanuschik, R. W. 1997, A&A, 320, 852

Hummel, W. & Štefl, S. 2001, A&A, 368, 471

Hummel, W. & Vrancken, M. 1995, A&A, 302, 751

—. 2000, A&A, 359, 1075

Hutchings, J. B. 1976, PASP, 88, 5

Hutchings, J. B. & Stoeckley, T. R. 1977, PASP, 89, 19

Ignace, R., Cassinelli, J. P., & Bjorkman, J. E. 1996, ApJ, 459, 671

—. 1998, ApJ, 505, 910

Jackson, S., MacGregor, K. B., & Skumanich, A. 2004, ApJ, 606, 1196

Janot-Pacheco, E., Jankov, S., Leister, N. V., Hubert, A. M., & Floquet, M. 1999, A&AS, 137, 407

Jarad, M. M., Hilditch, R. W., & Skillen, I. 1989, MNRAS, 238, 1085

Jaschek, C. & Jaschek, M. 1983, A&A, 117, 357

—. 1987, The classification of stars (Cambridge: University Press, 1987)

Jeffery, C. S. 1991, MNRAS, 249, 327

Kaiser, D. 1989, A&A, 222, 187

Kambe, E., Ando, H., Hirata, R., et al. 1993, PASP, 105, 1222

Kambe, E., Fabregat, J., & Hirata, R. 1998, in ASP Conf. Ser. 135: A Half Century of Stellar Pulsation

Interpretation: A Tribute to Arthur N. Cox, 145

Kambe, E., Hirata, R., & Fabregat, J. 2000, in ASP Conf. Ser. 214: IAU Colloq. 175: The Be Phenomenon in Early-Type Stars, 252

Katahira, J., Hirata, R., Ito, M., Katoh, M., Ballereau, D., & Chauville, J. 1996, PASJ, 48, 317

Kato, S. 1983, PASJ, 35, 249

Kaufer, A. 1998, in Rev. in Mod. Astron. No. 11, ed. E. Schielicke, 177

Kaufer, A., Stahl, O., Tubbesing, S., et al. 1999, ESO Messenger, 95, 8

Kaufer, A., Stahl, O., Wolf, B., et al. 1996, A&A, 305, 887

Kaufer, A., Wolf, B., Andersen, J., & Pasquini, L. 1997, ESO Messenger, 89, 1

Kilian, J. 1992, A&A, 262, 171

—. 1994, A&A, 282, 867

Koubský, P., Harmanec, P., Kubát, J., et al. 1997, A&A, 328, 551

Koubský, P., Horn, J., Harmanec, P., et al. 1993, A&A, 277, 521

Kroll, P. & Hanuschik, R. W. 1997, in ASP Conf. Ser. 121: IAU Colloq. 163: Accretion Phenomena and Related Outflows, 494

Lamers, H. J. G. L. M. & Pauldrach, A. W. A. 1991, A&A, 244, L5

Lamers, H. J. G. L. M. & Waters, L. B. F. M. 1987, A&A, 182, 80

Langer, N. 1998, A&A, 329, 551

Lee, U. & Saio, H. 1990, ApJ, 349, 570

Leone, F. & Lanzafame, A. C. 1998, A&A, 330, 306

Levenhagen, R. S., Leister, N. V., Zorec, J., et al. 2003, A&A, 400, 599

Limber, D. N. & Marlborough, J. M. 1968, ApJ, 152, 181

Lucy, L. B. 1974, AJ, 79, 745

Maeder, A. & Meynet, G. 2000, ARA&A, 38, 143

Maintz, M. 2003, PhD thesis, Landessternwarte Königstuhl, Ruprecht-Karls-Universität, Heidelberg

Maintz, M., Rivinius, Th., Tubbesing, S., et al. 2000, in ASP Conf. Ser. 214: IAU Colloq. 175: The Be Phenomenon in Early-Type Stars, 244

Maintz, M., Rivinius, Th., Štefl, S., et al. 2003, A&A, 411, 181

Mason, B. D. 1997, AJ, 114, 808

McAlister, H. A., ten Brummelaar, T. A., Gies, D. R., et al. 2004, ApJ, in press, astro-ph/0501261

McDavid, D. 1995, Be Star Newsletter, 30, 23

—. 2000, Be Star Newsletter, 34, 35

—. 2001, ApJ, 553, 1027

McDavid, D., Bjorkman, K. S., Bjorkman, J. E., & Okazaki, A. T. 2000, in ASP Conf. Ser. 214: IAU Colloq. 175: The Be Phenomenon in Early-Type Stars, 460

McLean, I. S. & Brown, J. C. 1978, A&A, 69, 291

Merrill, P. W. & Wilson, O. C. 1941, PASP, 53, 125

Millar, C. E. & Marlborough, J. M. 1999, ApJ, 526, 400

Millar, C. E., Sigut, T. A. A., & Marlborough, J. M. 2000, MNRAS, 312, 465

Moujtahid, A., Zorec, J., & Hubert, A. M. 1999, A&A, 349, 151

Moujtahid, A., Zorec, J., Hubert, A. M., Garcia, A., & Burki, G. 1998, A&AS, 129, 289

Neiner, C., Hubert, A. M., Floquet, M., et al. 2002, A&A, 388, 899

Neiner, C., Hubert, A. M., Frémat, Y., et al. 2003, A&A, 409, 275

Okazaki, A. T. 1991, PASJ, 43, 75

—. 1996, PASJ, 48, 305

—. 1997, A&A, 318, 548

Okazaki, A. T. 2000, in ASP Conf. Ser. 214: IAU Colloq. 175: The Be Phenomenon in Early-Type Stars, 409

—. 2001, PASJ, 53, 119

Osaki, Y. 1998, in IAU Colloq. 169: Variable and Non-spherical Stellar Winds in Luminous Hot Stars, 329

Oudmaijer, R. D. & Drew, J. E. 1997, A&A, 318, 198

Owocki, S. P. 2004, in IAU Symposium 215, 515

Owocki, S. P., Cranmer, S. R., & Blondin, J. M. 1994, ApJ, 424, 887

Owocki, S. P., Cranmer, S. R., & Gayley, K. G. 1996, ApJ, 472, L115

Pérez Hernández, F., Claret, A., Hernández, M. M., & Michel, E. 1999, A&A, 346, 586

Panko, E. & Tarasov, A. E. 2000, in ASP Conf. Ser. 214: IAU Colloq. 175: The Be Phenomenon in Early-Type Stars, 543

Papaloizou, J. C., Savonije, G. J., & Henrichs, H. F. 1992, A&A, 265, L45

Pavlovski, K., Harmanec, P., Božić, H., et al. 1997, A&AS, 125, 75

Penrod, G. D. 1986, PASP, 98, 35

Percy, J. R. & Bakos, A. G. 2001, PASP, 113, 748

Percy, J. R., Hosick, J., Kincaide, H., & Pang, C. 2002, PASP, 114, 551

Peters, G. J. 1983, PASP, 95, 311

—. 1988a, IAU Circ., 4682, 1

—. 1988b, PASP, 100, 207

—. 2001, Publications of the Astronomical Institute of the Czechoslovak Academy of Sciences, 89, 30

Peters, G. J. & Gies, D. R. 2000, in ASP Conf. Ser. 214: IAU Colloq. 175: The Be Phenomenon in Early-Type Stars, 375

Peters, G. J. & Penrod, G. D. 1988, in A Decade of UV Astronomy with the IUE Satellite, Volume 2, 117

Pinsonneault, M. H., Stauffer, J., Soderblom, D. R., King, J. R., & Hanson, R. B. 1998, ApJ, 504, 170

Poeckert, R. 1981, PASP, 93, 297

Poeckert, R., Bastien, P., & Landstreet, J. D. 1979, AJ, 84, 812

Poeckert, R. & Marlborough, J. M. 1978, ApJS, 38, 229

Pollmann, E. 2003, Informational Bulletin on Variable Stars, 5374, 1

Porri, A. & Stalio, R. 1988, A&AS, 75, 371

Porter, J. M. 1996, MNRAS, 280, L31

—. 1998, A&A, 336, 966

—. 1999, A&A, 348, 512

Porter, J. M. & Rivinius, Th. 2003, PASP, 115, 1153

Prinja, R. K. 1989, MNRAS, 241, 721

Quirrenbach, A., Bjorkman, K. S., Bjorkman, J. E., et al. 1997, ApJ, 479, 477

Quirrenbach, A., Buscher, D. F., Mozurkewich, D., Hummel, C. A., & Armstrong, J. T. 1994, A&A, 283, L13

Quirrenbach, A., Hummel, C. A., Buscher, D. F., et al. 1993, ApJ, 416, L25

Rivinius, Th. 1999, in IAU Colloq. 169: Variable and Non-spherical Stellar Winds in Luminous Hot Stars, 36

Rivinius, Th., Baade, D., Štefl, S., Maintz, M., & Townsend, R. 2002, The Messenger, 108, 20

Rivinius, Th., Baade, D., Štefl, S., et al. 1998a, in Cyclical Variability in Stellar Winds, ed. L. Kaper & A. Fullerton, ESO Astroph. Symp., 207

Rivinius, Th., Baade, D., & Štefl, S. 2003, A&A, 411, 229

Rivinius, Th., Baade, D., Štefl, S., & Maintz, M. 2001a, A&A, 379, 257

Rivinius, Th., Baade, D., Štefl, S., et al. 1998b, A&A, 336, 177

—. 1998c, A&A, 333, 125

—. 2001b, A&A, 369, 1058

Rivinius, Th. & Štefl, S. 2000, in ASP Conf. Ser. 214: IAU Colloq. 175: The Be Phenomenon in Early-Type Stars, 581

Rivinius, Th., Štefl, S., & Baade, D. 1999, A&A, 348, 831

Rivinius, Th., Štefl, S., Stahl, O., et al. 2001c, Journal of Astron. Data, 7, 5

Roche, P., Tarasov, A. E., Lyuty, V. M., Clark, J. S., & Larion ov, V. 2000, in ASP Conf. Ser. 214: IAU Colloq. 175: The Be Phenomenon in Early-Type Stars, 589

Royer, F., Gerbaldi, M., Faraggiana, R., & Gómez, A. E. 2002, A&A, 381, 105

Sackmann, I. J. 1970, A&A, 8, 76

Sareyan, J. P., Gonzalez-Bedolla, S., Chauville, J., Morel, P. J., & Alvarez, M. 1992, A&A, 257, 567

Sareyan, J. P., Gonzalez-Bedolla, S., Guerrero, G., et al. 1998, A&A, 332, 155

Savonije, G. J. & Heemskerk, M. H. M. 1993, A&A, 276, 409

Scargle, J. D. 1982, ApJ, 263, 835

Schmutz, W., Schweickhardt, J., Stahl, O., et al. 1997, A&A, 328, 219

Secchi, A. 1867, Astronomische Nachrichten, 68, 63

Shorlin, S. L. S., Wade, G. A., Donati, J.-F., et al. 2002, A&A, 392, 637

Slettebak, A. 1976, in IAU Symp. 70: Be and Shell Stars, 123

Slettebak, A. 1982, ApJS, 50, 55

Slettebak, A. 1987, in IAU Colloq. 92: Physics of Be Stars, 24

Smith, M. A. 1989, ApJS, 71, 357

—. 2001, ApJ, 562, 998

Smith, M. A., Peters, G. J., & Grady, C. A. 1991, ApJ, 367, 302

Spear, G. G., Mills, J., & Snedden, S. A. 1981, PASP, 93, 460

Stagg, C. 1987, MNRAS, 227, 213

Stee, P. 1995, Ap&SS, 224, 561

Štefl, S., Aerts, C., & Balona, L. A. 1999, MNRAS, 305, 505

Štefl, S., Baade, D., Harmanec, P., & Balona, L. A. 1995, A&A, 294, 135

Štefl, S., Baade, D., Rivinius, Th., Otero, S., & Setiawan, J. 2001, Informational Bulletin on Variable Stars, 5193, 1

Štefl, S., Baade, D., Rivinius, Th., et al. 1998, in ASP Conf. Ser. 135: A Half Century of Stellar Pulsation Interpretation: A Tribute to Arthur N. Cox, 348

Štefl, S., Baade, D., Rivinius, Th., et al. 2003a, A&A, 402, 253

—. 2003b, A&A, 411, 167

Štefl, S. & Balona, L. A. 1996, A&A, 309, 787

Štefl, S., Hadrava, P., Baade, D., et al. 2004, in IAU Symposium 215, 166

Štefl, S., Hummel, W., & Rivinius, Th. 2000, A&A, 358, 208

Štefl, S. & Rivinius, Th. 2000, in ASP Conf. Ser. 214: IAU Colloq. 175: The Be Phenomenon in Early-Type Stars, 356

Štefl, S., Rivinius, Th., & Baade, D. 2002, in ASP Conf. Ser. 259: IAU Colloq. 185: Radial and Nonradial Pulsationsn as Probes of Stellar Physics, 248

Stoeckley, T. R. 1968, MNRAS, 140, 141

Struve, O. 1931, ApJ, 73, 94

Tarasov, A. E. & Tuominen, I. 1987, in European Regional Astronomy Meeting of the IAU, Volume 5, 127–129

Telting, J. H., Heemskerk, M. H. M., Henrichs, H. F., & Savonije, G. J. 1994, A&A, 288, 558

Telting, J. H. & Kaper, L. 1994, A&A, 284, 515

Telting, J. H. & Schrijvers, C. 1997, A&A, 317, 723

Townsend, R. H. D. 1997a, PhD thesis, University College London

Townsend, R. H. D. 1997b, MNRAS, 284, 839

—. 2005, MNRAS, in press

Townsend, R. H. D., Owocki, S. P., & Howarth, I. D. 2004, MNRAS, 350, 189

Tubbesing, S., Rivinius, Th., Wolf, B., & Kaufer, A. 2000, in ASP Conf. Ser. 214: IAU Colloq. 175: The Be Phenomenon in Early-Type Stars, 232

Tycner, C., Hajian, A. R., Armstrong, J. T., et al. 2004, AJ, 127, 1194

Underhill, A. & Doazan, V. 1982, B Stars with and without emission lines (NASA)

Underhill, A. B. 1985, A&A, 148, 431

Vakili, F., Mourard, D., Stee, P., et al. 1998, A&A, 335, 261

van Kerkwijk, M. H., Waters, L. B. F. M., & Marlborough, J. M. 1995, A&A, 300, 259

von Zeipel, H. 1924, MNRAS, 84, 665

Waters, L. B. F. M. 1986, A&A, 162, 121

Waters, L. B. F. M., Coté, J., & Pols, O. R. 1991a, A&A, 250, 437

Waters, L. B. F. M. & Marlborough, J. M. 1992, A&A, 253, L25

Waters, L. B. F. M. & Marlborough, J. M. 1994, in IAU Symp. 162: Pulsation; Rotation; and Mass Loss in Early-Type Stars, 399

Waters, L. B. F. M., Marlborough, J. M., van der Veen, W. E. C., Taylor, A. R., & Dougherty, S. M. 1991b, A&A, 244, 120

Wilson, R. E. 1953, General Catalogue of Stellar Radial Velocities (Carnegie Institute Washington D.C. Publication)

Wood, K., Bjorkman, J. E., Whitney, B. A., & Code, A. 1996, ApJ, 461, 847

Wood, K., Bjorkman, K. S., & Bjorkman, J. E. 1997, ApJ, 477, 926

Yang, S., Walker, G. A. H., Hill, G. M., & Harmanec, P. 1990, ApJS, 74, 595

Yudin, R. V. 2001, A&A, 368, 912

Zorec, J. 1994, in IAU Symp. 162: Pulsation; Rotation; and Mass Loss in Early-Type Stars, 57

Zorec, J. & Briot, D. 1997, A&A, 318, 443

Zorec, J., Israelian, G., Ballereau, D., & Chauville, J. 1996, A&A, 308, 852

Appendices

Appendix A

Observational database

Over the past eight years more than 4000 spectra of Be stars were obtained in the framework of the HEROS project and successors (Baade et al. 2002a). Except for a few objects selected because of their well known variability, like μ Cen and ω CMa, most targets were observed on account of their apparent brightness and celestial position. Most of the data were taken with the instruments FLASH (≈ 400 spectra, at Tautenburg and Wendelstein) HEROS (≈ 3000 spectra, at various observatories) and FEROS (≈ 800 spectra, at the ESO 1.5m telescope). Several dozen of spectra were taken with other instruments like AURELIE at the OHP and the coudé echelle in Ondřejov.

HEROS is the dual-channel cross-dispersed echelle spectrograph of the Landessternwarte Heidelberg. Via a fibre link it was used with the ESO 50-cm telescope on La Silla, Chile, with the 1.23-m telescope on Calar Alto, Spain, and with numerous other telescopes. HEROS covers more than the entire Paschen continuum (3450 Å to 8600 Å) at a resolving power of $R = \lambda/\Delta\lambda = 20\,000$. The instrument was described in detail by Kaufer (Kaufer (1998)). The data reduction procedures are described in Rivinius et al. (2001c).

FLASH is the same instrument as HEROS, but used in a single channel configuration. It was used before 1996, typically covering the wavelength range of 4050 to 6750 Å with a larger fibre and thus lower resolving power of about 12 000. After 1996, it was used only once on Wendelstein, when the detector of the blue channel failed. There it was used with the smaller fibre giving $R = 20\,000$.

FEROS is a fibre linked echelle spectrograph permanently mounted at the ESO 1.52m telescope from the end of 1998 until 2002. FEROS covers the wavelength range of 365 to 920 nm in a single exposure, providing a resolving power of $R = \lambda/\Delta\lambda = 48\,000$. Further technical instrument characteristics, including the reduction, have been described in detail by Kaufer et al. (1997, 1999).

All above instruments are fibre-linked, predispersed echelle spectrographs, providing a large wavelength coverage over the Paschen continuum (and partly beyond) at high resolution (Table A.1). The observations aimed at a S/N of $100\ldots150$ with HEROS and $200\ldots300$ with FEROS, measured per extracted and rebinned pixel (0.1 Å wide for HEROS and 0.03 Å for FEROS) in the stellar continuum close to Hβ. Data from the observing runs at La Silla, both with HEROS and FEROS, were already introduced by Rivinius et al. (1998c) and Štefl et al. (2003a), assessing instrument stability and other questions.

The observations at La Silla were typically carried out in South American late summer with very good weather, so that the run lengths are almost equal to the number of nights with observations. For the European observations at the Landessternwarte Königstuhl, Calar Alto, Wendelstein, and Ondřejov only about 30 to 50 % of the nights could actually be observed in. An idea of the sampling can be obtained by combining the information in Tables A.1 and A.2 for individual stars. Note that the typical sampling rates and S/N ratios only exceptionally allowed to search also for higher modes with shorter periods.

Since August 2000, HEROS was mounted at the 2m telescope of the Czech Academy of Sciences in Ondřejov. As part of a long-term agreement, 50 % of the total time was available to our group, typically in a two-week alternating rhythm. Due to a fatal CCD failure the observations were ended in May 2003.

A few dozen spectra were obtained 2001 by Y. Goranova, A. Bik, and M. Stuhlinger at Observatoire de Haute-Provence with AURÉLIE at the 1.52m telescope during the 2nd NEON observing school, covering about 20 nm around 450 nm with high resolution.

For some program stars, particularly those discussed in part I, additional spectra could be used from the Ondřejov spectral archive, covering the Hα region at a resolving power of about 6000.

Table A.1: The Be star observing campaigns.

Run name	Season	Telescope	Instrument	Run length [d]	Typ. # of spectra per night&object	Resolving power	Spectral range [Å]
taut[1]	1988-1992	Tautenburg 2m	FLASH	–	–	12 000	4050-6700
ls95	1995 Feb.–May	ESO 0.5m	HEROS	118	1	20 000	3450-8620
ls96	1996 Jan.–April	ESO 0.5m	HEROS	103	1	20 000	3450-8620
ls96MJ	1996 May/June	ESO 0.5m	HEROS	27	5–10	20 000	3450-8620
ls97	1997 Jan.–April	ESO 0.5&1.5m	HEROS	82	1	20 000	3450-8620
lsw97	Late 1997–Early 1998	LSW 0.7m	HEROS	150	1–5	20 000	3450-8620
ca98	1998 Aug.–Okt.	CA 1.23m	HEROS	62	1–5	20 000	3450-8620
ls99a	1999 Jan.	ESO 1.5m	FEROS	7	5	48 000	3650-9200
ls99b	1999 Jan.–April	ESO 0.5m	HEROS	71	1	20 000	3450-8620
ls99c	1999 May/June	ESO 1.5m	FEROS	21	1–2	48 000	3650-9200
ls00	2000 Jan.	ESO 1.5m	FEROS	17	4–5	48 000	3650-9200
wn00	2000 May–July	WN 0.8m	FLASH	67	1	20 000	4050-6700
ohp01	2001 July	OHP 1.5m	AURÉLIE	2	5–10	50 000	4450-4600
ls02	2002 Jan.	ESO 1.5m	FEROS	2	60	48 000	3650-9200
ls02c	2002 Feb.	ESO 1.5m	FEROS	2	60	48 000	3650-9200
ond	2000–2003	Ond 2m	HEROS	ca. 900	1	20 000	3650-8620

[1]: This summarizes in fact various runs at the Landessternwarten Tautenburg and Königstuhl

Name	HR	HD	Sp. type	$v\sin i$ [km s^{-1}]	observed seasons (obtained spectra)
γ Cas	264	5 394	B0.5 IVe	230	ca98 (9), ond (55)
α Eri	472	10 144	B4 V(e)	225	ls96MJ (5), ls99a (20), ls99b (42), ls00 (44)
ϕ Per	496	10 516	B1.5 (V:)e-shell	450	lsw97 (12), ca98 (8), wn00 (21), ond (37)
μ For	652	13 709	B9 V		ls99 (1)
ψ Per	1087	22 192	B5 IIIe-shell	280	ond (8)
17 Tau	1142	23 302	B6 III	180	ond (12)
23 Tau	1156	23 480	B6 IV(e)	280	ond (7)
η Tau	1165	23 630	B7 IIIe	140	ond (12)
28 Tau	1180	23 862	B8 (V:)e-shell	320	taut (27), lsw97 (4), ca98 (8), ond (3)
48 Per	1273	25 940	B4 Ve	200	ond (10)
DU Eri	1423	28 497	B1 Ve	230	ls00 (6)
DX Eri	1508	30 076	B2 Ve	180	ls00 (42)
11 Cam	1622	32 343	B3 Ve	100	ond (3)
λ Eri	1679	33 328	B2 III(e)p	250	lsw97 (8), ca98 (29), ls00 (44)
ψ^1 Ori	1789	35 439	B1 Ve	320	ls00 (4)
ζ Tau	1910	37 202	B1 Ve-shell	320	taut (1), ca98 (3), ond (19)
ω Ori	1934	37 490	B2 IVe	160	lsw97 (16), ca98 (20)
HR 2142	2142	41 335	B2 IVe	350	ls99a (2), ls99b (11), ls99c (9), ls02c (8), ond (21)
FR CMa	2284	44 458	B1.5 IVe	200	ls95 (1)
ν Gem	2343	45 542	B6 IVe	170	ond (34)
ν Pup	2451	47 670	B8 III-(shell)	220	ls95 (1), ls96 (2), ls96MJ (6), ls97 (7), ls99a (2), ls99b (5), ls00 (1)
10 CMa	2492	48 917	B2 IIIe	200	ls00 (21)
κ CMa	2538	50 013	B2 IVe	220	ls00 (82)
FV CMa	2690	54 309	B2 IVe	200	ls00 (13)
27 CMa	2745	56 014	B3 III(e)p-shell	150	ls00 (23)
ω CMa	2749	56 139	B2.5 Ve	80	ls96 (97), ls97 (127), ls99a (32), ls00 (64), ls02 (127)
FW CMa	2825	58 343	B3 Ve	40	ls96 (9), ls97 (87), ls00 (40)
BN Gem	—	60 848	O8 V:pevar	360	taut (12)
—	—	76 534	B2 Vn	200	ls00 (6)
HD 76534	3642	78 764	B2 IVe	120	ls99b (6)

Table A.2: continued

Name	HR	HD	Sp. type	$v \sin i$ [km s^{-1}]	observed seasons (obtained spectra)
	4009	88 661	B2 IVe	220	ls99b (52), ls00 (66)
ω Car	4037	89 080	B8 IIIe-shell	220	ls95 (1), ls96 (2), ls96MJ (8), ls97 (7), ls99a (4), ls99b (5), ls00 (1)
	4074	89 890	B3 III	70	ls99c (15)
HR 4123	4123	91 120	B9 IVe	250	ls00 (1)
PP Car	4140	91 465	B4 Ve	250	ls99b (55)
HR 4221	4221	93 563	B8 III(e)-shell	280	ls00 (1)
δ Cen	4621	105 435	B2 IVe	220	ls99b (36)
	4625	105 521	B3 IVe	130	ls99b (50)
κ Dra	4787	109 387	B5 IIIe	200	taut (195), wn00 (20), ohp01 (1), ond (54)
HR 4823	4823	110 335	B6 IVe	250	ls00 (1)
HR 4830	4830	110 432	B1 IIIe	300	ls99a (2)
μ Cen	5193	120 324	B2 IV-Ve	155	ls95 (97), ls96 (87), ls96MJ (115), ls97 (83), ls99b (63), ls99c (44)
	5223	120 991	B2 IVe	70	ls99c (8)
η Cen	5440	127 972	B2 IVe	350	ls95 (46), ls96 (89), ls96MJ (202), ls97 (80), ls99b (28), ls99c (5)
κ^1 Lup	5646	134 481	B9 V(e?)	160	ls99b (3)
κ^1 Aps	5730	137 387	B3 IVe-2 sp.?	350	ls99b (50), ls99c (3)
θ CrB	5778	138 749	B6 III	320	taut (125), wn00 (2), ond (57)
HD 141 851	—	141 851	A3 Vn	185:	ls95 (1)
4 Her	5938	142 926	B7 IVe-shell	300	ca98 (2), wn00 (14), ohp01 (1), ond (29)
48 Lib	5941	142 983	B3: IV:e-shell	400	ls95 (1), ls95 (8), ca98 (2), ls99b (3), ond (4)
χ Oph	6118	148 184	B1.5 Ve	140	ls99b (49)
ι Ara	6451	157 042	B2.5 IVe	320	ls99b (38)
α Ara	6510	158 427	B3 Ve	250	ls99b (43)
88 Her	6664	162 732	B		ond (1)
66 Oph	6712	164 284	B2 IV-Ve	240	ohp01 (5), ond (51)
HR 6819	6819	167 128	B3 IIIe	50	ls99c (12)
λ Pav	7074	173 948	B1.5 III	170	ls99b (11)
HR 7316	7316	180 885	B3 V		ls99c (1)
HR 7355	7355	182 180	B2 Vn		ls99c (1)
28 Cyg	7708	191 610	B3 IVe	320	lsw97 (107), ca98 (107), wn00 (5), ond (88)
25 Vul	7789	193 911	B6 IVe	200	wn00 (2), ond (4)
v Cyg	8028	199 629	B2.5 Ve	180	wn00 (1), ond (18)

Table A.2: continued

Name	HR	HD	Sp. type	$v \sin i$ [km s^{-1}]	observed seasons (obtained spectra)
59 Cyg	8047	200 120	B1 Ve	260	taut (20), ca98 (38), wn00 (15), ohp01 (1), ond (50)
ε Cap	8260	205 637	B3 IIIe	250	ls95 (6), ls96 (23), ls96MJ (38), ca98 (4), ls99b (20), ls99c (7), ond (1)
o Aqr	8402	209 409	B7 IIIe-shell	300	ls99b (17), ls99c (6)
31 Peg	8520	212 076	B1.5 Ve	100	ls99c (11), ohp01 (14), ond (18)
π Aqr	8539	217 571	B1 III-IVe	300	ls99c (12), ohp01 (26), ond (11)
ε PsA	8628	214 748	B7 IVe	180	ls99c (12)
EW Lac	8731	217 050	B3: IV:e-shell	300	ca98 (2), ond (5)
o And	8762	217 675	B6 III	260	ca98 (104), wn00 (6), ond (110)
β Psc	8773	217 891	BB5 Ve	100	ls99c (12), ond (3)
ε Tuc	9076	224 686	B8 V	280	ls99b (1)

Appendix B

Bright Be-shell stars

The numerous HEROS observing runs of the past decade were primarily focused on the short-term variability of individual Be stars (see App. D). However, as a by-product, many observations were at irregular intervals obtained also of shell stars to follow their medium- and long-term variability. Special features or events sometimes prompted somewhat denser series of observations. The homogeneity of the database, its high spectral resolution, signal-to-noise, and wavelength coverage as well as its relatively long time baseline offer an excellent opportunity to assemble a statistically meaningful picture of the rotational properties of the disc, the disc structure and life cycles (see Part I). Eventually, they should result in a more complete knowledge and understanding of the dominant forces acting on and in the discs of Be stars.

For the sake of completeness, the sample of shell stars is augmented by 3 more stars, which have gone through phases of significant line emission with and without shell absorption lines (see Sect. B.2). In the other 23 stars shell absorption lines were never reported missing when significant line emission was present. This suggests that either the structure or the orientation of the discs of these 3 stars was different from the others.

In order to identify possible differences between Be stars and rapidly rotating B stars, that were never observed to exhibit emission lines, HEROS also observed nearly 20 Bn stars. They are presented in Sect. B.3.

Table B.1 summarizes the known Be shell stars brighter than about 6.5 mag, the three objects that have shown transitions between mixed shell/emission and pure emission type spectra, and three Bn stars that might be surrounded by weak discs. Most of the objects listed were observed with FLASH or HEROS in the past decade. The observations confirmed their shell classification according to the more restrictive definition by Hanuschik (1996). This definition requires that the residual shell absorption, i.e. after correction for the photospheric component, reaches deeper than the base level of the accompanying line emission. Such a criterion ensures that at least part of the central reversal of the emission line is due to absorption of light in front of the star. Only for four of these stars no own spectra are available. These are HR 7415, and 1 Del, marked as shell stars by Slettebak (1982), and HR 1772 and HD 193 182, noted to be shell stars by Hanuschik (1996). The data of ϕ Per were already discussed by Štefl et al. (2000) and Hummel & Štefl (2001).

Table B.1: The shell stars considered in this study and their observed parameters. Unless otherwise noted here or the detailed description, Spectral type and $v\sin i$ were taken from Slettebak (1982), but always cross-checked against the HEROS data where possible. $w = v_{\mathrm{rot}}/v_{\mathrm{crit}}$ was calculated using v_{crit} given in Table 2 of Yudin (2001), who interpolated values by Moujtahid et al. (1999). For stars without available luminosity class, the v_{crit} for dwarfs was used to obtain a lower limit to w. Since it is of some relevance whether phenomena can co-exist in the same star at the same time, the columns for V/R variability and CQE only list the state of the disc during our observations, although such information is available from the literature also for other times and the other stars.

HD number	HR number	name	Sp. type	$v\sin i$ [km s^{-1}]	$w\sin i$	V/R variable	CQE occurrence	binary	References
			Conventional shell stars (Sect. B.1)						
10516	496	ϕ Per	B1.5 (V:)e shell	450	0.90:	√	—	√	1
13709	652	μ For	A0 V	320	0.82	—	√	—	2
22192	1087	ψ Per	B5 IIIe shell	280	0.90	?	—	—	
35165	1772		B5 IVnp	280	0.73	no own spectra			3,4
37202	1910	ζ Tau	B1 IVe shell	320	0.66	√	—	√	5
41335	2142		B2 IVe	350	0.79	√	—	√	
45542	2343	ν Gem B	B8 IIIe	—	—	√	—	√	
45725	2356	β Mon A	B4 Ve shell	300	0.68	—	√	—	6
47760	2451	ν Pup	B8 III	230	0.84	—	—	—	7
56014	2745	27 CMa	B3 III(e)p shell	280	0.82	—	√	—	
89080	4037	ω Car	B8 IIIe shell	220	0.80	—	√	—	
91120	4123		B9 IVe	250	0.73	—	?	—	
93563	4221		B8 III(e) shell	280	1.02	—	—	—	
110335	4823	39 Cru	B6 IVe	250	0.67	—	—	—	
127972	5440	η Cen	B2 IV(e)	350	0.79	—	√	—	
137387	5730	κ^1 Aps	B3 IVe - 2 sp.?	350	0.83	—	√	—	
138749	5778	θ CrB	B6 III	320	1.08	—	√	—	
142926	5938	4 Her	B7 IVe shell	300	0.83	—	√	√	
142983	5941	48 Lib	B3:IV:e shell	400	0.95:	√	—	—	
162732	6664	88 Her	B6 IVe	300	0.80	—	—	√	8,9
183656	7415		B6e shell	300	>0.73	no own spectra			
193182			B8.5 III	200	0.73	no own spectra			10
195325	7836	1 Del	B8-9:(e) shell	280:	>0.71:	no own spectra			
205637	8260	ϵ Cap	B3 IIIe	250	0.74	—	√	√	

Table B.1: Table B.1 continued

HD number	HR number	name	Sp. type	$v \sin i$ [km s^{-1}]	$w \sin i$	V/R variable	CQE occurrence	binary	References
209 409	8402	o Aqr	B7 IIIe shell	300	1.06	—	√	—	
217 050	8731	EW Lac	B3:IV:e shell	300	0.71:	√	—	—	
217 675	8762	o And	B6 III	260	0.88	—	√	√	
Be stars having had both shell and emission phases (Sect. B.2)									
5394	264	γ Cas	B0.5 IVe	380	0.76	√	—	√	11
23 862	1180	28 Tau	B8 (V:)e shell	320	0.81:	√	—	—	
200 120	8047	59 Cyg	B1 Ve	$\geq$379	$\geq$0.73	√	—	√	7
Bn stars showing weak edge-on disc evidence (Sect. B.3)									
141 637	5885	1 Sco	B3 V	225	0.49	—	√	—	12
142 114	5904	2 Sco	B2.5 Vn	250	0.53	—	√	—	12
213 998	8597	η Aqr	B9 IV-Vn	245	0.68	—	√	—	12

1: Poeckert (1981), 2: Royer et al. (2002), 3: Hiltner et al. (1969), 4: Balona (1995), 5: Yang et al. (1990), 6: Chapter 2, 7: Chauville et al. (2001), 8: Divan & Zorec (1982), 9: Slettebak (1976), 10: Denizman et al. (1993), 11: Harmanec (2002), 12: Abt et al. (2002)
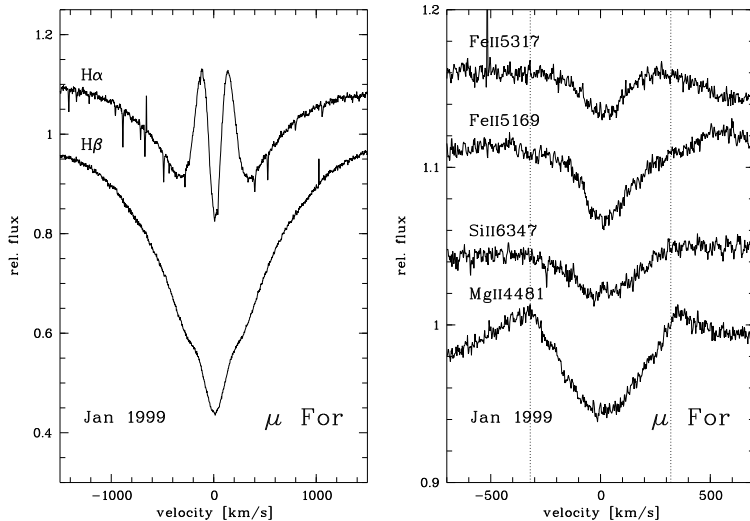
Figure B.1: Evidence for μ For being a shell star. The dotted lines mark $\pm v \sin i = 320 \, \mathrm{km^{-1}}$. Several lines show absorption cores typical of weak shells and even CQEs. The MgII 4481 line shows the undisturbed stellar rotational profile for comparison.

B.1 Shell type stars

μ For (= HR 652 = HD 13 709) is a star not previously known to show Balmer line emission. SIMBAD lists spectral type determinations from B9 V to A2 Vn. The shell phenomenon is common also in A- and even F-type stars. But since the presence of line emission is unusual among them, μ For is counted as 'Be-star' in this study, even if the 'median' spectral type is only A1 V and the most recent determination by Royer et al. (2002) is A0 V. The latter was adopted for the determination of the stellar parameters.

The star was observed only once with FEROS in January, 1999 (Fig. B.1). The FeII lines are narrow compared to the measured $v \sin i$ and do not exhibit a profile typical of rotational broadening, but rather of weak shells (cf. Chapter 2). The CQE apparent in SiII 6347 and the depth of the $H\alpha$ absorption core support the conclusion that μ For is a weak shell star. Royer et al. (2002) derived a $v \sin i$ of $320 \, \mathrm{km \, s^{-1}}$, but did not see anything unusual in spectra obtained between 1989 and 1995.

ψ Per (= HR 1087 = HD 22 192) was observed from Ondřejov thirteen times with the coudé spectrograph (1994 to 1999) and seven times with HEROS (2000 to 2002).

The profiles of this B5 IIIe-shell star did not exhibit significant shape variations. But the $H\alpha$ emission equivalent width increased slowly in absolute value from $W_\lambda = -34 \, \text{Å}$ to $-42 \, \text{Å}$. Although the coincidence of the jump in W_λ with the change from the Ondřejov coudé instrument to HEROS is suspicious, there is no other reason to dismiss it as spurious. Almost equally large variations are seen within the coudé instrument data alone, e.g. around JD=50 500. The various emission lines with $V/R \neq 1$ may indicate long-term V/R variability in the order of 1 % due to a weak global density wave pattern in the disc. But in the three years observed with HEROS no change was observed. The invariable differences in V/R between various lines (Fig. B.2) do not match the cyclic V/R behaviour expected from density waves (Hanuschik et al. 1995).

ζ Tau (= HR 1910 = HD 37 202) was observed 1991 with FLASH, 1993 to 2000 with the Ondřejov coudé, and finally 1998 and 2000 to 2002 with HEROS. It is a binary with a period of about 133 d (e.g. Harmanec 1984).

Inspection of lines with little circumstellar contribution, such as HeI 4009, 4026, or 4713, favours $v \sin i = 320 \, \mathrm{km \, s^{-1}}$, given by Yang et al. (1990, see also Fig. B.3), over lower values also sometimes published. In the strongest of these lines, HeI 4026, the orbital motion is clearly apparent also in the broad, supposedly photospheric component. The circumstellar shell itself is also variable with narrow, but strong absorption in 1998, becoming broader and shallower in the following years (Fig. B.3).

In the past years, ζ Tau continued its long-term V/R variations with cycle lengths of about 4 years. This is also reflected in the radial velocities (RV) of the shell lines, e.g., SiII 6347; 2 cycles of remarkable similarity were recorded (Fig. B.3). A formal period analysis of the SiII 6347 RVs yields $1503 \pm 18 \, \mathrm{d}$,
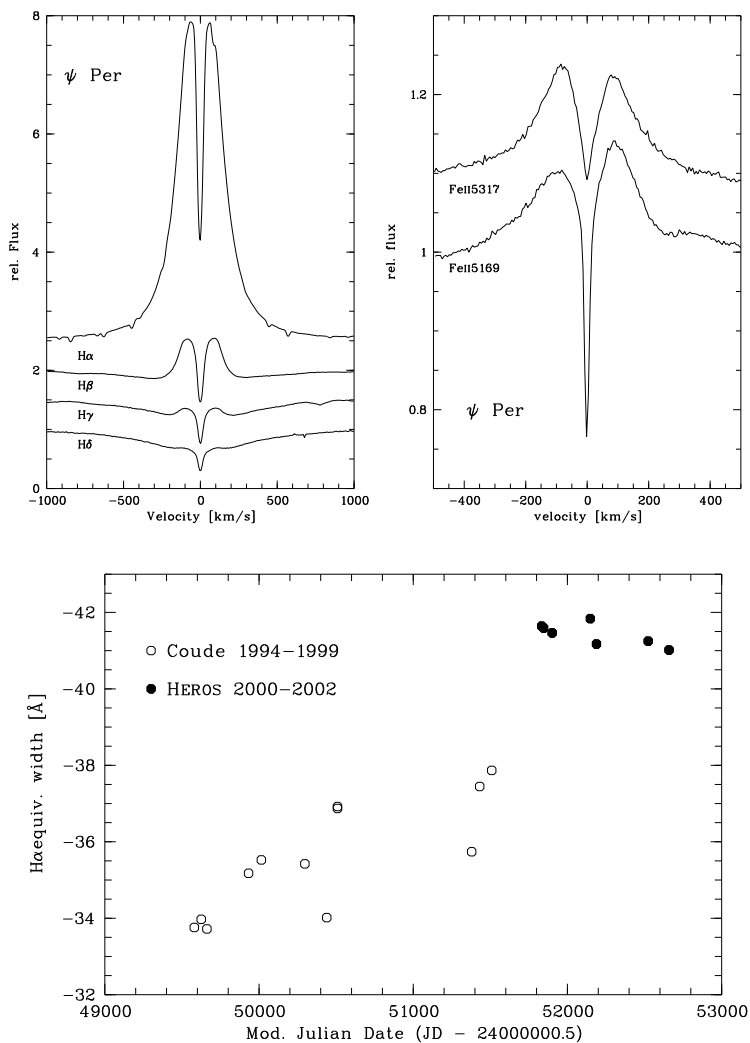
Figure B.2: Shell lines of ψ Per observed with HEROS in 2002. The V/R is unity for the Balmer lines, but greater than one for FeII 5317 and less than one for FeII 5169.

removing almost all power from the power spectrum. The binary motions, for which the present data suggest a period of 134.6 ± 0.6 d with a semi-amplitude of $10 \, \mathrm{km \, s^{-1}}$, only rank as the third-strongest feature, after the first harmonic of the 1503 d cycle.

On April 1, 1991 a very unusual Hα profile was observed, which was found later also in Ondřejov coudé observations in 1996 and 1999 (Fig. B.4). Similar profiles were seen already 1982 by Hanuschik et al. (1996) and ascribed to disc distortions due to the companion. However, the occurrence of this peculiar type of profile does not correspond to any special phase of the ephemeris given by Harmanec (1984). Rather, it appears linked to a change of the V/R-ratio from $\ll 1$ to $\gg 1$ (cf. Fig. 1 of McDavid et al. 2000). According to Telting et al. (1994), such a behaviour is consistent with a prograde precessing density wave (see also Vakili et al. 1998). It occurs when the dense part of the global wave is behind the star as seen from Earth, so that the V/R ratio changes from smaller to larger than unity.

Such a peculiar profile was seen to accompany a change in sign of $\log(V/R)$ also in ν Gem, which like ζ Tau is a binary. But contrary to ν Gem the positions of the peak substructure in ζ Tau were not stable in radial velocity (Fig. B.4).

Similar profiles were reported also for ϕ Per (Galkina 1990), which is another binary with V/R variations seemingly unrelated to the orbital motions. Two profiles in the present database confirm this.

HR 2142 (= HD 41 335) shows periodic shell absorptions, similar to ϕ Per, and is a binary with $P = 80.86$ d (Peters 1983). However, the nature of the secondary is not entirely clear. It could either a hot subdwarf, causing the same phenomenon as in ϕ Per (Waters et al. 1991a; Hummel & Štefl 2001), or a
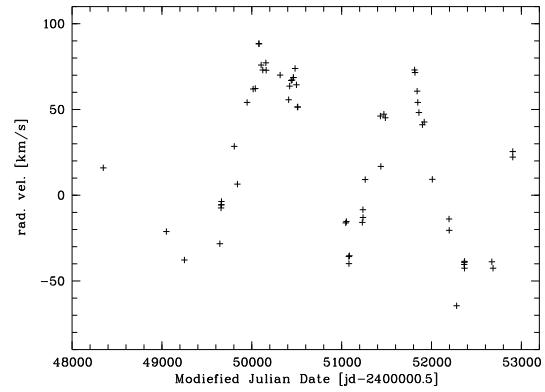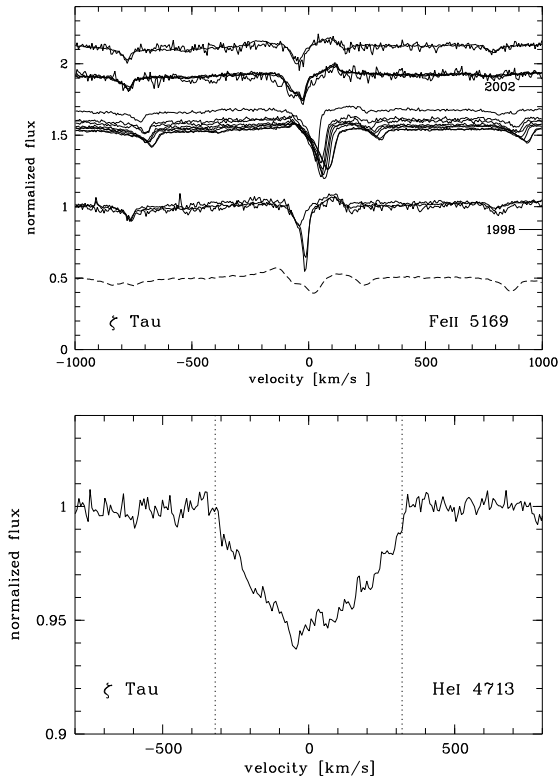
Figure B.3: The evolution of the circumstellar shell FeII lines of ζ Tau (upper left panel). The 1991 spectrum is included as dashed line. The radial velocity curve of the SiII 6347 shell absorption is shown in the upper right panel. The lower panel displays HeI 4713, relatively unaffected by the shell, and two dotted lines at $\pm v \sin i = 320 \, \mathrm{km \, s^{-1}}$.
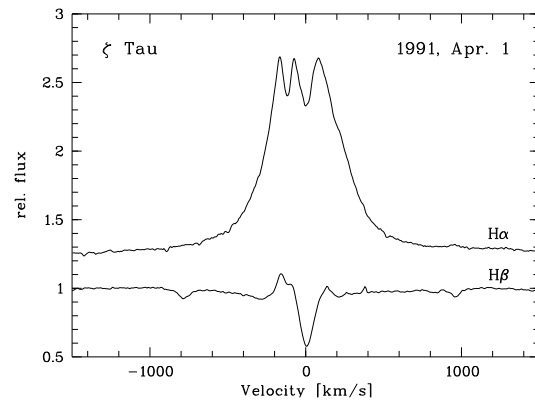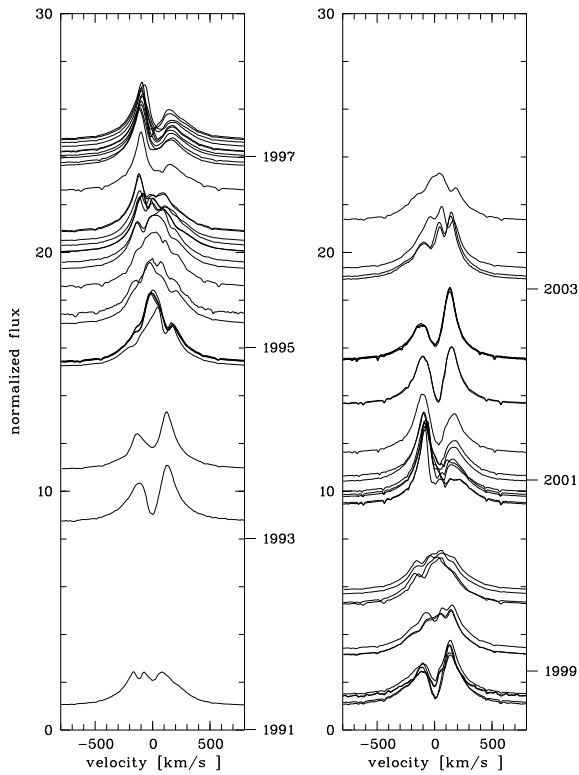

Figure B.4: Triple-peaked profiles in ζ Tau. The right panel shows the spectrum taken on April 1, 1991. The evolution of the Hα line from 1991 to 2003 is shown in the eft panels. The vertical offset of the profiles is proportional to time and corresponds to one continuum unit per 1/4 year. The lowermost spectra were taken Apr. 1, 1991 (left) and Aug 19, 1998 (right), respectively.

Table B.2: Binary parameters derived from the radial velocities (RVs) of ν Gem (Fig. B.5) and ε Cap (Fig. B.15) by means of VELOC (Schmutz, unpublished, e.g. used also by Schmutz et al. 1997) and FOTEL (Hadrava 2002). Since the eccentricity is zero for ε Cap, T_0 denotes the time of maximal RV. The VELOC and FOTEL solutions agree very well within their errors.

γ [km s^{-1}]	K [km s^{-1}]	P [d]	T_0 JD	ϕ °	e
ε Cap, VELOC					
-8.9	8.7	128.5	51030	$-$	0.00
FOTEL					
-9.2 ± 0.2	8.8 ± 0.3	128.3 ± 0.2	51029.1 ± 0.6	$-$	0.00
ν Gem, VELOC					
34.4	37.6	53.733	51005	316	0.11
FOTEL					
34.5 ± 1.1	38 ± 8	$53.731 \pm .017$	51004.7 ± 4.2	315 ± 29	0.11 ± 0.05
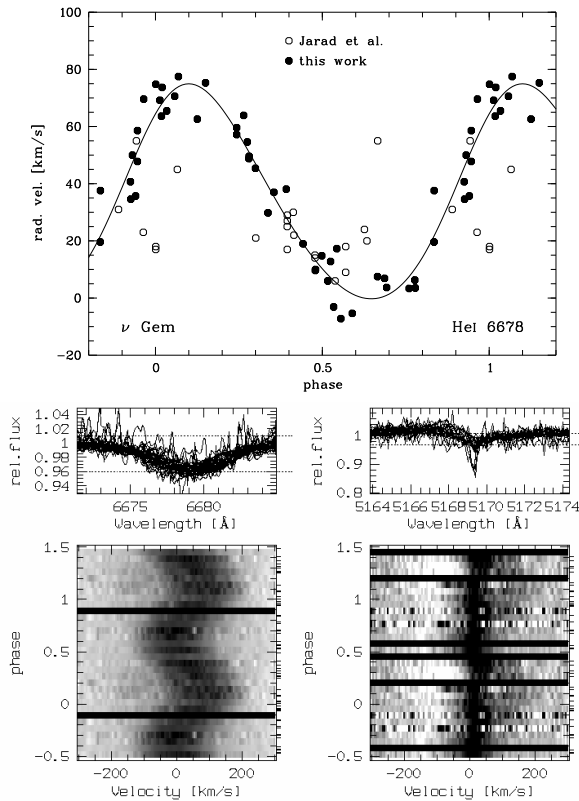
Figure B.5: Upper panel: HeI 6678 radial velocity curve of ν Gem, phased with $P = 53.72$ d. (Table B.2, VELOC). Open symbols taken from Jarad et al. (1989). Lower panels: Photospheric lines like HeI 6678 are RV variable, while circumstellar shell lines like FeII 5169 (only covered by HEROS spectra) do not follow this period.

mass-transferring cool star, in which case the shell absorption would arise from the mass-transfer stream passing the line of sight (Peters 2001). In the latter case the inclination would be less than about 77°, since no eclipses are observed, which would make the listed $w = 0.79$ a lower limit, but probably not much less, since then the mass-transfer stream would not intersect the line of sight (under the assumption that orbit and stellar rotation are co-planar). In this sense, HR 2142 is kept in Table B.1.

In addition, HR 2142 is a V/R variable. But because of the orbital variations of the Balmer lines this is better visible in FeII and similar lines, which are relatively unaffected by the companion.

ν **Gem** (= **HR 2343** = **HD 45 542**) is part of a very close visual pair ($< 0.2''$) with a magnitude difference of the order of 1 mag, for which micrometer, speckle and lunar-occultation observations are available
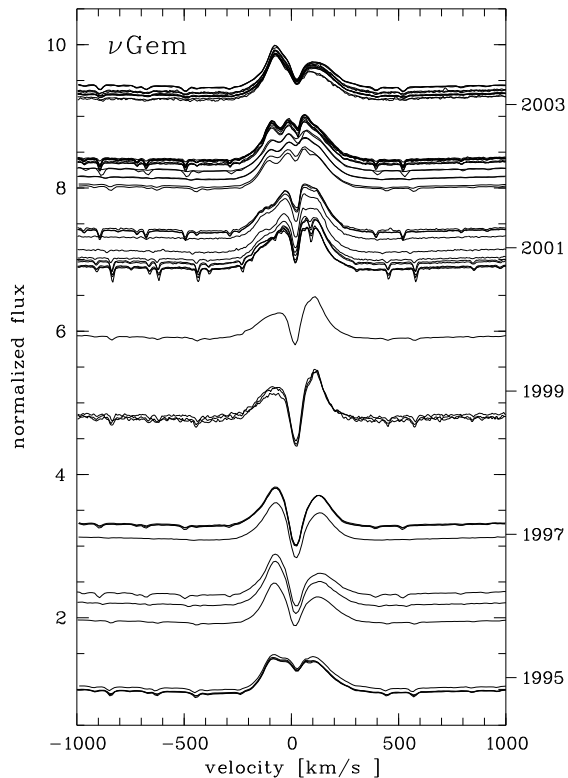
Figure B.6: Line profiles of Hα of ν Gem. A vertical offset of one flux unit corresponds to one year. The first spectrum was taken Nov. 2, 1994. Note the remarkable similarity of the Hα profiles in 2002 to that of ζ Tau in 1991 (Fig. B.4). Both stars are binaries. The red peak of the late 2000 profiles is affected by strong telluric absorption.

(e.g. Blow et al. 1982; Baize 1992; Mason 1997, and references therein). It was also reported to be a spectroscopic binary with $P = 40.198\,\mathrm{d}$, $K = 19.9\,\mathrm{km\,s^{-1}}$ and $\gamma = 34.7\,\mathrm{km\,s^{-1}}$ (Jarad et al. 1989), but the authors caution that the "period may well be spurious". Our data were taken from 1994 to 2003 and clearly confirm strong radial velocity variations. The Ondřejov coudé and HEROS data, however, cannot be sorted with the 40-d period, but with 53.72 d (Fig. B.5). Older photographic data by Jarad et al. (1989, 21 points spanning 475 days in 1983–1985) are unfavourably distributed to permit a check on the 53-d period; some points do not fit the corresponding radial velocity (RV) curve. Still older are 39 measurements from 1919 to 1932 by Harper (1934) and so cannot be co-phased with the present data. However, although the measurements are of a different line and their errors are large, they are consistent with the 53.7-d period, in the sense that they provide an RV curve similar to the one in Fig. B.5 when phased with that period.

Accordingly, ν Gem has at least three components: The main system Aa+Ab with $P = 53.72\,\mathrm{d}$ and the speckle component B, orbiting Aa+Ab in about a decade. Conspicuously, the circumstellar lines, i.e. Balmer emission and shell lines, do not take part in the 53.72 d orbital motion, but only show secular motions (Figs. B.5 to B.8). This poses the question if the disc is surrounding the entire Aa+Ab system, or if the shell star is component B. Given the relatively long period of 53.72 d, the former hypothesis is unlikely. In addition, the depth of the shell absorption of only 10 % in FeII is, judging by *bona fide* single shell stars, very small relative to the strength and shape of the Balmer emission (Fig. B.6). This, too, does not support the possibility of the shell absorption forming on the line of sight towards the primary Aa+Ab components of ν Gem. Consequently, the spectrum of type B6 III with $v\sin i = 170\,\mathrm{km\,s^{-1}}$ would not belong to the emission line star. In fact, such a $v\sin i$ is extraordinarily low for a shell star (see Table B.1). Therefore, spectral type B8 III is adopted for the shell star, following the classification by Mason (1997) of component B.

For the speckle-resolved subsystem, i.e. A+B, Mason (1997) gives an eccentricity of 0.923 ± 0.010. Hence one should expect large RV variations around the periastron times ($T_0 = 1983.51 \pm 0.05 + E \times 13.00 \pm 0.17$) in the spectral features arising from component B, namely the line emission. Owing to the period of 13.00 years, the periastron itself would always be unobservable (the sun being only a few degrees away in early July). But the spectra taken in 1996 on Jan. 22, Mar. 16, Nov. 23, and Dec. 22
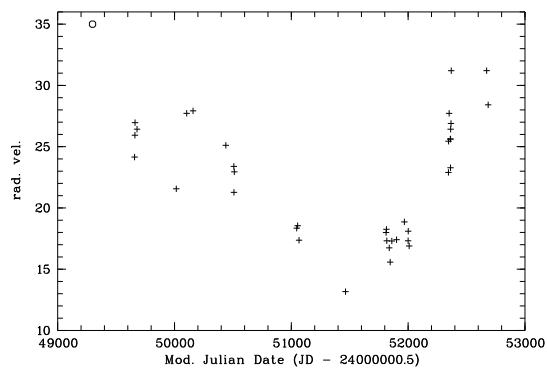
Figure B.7: Radial velocity of the Hα core of ν Gem. The circle was taken from Hummel & Vrancken (1995).
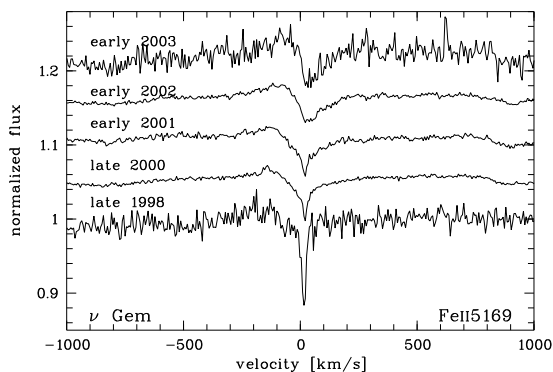

Figure B.8: Mean circumstellar shell component of the spectrum of ν Gem in Fe II 5169. This spectral range is covered by HEROS data only. Note the early 2002 profile, which is similar to the Fe II profile of ζ Tau in 1991 (Fig. B.3), as are the Hα profiles.

do not show a trace of such a behaviour, either. Fig. B.7 illustrates the actually observed smooth RV curve of the sharp absorption core in the Hα emission line (which should follow component B). It appears to be inconsistent also with the provisional orbital elements by Baize (1992, $e = 0.86, T_0 = 1986.44 + E \times 11.70$).

These proposed orbital motions cannot explain the RV variations of the sharp absorption core in the Hα emission line. Instead, the disc oscillations causing the V/R variability might explain the smooth RV curve of the sharp Hα absorption.

The peculiar Hα profile observed in Mar./Apr. 2002 (Fig. B.6) is reminiscent of the disturbed profile of ζ Tau observed in 1991 which, too, is a binary. Previously, Hanuschik et al. (1996, see also Hummel & Vrancken 1995) observed towards the end of 1993 the onset of a phase with a similar triple-peaked Hα emission profile, which after nearly 3 months was fully developed. For the present project ν Gem was observed from Nov. 15 2001 to Feb. 16 2002 with the Ondřejov coudé instrument and from Mar. 5 to Apr. 4 2002 with HEROS, i.e. 140 days, with the RV-stable triple peaked profile present in all spectra (Fig. B.6) . The blueshifted emission minimum resided at $-52.4 \pm 1.5 \, \text{km s}^{-1}$ all the time. The occurrence of such a peculiarity is, therefore, not dependent on the phase of the Aa+Ab 53.7-d orbit. This is the same conclusion as for ζ Tau where, furthermore, there are reasons to attribute it to the V/R variability.

β **Mon A (= HR 2356 = HD 45 725,)** is one of the longest observed shell stars. It used to be V/R variable in the past (Cowley & Gugula 1973; Telting et al. 1994), but the cycle seems to have stopped and only marginal asymmetries are present in the data, taken during January 2000. The spectrum of β Mon A showed CQEs in lines like Ti II 4824, as well as very narrow and deep cores in profiles like the one of Fe II 5169. Another spectrum of β Mon A was obtained in the framework of the Paranal Observatory Project (POP[1]) with UVES in March 2001. The V/R ratios are mostly unity also in this spectrum, at best as asymmetric as in ψ Per (see Fig. B.2).

The UVES spectrum covers the range from 310 to 1060 nm. In the blue region, not observable with HEROS and FEROS, various strong and again very narrow shell lines can be attributed to Ni II, most notable at 3514, 3577, and 3769 Å. Fig. B.9 presents such shell absorptions for five different ions.
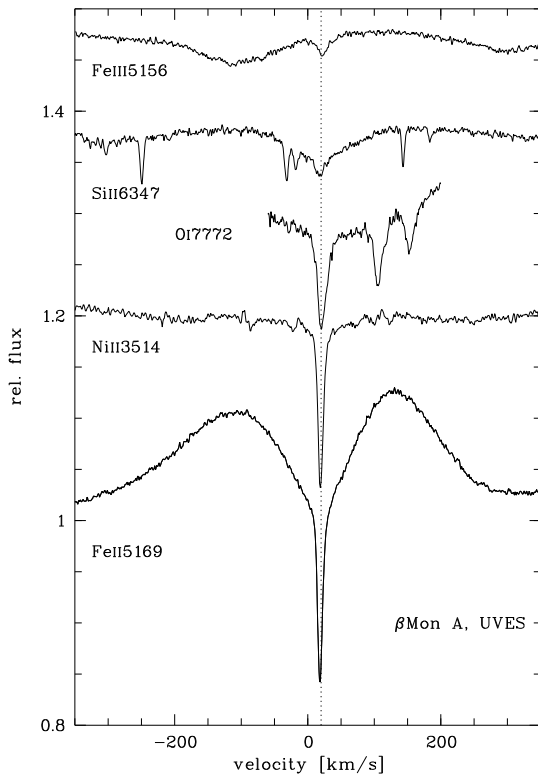
[1]http://www.eso.org/santiago/uvespop/

Figure B.9: Narrow shell lines in the UVES spectrum of β Mon A. These lines are seen in our own FEROS data as well, but are fully resolved only by UVES. The dotted line marks the systemic radial velocity given in the GCRV, $20 \, \mathrm{km \, s^{-1}}$ (Wilson 1953). Narrower absorptions around the SiII 6347 line are of telluric origin.

The star is part of a visual multiple system, with periods in the order of at least millenia (Abt & Cardona 1984). Since this can impossibly have any influence on the Be star, it is not listed as binary in Table B.1. The core velocities of the sharp shell absorptions are stable in all our data as well as in the UVES spectrum and agree well with published values for the systemic velocity.

27 CMa (= HR 2745 = HD 56 014) has one of the strongest metallic shells among early-type Be stars. In most of our spectra there are almost no uncontaminated stellar lines. Of the shell stars listed by Slettebak (1982) it has the lowest $v \sin i = 150 \, \mathrm{km \, s^{-1}}$, indicated as uncertain, however. The rotational velocity could, therefore, be underestimated. Indeed, recent spectra taken with FEROS do reveal a few lines hardly affected by the shell, like CII 4267, NII 3995, and SiIII 4553. These profiles have a full width of about $600 \, \mathrm{km \, s^{-1}}$ (Fig. B.10, upper panel), favouring about twice as fast an equatorial rotation as estimated during a strong shell phase. Chauville et al. (2001), too, derived a $v \sin i$ of $280 \, \mathrm{km \, s^{-1}}$. Some weaker shell lines, like several FeII transitions or MgII 4481, show a clear CQE signature (Fig. B.10, lower panel).

ω Car (= HR 4037 = HD 89 080)

Central quasi-emission peaks in ω Car (HD 89 080, HR 4037) were found by Baade (1989a) in his search for line profile-variability in late-type B stars. The Hα profile was stable during the monitoring from 1995 to 1999. Of the stars investigated here, ω Car has the strongest emission with an Hα peak height of 2 in units of the local continuum. The central absorption is rather deep, but the minimum flux is still above the continuum. CQEs are seen in partly photospheric lines like MgII 4481, being broadest there, as well as in shell lines of TiII and CrII. However, in FeII, the most typical shell lines of Be stars, only deep pure absorption cores are visible (Fig. B.11, left panel). Strengths and widths of the CQEs as observed with FEROS are given in Table 2.1.

HR 4123 (= HD 91 120) is confirmed as a shell star (first reported by Hanuschik (1996)). The circumstellar FeII lines show a typical shell profile, with the absorption cores being below the ambient stellar continuum. The S/N of the spectra is not high enough for an unambiguous detection; but some FeII lines might have CQE-type profiles.
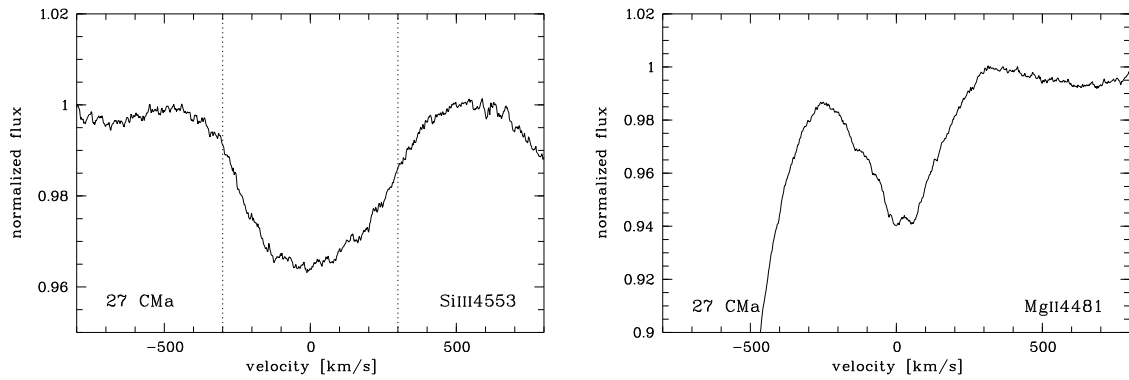
Figure B.10: Averaged profiles of spectral lines of 27 CMa in 2000. An almost uncontaminated line, indicative of a stellar $v \sin i$ of at least $300 \, \mathrm{km \, s^{-1}}$ is shown in the upper panel. The lower profile has intermediate shell contribution, a typical CQE can be seen.
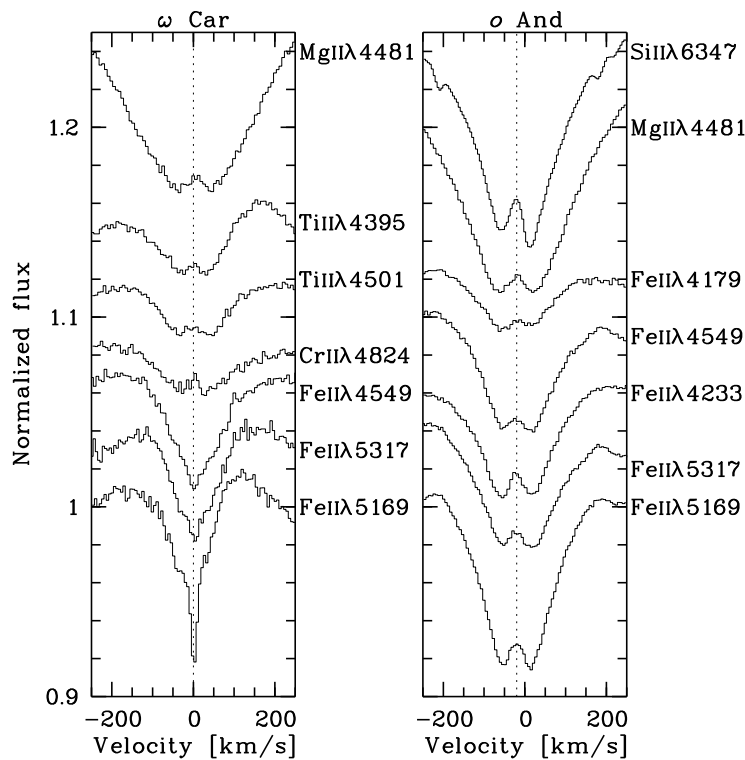

Figure B.11: Selected profiles of lines with circumstellar contributions in ω Car (left, 1996 data) and o And (right, 1998 data). The dotted vertical lines indicate the mean radial velocity of the CQEs. Note the good alignment of all CQEs even though the parent absorption profile varies rather significantly.

HR 4221 (= HD 93 563) possesses a shell only slightly stronger than that of HR 4123. The Fe II lines do not have CQEs but show flat-bottom profiles, which are intermediate between classical shell absorptions and CQE-type profiles (for theoretical and observational examples see Hanuschik 1995 and Chapter 2, respectively).

39 Cru (= HR 4823 = HD 110 335) exhibits strong Balmer and Fe II emission. The central absorption core of the Fe II lines is only marginally below the local continuum. The object was classified as a shell star by Hanuschik (1996).

κ^1 Aps (= HR 5730 = HD 137 387) is an obvious shell-type star, with CQEs in most He I and some other lines, like Mg II 4481 (Fig. B.12, lower panel). The star was observed quite intensively in 1999 (49 spectra taken May-July). But the peculiar variability in line width between 250 and $350 \, \mathrm{km \, s^{-1}}$ described by Slettebak (1982) was not present. The photospheric profiles affected least by emission favour the higher $v \sin i$ of $350 \, \mathrm{km \, s^{-1}}$ (Fig. B.12, upper panel).
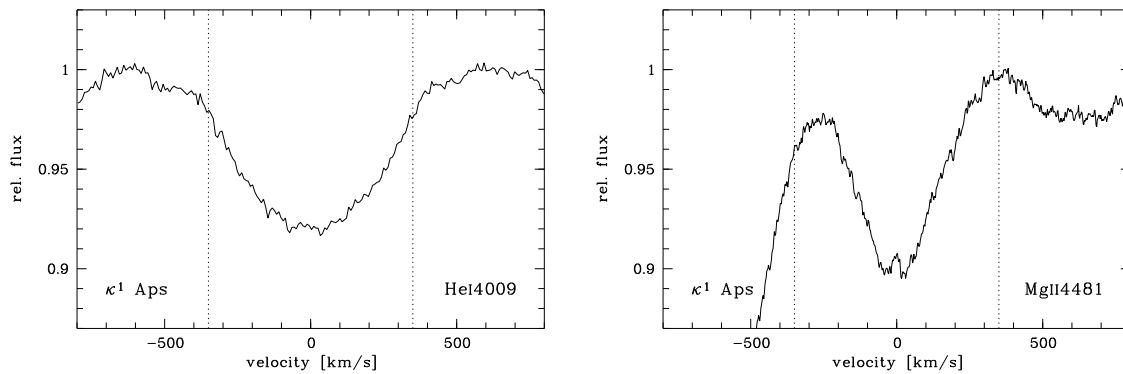
Figure B.12: Photospheric profile (left) and sample CQE (right) of κ^1 Aps in the 1999 season. A $v \sin i = \pm 350\,\mathrm{km\,s^{-1}}$ is indicated by dotted lines. Lower $v \sin i$ values may have resulted from the contamination by narrow shell absorptions.
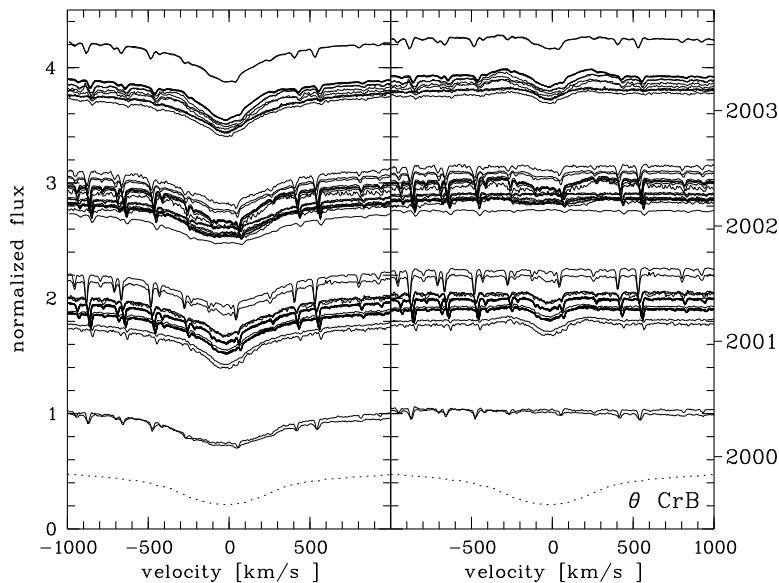

Figure B.13: Evolution of the Hα profile of θ CrB from 2000 to 2003. A vertical offset of one flux unit corresponds to one year. The mean of the 1991 Tautenburg data is shown as dotted line for comparison. In the right panel the residuals are plotted w.r.t. the Tautenburg 1991 data, which is repeated for convenient comparison.

θ **CrB (= HR 5778 = HD 138 749)** was extensively studied with IUE by several investigators (e.g. Underhill 1985; Doazan et al. 1986a). This B6 III star became particularly interesting when the shell signature due to the circumstellar matter faded and finally disappeared in 1980. Since then, the star has been in a stable B-star phase, in the UV and optical spectral range indistinguishable from a normal rapidly rotating B star. Several, mostly photometric, monitoring projects covered θ CrB in case it would become active again (e.g. Fabregat & Adelman 1998; Percy & Bakos 2001).

θ CrB was observed from Tautenburg in 1991 and 1992 with FLASH, with the Ondřejov coudé instrument 1993 to 2000, and with HEROS from Wendelstein in 2000 as well as from Ondřejov since 2001. The Tautenburg, Ondřejov coudé, and Wendelstein data show the purely rotational Hα profile present since 1981. By 2001 February, the spectrum had developed a weak shell signature with a rather broad core. This signature remained stable until May, then disappeared in July. In March, 2002, a weak and broad CQE-type signature was present in the core of Hα that finally disappeared in April, 2002 (Fig. B.13). In February, 2003, however, circumstellar contribution is visible again. Only Hβ showed a similar, but weaker shell effect, while no other line reflected this brief and weak shell episode.

Although the disc signature is feeble and only transiently present, it seems that the star has restarted its circumstellar activity (see Panko & Tarasov 2000, for comparison with o And). It has to be seen if θ CrB will develop a stable shell or if the current observations show a failed attempt of disc build-up. Photometric monitoring in the 1999–2002 period did not reveal any changes (Adelman 2002) so that the
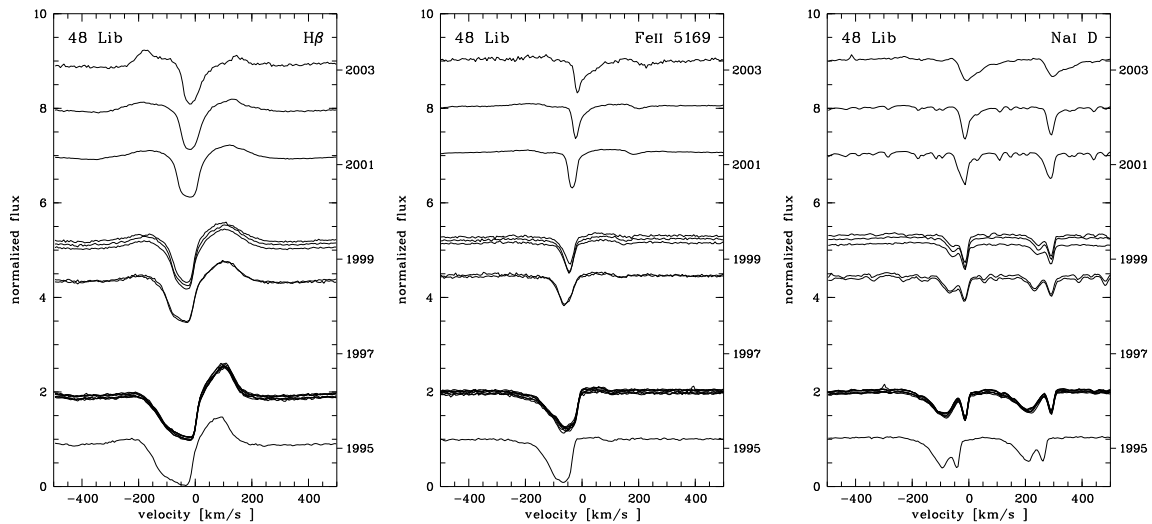
Figure B.14: Evolution of Hβ, FeII 5169, and NaI D shell absorption in 48 Lib between 1995 and 2002.

amount of accumulated material was probably too small to reduce the continuous light by a measurable fraction.

4 Her (= HR 5938 = HD 142 926) The first report on CQEs in the shell star 4 Her was given by Koubský et al. (1993), a more detailed description by Koubský et al. (1997). Being visible in many shell lines, these features are present at the beginning of new shell phases, when the star is faintest. They vanish when the Hα emission strengthens. It should also be noted that the shell lines are reported to be unusually broad. Compared to classical shell stars such as ζ Tau or EW Lac, this is true of all CQE stars. In two HEROS spectra of 1998 August, CQEs are not detectable. However, it can hardly be judged if this is so as a result of the limited S/N or because they have really disappeared.

Koubský et al. (1997) showed that Hα V/R and its shell radial velocity as well as the RVs of other shell lines follow a 46.18 d period. They interpreted it as a binary period and derived orbital elements. However, they concluded that a Roche-lobe filling secondary, even as cool as 3500 K is ruled out. The spectral coverage of their data did not permit them to look for a hot sdO companion similar to that one in ϕ Per.

Our data (the Ondřejov spectra partly overlapping with the ones of Koubský et al. 1997) confirm the 46.18 d periodic variations of the shell and emission line characteristics. Just the emission had decreased from $W_\lambda \approx -6$ Å at the end of the observations of Koubský et al. (1997) in early 1997 to $W_\lambda \approx -1$ Å in mid 1999, only to climb again to $W_\lambda \approx -5.5$ Å in the following season, then having remained unchanged at least until March 2003.

A search for similarities to other stars with confirmed or suspected sdO companions remained unsuccessful also in our data. Our blue HEROS spectra allowed to search for a HeII 4686 line of the suspected sdO secondary. Due to much lower temperature of 4 Her, compared to ϕ Per and 59 Cyg, the detection of HeII 4686 should have been easier. However, even in the phase-averaged HEROS spectra of 4 Her, no trace of such a HeII 4686 feature could be found. The orbital interpretation of the 46.18 d variability in 4 Her as well as the nature of its secondary component still needs to be further investigated.

48 Lib (= HR 5941 = HD 142 983) has a very strong shell, rendering the determination of the spectral type quite uncertain. In the recent decade, the strong and unusually broad shell absorption observed in 1995 has weakened and narrowed (Fig. B.14). This broad absorption was not present in observations by Hanuschik et al. (1995, taken 1985 to 1993), but only in 1995 and 1996. The absorption reached velocities as high as -200 km s^{-1} projected against the stellar surface in the line of sight, with a similarly large dispersion (Fig. B.14, lowermost panel). During these years, additional moving narrow absorption components were observed by Hanuschik & Vrancken (1996).

In the past 50 years, 48 Lib underwent long-term V/R cycles of 11.8, 6.8 and recently 9 years (Okazaki 1997). The current cycle started 1990 at $V = R$, with $V > R$ until 1994, as reported by Hanuschik et al.
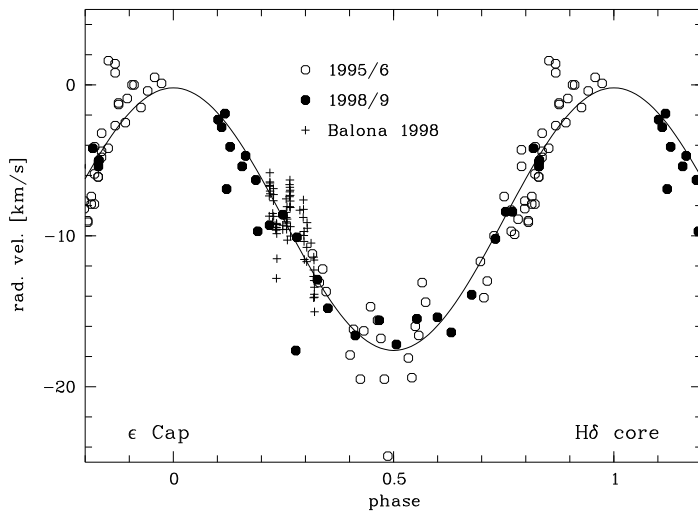
123

Figure B.15: Periodic radial velocity variations of the Hδ absorption core of ε Cap, sorted with $P = 128.5$ d. The parameters for the plotted radial velocity curve are compiled in Table B.2 (VELOC solution). Additional points were measured in 76 spectra taken over two weeks in Sep. 1998 by Balona (2002).
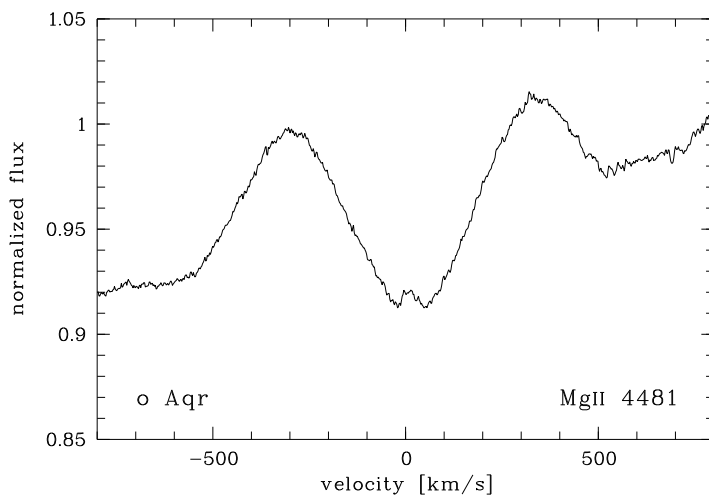

Figure B.16: CQE in the MgII 4481 profile of o Aqr in 1999.

(1995). After that, the red peak was dominant for almost eight years (see Fig. B.14). In particular, in the beginning of 2003 the $V/R_{\mathrm{H}\alpha}$ was still larger than 1, but becoming smaller, while $V/R_{\mathrm{H}\beta}$ was already less than unity. This points to a very asymmetric V/R cycle, or to a change in cycle length.

88 Her (= HR 6664 = HD 162 732) possesses a strong shell with relatively narrow absorption lines, mainly seen in hydrogen and FeII. The shell absorbs up to 30 % of the stellar flux in the strongest FeII lines of multiplet 42. Shell absorption is weakly apparent in SiII or OI. The red peak in Hα is slightly higher than the violet one.

ε Cap (= HR 8260 = HD 205 637) was suggested by Abt & Cardona (1984) as double with a possible period of 0.3 yr. Analysis of the radial velocities of the absorption core of Hδ show that a period of $P = 128.5$ d sorts the data well; the 96.3 d suggested by Rivinius et al. (1999) is a seasonal alias (Fig. B.15 and Table B.2). Since part of the RV curve is not well covered by our observations, the uncertainty might be as high as ± 2 d, although the formal error is smaller, since it relies on zero eccentricity (Table B.2). The radial velocities of the CQEs in ε Cap trace well the RV curve of the shell absorption cores. This confirms that CQEs are markers of the stellar radial velocity (Chapter 2).

o Aqr (= HR 8402 = HD 209 409) displayed remarkably narrow and deep shell lines of FeII already in 1993 (Hanuschik 1996). Between then and 1999, the disc seems not to have undergone any changes. In addition to the narrow shell absorption, MgII 4481 shows a clear CQE (Fig. B.16).

EW Lac (= HR 8731 = HD 217 050) was observed a few times with HEROS and more than 60 times with

the Ondřejov coudé spectrograph. Similar to o Aqr, the FeII multiplet 42 shell-absorption lines are too narrow to be resolved with HEROS. The hydrogen shell absorption reaches zero intensity even for the higher Balmer lines up to H10.

The star is a weak V/R variable. The cycles are strongly different from each other in length and amplitude (Fig. B.17). The $\pi/2$ phase shift between the radial velocity of the SiII shell line and the Hα V/R ratio is explained well by a global density wave (cf. model computations by Hummel & Hanuschik 1997).

o **And** (= **HR 8762** = **HD 217 675**) was the first star for which CQE was reported (Doazan 1976) but at the time taken to be genuine emission. These features were seen in Balmer lines and rapidly variable. As in the case of η Cen, it is not clear if the structures were intrinsically variable or reflected underlying stellar variability. No subsequent study reported such features. However, shortly after Doazan's observations of CQEs, the star entered into a new shell phase (Fracassini et al. 1977).

CQEs can be recognized again in the spectra taken in 1998. But this time they are present in shell rather than in Balmer lines (see Fig. B.11, right panel). The weak Hα emission with a peak height of about 1.1 looks similar to that in ε Cap or η Cen (Fig. 2.2). The absorption core drops as low as 0.2 of the ambient continuum. Lines of the Balmer series can be detected up to H26 at 3666 Å in the high-quality, averaged spectrum.

As part of a long term-monitoring programme at Ritter Observatory, K. Bjorkman (1999, private comm.) observed o And in fall 1997 and fall 1998 and found both narrow shell absorption and emission peaks. In late 1998, the emission strengthened somewhat. Peters (1999, private comm.) concluded from observations of the Hδ and Hβ regions that "a weak shell was present in mid-January" (1999). Noteworthy is also a recent report by McDavid (2000), who within only a few months of the present observations measured the highest linear polarization ever published for this star.

Previous shell episodes are known to have started in 1966, 1975, 1983, 1988 (cf. Sareyan et al. 1992), and 1994 (Harmanec 1994). For the latter event it is also known that it was accompanied by a similar rise in polarization (McDavid 1995) as observed recently. Therefore, it seems possible that a new shell phase, or an enhancement of shell characteristics, started only a short while ago. Since shell phases of o And typically last a few years, observations in the next observing season should easily confirm or reject this hypothesis.

o And is the star in which a further typical property of CQEs can be seen best. Although the absorption component of the various parent lines may have different radial velocities, the CQEs always occur at one radial velocity common to all CQEs (see Fig. B.11 and Table 2.1).

The multiplicity of o And (Hill et al. 1988) has most probably negligible physical influence on the phenomenon. The 33-d period only concerns companion B which orbits the Be star and another, much fainter companion a, in about 30 years at least. The period of component a is still of the order of 4 years. Therefore, averaging spectra over some weeks to months does not grossly affect any conclusion about the CQEs of the Be star. Only for measurements with very high precision do the values of the derived parameters depend on the disentangling of the component spectra and require a dedicated study.

B.2 Stars with alternating emission & shell phases

Three Be stars are known to have undergone transitions between emission & shell appearance, as in the above shell stars, and pure emission appearance, as in other Be stars. From what little statistics is available, it seems that these stars are typically observed without shell absorption lines, and only exceptionally with. In fact, in all spectra of the present dataset the 3 stars look like ordinary Be stars without any shell component. Section 2.1.1.2 reviews a hypothesis by Hummel (1998) to explain this behaviour.

γ **Cas** (= **HR 264** = **HD 5394**) went through a cycle of shell phases in the 1930s (see Hummel 1998, and references therein). The so-called "giant outburst" of γ Cas in the mid 1930s was part of this pattern, with the emission peaks highest outside the shell phases (Underhill & Doazan 1982). Since then, γ Cas was not observed to show shell behaviour any more.

Recently, Harmanec et al. (2000) have shown the star to be a single-lined spectroscopic binary with a low amplitude of about $5 \, \text{km} \, \text{s}^{-1}$ and a period of 203.59 d. Harmanec (2002) analyzed the photospheric wings of the HeI 6678 line and gave a $v \sin i$ of $380 \, \text{km} \, \text{s}^{-1}$, while Chauville et al. (2001) derived even $v \sin i = 432 \, \text{km} \, \text{s}^{-1}$.
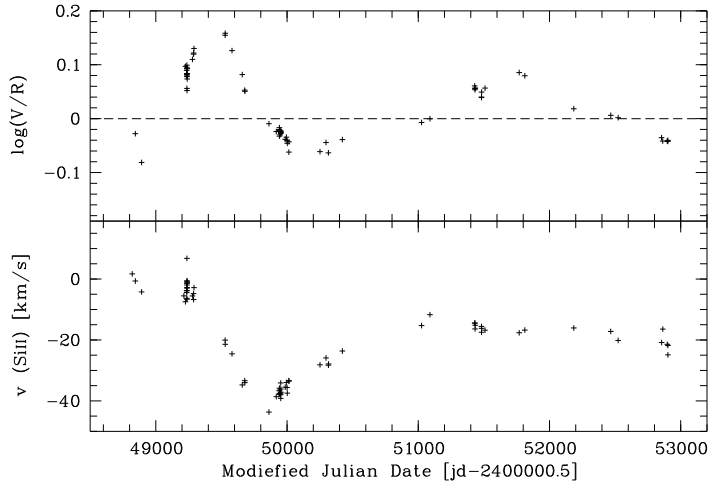
Figure B.17: V/R ratio of Hα and radial velocity of the Si II 6347 shell absorption of EW Lac. Note the strong cycle-to-cycle variations of amplitude and cycle length.
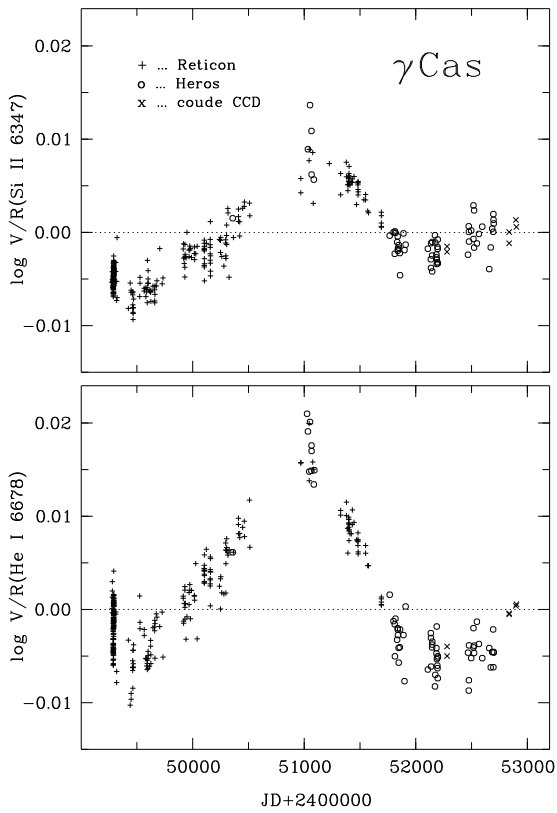

Figure B.18: V/R peak height ratios observed in Si II 6347 and He I 6678 of γ Cas.

In our data taken between 1996 and 2003, the presence of the above orbital period is confirmed, as is the large width of He I 6678. The star continued its long-term V/R cycle (Fig. B.18). No line in the observed wavelength range would have justified a shell classification in this period. Like in other stars (see Baade 1985, for a summary) the V/R cycle undergoes phase lags between different lines, which is seen best when V/R changes from R-dominated to V-dominated (and vice versa) in some lines earlier than in others (Fig. B.19). In the frame of the global density wave pattern such phase lags are explainable by a (trailing) spiral geometry (Okazaki 1991 was the first to propose a spiral pattern; later McDavid et al. 2000 suggested it to explain phase lags in 48 Lib). The density pattern is, then, not at the same azimuth for all radii, so that the bulk of (e.g.) He I 6678 emitting plasma, close to the star, crosses the line of sight earlier than the bulk of Hα emitting plasma does, farther away from the star. A similar behaviour is apparent for 28 Tau (Fig. B.20) and 48 Lib (Sect. B.1, 1998 data).
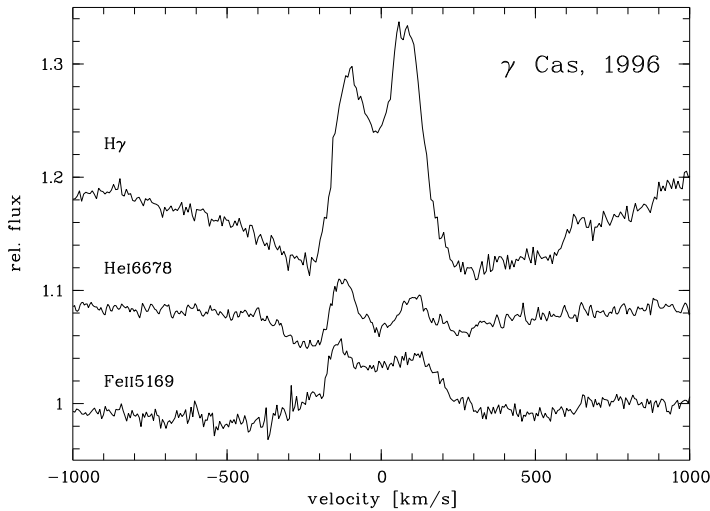
Figure B.19: A spectrum of γ Cas on JD=50358, showing different V/R ratios in different lines. This indicates a trailing spiral structure of the density wave causing the V/R variations (see Sect. B.1 about γ Cas for detailed explanation). The red absorption wing of Hγ is blended with another FeII emission line.
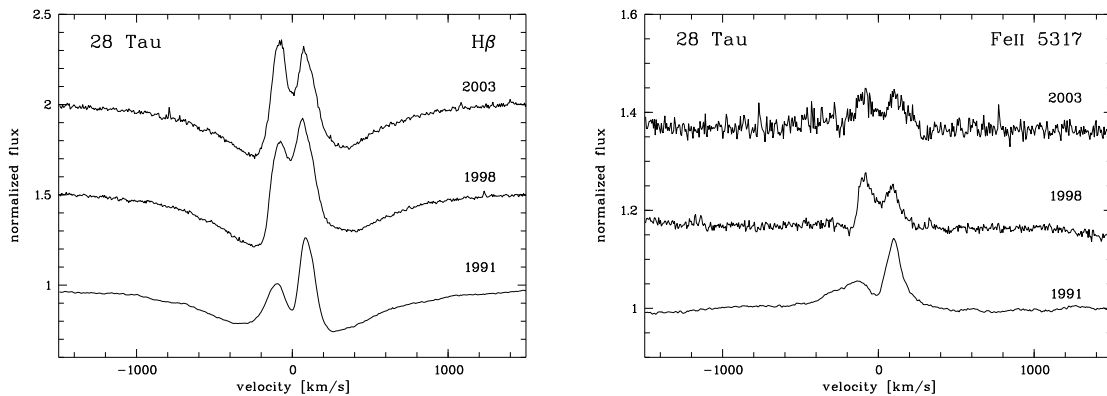

Figure B.20: The changes of the emission profile of Pleione between 1991 and 2003. Note the strong variable asymmetry of the Balmer absorption wings vs. the V/R ratio of the emission, which in FeII is ahead of Hβ, while in Hα the red peak is even in 2003 still higher than the blue one (Fig. B.21).

28 Tau (= HR 1180 = HD 23 862 = Pleione) is a well-observed Be star. The last shell phase ended 1988 (e.g. Ballereau et al. 2000), although absorption was still visible in our FLASH spectra taken 1991 in a few FeII lines, but not all of them. Because of their limited wavelength coverage of the Hα region only, the available 32 Ondřejov coudé spectra obtained between 1994 and 2000 do not permit the disappearance of these FeII shell absorption remnants to be traced. But a set of HEROS spectra obtained in 1998 evidenced unambiguously that the shell signature had completely vanished.

In addition, Pleione is subject to a very strong cyclic V/R variability that affects not only the peak heights but even the filling-in of the absorption wings of the Balmer lines (Figs. B.20 and B.21). Inspection of HeI and metal lines does not show their radial velocities (RV) to be variable. This excludes orbital motions as the cause of the variability of the Balmer line wings.

The 218-d period reported by Katahira et al. (1996) could not be confirmed from the present data. Therefore, 28 Tau is not listed as a binary in Table B.1.

The long-term trend of the Hα emission reported by Pollmann (2003) is confirmed by the present data. But they do not cover the claimed sudden breakdown and recovery of the line emission. On the other hand, only 10 days before Pollmann's measurement of $W_\lambda = -5\,\text{Å}$ (JD=51585.36), $W_\lambda = -29\,\text{Å}$ was observed (JD=51575.28, last profile taken in 2000 in Fig. B.21). Since a Keplerian disc cannot dissipate in so few days, an independent confirmation of the unusual behaviour of Pleione as reported by Pollmann (2003) is highly desirable.

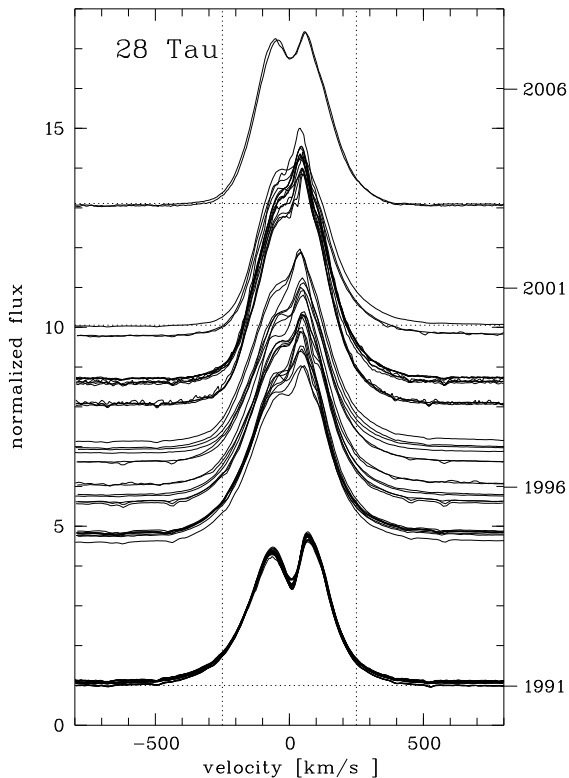**59 Cyg (= HR 8047 = HD 200 120)** exhibited two shell phases in the mid-1970s (Hummel 1998, and refer-

Figure B.21: Hα line profiles of 28 Tau. A vertical offset of one flux unit corresponds to one year. The first spectrum was taken Jan. 8, 1991, the last one on Feb. 15, 2003. Horizontal lines mark the continua of the first and last spectra, and the one with the most pronounced red displacement of its base. Vertical lines at $\pm 250\,\mathrm{km\,s^{-1}}$ are to visualize the secular shift of the emission base towards the red.

ences therein). The phenomenology of these shell phases was the same as in γ Cas, and also very similar to the one of Pleione. The star was observed in 1998 and from 2000 to 2002.

The published $v\sin i$ values range from $260\,\mathrm{km\,s^{-1}}$ (Slettebak 1982) over $379\,\mathrm{km\,s^{-1}}$ by Chauville et al. (2001) to $450\,\mathrm{km\,s^{-1}}$ by Hutchings & Stoeckley (1977), confirmed by Harmanec et al. (2002) and Maintz (2003). For Table B.1, $379\,\mathrm{km\,s^{-1}}$ was adopted as a lower limit.

59 Cyg underwent strong V/R variability in the past, which was still weakly present in 1998, but had completely ceased by 2000. Since then, the profiles have been symmetric, except for variability phase-locked to the orbit.

The binarity suspected by Tarasov & Tuominen (1987) was confirmed by Rivinius & Štefl (2000), who found a period of about $27.17\,\mathrm{d}$ and an RV amplitude of $27\,\mathrm{km\,s^{-1}}$. Because of striking phenomenological similarities to ϕ Per, the companion was proposed to be an He-sdO star. Harmanec et al. (2002) improved the period, gave a smaller amplitude and put the nature of the companion into question. However, Maintz (2003) meanwhile detected a HeII 4686 absorption. Because of its radial velocity variations it can undoubtedly be attributed to a very hot, small companion; the larger RV amplitude of the primary is also confirmed. A detailed publication is in preparation.

B.3   Bn stars with weak disc absorption signature

The search for rapid line profile variability included also 19 Bn stars, i.e. rapidly rotating B stars without a record of line emission.

For three of these stars observed in 1999, namely 1 Sco, 2 Sco, and possibly also η Aqr (Fig. B.22), CQE-like distortions of the Hα line suggest that they are surrounded by weakly developed rotating discs. Similar weak CQEs are seen also in the Balmer lines of classical Be shell stars, when the disc is about to form (e.g. o And, Doazan 1976, Panko & Tarasov 2000; and η Cen, Baade 1983), or when it simply is extremely weak (θ CrB, Fig. B.13).

The quasi-resonance line character of Hα implies that low hydrogen column densities can be seen well before appreciable line emission occurs. This is aggravated in stars with large $v\sin i$, which Bn stars are by
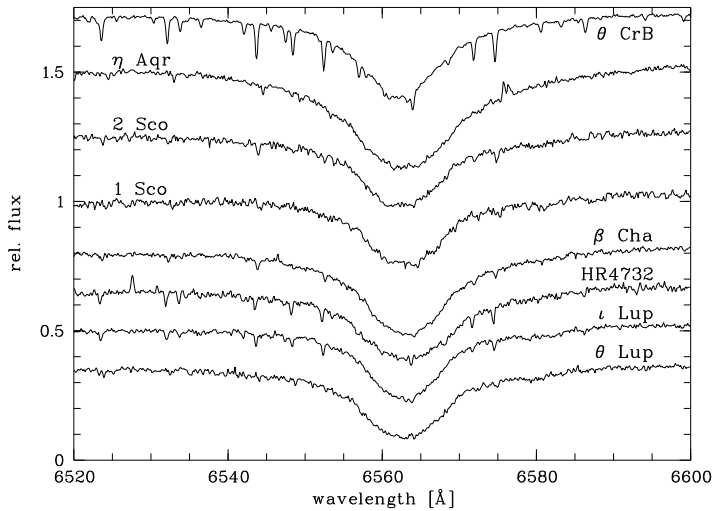
Figure B.22: The Hα lines of the Bn stars 1 Sco, 2 Sco, and η Aqr. The line cores show a CQE-like deformation, which is known also from Be stars in a weak disc state (cf. θ CrB, Fig. B.13). Several Bn stars with normal Hα profiles are plotted in the lower part for comparison.

definition. Therefore, it is plausible that, while there is a relatively clear-cut division between Be and non-Be stars, self-absorption in edge-on discs has a much larger dynamical range. Accordingly, the circumstellar matter of some Bn stars might be the low-density tail of the discs of Be stars.

The mean fraction $\overline{w} = 0.57$ of the critical rotation velocity is considerably lower than the one of any of the shell stars (Table B.1). But, with only 3 such stars known, it would be premature to speculate whether the amount of circumstellar matter somehow depends on w.

CQE stars might play a similar role among non-Be stars as shell stars do among Be stars: They would permit a sample of equator-on stars to be compiled from which the high-rotation limit of non-Be stars could be determined. A comparison with the distribution of rotation velocities in shell stars might, then, offer a clue as to whether Be and Bn stars are entirely different populations of stars or possibly only differ in evolutionary stage.

Appendix C

Evolution of disc emission lines

Next to the absorption line profiles presented in the previous part, also the emission lines can provide important insights into the disc structure and temporal evolution. While a statistical approach is more problematic due to the unknown inclination angle, a sufficient database of an individual star is still valuable. Although for such an object the inclination is hardly constrained, it is clear that is is constant for all observations. In this sense, if an individual observation allows to set a limit on a quantity, this limit is applicable to all spectra of that star. Sometimes even single snapshot observations reveal such an unusual structure that the paradigm of a disc that might be parametrized in a relatively simple way clearly fails at first sight, like for FY CMa, so that also these data provide important insights,

The echelle spectra on which this part is based were mainly secured during observing campaigns with the HEROS (Štefl & Rivinius 2000), and more recently also with the FEROS spectrograph (Kaufer et al. 1999). The discussions below focus on the medium-and long-term development of emission lines between 400 and 850 nm. The following stars were investigated in detail for the dynamical evolution of the disc, the results are presented in Chapter 3. All spectral types given are from Slettebak (1982):

C.1   Own observations

ω **(28) CMa (= HD 56 139 = HR 2749; B2.5 Ve):** The temporal evolution of the maximum width of the emission lines is seen best in this star. It is one of the main targets of the *lpv* program, having been observed from 1996 to 2000 (see App. D). Fig. 3.1 shows the average spectrum from each observing run. An outburst in 1996 is well flagged by the broad HI emission wings and the observed variability (Štefl et al. 1998). Optically thin emission lines like FeII 5169 are also quite broad. By the following year, the broad HI emission wings had disappeared and the disc emission lines had evolved to their maximum peak height. In January 1999, the hydrogen emission was still high, but the emission from the FeII and SiIII lines had significantly weakened and narrowed, and finally disappeared in the first half of 1999.

In the beginning of 2000, however, the HI emission wings were present again, which is a reliable indicator of a new outburst *á la* μ Cen (Rivinius et al. 1998c). At the same time the FeII and SiIII line emission re-appeared with large width. The narrower double-peaked emission in OI 8446 had lost a bit in width and two-thirds in peak height. But it had acquired a broad pedestal with the same total width as the other two lines. Like the Hα emission, this oxygen emission line is pumped by Lyβ emission, but it is optically thin. It should, therefore, trace large parts of the disc without its profile being contaminated by self-absorption or scattering.

FV CMa (= HD 54 309 = HR 2690; B2 IVe): Unfortunately, this star was observed during one observing run only so that nothing can be stated about a possible temporal evolution. Thirteen spectra were taken with FEROS at the ESO 1.52-m telescope over a period of 17 days in January, 2000. All spectral features discussed here were stable during the entire observing period. Therefore, the data were averaged. The emission in the Balmer lines shows two quite clearly separated constituents. In Hβ a strong narrow and a broad weaker component are apparent. Towards the higher Balmer lines, the narrow component weakens more rapidly than the broad one. At their base, the total widths of these two constituents are 415 km s^{-1} and 670 km s^{-1}, respectively (Fig. 3.3).
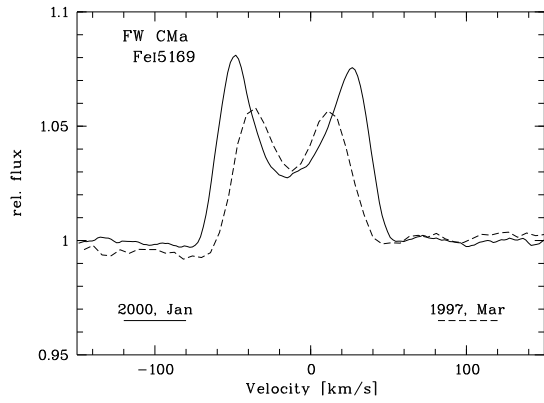
Figure C.1: FW CMa behaves very similarly as ω CMa (Fig. 3.1), except that no broad base in the O I 8446 emission line is seen. Only spectra exhibiting the extreme maximum and minimum width, respectively, of the Fe II 5169 emission observed between 1996 and 2000 are shown.
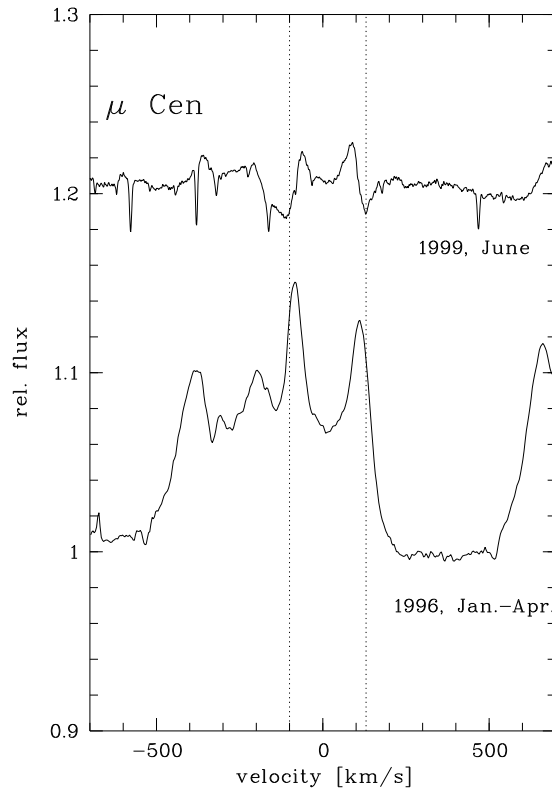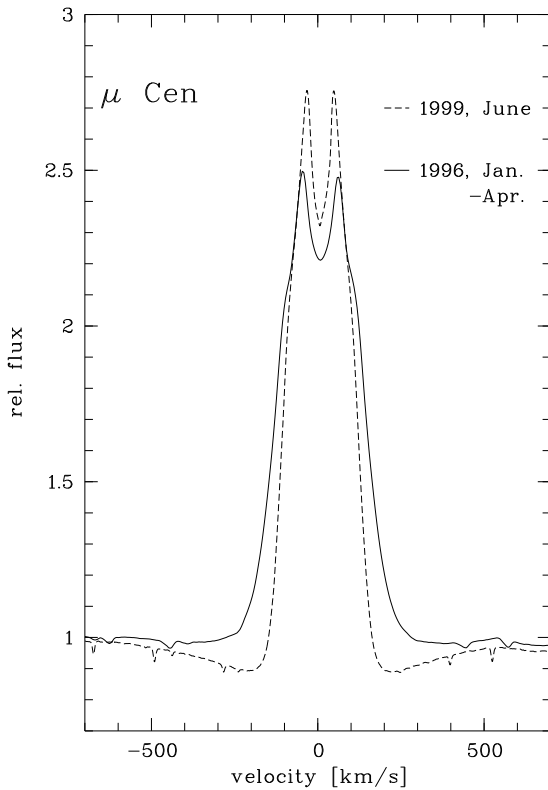

Figure C.2: The Hα and O I 8446 emission lines of μ Cen in 1996 and 1999. The narrowest width of O I 8446, $[-100, +130]$ km s^{-1}, is indicated by vertical lines. The variability of the broad Hα wings is similar to that in ω CMa (Fig. 3.1.)

FW CMa (= HD 58 343 = HR 2825; B3 Ve): The variable base width of the emission in Fe II is clearly visible in observations extending over the years 1996-2000 (Fig. C.1). The emission peak separation is variable in the same sense as in ω CMa (Fig. 3.1) as well. The timescales are, however, long. For instance, there was only a slight decrease in peak height from 1996 to 1997, but no width variation at all. In 1999, the Fe II 5169 line had turned into absorption, with some central emission component still seen, however. In 2000, when Fe II 5169 was in emission again, also the H I lines had developed broad emission wings.

μ **Cen (= HD 120 324 = HR 5193; B2 IV-Ve):** Fig. C.2 complements Figs. 1, 5, 6, and Sect. 7 in Rivinius et al. (1998c) and extends them in temporal coverage. Especially in Fig. 5 of Rivinius et al. (1998c, panel for Si II) it can well be seen how the narrower emission line of an older circumstellar structure is complemented during an outburst by a broader emission component. By 1999, only the Balmer lines
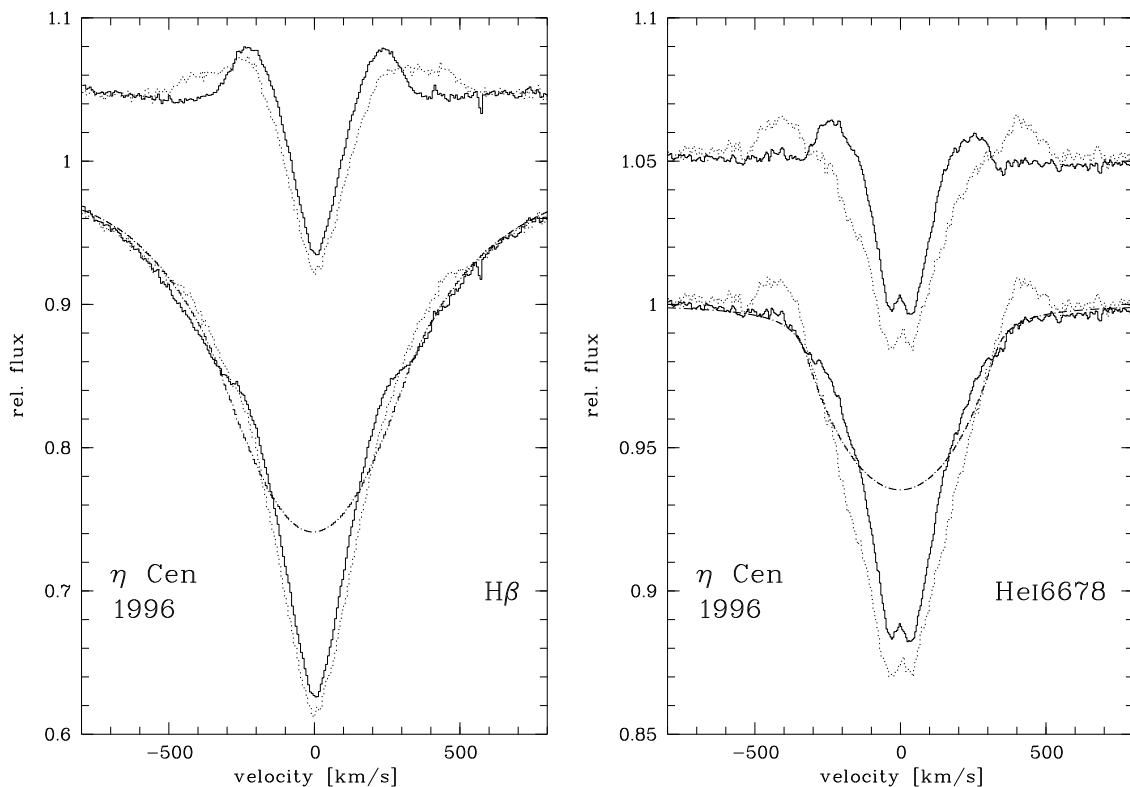
Figure C.3: The Hβ and HeI 6678 lines of η Cen in 1996 before and after an outburst. A synthetical spectrum, using the parameters by Balona (1999, dash-dotted profile, 25 000 K, $\log g = 4.0$, $v \sin i = 331 \, \mathrm{km \, s^{-1}}$) was subtracted to make the differences of the emission more visible (residuals plotted above the spectra).

have retained their emission at their approximate previous strength. Even the Paschen and OI emissions have nearly vanished, and all other emission lines are no longer detectable.

η **Cen (= HD 127 972 = HR 5440; B2 IV(e)):** The shell nature of this star makes it difficult to determine the position of emission peaks in weak lines. But an obvious sudden change occurred in February, 1996 (Fig. C.3), when the maximum base width of the HeI 6678 emission increased from $[-330, +350] \, \mathrm{km \, s^{-1}}$ to $[-540, +560] \, \mathrm{km \, s^{-1}}$. A similar increase was seen in the Balmer lines, although numbers are hard to give because of electron scattering blurring the footpoints of the emission.

o **And (= HD 217 676 = HR 8762; B6 III):** Among the Be stars, in which outbursts were seen, o And has (one of) the latest spectral subtypes. The Hα emission developed a second component at higher velocities from the end of August, 2000 to mid September (Fig. C.4; the star was not observed in the beginning of September). From September on, transient period type variability (Štefl et al. 1998, rapid V/R variations) was seen, although the data are not sampled well enough to derive a period, especially during the beginning of the outburst.

The metallic shell absorption observed in 1998 (Rivinius et al. 1999) has almost completely disappeared. Similarly, the Paschen shell absorption cores have weakened, but the Balmer absorption profiles are largely unchanged between 1998 and 2000. This behaviour is typical of the evolution of Be star discs, see e.g. μ Cen and ω CMa.

28 Cyg (= HD 191 610 = HR 7708; B3 IVe): A very similar behaviour of varying FeII emission line width and multiple outbursts as in μ Cen was reported by Tubbesing et al. (2000, their Fig. 1), based on 1997 and 1998 data. Meanwhile, new observations in spring/summer 2000 (with FLASH at the Wendelstein 80-cm telescope) and fall 2000 (with HEROS and the Ondřejov 2-m telescope) have confirmed this behaviour. Interestingly, the high velocity tails have disappeared, but the position of the emission peaks remained largely unchanged in FeII 5169 (Fig. C.5).
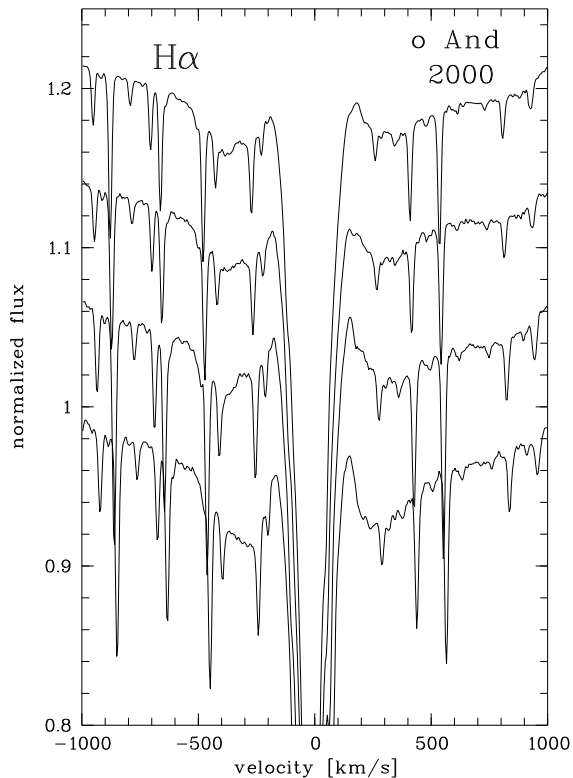
Figure C.4: *o* And showed signs of a typical outburst in the second half of 2000. Shown is the increase of the Hα emission wings from August to November 2000. The spectra have been averaged in roughly 20-day intervals (from bottom to top: MJD 51 766–783, 51 798–816, 51 826–845, and 51 855–875). While the star was quiet in August (until MJD 51 783), clear additional emission appeared at higher velocities around mid September. The V/R ratio of this emission was highly variable on timescales of days or shorter for some time. Unfortunately, not enough spectra were taken in this phase that a time series analysis could be attempted. This rapid V/R variability excludes an interpretation by electron scattering, since this should produce a symmetric profile.

C.2 Other published evidence

A search in the literature showed that DU Eri (= 228 Eri = HD 28 497 = HR 1423; B1 Ve) was once reported to display an unusual Hα profile (Hanuschik et al. 1996, their Fig. 10d). In comparison to other observations of the same star, the inner two emission peaks were relatively narrow and arose above a weaker but much broader emission constituent highly akin to the dual structures in ω CMa and FV CMa. FEROS spectra taken of DU Eri in January 2000 also show some structure in Hβ similar to the same line in FV CMa (Fig. C.6).

Waters & Marlborough (1994, their Fig. 1) reported a broad emission plateau in the Brγ line of ψ Per, observed in 1992, to which the normal Be double peak profile was superimposed. They described the plateau as symmetric and disappearing in Brα. Electron scattering as the process of formation is ruled out because of the sharp edges separating plateau and normal emission profile. From this, a formation of the plateau in the part of the disc close to the stellar surface is suggested.

Observations by Smith et al. (1991) of variable peak separation in the Hα profile of λ Eri also fit the above picture well, and were interpreted already by these authors as a ring. However, this could also be understood in terms of a variable outer disc radius and without further support is not sufficient to unambiguously establish a detached ring.

X Per (= HR 1209 = HD 24534) is a highly active X-ray binary with a probable orbital period of 250 d (Delgado-Martí et al. 2001) and consists of a B0e primary and a neutron star. Observations by Roche et al. (2000) and spanning a decade of the variability of the emission in Hα and HeI 6678 are dominated by the initial complete loss of the disc, its later recovery, and large-scale V/R variations. After abstraction from these phenomena, the relatively quick appearance and slower decay of broad emission wings closely resembles the outbursts described above for other, single Be stars. Still more interestingly, at several epochs the HeI 6678 emission displayed a broad plateau underlying a narrower double-peaked emission. In at least one instance, this plateau even rose to two discrete outer peaks, which were yet more pronounced than in 28 CMa, FV CMa or DU Eri.
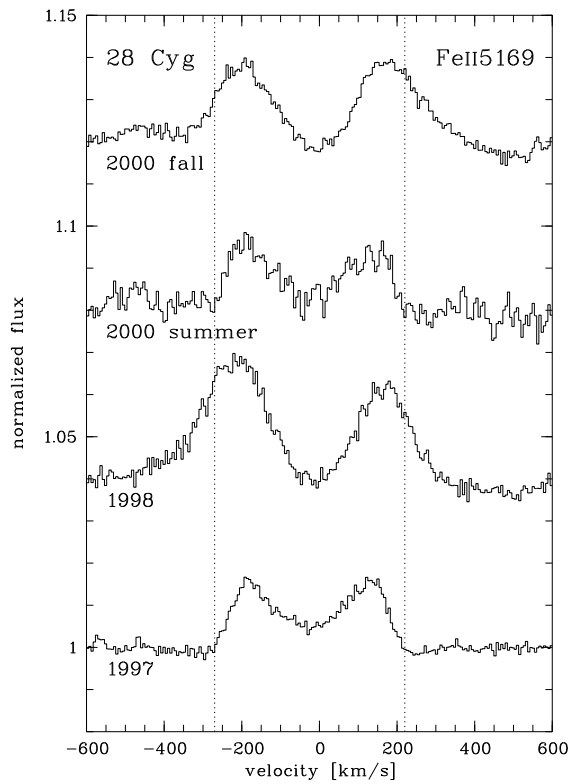
Figure C.5: The appearance of the FeII 5169 line of 28 Cyg in the average spectra of four different observing campaigns. The dotted lines represent the narrowest appearance of the FeII 5169 emission of [-270,220] km s^{-1}. The disappearance of the high velocity tails in the emission, while the narrower component remains largely unchanged, is in agreement with the hypothesis that only the emission contribution from the inner parts of the disc is gone.
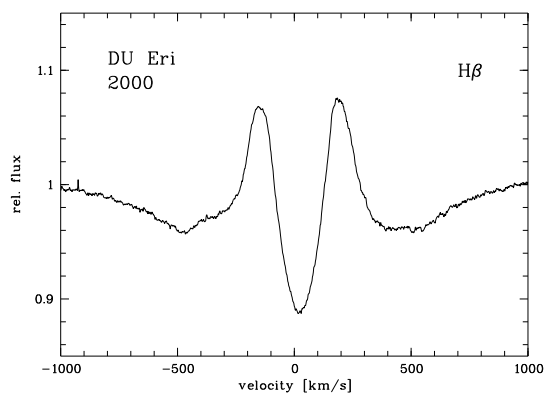

Figure C.6: The Hβ line of DU Eri in January 2000. The unusual morphology of the emission wings is reminiscent to FV CMa, but the metallic emission is too weak (i.e. below the detection threshold) to provide further evidence from optically thin lines.

Appendix D

Short periodic Be stars

In the following findings about the observed stars are summarized, both derived from own data and the literature. For most of the stars investigated sufficient data were obtained to study the periodic line profile variability. For many the periodic behaviour was found in previous studies already. But wherever possible the period analyses were re-performed on the HEROS and FEROS data, using the published periods as initial guesses (Table 6.1).

Figures 6.1, 6.2 and D.1 show the phase-sorted residual *lpv* of stars with ω CMa like behaviour (see Sects. 5.2 and 6.3.1). In Fig. 6.4, the three stars with different variability are presented. Each star is briefly commented in the following:

α **Eri:** Balona et al. (1987) derived a period of 1.26 days from simultaneous spectroscopy and photometry. Later, Porri & Stalio (1988) showed spectra displaying asymmetric *lpv*. The period derived here, 1.291 d, bases on observations taken from 1996 to 2000. The seasons have been analyzed both individually and as combined data, all pointing to the longer period as used here.

Due to its brightness, α Eri became a frequently observed target also with space experiments. Smith (2001), analyzing the UV spectrophotometric variability observed with IUE, concluded the stellar continuum to vary with higher amplitude in the blue part than in the red, but not showing distinct spectral features that would clearly point to either *nrp* or other investigated scenarios causing the variations. The recent measurement of α Eri's large equatorial radius of $12\,R_\odot$ and high rotational flattening, together with the rotational velocity of at least $225\,\mathrm{km\,s^1}$ exclude the *lpv* period to be rotational (Domiciano de Souza et al. 2003).

DU Eri: For this star only very few spectra are available, so that these are sorted only into 8 phase bins instead of 16 (Fig. 6.2), as with the other figures. The period used to sort the data is very tentative with 0.577 d. However, the variable shape of the individual line profiles clearly is of the same type of variability as for the other pulsating stars in this sample, i.e. the symmetry of the profile changes in a low-order fashion. Dachs & Lemmer (1991) found a double-wave period of 0.65 d, while from HIPPARCOS photometry a single-wave value of 0.654 d was derived (Hubert & Floquet 1998). Smith (2001) found DU Eri to exhibit *nrp* type spectrophotometric UV variability with a period of 1.2 d, which is about twice the period presented here, while Peters & Gies (2000) found a period of 0.61 ± 0.08 d in the UV line profiles and 1.2 d in the UV wind lines, tentatively proposing an $\ell = -m = 2$ mode.

DX Eri: Štefl & Balona (1996) investigated this star in detail, deriving a consistent period from both photometry and spectroscopy of 1.26708 d. This period is confirmed by FEROS observations in 2000. The circumstellar emission increased somewhat during the two weeks of observations, but there was no obvious outburst. The period derived from Hipparcos photometry, 1.383 d (Hubert & Floquet 1998), does not sort the data well and might be an alias, but could also indicate transient activity, as described in Sect. 6.3.4.

λ **Eri:** The *lpv* period was derived in many independent studies to be 0.702 d. Kambe et al. (1993, 1998) carried out an extensive campaign over several seasons and found not only this period, but a second coherent one of 0.269 d and intermittently present ones of 0.6 d and 0.75 d. The appearance of those intermittent periods is similar to the transient ones found in ω CMa, μ Cen and η Cen by Štefl et al. (1998). λ Eri is one of the few stars with clearly different *lpv* than ω CMa (Fig. 6.4). Although the

HR 3642
$v \sin i = 130\,\mathrm{km\,s}^{-1}$
HeI 4388

31 Peg
$v \sin i = 100\,\mathrm{km\,s}^{-1}$
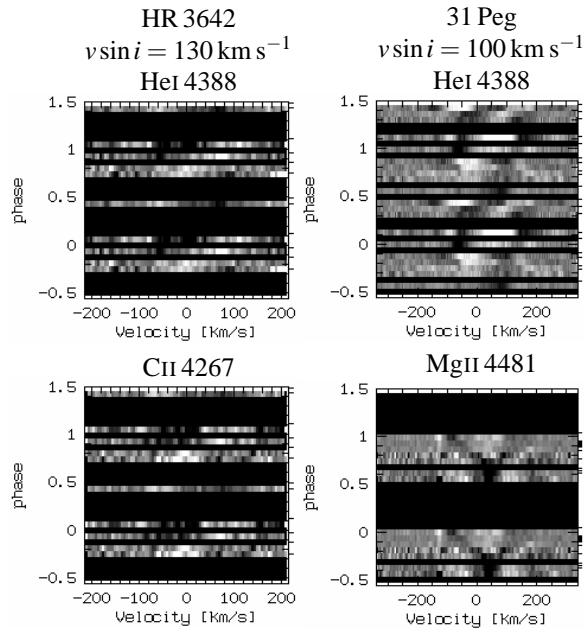HeI 4388

CII 4267

MgII 4481

Figure D.1: Phased main *lpv* of HR 3642 and 31 Peg. The period for HR 3642 was taken from Carrier et al. (2002). For 31 Peg the ls99c data is shown for HeI 4388, the ohp01 data for MgII 4481 (see Table A.1 for notation used for observing runs). The periods are given in Table 6.1.

general appearance is that of low-order variation, the *lpv* shows additional substructure in particular in the line wings.

Smith (1989) reported a large number of aperiodic small-scale transient features. Such features are weakly seen also in FEROS data, but are not detected in the noisier (and less resolved) HEROS data. The sampling, optimized for phase coverage of the 0.7 d period, does not trace those features, and is therefore not suited for their investigation.

ω **Ori:** Although the data is not sufficient to cover the unfavourable period of almost exactly one day, the type of *lpv* as shown by Neiner et al. (2002, their Fig. 16), similar to most other Be stars, can be confirmed.

10 CMa: Baade (1984a) found periodic *lpv* and gave a period of 1.36 ± 0.05 d. The 21 FEROS spectra taken 2000 confirm this value, although the latter spectra alone do not suffice to distinguish between this period and its 1-day aliases. Dachs & Lemmer (1991) found a photometric 1.34 d period, later Balona et al. (1992) reported a double wave period of 2.632 d, which is just about twice these values. HIPPARCOS photometry gives 1.338 d (Hubert & Floquet 1998), but Percy et al. (2002) did not confirm this value and noted a period of 0.5 d to be more consistent with the data.

κ **CMa:** This star was observed intensively with FEROS in 2000. The period that sorts the *lpv* best is 0.548 d with no confusion due to aliasing. The residual *lpv* is one of the few that does not resemble the $\ell = m = 2$ patterns derived from modelling (Sect. 6.2). Instead of a single low-order bump travelling from blue to red in the line profile, a similar bump is present, but shows clear substructure in metal lines, as if two such patterns would follow each other with a separation of about 0.25 cycles (Fig. 6.4).

κ CMa shows also a secondary period of 0.617 d with the typical properties of what Štefl et al. (2003a) called a transient period in ω CMa. Only sparse data were taken in other observing seasons (1997, 1999, 2002), but already these few data make clear that κ CMa is extraordinarily active on short timescales. Comparison with the outbursts directly witnessed in μ Cen and ω CMa suggests that κ CMa underwent such outbursts most of the time when it was observed.

Photometric period determinations do not agree with these spectroscopic values. Percy et al. (2002) confirm the short periodic behaviour found by Hubert & Floquet (1998, 1.337 d), while Balona (1990) derived 1.408 d from 1988 data, but data obtained 1987 just previous to a photometric outburst seem to be sorted better with ≈ 1 d (c.f. his Fig. 5).

ω **CMa:** The periodic *lpv* of this object has been discussed in detail already by Štefl et al. (2003b) and modelled in Sect. 5.2. The outbursts of ω CMa are described by Štefl et al. (2003a). During such outbursts, a secondary period of about 1.47 d is apparent. It is seen only in lines with at least some
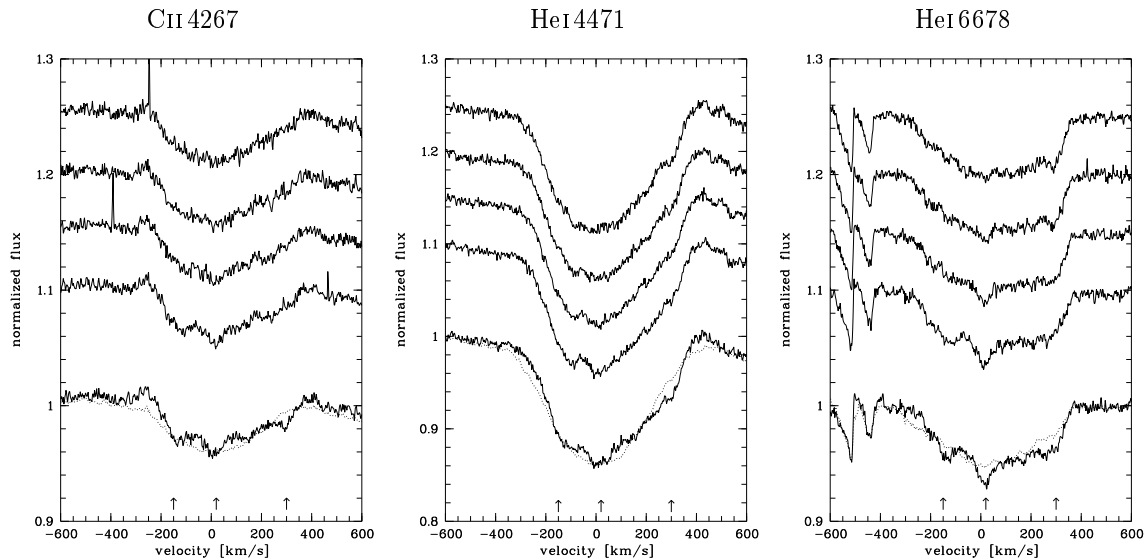
	C II 4267	He I 4471	He I 6678

Figure D.2: Evolution of three short-lived transients in three different lines of HR 4009 observed with FEROS. The dotted line overplotted to the lowermost profiles corresponds to the mean of all observations. The structure between -600 and $-400 \, \mathrm{km \, s^{-1}}$ in He I 6678 is due to detector blemishes. Time increases towards the top, proportional to the offset. The observations span 95 minutes.

circumstellar contribution, but not in purely photospheric lines. There is only very weak photometric variability, which is not dominated by the photospheric 1.37 d period, but the only transiently present 1.49 d period. For a detailed discussion of the variability and previous investigations the publications listed above are referred to.

FW CMa: The period of 0.83 d has tentatively been published already on account of the first HEROS data (Rivinius 1999). Further observations confirmed this period as coherent at least between 1996 and 2000. The star is not known to show periodic behaviour in photometry, but already Hanuschik et al. (1996) found FW CMa comparable to ω CMa in terms of the emission outburst behaviour. This was confirmed with HEROS and FEROS spectra.

HR 3642: Carrier et al. (2002) detected short-periodic *lpv* with 1.13028 d in spectroscopic data, while no such period was present in HIPPARCOS photometry. The variability shown (their Figs. 13 to 15) looks like the *lpv* presented here of objects of similarly low $v \sin i$. *lpv* is also clearly present in our few spectra of this star, but only six spectra at a relatively low S/N of 60 do not allow to search for this period independently or determine the type of the *lpv*. Adopting the given period, however, the data is acceptably sorted (Fig. D.1).

HR 4009: No period was given for this star so far. A periodic signal in the analysis is very weak, but undoubtedly present in both observing seasons in 1999 and 2000. Next to the periodic *lpv* HR 4009 shows also short-lived aperiodic phenomena (Fig. D.2), which resemble the ones reported by Smith (1989) for λ Eri.

HR 4074: The spectroscopic *lpv* found initially by Baade (1984a) is very similar to the one of ω CMa. The star was classified as a Be star from a spectrum taken in the 19$^{\mathrm{th}}$ century, but currently does not show any traces of circumstellar material (Štefl et al. 2002, and references therein), excluding any interpretation of its variability in terms of circumstellar matter. Percy et al. (2002) do not find short-periodic variability in HIPPARCOS photometry.

PP Car: The period analysis performed here indicates a weak signal, but clearly above the noise at about 1.0 d or its 1-d aliases. Porri & Stalio (1988) published spectra in which *lpv* is apparent, and a period of 0.35 d is suggested for the variability of the full width at half maxima of the He I 6678 line. In fact, the extreme red asymmetry of the profiles in their data (their Fig. 8) repeats on a timescale of slightly more than a day. In one case, the opposite asymmetry was observed 0.22 d earlier. Computing the phase
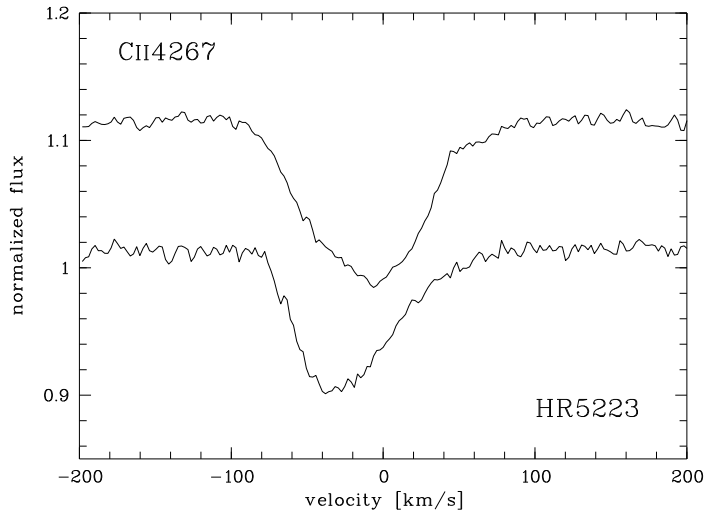
Figure D.3: The *lpv* of HR 5223. The few spectra do not enable a period determination, but the *lpv* is of the same type as in FW CMa, which has a similarly low $v\sin i$. The spectra are the two most different ones observed.

differences resulting from the potential period values (1.0, 0.504, and 0.33 d), phase differences of 0.21, 0.44 and 0.66 cycles are derived. Similar to the arguments for μ Cen (Rivinius et al. 1998b), a phase difference of 0.44 cycles between these two spectra (i.e. close to 0.5 for opposite asymmetry) seems more likely than the others, so here 0.504 d are adopted as *lpv* period, but still the one day aliases cannot firmly be excluded with the current data.

δ Cen: Balona et al. (1992) report a tentative photometric period of 1.923 d seen in 1988, but absent in 1990. Percy et al. (2002) find either 0.55 or 1.1 d in HIPPARCOS photometry, favouring the shorter value. In the 1999 HEROS spectroscopy, also both values are present, 0.532 d and 1.139 d, being 1-d aliases of each other, but with a formally somewhat higher significance of the longer period, which is adopted here.

HR 4625: Unpublished single previous spectra taken by S. Štefl suggested this star to be a good candidate to search for periodic *lpv*. It was observed intensively with HEROS in 1999. Over the $2\frac{1}{2}$ months of observations no outburst occurred, but the Balmer emission underwent the typical evolution of a relaxation phase, i.e. the wings became narrower while the emission height increased. The photospheric lines showed typical *lpv* with a period of 1.69 d.

μ Cen: This multiperiodic Be star was investigated in detail by Rivinius et al. (1998b,c). Modelling the short-periodic *lpv* resulted in the same mode properties as for ω CMa. The spectral data was made public by Rivinius et al. (2001c). Only the main period of 0.503 day is shown here. In addition to this period there are three more periods with very similar values, together called the "longer period group" by Rivinius et al. (1998b), and two more periods at 0.28 d which constitute the "shorter period group". Similar to ω CMa, there are also transient periods present during outbursts.

From several independent photometric data sets a period of about 1.06 d was derived (Cuypers et al. 1989; Dachs & Lemmer 1991; Percy et al. 2002). For this reason Balona et al. (2001b) favour a 1d double-wave period over a 0.5 d single wave also for spectroscopy. However, neither is the photometric period a double wave, nor do the two assumed half-waves for spectroscopy differ from each other, which in the absence of other evidence, is the only justification to assume a double-wave pattern. The secondary period group at 0.28 d, also due to non-radial pulsation, but in a higher mode, is not seen in photometric data at all.

HR 5223: During the 20 nights spanned by the observations, the broad Balmer emission wings decreased, while the Hα peak height rose. This is a usual early post-outburst evolution, observed in detail e.g. in ω CMa, FW CMa, and μ Cen. Low-order *lpv* is clearly present in the 8 observed spectra.

The two spectra with the most extreme asymmetry (Fig. D.3) compare well with the typical appearance of asymmetric phases in other low $v\sin i$ stars. No period can be derived from the limited data, however.

η Cen: The photometric period given by Cuypers et al. (1989) is 1.927 d with a triple-wave shape. Štefl et al. (1995) took into account both photometric and spectroscopic data and derived a single-wave period of $\frac{1}{3}$ of the triple-wave value, 0.642 d, which was confirmed by later works (e.g. Janot-Pacheco et al. 1999;

Balona 1999; Levenhagen et al. 2003). Štefl et al. (1995) also detected traces of a period at about 0.57 d, but due to unfortunate sampling could not confirm its reality. Such a shorter period was, however, also found by Janot-Pacheco et al. (1999) and Levenhagen et al. (2003), in the HEROS data, and by Balona (1999). The latter author rejected this period as not real, since it was not found in all spectroscopic lines, but this is similar with the HeI vs. SiIII lines of e.g. μ Cen (Rivinius et al. 1998b). Given all the detections in independent data, however, η Cen can be concluded to be a multiperiodic Be star. Taking into account the obtained results about secondary "transient" periods in other stars, the photospheric main period should be the shorter one, which is weaker in photometry, but almost dominant in HeI lines.

Analysis of the data of all seasons from 1995 to 1999 permits the 0.57 d period to be resolved into two with values of 0.577 d and 0.565 d. Although the weaker one is also weaker than the 0.642 d secondary period, it is clearly detected in all stronger HeI lines.

Sorting the data with the shorter periods, the patterns are well comparable to other Be stars (Fig. 6.2). In fact, both 0.577 and 0.565 d have very similar patterns, just like the group of longer periods present in μ Cen (Rivinius et al. 1998b). Similar to other high $v \sin i$ Be stars, these periods are only very weakly present in metal lines like SiIII, but still detectable in e.g. CII 4267.

For the secondary period, i.e. 0.642 d, which was the only one taken into account by most previous investigators, striking differences are seen between the *lpv* of Hδ, HeI 6678, and HeI 4388 lines (Fig. 6.5, discussed in Sect. 6.3). The secondary period is coherently present through all observing seasons from 1995 to 1999. The same variability pattern can be identified in Fig. 10 of Balona (1999), but since the main period of 0.577 d and eventual transient features will not perfectly cancel out during such a short run of twenty days, the pattern is much less evident.

η Cen shows line emission outbursts about once every couple of weeks. This is almost as frequent as in μ Cen, but the outbursts of η Cen are less prominent, and detectable only in data with relatively good spectral coverage and S/N. The beat frequency of the two main periods (0.565 d and 0.577 d) is in the same order of magnitude, 29 d, but the outbursts are not regular enough to be explained with just these two frequencies. The secondary period, 0.642 d, is unlikely to contribute to such a beating mechanism, as it probably is not associated with photospheric *nrp*.

χ **Oph:** Hubert & Floquet (1998) reported cyclic behaviour of the HIPPARCOS photometry, but could only constrain the period to be > 0.45 d. The spectroscopic HEROS data also shows a periodic signal, but cannot distinguish between 0.649 d and the 1-day alias at 0.393 d. Re-investigating HIPPARCOS data Percy et al. (2002) propose 0.55 d. Taking into account the results by Hubert & Floquet (1998), 0.649 d is adopted for this work.

ι **Ara:** There is no *lpv* apparent for the available HEROS data. A period of ≈ 0.56 d was derived by Cuypers et al. (1989), switching from single- to double-wave appearance, while Dachs & Lemmer (1991) published a 0.61 d double-wave period.

From HIPPARCOS data, Hubert & Floquet (1998) deduced 0.565 d, not mentioning a double wave nature. If this period is present also in spectroscopy, it is below the detection threshold for HEROS data, which shows the spectrum to be stable within the limits. The star has not been observed with FEROS, which would have provided better resolution at higher S/N.

α **Ara:** Neither the photometric period reported by Cuypers et al. (1989), 0.9807 d with a double-wave lightcurve, nor the single wave period of 0.490 d found by Hubert & Floquet (1998) can be confirmed by spectroscopy. Although these periods are close to one day or half a day, the phase coverage would almost be complete for both of them in our data, so this is not a sampling problem. However, a slow secular shift in the overall velocity of the emission lines is apparent, so that α Ara could be a binary with a period longer than the run length of 71 d. This would severely hamper the detection of short periods in data with one spectrum per night.

66 Oph: A spectroscopic period of 0.45 d, together with a shorter one of 0.25 d, was published recently by Floquet et al. (2002) and ascribed to *nrp*. While the data available for the present work are not suited to confirm the shorter period, the 0.452 d sort the HEROS spectra well.

Štefl et al. (2004) report 66 Oph to be a spectroscopic triple system similar to *o* And, where a close pair of late B/early A type stars is seen in singly ionized metal lines. This pair orbits the Be star on a very long timescale at large distance, so that no influence on the Be star is to be expected.
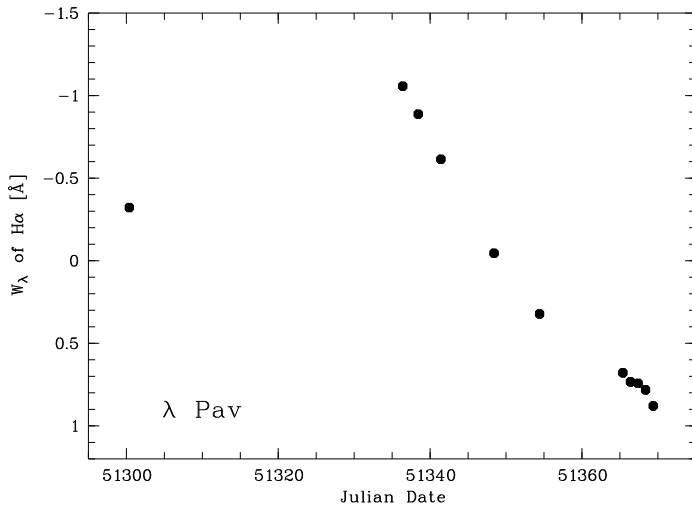
Figure D.4: The Hα equivalent width of λ Pav. An outburst probably occurred between JD 51 300 and 51 340, confirming the photometric outburst behaviour of λ Pav found by Hubert & Floquet (1998).
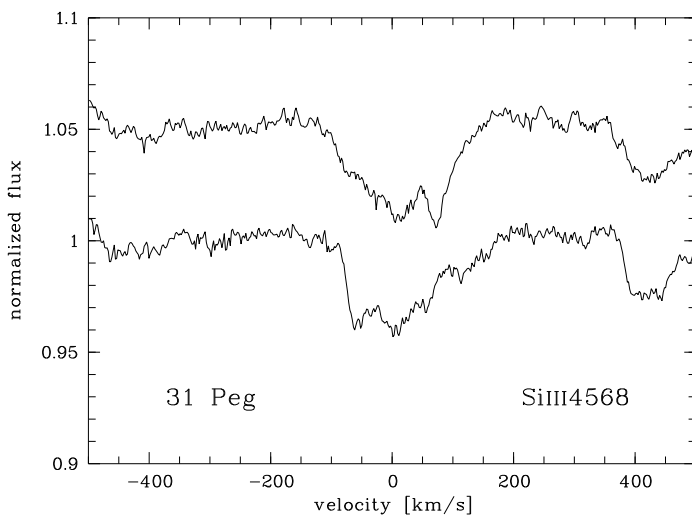

Figure D.5: ω CMa-like spikes in the *lpv* of 31 Peg observed with FEROS.

λ Pav: In the spectra *lpv* is apparent, but the limited database of 11 spectra over 70 days does not allow one to determine a period. The variability is close to the detection threshold, so that the individual profiles neither permit the variability type to be derived from them, like in HR 5223. Hubert & Floquet (1998) give a photometric period of 0.6 d and note outburst behaviour. The Balmer emission during our observations was highly variable (Fig. D.4), comparable to μ Cen in its "flickering" stage (Hanuschik et al. 1993).

28 Cyg: Periodic behaviour with 0.7 d was initially found by Spear et al. (1981) in photometry and later confirmed as 0.68 d by Peters & Penrod (1988). Further works agree with this period, and also found other periods, which were not present in all data sets, however (Pavlovski et al. 1997, for a review). The period given here, 0.64 d was found also by Hahula & Gies (1994). The values ranging from 0.64 d to 0.7 d seem incompatible. But the multiperiodicity with two close periods around 0.64 d reported by Tubbesing et al. (2000), based on a subset of the HEROS data presented here, potentially explains slightly different periods found from run to run, if these runs are too short to resolve the period doublet.

31 Peg: The period tentatively given here, 0.724 d, was derived from the ls99c and ohp01 data independently, but both data sets suffer from 1-d aliasing. No other period determination was published by now. The presence of rapid *lpv* itself is, however, clearly seen in the ohp01 data, which consists of 14 spectra taken in two separate nights.

The *lpv* is also obvious in the ls99c data and published data (e.g. Zorec et al. 1996), and several spectra clearly show spikes like in ω CMa (Fig. D.5). Metal line emission was strong in 1999, but weak in the
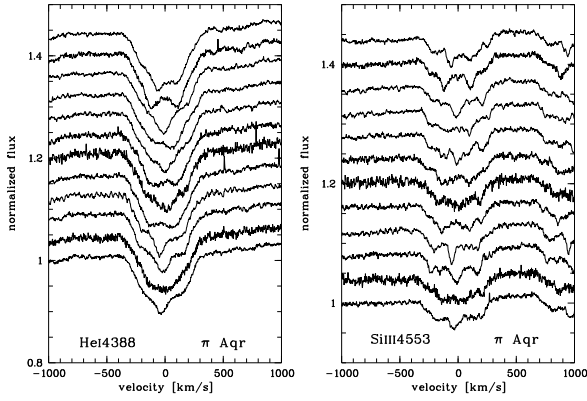
Figure D.6: The *lpv* of π Aqr observed in 1999 with FEROS is clearly of a different type than in most other objects. The individual spectra are separated by a few days, but the evolution of the features is much faster.
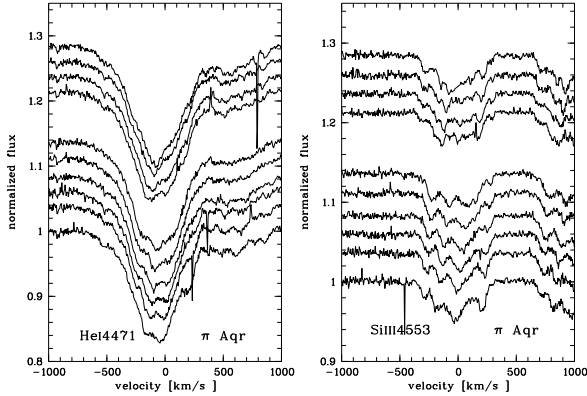

Figure D.7: π Aqr observed with AURÉLIE at the OHP ($t_{exp} \approx 10$ min). The sharp features clearly propagate across the line profile quickly. The spacing of the spectra is proportional to time (increasing upwards), spanning exactly two hours in total.

ohp01 and ond observations (see Table A.1), with traces of outburst-like activity in the outer wings of the Balmer lines. Due to this and the limited number of spectra, the data sets cannot be combined to better constrain the period.

To give an impression of the ls99c and ohp01 data, the HeI 4388 line is shown from the ls99c run, while the figure for SiIII 4568 was constructed from the ohp01 observations (Fig. D.1).

π Aqr: The star had a very strong emission spectrum before 1995/96 (Bjorkman et al. 2002). No short-term periodic behaviour is known for π Aqr, but recently Bjorkman et al. (2002) reported it to be a binary with a period of 84.1 d. Our data, obtained during the low emission phase after 1996 confirms such a timescale in the Balmer emission lines. Three spectra in October 2001 show a relatively strong Hα emission filling up the absorption and a peak height of about 1.1 of the continuum, but by 2002 the emission had weakened again to the previous value, with peak heights of about 0.9 of the ambient continuum. Since late 2004, the emission is rebuilding to the strong values observed before 1996.

Multiple, very sharp and rapidly variable absorption spikes are present in all lines normally formed photospherically (Figs. D.6 and D.7). They were present in every spectrum taken. The width of the absorption spike scales with the expected thermal broadening of the respective element forming the line. No other star in the observed sample exhibits such strong sharp transients. These features might be due to similar processes as the line transients described by Smith (1989) for HeI lines of λ Eri and also present in HR 4009 (see Fig. D.2).

Meanwhile, Peters et al. have presented data on a conference 2004 in Tennessee (not yet published), which clearly attributes the variations to high-order non-radial pulsation. The key to this finding were several hundred high-resolution spectra taken over only a few days, so that the problems our data typically pose with only one or a few spectra per night do not arise. In any event, however, the strength and sharpness of the pseudo-absorption features, especially in metal lines, are unique.

o And: Being well known for its photometric variability with highly variable amplitude, this star has the latest spectral subtype in the sample (B6). The dominant photometric period is 1.58 d (double wave).

The main spectroscopic period presented here (0.694 d) is clearly different from this value and its single-wave equivalent, but also present in the photometric data as third strongest periodicity (Sareyan et al. 1998). The amplitude of the spectroscopic variations may vary strongly. In spectroscopic data taken in late 1998 no periodic signature could be found at all (Budovičová et al. 2005). When present, the *lpv* is different from the one in most other Be stars because the propagation of a feature from the blue to the red side of the line takes longer in phase (about a full cycle) whereas in other Be stars the feature crosses the line width in about 0.6 to 0.7 cycles (Fig. 6.4). Other periods tested on the data, in particular the dominant photometric ones, do not sort the spectroscopic *lpv* at all.

Table D.1: Types of *lpv* observed. Parentheses denote uncertain detections, periods taken from the literature (see above) but not confirmed here are marked with ∗. A double √√ indicates μ Cen-style multiperiodicity. Mode determinations derived by other authors are given in the last three columns.

| Name | HR | Line profile variability type | | | | | | other authors | | |
		ω CMa-like period	non-ω CMa period	stable	aperiodic or N/A	additional short period	secondary period	ℓ	m	ref.
α Eri	472	√	—	—	—	—	—	2	−2	1
DU Eri	1423	√	—	—	—	—	—	2	−2	1
DX Eri	1508	√	—	—	—	—	—	—	—	—
λ Eri	1679	—	√	—	—	—	—	2,4	−2,−2	1,2
ω Ori	1934	∗,(√)	—	—	∗	∗	—	2–3	±2	3
10 CMa	2492	√	—	—	—	—	—	—	—	—
κ CMa	2538	—	√	—	—	—	√	—	—	—
ω CMa	2749	√	—	—	—	—	√	2	+2	4
FW CMa	2825	√	—	—	—	—	—	—	—	—
	3642	(√)	—	—	—	—	—	—	—	—
	4009	√	—	—	√	—	—	—	—	—
	4074	√	—	—	—	—	—	—	—	—
PP Car	4140	√	—	—	—	—	—	—	—	—
δ Cen	4621	√	—	—	—	—	—	—	—	—
	4625	√	—	—	—	—	—	—	—	—
μ Cen	5193	√√	—	—	—	√	√	2	+2	5,6
	5223	(√)	—	—	—	—	—	—	—	—
η Cen	5440	√√	—	—	—	—	√	2,1–3,3	−2,−-	1,7,8
χ Oph	6118	√	—	—	—	—	—	—	—	—
ι Ara	6451	—	—	√	—	—	—	—	—	—
α Ara	6510	—	—	√	—	—	—	—	—	—
66 Oph	6712	√	—	—	—	∗	—	2–3	—	9
λ Pav	7074	—	—	—	√	—	—	—	—	—
28 Cyg	7708	√√	—	—	—	—	—	2	−2	1
31 Peg	8520	(√)	—	—	—	—	—	—	—	—
π Aqr	8539	—	—	—	√	—	—	—	—	—
o And	8762	—	√	—	—	—	—	—	—	—

1: Peters & Gies (2000), 2: Kambe et al. (1998), 3: Neiner et al. (2002), 4: Baade (1982), 5: Baade (1984b), 6: Chapter 5, 7: Janot-Pacheco et al. (1999), 8: Levenhagen et al. (2003), 9: Floquet et al. (2002)